Structural and Functional Investigations of Plant Metallothioneins

---

Dissertation
zur
Erlangung der naturwissenschaftlichen Doktorwürde
(Dr. sc. nat.)
vorgelegt der
Mathematisch-naturwissenschaftlichen Fakultät
der
Universität Zürich

von
Tamara Huber
von
Reiden, LU

Promotionskomitee
Prof. Dr. Eva Freisinger (Vorsitz und Leitung der Dissertation)
Prof. Dr. Julia Fritz-Steuber
Prof. Dr. Roland K. O. Sigel

Zürich, 2013

Acknowledgment

I like to thank all those people who made this thesis possible, also the ones which are not specially mentioned here. Without your help and support, I could not have accomplished this challenging work.

First of all, I am indebted to Prof. Dr. Eva Freisinger. I like to thank her for giving me the opportunity to work in her lab, for keeping the ball rolling and putting me on the right track. I appreciated to work with the extraordinary amount of freedom and manifoldness. I enjoyed her confidence to let me develop my own ideas and to get the chance to present them on conferences. It was a pleasure to spend the last four years in the Freisinger group.

My special thanks also go to the members of my PhD committee, Prof. Dr. Roland K. O. Sigel from the University of Zürich and Prof. Dr. Julia Fritz-Steuber from the University of Hohenheim for kindly acting as referee.

I also like to thank for the great financial support from the Swiss National Science Foundation, the Swiss Academy of Science, the Swiss Chemical Society, the University of Zurich, the Inorganic Chemical Institute, and the CMSZH graduate school.

Then, I also like to thank all other peoples from the university, especially the different chemical institutes, for helping me in various technical tasks and giving me helpful advices. But also a special thank also goes to the people, who supported me with specific material and knowledge: Prof. Dr. Julia Fritz-Steuber for the NifS protein and plasmid, Prof. Dr. Milan Vašák for the rabbit liver MT2A protein and huMT plasmid, Prof. Dr. Sílvia Atrian and Prof. Peter Goldsbrough for the yeast strains, Prof. Dr. Yves Barral for yeast marker plasmids, Dr. Silke Johannsen, Dr. Daniela Donghi, Dr. Maria Pechlaner, and Dr. Maximiliane Korth for recording and evaluating NMR spectra, Dr. Ilian Jelezarov and Dr. Christine Berger for access to the MCD spectropolarimeter.

A special acknowledgement goes to Dr. Jens Löbus for introducing me into the field of metallothioneins, answering all my questions, giving me tremendous amount of advices and inspired me for further experiments. Our endless and fruitful discussions which most started with opposite opinions were very helpful for my PhD.

I also like to thank Dr. Xiaoqiong Wan and Dr. Estevão Aun Peroza Galli for starting my interesting projects and advising me in several technical details. Then to Sandra Rezzonico and Mareike Anna Schmidt for advising me endlessly patient for the work with yeast. To Dr. Silke Johannsen for helping me uncomplaining with the NMR experiments and the DLS. And to Dr. Christine Berger and Dr. Simone Tix for the help with the MCD.

Further thank goes to the whole MT group and Prof. Dr. Milan Vašák for great scientific discussions, Dr. Augusto César dos Santos Cabral, Dr. Barbara Leitenmaier, Dr. Silke Johannsen, Katsiaryna Tarasava, Jovana Jakovleska for being me great labmates, and also our guests visiting shortly or longer the lab, Aleksandar Salim, Alessia Dürst, Blanca Puigdelloses, Mansoore Esmaili, Manuela Bruetsch, Matthias Winnerlein, Michelle Burkart, Philipp Pfingstag, and Sonja Giger. But I also like to thank the rest of the Freisinger group, David Egloff, Igor Oleinich and Joachim Schnabl.

Likewise I thank all past and present members of the SF-group from the last four years for the great time, the unique familiar atmosphere and daily support. The thank goes to Aleksandar Salim, Alessia Dürst, Alicia Dominguez-Martin, Anastasia Musiari, Anita Schmitz, Augusto César dos Santos Cabral, Barbara Leitenmaier, Bhaumik Dave, Dania Marthaler, Daniela Donghi, Danny Kowerko, David Egloff, Erica Fiorini, Estevão Aun Peroza Galli, Fawzia Al-Sogair, Eva Freisinger, Helena Guiset Miserachs, Igor Oleinich, Jens Löbus, Joachim Schnabl, Johanna-Elena Penner-Jacobi, Jovana Jakovleska, Katsiaryna Tarasava, Lucia Cardo, Lukas Kopp, Magdalena Grazul, Magdalena Rowińska-Żyrek, Maria Pechlaner, Marianthi Zampakou, Maximiliane Korth, Mélodie Hadzic, Michelle Schaffer, Milan Vašák, Miquel Barceló Oliver, Miriam Skilandat, Mokrane Khier, Pallavi Choudhary, Richard Börner, Roland Sigel, Sebastian König, Serranda Gashi, Silke Johannsen, Sofia Gallo, Sonja Giger, Susann Paulus, Theodor Marsoner, Viviane Zelenay, Xiaoqiong Wan for inputs, discussions, advices and helpfulness.

Besides the scientific help, I also appreciated magnificent personal support from the SF-lab during various memorable events, as ski trips, boat trips, barbecues, cake time, and so one. Especially to mention the lunch group for sharing with me ups and downs of the daily life.
Also I like to thank the CMSZH graduate school for organizing various socializing events, where I met various interesting people and friends spending long nights at apéros, barbecues, and retreats.

Some special thanks goes to Silke and Susi for hours of discussions, mostly not related to science but about all aspects of the lab life. And a great thank also to David and Jay always willed for having a break, especially in the last year, when we spent hours drinking coffee and by the way forgetting about the lab; but I also appreciated the time we spent beside with other activities.

Finally, I would like to thank Alex, without him this thesis would not exist. He always supported me and had a non-chemical look at my activities.

1. Content

2. Abbreviations

aa	amino acids
Ac	acetate
Amp#	ampicillin concentration [ug/mL]
bp	base pairs
calc	calculated
CD	circular dichroism
COSY	correlation spectroscopy
Da	dalton
ddH_2O	deionised and distilled water
DNA	deoxyribonucleic acid
DLS	dynamic light scattering
DOSY	diffusion ordered spectroscopy
DPD	*N*,*N*-dimethyl-*p*-phenylenediamine
DTNB	5,5'-dithiobis(2-nitro-benzoic acid)
DTT	1,4-dithiothreitol
EDTA	ethylenediaminetetraacetic acid
ESI	electrospray ionization
EtBr	ethidium bromide
$\varepsilon_{\#}$	extinction coefficient wavelength [nm]
F-AAS	flame atomic absorption spectroscopy
FPLC	fast protein liquid chromatography
γ-ECS	γ-glutamyl-cysteine-synthetase
GFLC	gravity flow liquid chromatography
GS	glutathione synthetase
GSH	glutathione
GST	glutathione *S*-transferase
G418	geneticin
HPLC	high pressure liquid chromatography
HR	homologous recombination
HSQC	heteronuclear single quantum correlation
IDS	intrinsically disordered structures
IPTG	isopropyl β-D-1-thiogalactopyranoside
kb	kilo base
LB	luria-bertami
LMCT	ligand to metal charge transfer
MALDI	matrix-assisted laser desorption / ionization
mBBr	monobromobimane
MBSR	mB-thioether
MCD	magnetic circular dichroism
M-MT	metallated MT
M,S-MT	metallated MT with additional sulfide ligands
M_r	molecular weight
MS	mass spectrometry
MT	metallothionein
mut	mutant
MWCO	molecular weight cut off
NMR	nuclear magnetic resonance
NOESY	nuclear overhauser effect spectroscopy
NTA	nitrilotriacetic acid
NTB	2-nitro-5-thio-benzoic acid
NTSB	2-nitro-5-thiosulfo-benzoic acid
OD#	optical density wavelength [nm]
PAGE	polyacrylamide gel electrophoresis
PBS	phosphate buffered saline
PC	phytochelatin
PCR	polymerase chain reaction
PDB ID	RSCB protein data bank identification code
PEG	polyethylene glycol
ppm	parts per million
PS	phytochelatin synthetase
QD	quantum dot
$\theta_{\#}$	ellipticity coefficient wavelength [nm]
$\theta_{M\#}$	magnetic ellipticity coefficient wavelength [nm]
rpm	rounds per minute
SD	synthetic defined
SDS	sodium dodecyl sulfate
SEC	size exclusion chromatography
TEV	tobacco etch virus
TOCSY	total correlation spectroscopy

Tris-HCl	tris(hydroxymethyl) aminomethane-hydrochloride
U	enzymatic units [µmol/min]
UV/Vis	ultraviolet and visible light
WT	wild-type
x g	gravitational acceleration
YNB	yeast nitrogen base
YPD	yeast extract peptone dextrose
2-PDS	2,2'-dithiodipyridine
3D	3 dimensional

3. Summary

Metallothioneins (MTs) are small cysteine-rich proteins coordinating various transition metal ions preferably with the electron configuration d^{10}. They are ubiquitously present in most phyla, and next to phytochelatins they represent a successful molecular concept for metal complexation in cells. Although MTs have been studied for decades still limited information is available. Especially plant MTs are not examined sufficiently, neither in structural nor in functional aspects.

This study deals mainly with elucidating the structural and functional characteristics of the plant MT2 (cicMT2) from chickpea (*Cicer arietinum*). As a typical member of the plant MT subgroup p2, it has an *N*- and *C*-terminal metal binding region with a long cysteine-devoid linker region in between. The binding of five divalent metal ions (mainly Zn^{2+} and Cd^{2+} ions) to the 14 thiolate groups of the cysteines leads to a single metal-thiolate cluster.

Recent studies showed the incorporation of sulfide ions into the metal-thiolate cluster of cicMT2. Although the presence of sulfide ions in plant and other MTs has already been reported previously, many details remained unclear. The further *in vitro* characterization with various analytical techniques could enlighten the features of the cluster in terms of mono- and divalent metal ions, stability, sulfide-modulated increase in cluster size, the influence of the environment on the various isoforms, and the mechanism of the incorporation itself. From our findings we can conclude that sulfide ion incorporation is highly influenced by the metal ion and sulfide ion availability in the experimental setup. While a clear incorporation of sulfide ions can be shown with divalent metal ions, also a change in cluster structure can be reported for monovalent metal ions but its specific features are still under discussion. The size of the cadmium-sulfide-thiolate cluster shows a dependence on the initial available free sulfide ion concentration. In case of cicMT2, the cluster can be enlarged to a multiple size of the one without sulfide ions. Evaluation of the mechanism of sulfide containing Cd^{2+}-thiolate cluster formation reveals a slight distortion or opening of the preformed cluster structure by sulfide ions prior to insertion of additional metal ions into the cluster. To probe the general ability of metallothioneins to form sulfide containing metal-thiolate clusters, analogous experiments were performed with a mammalian MT revealing a probable role of the long cysteine-free linker region present in most plant MTs.

Further, determination of the overall 3D structure of cicMT2 was attempted by nuclear magnetic resonance spectroscopy. The obtained spectra indicate intrinsically disordered structures, which might however even be favorable for the metal related function of the protein. Next to the structural features of cicMT2, the function of a variety of plant MTs was approached with yeast complementation assays. These experiments will require further efforts.

All in all, we elaborated different aspects of plant metallothioneins, yet a lot of facets are hidden in the dark.

4. Zusammenfassung

Metallothionine (MTs) sind kleine cystein-reiche Proteine, die bevorzugt Übergangsmetalle mit einer d^{10} Elektronenkonfiguration binden. Sie kommen in einem grossen Teil der bekannten Lebensformen vor und repräsentieren neben den Phytochelatinen ein erfolgreiches molekulares Konzept für die Metallkomplexierung in Zellen. Obwohl MTs seit Jahrzehnten studiert werden, sind die vorhandenen Informationen immer noch beschränkt. Insbesondere die pflanzlichen MTs sind wenig untersucht, weder in struktureller noch funktioneller Hinsicht.

Diese Studie behandelt hauptsächlich strukturelle und funktionelle Aspekte des pflanzlichen MT2 (cicMT2) der Kichererbse (*Cicer arietinum*). Als typisches Mitglied der pflanzlichen MT-Untergruppe p2 hat cicMT2 eine *N*- und *C*-terminale Metallbindungsregion mit einer dazwischengeschalteten cystein-freien Linkerregion. Die Bindung von fünf zweiwertigen Metallionen (hauptsächlich Zn^{2+}- und Cd^{2+}-Ionen) an die 14 Thiolatgruppen der Cysteine führt zu einem einzelnen Metall-Thiolat-Cluster.

Jüngste Studien zeigen die zusätzliche Koordination von Sulfidionen im Metall-Thiolat-Cluster von cicMT2. Obwohl die Anwesenheit von Sulfidionen schon früher nachgewiesen wurde, sind noch viele Details unklar. Die weitere *in vitro* Charakterisierung konnte die Eigenschaften des Clusters bezüglich ein- und zweiwertiger Metallionen, Stabilität, Sulfid-moduliertem Anstieg der Clustergrösse, den Einfluss der Umgebung auf die verschiedenen Isoformen und den Mechanismus der Aufnahme selbst aufklären. Von unseren Resultaten können wir auf die starke Abhängigkeit der Sulfid-Aufnahme von der Metall- und Sulfidionen-Verfügbarkeit schliessen. Während mit zweiwertigen Metallionen die Sulfid-Aufnahme klar bestätigt werden konnte, wurde mit einwertigen Metallionen zwar eine Änderung in der Cluster-Struktur gezeigt, jedoch verbunden mit offenen Fragen zu den spezifischen Eigenschaften. Die anfängliche Konzentration an frei verfügbaren Sulfidionen bestimmt die Grösse des Cadmium-Sulfid-Thiolate-Clusters. Im Falle von cicMT2 konnte gezeigt werden, dass der Cluster in Gegenwart von Sulfidionen signifikant mehr Metallionen binden kann als in ihrer Abwesenheit. Die Untersuchung des Bildungsmechanismus des Sulfidionen enthaltenden Clusters zeigt eine Sulfid-induzierte geringe Verformung oder Öffnung der vorhandenen Clusterstruktur vor dem Einbau zusätzlicher Metallionen. Um die prinzipielle Existenz von Sulfid-enthaltenden Metall-Thiolat-Clustern in MTs abzuschätzen, wurden analoge Experimente mit Säugetier-Metallothioninen durchgeführt, die eine mögliche Rolle des langen cystein-freien Linkers in gewissen pflanzlichen MTs aufdeckten.

Des Weiteren gab es Bestrebungen, die dreidimensionale Struktur des cicMT2 mit Kernspinresonanzspektroskopie zu untersuchen. Die Spektren lieferten Hinweise auf intrinsische ungeordnete Strukturen, die durchaus von Bedeutung für die funktionellen Interaktionen mit den Metallionen sein könnten. Neben den strukturellen Analysen bezüglich cicMT2 versuchten wir, die Funktion von einer Vielfalt pflanzlicher MTs mit der Komplementierung von Hefen zu untersuchen, was allerdings nicht abgeschlossen werden konnte.

Alles in allem konnten wir Licht auf verschiedene Aspekte der pflanzlichen Metallothionine werfen, es liegen jedoch noch immer viele Facetten im Dunkeln verborgen.

5. Introduction

Metallothioneins (MTs) constitute an extremely heterogeneous family of ubiquitous, low molecular weight, cysteine-rich proteins (close to 30 % of their amino acid content) that give rise to metal-thiolate complexes ensuing on metal ion coordination.[1] The designation "metallothionein" reflects the extremely high thiolate sulfur and metal content.

MTs were first recognized in 1957 in equine renal cortex, and in the following decades, the protein was found throughout the animal kingdom, from bacteria to human, except arachea.[2-4] The omnipresence of these proteins indicates a key role in life what was raising the interest in MT research. Newer investigations do not only focus on the elucidation of their structure and function, they also become known as tools and for disease treatments, e.g. biomarkers or for chemotherapy of certain cancers.[5-6]

The biological role of MTs is often considered to be enigmatic, however it is increasingly clear that MTs fulfill protein functions, the relative importance of which depends very much on specific evolved requirements of the particular organism.[7] This is not unexpected, as its unique structural characteristics, potent metal binding, and striking chemical reactivity have bearing on numerous biochemical processes. Vital roles often result from sequestration of environmental toxic metal ions such as cadmium and mercury or its involvement in homeostasis of essential trace metals as zinc and copper. Apart from these roles, recent studies suggest their involvement in a number of biological processes, among others, protection against reactive oxygen species, adaptation to stress, protection against brain injury, antiapoptotic effects, or regulation of neuronal outgrowth.[8-10]

5.1. Structural aspects of MTs

5.1.1. Occurrence and elementary structure of MTs

MTs have been isolated from vertebrates, invertebrates, plants, and eukaryotic microorganisms and from some prokaryotes. The expression levels of MT genes depend on the species, the isoform, the tissue, the growing stages and environmental factors. Most MTs isolated to date are inducible by cellular products and stress conditions, including hormones, cytokines, reactive oxygen species, metal ions, and a variety of environmental factors like low temperature, heat shock, inflammation, nutrient deprivation, UV exposure.[11-14]

In contrast to the relatively detailed knowledge about the regulation of MT gene expression in mammalians and yeasts, little is known about the mechanisms that regulate transcription of plant MT genes. The promoter region of some plant MT genes was found to contain both metal and hormone regulatory elements mediating the induction and efficient expression of the protein.[15-18] The abundance of RNA transcripts is also dependent on the respective MT subfamily. Plant MTs from the p1 subfamily show a lower abundance in shoots than in roots, whereas the opposite is true for the p2 subgroup.[19] RNA from the p3 subgroup is highly expressed in fleshy

Tab. 1 Alignment of metallothioneins and classification into different taxonomical families and subfamilies according to Kojima et al.[3]. Cysteine residues are highlighted.

UniProtKB	Name	Species		Amino acid sequence
vertebrate (family 1)				
P02802	MT1	*(Mus musculus)*	mouse	MDP-NCSCST-GGSCTCTSSCACKNCKCTSCKKSCCSCCPVGCSKCAQGCVCKG------AADKCTCCA
P04355	MT2	*(Rattus norvegicus)*	rat	MDP-NCSCAT-DGSCSCAGSCKCKCQCKCTSCKKSCCSCCPVGCAKCSQGCICKE------ASDKCSCCA
P18055	MT2A	*(Oryctolagus cuniculus)*	rabbit	MDP-NCSCAAAGDSCTCANSCTCKACKCTSCKKSCCSCCPPGCAKCAQGCICKG------ASDKCSCCA
P28184	MT3	*(Mus musculus)*	mouse	MDPETCPCPT-GGSCTCSDKCKCKGCKCTNCKKSCCSCCPAGCEKCAKDCVCKGEEGAKAEAEKCSCCQ
P47945	MT4	*(Mus musculus)*	mouse	MDPGECTCMS-GGICICGDNCKCTTCSCKTCRKSCCPCCPPGCAKCARGCICKG------GSDKCSCCP
fungae and yeast (family 8-13)				
P07215	CUP1	*(Saccharomyces cerevisiae)*	baker's yeast	MFSELINFQNEGHECQCQCGSCKNNEQCQKSCSCPTGCNSDDKCPCGNKSEETKKSCCSGK
P41902	CRS5	*(Saccharomyces cerevisiae)*	baker's yeast	MTVKICDCEGECCKDSCHCGSTCLPSCSGGEKCKCDHSTGSPQCKSCGEKCKCETTCTCEKSKCNCEKC
plant (family 15)				
subfamily p1				
Q39458	MT1	*(Cicer arietinum)*	chickpea	M--SGCNCGSSCNCGDQCKCNKRS-----GLSYVEAGETTETVVLGVGPTKIHFEGAEMSVAAEDGCKCGSSCTCDP-CNCK
P20830	MT1	*(Pisum sativum)*	garden pea	M--SGCGCGSSCNCGDSCKCNKRSS----GLSYSEM-ETTETVILGVGPAKIQFEGAEMSAASEDGCKCGDNCTCDP-CNCK
P43400	MT1	*(Triticum aestivum)*	wheat	M--S-CNCGSGCSCGSDCKCGKMYPDLTEQGSAAAQVAAVVVLGVAPENKAGQFEVA---AGQSGEGCSCGDNCKCNP-CNC
P43392	MT1A	*(Arabidopsis thaliana)*	mouse-ear cress	MADSNCGCGSSCKCGDSCSCEKNY----------NKECDNCSCGSNCSCGSNCNC
subfamily p2				
Q39459	MT2	*(Cicer arietinum)*	chickpea	MSCCGGNCGCGSSCKCGSGCGGCKMYPDMSYTEQTTSE--TLVMGVASGKTQFEGAEMGFGAENDGCKCGSNCTCNPCTCK
Q93X22	MT	*(Quercus suber)*	cork oak	MSCCGGNCGCGTGCKCGSGCGGCKMFPDISSEKTTT-E--TLIVGVAPQKTHFEGSEMGVGAEN-GCKCGSNCTCDPCNCK
O22319	MT2	*(Musa acuminata)*	banana	MSCSGGNCGCGSSCSCGSGCGGCRMLTDLGEERSSTSQ--TMIMGVAPQKGHFEELETAAGSDN-GCKCGSNCTCDPCNCK
P25860	MT2A	*(Arabidopsis thaliana)*	mouse-ear cress	MSCCGGNCGCGSGCKCGNGCGGCKMYPDLGFSGETTTTETFVLGVAPAMKNQYEASGESNNAENDACKCGSDCKCDPCTCK
subfamily p3				
P43389	MT3	*(Actinidia deliciosa)*	kiwi	MSDKCGNCDCADSSQCVKKGNS--IDIVETDKSYIEDVVMGVPAAESGGK--CKCGTSCPCVNCTCD
D2CGP2	AMT2	*(Malus domestica)*	apple	MSGKCDNCDCADSTQCVKKGNSYDLVIVETENRSMDTVFVDAPAAEHDGK--CKCGTGCSCVSCTCGH
Q40256	MT3	*(Musa acuminata)*	banana	MS-TCGNCDCVDKSQCVKKGNSYGIDIVETEKSYVDEVIVAAEAAEHDGK--CKCGAACACTDCKCGN
O22433	MT3	*(Arabidopsis thaliana)*	mouse-ear cress	MSSNCGSCDCADKTQCVKKGTSYTFDIVETQESYKEAMIMDVGAEENNANCKCKCGSSCSCVNCTCCPN
subfamily p4/pec				
P30569	E_c-1	*(Triticum aestivum)*	wheat	MGCDDKCGCAVPCPGGTGCRCTSAR-SGAAAGEHTTCGCGEHCGCNPCACGREGTPSGRANRRANCSCGAACNCASCGSATA
P43401	E_c	*(Zea mays)*	maize	MGCDDKCGCAVPCPGGKDCRCTS---GSGGQREHTTCGCGEHCECSPCTCGRATMPSGRENRRANCSCGASCNCASCASA
P93746	E_c-1	*(Arabidopsis thaliana)*	mouse-ear cress	MADTGKGSSV---AGCNDSCGCPSPCPGGNSCRCRMR-EASAGDQGHMVCPCGEHCGCNPCNCPKTQTQTSAKG----CTCGEGCTCASCAT
O22378	E_c-1	*(Glycine max)*	soybean	MADTSGGDAVRPVVICDNKCGCTVPCTGGSTCRCTSVG-MTTGGGNHVTCSCGEHCGCNPCNCPKT-AAS-GTG----CRCGTDCSCASCRT

fruits such as apple, banana, and kiwi during the ripening process, in plants, which do not produce fleshy fruits such as buckwheat, MT3 is predominantly expressed in leaves.[20-22] Finally, the pec subfamily is restricted to a single organ, the seed.[23-24]

The classification of MTs is based on amino acids similarities and phylogenetic relationships and divides MTs into fifteen families (Tab. 1).[3] For example, the mammalian MTs are part of family one, the vertebrate MTs, while all MTs of plant origin constitute family fifteen. The plant MT isoforms are additionally subdivided into four subfamilies called p1, p2, p3, and pec, based on the number of cysteine residues per protein and their distribution along the peptide chain.

A typical plant MT is composed of 60-85 amino acids therefore it is slightly larger than the members of the mammalian MT. The exact length depends on the respective subfamily. The subfamilies p1, p2, and p3 show some distinct different features than the one of the subfamily pec.

The primary sequences of the subfamilies p1-3 show assemblies of cysteine residues in the *N*- and *C*-terminal regions. In a subfamily, the *N*-terminal sequences are strictly conserved and present the main characteristic for discriminating them. The amino acid sequence of the *C*-terminal region is however very similar for all three subfamilies. These cysteine-rich regions are connected by a long (30-45 amino acids) cysteine-free linker region. Differently from mammalian MTs with an overall cysteine content of twenty residues, the amount of cysteines in p1-3 sums up to 10-14 residues. An additional specialty is the presence of aromatic amino acids as phenylalanine, tyrosine, and histidine in the linker region.

The main difference of the pec subfamily in comparison to the subfamilies p1-3 is the different organization of the cysteine-rich regions. The pec MTs contain a third cysteine-rich region with accordingly shorter linker regions in between (11-15 amino acids). The cysteine-free linkers are completely devoid of phenylalanine, tyrosine, and tryptophan. The central cysteine-rich region however encloses two highly conserved histidine residues. The cysteine-pattern of this central region is identical to the one found in the *C*-terminal cysteine-rich part of plant MTs from the other three subfamilies.[25] With totally 17 cysteine residues, the pec subfamily comprise a higher amount of cysteine residues than the other plant MT subfamilies and is thus more comparable to the mammalian isoforms.

5.1.2. Metal binding properties of MTs

MT genes were isolated from basically all living phyla, most of them are found as RNA, and only a few MTs as proteins. Those MTs, which were investigated on the protein level, all comprise a sulfur-based metal ion cluster.[26-27] Although the high metal-binding capability of MTs was ascribed mainly to the amount of cysteine residues present in these proteins, also other amino acids including histidine, lysine, and polar amino acid residues such as aspartic acid are taking part in the metal binding.[28-34]

The metal ion composition of native MTs depends on the natural source and/or on the previous exposure of the organism to metal ions. As cysteines are soft bases they preferentially coordinate soft acids according to the hard and soft acids and bases (HSAB) concept.[35] Especially closed shell

metal ions are favored, which give not rise to ligand field stabilization energy, including all d^{10} metal ions like essential Cu^{+} and Zn^{2+} ions but also non-essential Cd^{2+} and Hg^{2+} ions.

A more recent metallothionein classification is oriented on the metal binding selectivity differentiating among Zn^{2+} and Cu^{+} ion associated MTs claiming that according to the difference in binding geometry, MTs are either involved in Zn^{2+} or in Cu^{+} ion homeostasis.[36]

For the mammalian MTs, species containing Zn^{2+}, Cd^{2+}, Co^{2+}, Cu^{+}, Hg^{2+}, and Ag^{+} ions were analyzed, whereby the affinity of the metal ions for the cysteine-thiolate groups follows the order of the Irving William series: $Hg^{2+} >> Cu^{+}$, Ag^{+}, $Bi^{3+} >> Cd^{2+} > Pb^{2+} > Zn^{2+} > Co^{2+} > Fe^{2+}$.[37]

The metal ions Zn^{2+}, Cd^{2+}, and Co^{2+} are generally tetrahedrally coordinated and Cu^{+}, Hg^{2+}, and Ag^{+} ions prefer trigonal or diagonal coordination geometries.[38-42] In contrast to MTs from mammalian sources, in which zinc, cadmium, and copper can be simultaneously bound, there is no structural evidence from yeast and fungal MTs to host different coexisting metal ions. Specific binding of cadmium or copper to different tissue specific MT-forms *in vivo* has been encountered in the snail.[43] Plant MTs are so far shown with Cu^{+} and Zn^{2+} ions *in vivo*, but at least *in vitro* also with the other ones as shown for mammalian MTs.[25] As essential and highly abundant metal ions, Zn^{2+} and Cu^{+} ions are most extensively studied *in vitro*. Additional Cd^{2+} and Ag^{+} ions are well characterized mimicking the essential ones, although Ag^{+} ions show sometimes a different coordination than Cu^{+} ions.[38, 44-45]

Except the structure of the yeast metallothionein Cup1, all other published structures in the RSCB protein data bank are solved either with Cd^{2+} or Zn^{2+} ions as ligands, whereby both metals seem to be isostructurally exchangeable.[46] Zinc ions have a rather flexible coordination sphere, which is mostly dictated by the steric requirements of the ligands. Due to the lack of redox activity, Zn^{2+} ions are found as structural elements in a variety of biological molecules and they can undergo relatively fast ligand exchange reactions with low energy requirements.[47] Copper is commonly supposed to bind to MTs in its monovalent state because Cu^{2+} ions can be easily reduced by thiolate ligands.[48] The variety of outcomes of independent investigations on the Cu^{+} ion binding capability, the coordination geometry, and the cluster organization of Cu-MTs makes it even more difficult to generalize properties of Cu-MTs than those of Zn-, and Cd-MTs.[49-51] Multiple coordination numbers are possible showing Cu^{+} ion coordination to two, three, and four thiolate ligands in synthetic Cu-thiolate clusters, often adopting more than one Cu^{+}-geometry within the same molecule.[52]

5.1.3. General structure of MTs

The most important structure determining elements of MTs are the bound metal ions. In the absence of metal ions, MTs were estimated to contain a predominantly disordered structure.[53-54] Structural studies of apo-MTs using molecular dynamics calculations show that the cysteine side chains predominantly populate the outside surface of the protein to make the residues easily accessible for metal ions.

As long as metal ions are bound to the thiolate groups of the MTs, another structural characteristic appears. MTs can form either one or two metal-thiolate clusters. While mammalian

MTs always fold with two separate clusters to a dumbbell like shape, the baker's yeast Cup1 is known to form a single cluster connecting the *N*- and *C*-terminus of the protein. The number of metal-thiolate clusters of plant MTs is not clear so far but it seems to depend on the respective subfamily. Proteolytic digestion experiments show a coordination in two distinct clusters of the wheat E_c-1 (*Triticum aestivum*) which belongs to the pec subfamily and which structure was determined by nuclear magnetic resonance (NMR) spectroscopy (Fig. 1).[29, 55-57] In contrast, proteolytic digestion experiments and comparative metal ion binding studies of the garden pea MT1 (*Pisum sativum*) and the cork oak MT2 (*Quercus suber*) from the subfamilies p1 and p2 point towards one single metal-thiolate cluster.[58-59]

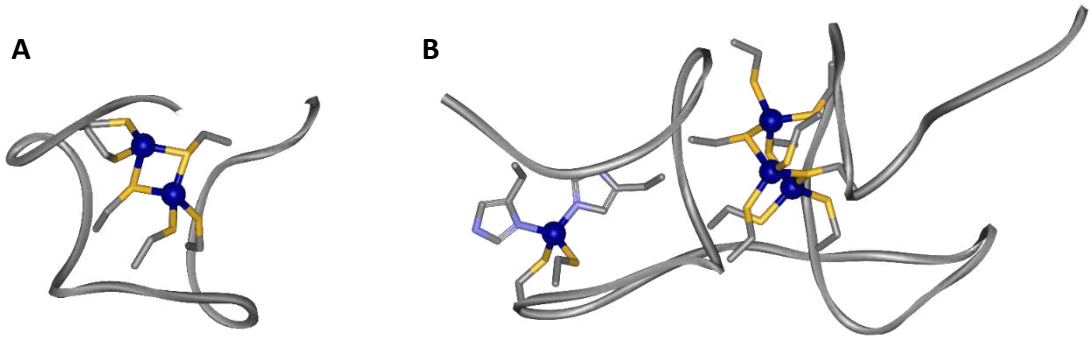

Fig. 1 NMR solution structure of the Zn^{2+} ion loaded **(A)** γ-domain (PDB ID: 2L62) and **(B)** β_E-domain (PDB ID: 2KAK) of wheat E_c-1. Grey ribbon is the backbone, cysteines and histidines are indicated as sticks, Zn^{2+} ions as blue spheres.[29, 55]

The investigation of the detailed overall structure of MTs is challenging because of the strong dependence of the protein backbone structure on the metal-thiolate cluster. While various methods for analyzing the metal-thiolate cluster exist, the protein backbone structure has either to be investigated by cryo-electron microscopy, X-ray crystallography, or NMR spectroscopy. Due to the intrinsic dynamic of the metal cluster, NMR spectroscopy has gained prominence as most reliable method for predicting the correct structure of metallothioneins. While X-ray crystallography requires a complete rigid structure of the mono-isomeric protein to form crystals, solution NMR spectroscopy is able to solve structures although a part of the whole molecule remains flexible. Additionally, MTs are rather small proteins and still able to be analyzed by NMR spectroscopy.

In conclusion, 94 % of the published structures of MTs in the RSCB Protein Data Bank are NMR solution structures, i.e. human MT2 and MT3 (*Homo sapiens*), rat MT2 (*Rattus rattus*), mouse MT1 and MT3 (*Mus musculus*), rabbit MT2A (*Oryctolagus cuniculus*), lobster MT1 (*Homarus americanus*), blue crab MT1 (*Callinectes sapidus*), antarctic fish MT_nc (*Notothenia coriiceps*), sea urichin MTA (*Strongylocentrotus purpuatus*), yeast Cup1 (*Saccharomyces cerevisiae*), wheat E_c-1 (*T. aestivum*), cyanobacteria SmtA (*Synechococcus elongates* PCC7942), and red bread mould NcMT (*Neurospora crassa*).[29-30, 38, 46, 55, 60-73]

Solution and crystal structures do not necessary overlap and can reveal differences. The crystal structure of rat Cd_5Zn_2-MT2 and the solution NMR structure of rat $^{113}Cd_7$-MT2 show identical

metal-thiolate cluster structures and closely similar global polypeptide folds (Fig. 2 A, B, D).[7, 62, 69, 74]

However, Cup1 of *S. cerevisiae* was found to harbor 8 Cu^+ ions with X-ray crystallography, while only 7 Cu^+ ions were found with NMR spectroscopy. Both structures show differences in the connectivity of the metal ions as well as in the overall shape, e.g. the amount of formed α-helices (Fig. 2 C, E).[67, 75]

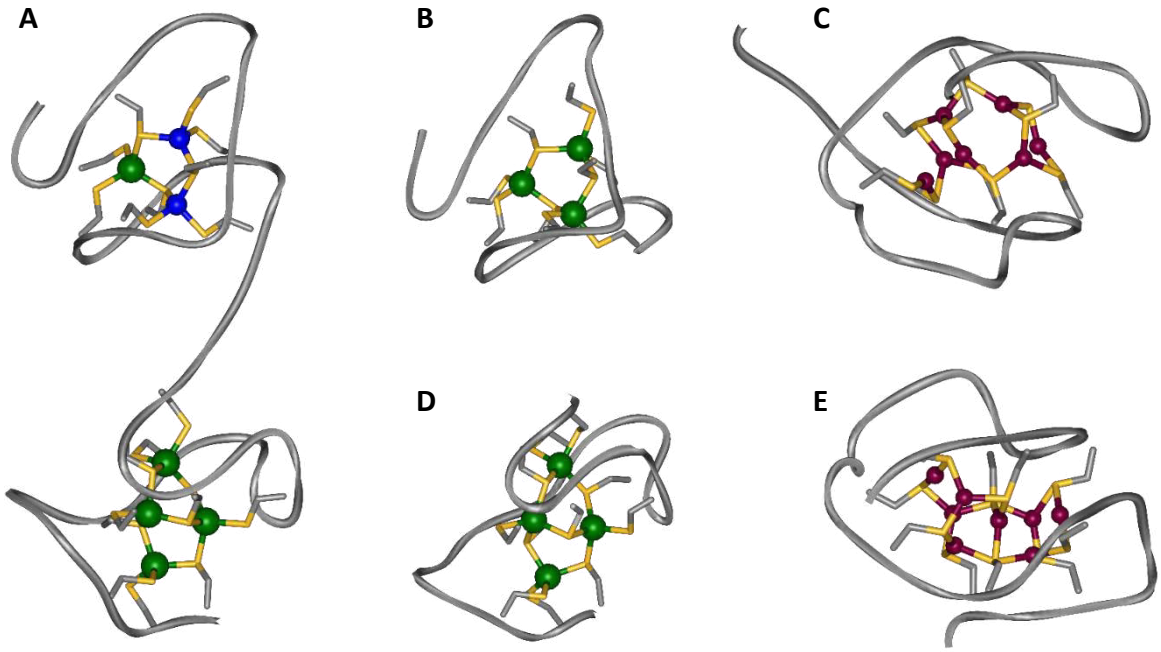

F

	protein sequence	helices
full-length	MFSELINFQNEGHECQCQCGSCKNNEQCQKSCSCPTGCNSDDKCPCGNKSEETKKSCCSGK	
NMR (1AQR)	QNEGHECQCQCGSCKNNEQCQKSCSCPTGCNSDDKCPCGN	7 %
X-ray (1RJU)	HECQCQCGSCKNNEQCQKSCSCPTGCNSDDKCPCGN	16 %

Fig. 2 **(A, B, D)** Three-dimensional structure of rat MT2 as determined by **(A)** X-ray crystallography of Cd_5Zn_2-MT2 (PDB ID: 4MT2) and **(B, D)** NMR spectroscopy in aqueous solution of $^{113}Cd_7$-MT2 (PDB ID: 1MRT and 2MRT).[62, 69] **(C, E)** Three-dimensional structure of Cup1, solved by **(C)** NMR spectroscopy of Cu_7-Cup1 (PBD ID: 1AQR) and **(E)** by X-ray crystallography of Cu_8-Cup1 (PBD ID: 1RJU).[67, 75] Protein backbone is shown as grey ribbon, cysteine thiolate ligands as yellow sticks, Cd^{2+} ions as green spheres, Zn^{2+} ions as blue spheres, Cu^+ ions as purple spheres. **(F)** Sequences of solved structures for full-length Cup1, for solved NMR structure (PDB ID: 1AQR) and solved X-ray structure (PBD ID: 1RJU). Color in sequence indicate connectivity to Cu^+ ions, underlined amino acids are forming a α-helical structure.

One of the main problem in 3D structure determination of metallothioneins are the flexible parts, especially the long linker region in the plant MTs. Recent investigations on floppy proteins go into the direction of stabilizing the backbone structure by an attached tag, e.g. glutathione-*S*-transferase (GST). These tags are mainly used for protein purification but are now also utilized as stabilization agents in crystallization experiments and NMR spectroscopy.[76-77] The dimerizing GST is interfering with spectroscopic methods such as UV/Vis, but due to the much bigger size of the tag compared to the MT, in NMR spectra only a negligible number of GST-signals can be

detected.[78] The advantage of the fusion system is already proven for the γ-domain of wheat E_c-1 and the fungal metal binding protein Neclu_MT1.[79] The fusion protein GST-γ-E_c-1 and the isolated γ-E_c-1 showed comparable NMR spectroscopy pattern and an overlapping 3D structures.

5.1.4. Additional sulfide ligands in the metal-thiolate cluster of MTs

In 2004, acid-labile ligands were observed in the Cd-MT2 of cork oak.[80] It was proposed that they are sulfide ligands, a finding that was corroborated later with ESI-MS analysis.[81] Later on, inorganic sulfide ions were also detected in the Zn^{2+}- and Cd^{2+}-forms of MTs from a broad range of different species including the mammalian MT1 and MT4 forms.[80-83] Recently, sulfide ions were shown to exist in the native Cd^{2+}- and Zn^{2+}-MTs Cup1 of the baker's yeast *S. cerevisiae*, whose growth media was supplemented with metal ions.[84]
So far, only acid-labile sulfide ions were found in Zn^{2+} and Cd^{2+} metallated forms, but never in Cu^{+}- or Ag^{+}-MTs. Moreover, these MTs were always in equilibrium with the S^{2-} ion devoid forms (native and recombinant).[85-86]

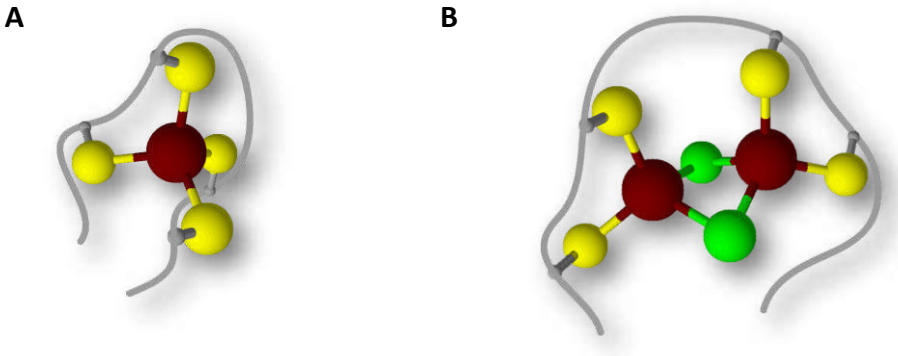

Fig. 3 Schematic representation of an exemplary **(A)** Cd-thiolate cluster and **(B)** Cd,S-thiolate cluster. In red are shown the Cd^{2+} ions, in yellow the thiolates, in green the S^{2-} ions, and in grey the protein backbones.

The stoichiometry of the sulfide containing MTs displays a high degree of heterogeneity, similar to the native isolates of MT complexes from many species which contain significant heterogeneity of isoforms and metal compositions.[87-88] Hence, it was not possible so far to establish a general rule with respect to the ratio between incorporated sulfide ions and coordinated metal ions or even between the combined content of cysteine thiolate groups and sulfide ions and the metal ions. The main consensus seems to be a S^{2-} ion to metal ion ratio below one, which is to be expected considering charge compensation of the additional negative charges introduced into the cluster by the sulfide ions with additionally coordinated metal ions (Fig. 3). In general, the MTs seem to be flexible in their metal and sulfide ion load, maybe as an adaption to their environment. 3D structures from MTs with incorporated sulfide ions are so far not published.

5.2. Functional aspects of MTs

Despite many decades of intensive investigations since the discovery of the first MTs, their precise functions remain elusive. In considering the functions of metallothioneins, one must remember that it is present in varying amounts in most tissues, it binds several essential and nonessential metals, and its synthesis is induced by these metals and also by physical or inflammatory stress. Therefore, the protein either performs one basic role common to all these conditions or has a multiplicity of functions, depending on the particular circumstance. The consensus view appears to favor the latter option.[89] The generally proposed functions of MTs include homeostasis and metabolism of essential metal ions, metal detoxification, free radical scavenging, signal transduction, and adaptation to stress (Fig. 4).[10, 19, 80, 90-95] In this functions, MTs were also associated with various diseases, e.g. Alzheimer's disease, diabetes, cancer, Lyme disease, Parkinson.[96-103]

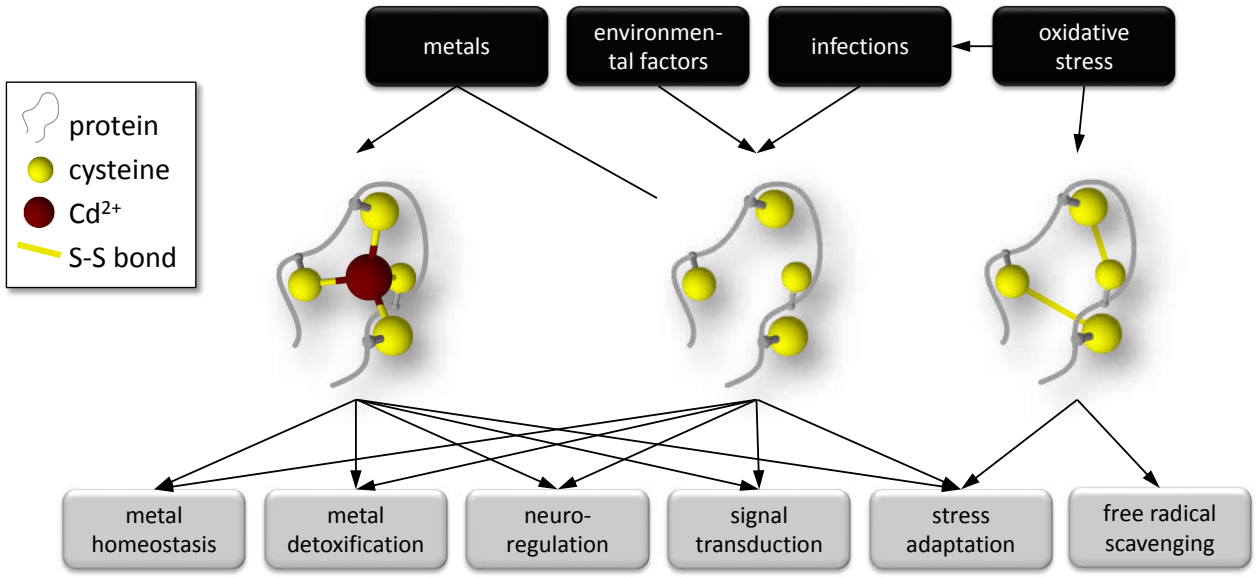

Fig. 4 Scheme of impacts of metallothioneins, stress and metal ions interplay. Infections, stress, and other environmental factors trigger an inflammatory response by increasing the production of pro-inflammatory cytokines, which, in turn, stimulate the gene expression of metallothioneins. For proper conducting of most of their functions they need metal ions. Binding and releasing of metal ions has numerous impacts on the regulation of the organism.

There is more and more evidence that MTs can act as scavengers of cell damaging reactive oxygen species. E.g. rabbit liver MT1 appears to scavenge free hydroxyl ($^{\cdot}OH$) and superoxide (O_2^{-}) radicals with the help of the metal-thiolate cluster by metal release and thiolate oxidation:

$$2\ \text{-SH} + 2 \bullet\ ^{\cdot}\text{OH} \longrightarrow \text{-S-S-} + 2\ H_2O$$

This effect could be reversed, what makes the MTs an extraordinary efficient $^{\cdot}OH$ radical scavenger. MTs have the characteristics of a sacrificial but renewable cellular target for

·OH-mediated cellular damage.[104] Additionally, *in situ* hybridization experiments with the plant MT2 from *Q. suber* (cork oak) provided evidence for a function of the thiolate groups as scavengers for free radicals.[80]

5.2.1. Metal ions in life

Metal ions are essential to the structure and function of many proteins, from DNA-binding zinc fingers to respiratory proteins that require iron or copper.[105] It has been estimated that nearly half of all enzymes are metalloproteins.[106] Therefore, an exact control of the essential as well as toxic metal ions is indispensable. All organisms show mechanisms to maintain an optimal concentration of metal ions by a complex set of physiological reactions.

Fig. 5 shows the dependence of a compound concentration on the physiological state of an organism.[107] Essential metal ions show an immediate positive response above zero concentration. They level off at an optimal level, which wide depends on the nutrient. Finally, at excess concentrations deleterious effects settle in, the biological response becomes unfavorable, and the once nutritious substance becomes toxic. Toxic metal ions show a lag region at low concentration under the assumption that an organism can cope with some amount of a substance before toxic effects become evident (threshold).

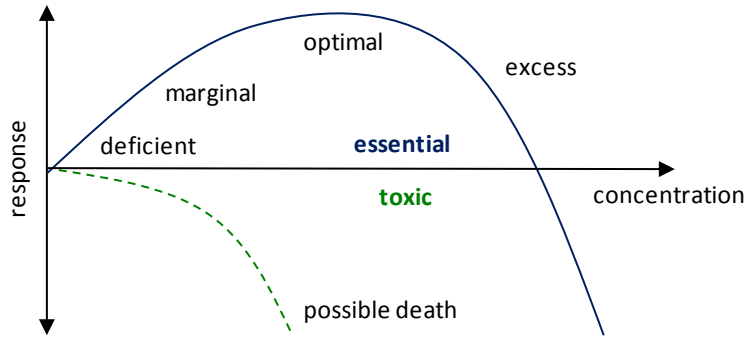

Fig. 5 Biological response dependence on tissue concentration of an essential nutrient (blue solid curve) and of a deleterious substance (green dashed curve). Scheme adapted from Martin[107].

5.2.1.1. Role of MTs in metal homeostasis

The role of MTs in homeostasis and metabolism of essential metal ions such as zinc and copper is based on the fact that they are the major zinc and copper binding proteins in many tissues, and that there is also a close relationship between zinc content and tissue MT concentration.[14, 108] Zinc ions bind most tightly to MTs suggesting that MTs are behaving effectively as a sink for zinc. But it was also found, that the cellular redox state can directly influence the availability of the zinc ions, by oxidation/reduction of the solvent accessible thiolate ligands.[74, 93] There is also evidence that MTs are involved in copper homeostasis, e.g. MT transcript abundance in senescing leaves is associated with a set of gene transcripts involved in copper homeostasis.[19]

5.2.1.2. Detoxification properties of MTs

In view of their unusual metal binding properties, MTs are supposed to play a role in metal detoxification by sequestering excess amounts of essential and non-essential heavy metal ions such as cadmium and mercury.[109]

The detection of additional sulfide ligands supports this idea. In biological systems, compounds containing sulfide ions exhibit a variety of physiological functions including redox processes, structure stabilization of proteins, enzyme regulation as well as the formation of important parts of catalytic centers and of sensors for iron and oxygen.[110-119] It can be assumed, that sulfide ligands fulfill a similar function in MTs and in phytochelatins (PCs).[19, 94]

Phytochelatins, also called cadystines or γ-EC peptides, are a second group of cysteine-rich molecules occurring mainly in plants and fungi.[120-122] They share many characteristics with MTs and are considered to be the main cadmium and arsenic detoxification molecules in those cells.[19] Their general formula is $(\gamma\text{-Glu-Cys})_n\text{-Gly}$, where n varies in the range of 2-11 depending on the organisms.[123-125] Unlike the gene-encoded MTs, phytochelatins are enzymatically synthesized from glutathione upon heavy metal ion exposure (Fig. 6).[19, 125]

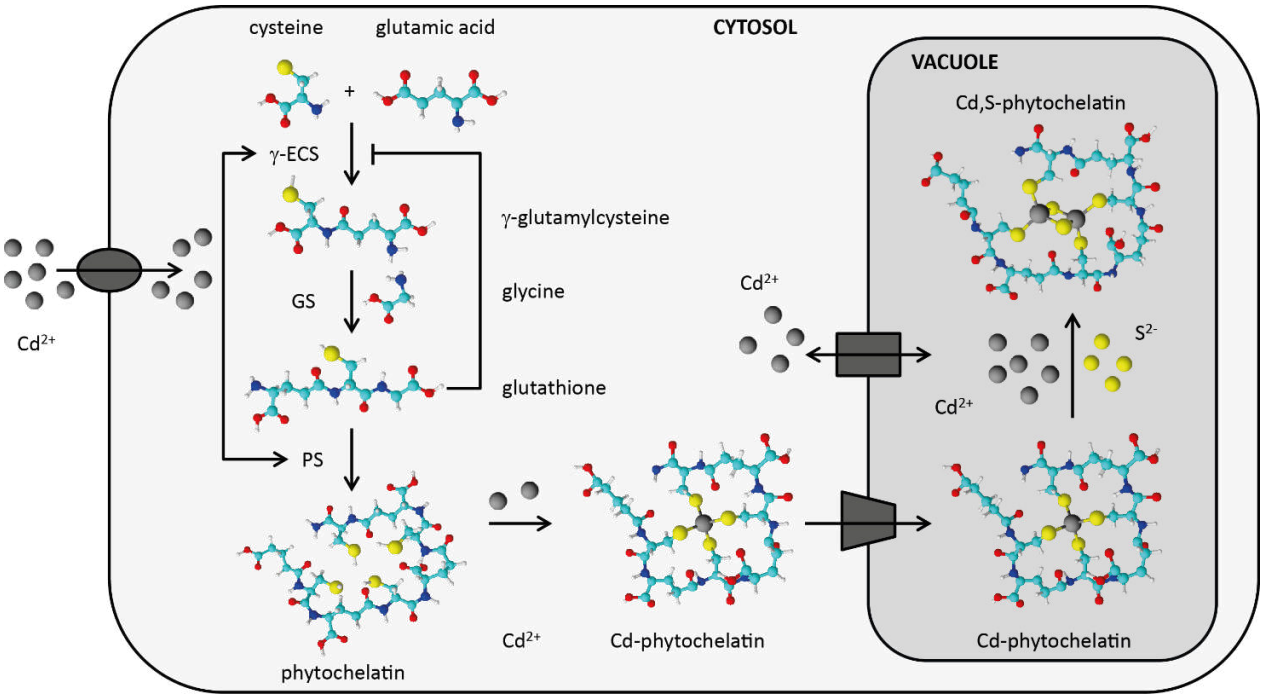

Fig. 6 Scheme of phytochelatin pathway in the cell.[19, 126-127] Highly abundant of Cd^{2+} ions are imported into the cell by a ZIP transporter. In the cytosol, the translation of γ-glutamyl-cys-synthetase (γ-ECS) and phytochelatin synthetase (PS) starts immediately. γ-ECS synthesizes from cysteine and glutamic acid γ-glutamylcysteine, which is elongated with a glycine by glutathione synthetase (GS) forming glutathione. Several glutathiones are subsequently connected by PS to phytochelatins, which are in the following loaded with Cd^{2+} ions (Cd-phytochelatin). ABC transporter bring the Cd-phytochelatin from the cytosol to the vacuole, where with the help of sulfide ions the Cd^{2+} ion binding capacity is increased and Cd,S-phytochelatins are formed.

For example, suppression of PC synthesis in the fission yeast *Schizosaccharomyces pombe* leads to a metal sensitive phenotype.[128-129] Most phytochelatin isoforms characterized so far contain sulfide ions, increasing the thermodynamic stability and metal binding capacity.[85-86, 121, 130] The generation of sulfide ions might be in part a cellular response to enhance the detoxification efficiency for heavy metal ions.

Sulfide ions were also found in some Zn^{2+} and Cd^{2+} ion containing MTs. Presuming that incorporation of sulfide ions has *in vivo* relevance for certain MTs, flexible metal ion and sulfide ion contents would provide a simple and fast way to adapt to changes in the physiological environment. The exact role of metallothioneins however remains to be investigated further.

5.2.2. Yeast complementation studies as a tool for functional analysis of plant MTs

There is not a lot of information known about the function of plant MTs, but the function of other MTs is often related to metal ion binding/releasing. As plant MTs also have a high affinity for metal ions, the behavior of plant MTs should be studied in an environment with a high metal concentration. Such *in vivo* tests are very time consuming to perform in plant cells. Therefore, the genetically easy to manipulate yeast *S. cerevisiae* is often chosen as model organism for studying the function of eukaryotic proteins.

In yeast complementation assays, the target protein production (MT) is disrupted so that the host is incapable for their synthesis. The host indeed gets the ability to express another protein with a supposed similar function, which should overtake the function of the original protein (Fig. 7). Thus, the function of the target protein is indirectly shown by the yeast complementation assay.

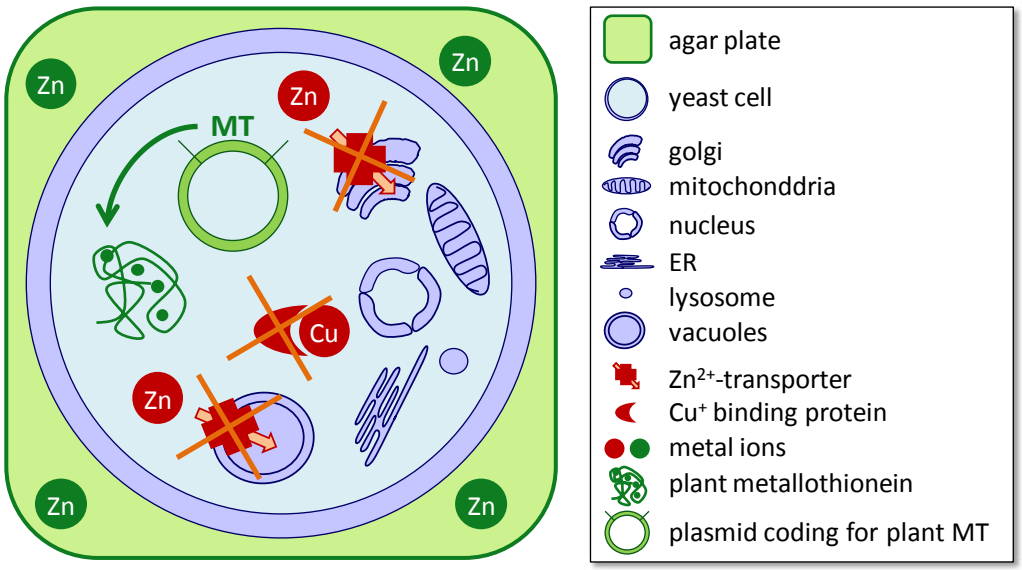

Fig. 7 Scheme of yeast complementation assay. Yeast defense mechanisms against high metal concentration are disrupted by gene deletion. As an alternative they are complemented with plasmids coding for different plant MTs, which are supposed to overtake the function of the lacking proteins.

For the elucidation of the function of metallothioneins, *S. cerevisiae* can act as a model system. Yeast cells have two protection systems against high metal ion concentration, i.e. scavenging by proteins and transport into vacuoles.

Metal scavenging is performed by copper binding proteins (Cup1 and Crs5), which decrease the free metal ion concentration in the cytosol. Cup1 and Crs5 are involved in copper resistance and sensitivity and show properties analogous to MTs studied from higher eukaryotes.[131-132] Yeast complementation studies with the plant MT2 from *Q. suber* show that over-expression of this protein restores viability in high Cu-concentrations.[82, 133] Expression of MT1a, MT2a, MT2b, MT3, E_c-1, or E_c-2 from *A. thaliana* can re-establishes copper tolerance in all instances.[18, 92]

Metal transport into vacuoles by zinc transporters (Zrc1 and Cot1) removes metal ions from the cytosol and stores them in a separate compartment, the vacuoles. To investigate sensitivity against Zn^{2+}, Cd^{2+}, and Co^{2+} ions of *A. thaliana* MTs, a yeast double deletion mutant for Zrc1 and Cot1 was chosen that is hypersensitive to zinc due to a deficiency for expression of the two vacuolar Zn^{2+} transporters.[92] It was shown, that the inserted plant MTs of *A. thaliana* were able to restore zinc tolerance of the mutant to the wild-type level.

5.3. Metallothionein 2 from chickpea

The focus of this work is set on the plant MT2 from *C. arietinum* (chickpea), cicMT2 (UniProt: Q39459). The mRNA of this protein is up-regulated during epicotyls growth and shows increased expression in mature tissues.[134] The existence of the protein is inferred from homology. cicMT2 shows the characteristic cysteine distribution pattern of the p2 subfamily of the plant MT family 15. The amino acid sequence of cicMT2 consists of 78 amino acids and features two cysteine-rich regions containing eight and six cysteine residues, respectively, separated by a 41 amino acids long linker region (Fig. 8).

SCCGGNCGCGSSCKCGSGCGGCKMYPDMSYTEQTTSETLVMGVASGKTQFEGAEMGFGAENDGCKCGSNCTCNPCTCK

Fig. 8 Amino acid sequence of cicMT2. In black the cysteines are highlighted, squares indicate the *N*- and *C*-terminal metal binding regions with the cysteine free linker region in between.

As typical for all MTs, cicMT2 shows a high affinity to d^{10} metal ions. cicMT2, obtained by recombinant expression in *Escherichia coli*, is able to coordinate five divalent metal ions such as Zn^{2+}, Cd^{2+}, and Co^{2+} *in vitro*.[135] Results strongly suggest further that the coordinated metal ions are arranged in a single metal-thiolate cluster formed by the combined *N*- and *C*-terminal cysteine-rich regions of the protein leading to a hairpin-like structure.[135] Recently, the incorporation of sulfide ions into the Cd^{2+}-thiolate cluster of cicMT2 *in vitro* was evaluated.[136] In presence of initially ten equivalents of sulfide ions a protein complex of the average composition Cd_9S_7-cicMT2 is formed. In addition to significantly increasing the binding capacity of cicMT2 for Cd^{2+} ions, the incorporation of sulfide ions also raises the pH stability of the formed cluster by approximately 0.5 pK_a units compared to Cd_5-cicMT2.

6. Material and Methods

6.1. Material

6.1.1. Chemicals and enzymes

Enzymes and kits were purchased from Promega AG, Dübendorf, Switzerland (www.promega.com), Fermentas, Le Mont-sur-Lausanne, Switzerland (www.fermentas.ch), Finnzymes, Vantaa, Finland (www.finnzymes.com), New England BioLabs, Ipswich, USA (www.neb.com), Roche, Rotkreuz, Switzerland (www.roche-applied-science.com) or GE Healthcare, Uppsala, Sweden (www.gelifesiences.com). Vectors used for plasmid construction were purchased from GE Healthcare, Uppsala, Sweden (www.gelifesiences.com) and Addgene, Cambridge, USA (www.addgene.org). Cell strains were purchased from Life Technologies, Zug, Switzerland (www.lifetechnologies.ch) and Stratagene, Agilent Technologies, Basel, Switzerland (www.genomics.agilent.com). Oligonucleotides were ordered from and DNA sequencing was performed by Microsynth, Balgach, Switzerland (www.microsynth.ch).

ZipTips (C18) were purchased from Millipore, Zug, Switzerland (www.merckmillipore.ch), PicoTips from New Objective, Woburn, USA, (www.newobjective.com), and dialysis tubing from Pierce, Rockford, USA (www.piercenet.com). Cellulose acetate filters 0.2 μM were purchased from Whatman GmbH, Dassel, Germany (www.whatman.com), Sartorius AG, Goettingen, Germany (www.sartorius-stedim.com), or Millipore, Zug, Switzerland (www.merckmillipore.ch). Deuterated reagents were bought from Armar Chemicals, Döttlingen, Switzerland (www.armar.ch) or Euriso-Top, Gif sur Yvette Cedex, France (www.eurisotop.com), $^{113}CdCl_2$ from Cambridge Isotope Laboratories Inc., Innerberg, Switzerland (www.isotope.com).

All other buffers and chemicals were ACS grade or comparable and were purchased from Sigma-Aldrich, Buchs, Switzerland (www.sigmaaldrich.com), Merck, Zug, Switzerland (www.merckmillipore.ch), Chemie Brunschwig, Basel, Switzerland (www.brunschwig-ch.com), or Carl-Roth AG, Arlesheim, Switzerland (www.carlroth.ch).

All solutions were prepared using water treated with a TKA genepure water purification system from TKA Wasseraufbereitungsysteme, Niederelbert, Germany (www.tka.de). If appropriate, solutions were saturated with nitrogen or argon. Whenever complete absence of oxygen was required, water was degassed by three consecutive freezing–thawing cycles under vacuum.

6.1.2. Instrumentation

Anaerobic working was performed in a glove-box from Coy Laboratory Products Inc., Grass Lake, USA (www.coylab.com).
Various spectrophotometers were used. UV/Vis spectra were collected with a Cary 100 Bio UV-Vis spectrophotometer and a Cary 500 Scan UV-Vis-NIR spectrophotometer from Agilent Technologies, Basel, Switzerland (www.agilent.com) equipped with Varian UV 3.00 software, or a Nanodrop 2000 Spectrophotometer from Thermo Fisher Scientific, Wohlen, Switzerland (www.thermoscientific.com) analyzed with Nanodrop 2000 1.3.1 software. UV/Vis spectra of microplates were recorded with a Microplate Spectrophotometer Power Wave XS2 from Biotek Instruments, Luzern, Switzerland (www.biotek.ch) and evaluated with Gen5 1.11.5 software. CD and MCD spectra were recorded with a J-810 spectropolarimeter from Jasco Corporation, Tokyo, Japan (www.jasco.com) equipped with Spectra manager 1.53.00 software, Jasco Corporation, Tokyo, Japan (www.jasco.com). Fluorescence spectra were taken with a Cary Eclipse Fluorescence Spectrophotometer from Agilent Technologies. Cuvettes used for spectra recording were purchased from Hellma AG, Zumikon, Switzerland (www.hellma.ch), and microplates from Corning, Corning, USA (www.corning.com).
The thermomixer used was from Eppendorf, Hamburg, Germany (www.eppendorf.de), other shaking devices such as the Stuart Rotor Drive STR4 from Bibby Scientific, Staffordshire, UK (www.stuart-equipment.com) and KL2 Schüttler from Edmund Bühler GmbH, Hechingen, Germany (www.edmund-buehler.de) were used.
Ultrafiltration was performed with an ultrafiltration cell equipped with a regenerated cellulose membrane, both from Amicon, Millipore, AG, Zug, Switzerland (www.millipore.com). Concentration of solution was done with a Concentrator 5301 from Vaudaux-Eppendorf AG, Schönenbuch BL, Switzerland (www.eppendorf.ch).
Autoclaving was carried out in a Systec VX-100 of Systec Schweiz GmbH, Hünenberg, Switzerland (www.systec-lab.ch). PCR reactions were performed either in a Mastercycler personal from, Vaudaux-Eppendorf AG or a Thermocycler T1 from Biometra, Goettingen, Germany (www.biometra.com) and were designed with Vector NTI 10.1.1. of Invitrogen Corporation, Zug, Switzerland (www.invitrogen.com) and pDRAW32 1.0 of AcaClone software, USA (www.acaclone.com). Sequences were analyzed with Scanner software v1.0 of Life Technologies Corporation, Carlsbad, USA (www.appliedbiosystems.com). Agarose gel electrophoresis was performed in a Sub-Cell GT agarose gel electrophoresis system from Biorad, Reinach, Switzerland (www.bio-rad.com) and fluorescence imaging was performed with a Bio Vision 3026 from Vilber Lourmat, Eberhardzell, Germany (www.vilber.de). Cells were incubated in a Heraeus Function line incubator, Fisher Scientific, Wohlen, Switzerland (www.thermofisher.com) and for liquid cultures in the shaking incubator Innova 40, New Brunswick Scientific, Vaudaux-Eppendof AG, or in a Unitron incubator, Infors AG, Bottmingen, Switzerland (www.infors-ht.com). Cells were lysed with a Brandson Sonifier 250 from Branson Ultrasonics, Danbury, USA (www.emersonindustrial.com). Protein gel electrophoresis was performed with a Mini-Protean® 3 Cell gel electrophoresis system from Biorad.

FPLC runs were performed on an ÄKTA prime or an ÄKTA prime plus, GE Healthcare, Glattbrugg, Switzerland (www.gelifesiences.com) and analyzed with the Prime view 5.0 software. Affinity and size exclusion columns as GSTPrep FF 16/10, Hiload 16/60 Superdex 75 prep grade, Hiload 16/60 Superdex 200 prep grade, HiTrap desalting, and Superdex 75 10/300 GL for the automated FPLC system were purchased from GE Healthcare. Gravity flow column material for affinity chromatography as nickel loaded nitrilotriacetic acid agarose column was purchased from Qiagen AG, Hombrechtikon, Switzerland (www.qiagen.com).

Atomic absorption spectroscopy was measured with a Spectra AA240FS and AA110 atomic absorption spectrometer equipped with a UltraAA high intensity boosted hollow cathode lamp for the metals Ag, Cd, Pb, and Zn or for Co, Cu, Cr, Fe, Mn, and Ni, and the SpectraAA 5.1 Pro software, all from Agilent Technologies, Basel, Switzerland (www.agilent.com). Dynamic light scattering was recorded with a DynaPro Titan instrument and the corresponding software Dynamics, both from Wyatt Technology Corporation, Santa Barbara, USA (www.wyatt.com). Mass analysis was performed with a Q-TOF Ultima API mass spectrometer equipped with a MassLynx 4.1 software, both from Micromass, UK (www.micromass.co.uk) or an Autoflex mass spectrometer from Bruker Daltonic GmbH, Fällanden, Switzerland (www.bruker.ch). NMR spectra were recorded on a Bruker AV700 MHz spectrometer equipped with a TXI z-gradient CryoProbe®, on a Bruker AV600 MHz spectrometer equipped with a TCI z-gradient CryoProbe®, and on a Bruker AV500 MHz equipped with a BBI probehead and were analyzed with Topspin 3.0, all from Bruker Daltonic GmbH, Fällanden, Switzerland (www.bruker.ch).

Calculations and fittings were performed with Origin 7.0, OriginLab, Northampton, USA (www.originlab.com) or Microsoft Office Excel 2007, Microsoft, USA (www.microsoft.com).

6.2. Bacterial recombinant DNA techniques

6.2.1. General plasmid generation

DNA amplification was performed in a Mastercycler personal or a Thermocycler T1. PCR was performed with a three step protocol with 30 repeating cycles as described by the DNA polymerase supplier. A high-fidelity DNA polymerase, either Pfu Polymerase or Phusion Polymerase was used. The primers were designed with Vector NTI and were synthesized by Microsynth. DNA restriction-digest, dephosphorylation, and ligation was performed according to manufacturer of the enzyme. DNA purification was done by mini-kits or agarose gel extraction. Plasmid DNA was isolated using High pure plasmid isolation kit, PCR products were purified using Wizard SV Gel and PCR Clean-Up System. For the preparative separation of DNA fragments agarose gel electrophoresis was used and the excised fragments purified with Wizard SV Gel and PCR Clean-Up System. DNA sequence was verified by DNA sequencing performed by Microsynth. The resulting sequencing chromatograms were analyzed with the Sequence Scanner software and were aligned with the expected sequence using pDRAW32 and Vector NTI.

6.2.2. Plasmid generation for cicMT2

Primers used for PCR and generation of cicMT2 plasmids are listed in Tab. 2. Plasmids and their characteristics are listed in Tab. 3.

Tab. 2 Primers used for the cicMT2 constructs. Indicated sequences are in the direction 5' to 3'. Restriction sites are underlined.

Primer	DNA Sequence 5'-3'	Restriction site
TH001 cicMT2 F1-F	ATACATGGAGATATACATGGATCCTGCTGTGGCGGC	*Bam*HI
TH002 cicMT2 F1-R	AAAGCACCCGGGTTTGCAGGTGCACGGATTGCTGGT	*Xma*I, *Apa*LI
TH003 cicMT2 F2-F	ACCCCGTGCACCTGCAAAGGCCGTGGCTCTTGCTGTGGCGGCAATTG TGGGTGT	*Apa*LI
TH004 cicMT2 F2-R	ACCCTTCCCGGGGCCGCGGCCTTTGCAGGTACACGG	*Xma*I, *Sac*II
TH005 cicMT2 F3-F	GAAGGAGATATCCGCGGATCTTGCTGTGGG	*Sac*II
TH006 cicMT2 F3-R	CTTGGCCCCGGGTCATTATTTGCAGGTGCA	*Xma*I
TH016 cicMT2 GST/TEV-F	ATCTTAGTGTGGATCCGAGAACCTTTACTTCCAATCCTGCTGTGGCGG CAATTGTGCATGTCAA	*Bam*HI, *Mfe*I
TH017 cicMT2 GST/TEV-R	TTGACATGCACAATTGCCGCCACAGCAGGATTGGAAGTAAAGGTTCT CGGATCCACACTAAGAT	*Mfe*I, *Bam*HI

6.2.2.1. pG1xMT

Generation of an expression vector coding for a GST-tag followed by cicMT2 containing a thrombin cleavage site in between (Fig. 9 A).
The DNA coding sequence of the *C. arietinum* mt2 gene was amplified with primers introducing a *Bam*HI restriction site at the 5'-end (TH001 cicMT2 F1-F) and a *Xma*I restrictions site at the 3'-end (TH002 cicMT2 F1-R) with the pTYB2 cicMT2 plasmid as a template for PCR.[135] The resulting construct was cloned into the pGEX-4T-1 expression vector using the appropriate restriction enzymes. The construct identity of pG1xMT was subsequently verified by DNA sequencing.

6.2.2.2. pG3xMT

Generation of an expression vector coding for a GST-tag followed 3 times by the cicMT2 with in between a thrombin cleavage site (Fig. 9 B).
The DNA coding sequence of the *C. arietinum* mt2 gene was amplified with 3 different primer sets and pTYB2 cicMT2 plasmid as a template for PCR.[135] The first fragment introduced a *Bam*HI restriction site at the 5'-end (TH001 cicMT2 F1-F) and an *Apa*LI and an *Xma*I restrictions site at the 3'-end (TH002 cicMT2 F1-R). The second fragment introduced an *Apa*LI restriction site at the 5'-end (TH003 cicMT2 F2-F) and a *Sac*II and *Xma*I restrictions site at the 3'-end (TH004 cicMT2 F2-R). The third fragment introduced a *Sac*II restriction site at the 5'-end (TH005 cicMT2 F3-F) and an *Xma*I restrictions site at the 3'-end (TH006 cicMT2 F3-R). The resulting fragments were cleaved with the appropriate restriction enzymes and ligated to one insert (fragment 1 – fragment 2 – fragment 3). The insert was cloned into the pGEX-4T-1 expression vector using the appropriate restriction enzymes. The construct identity of pG3xMT was subsequently verified by DNA sequencing.

6.2.2.3. pGtMT

Generation of an expression vector coding for a GST-tag followed by the cicMT2 with featuring a TEV protease cleavage site in between (Fig. 9 C).
The additional TEV protease cleavage site was introduced into the pG1xMT by an additional fragment consisting of two complementary primers (TH016 cicMT2 GST/TEV-F and TH017 cicMT2 GST/TEV-R). Two restriction sites (upstream *Bam*HI, downstream *Mfe*I) allowed the introduction into the pG1xMT expression vector. The construct identity of pGtMT was subsequently verified by DNA sequencing.

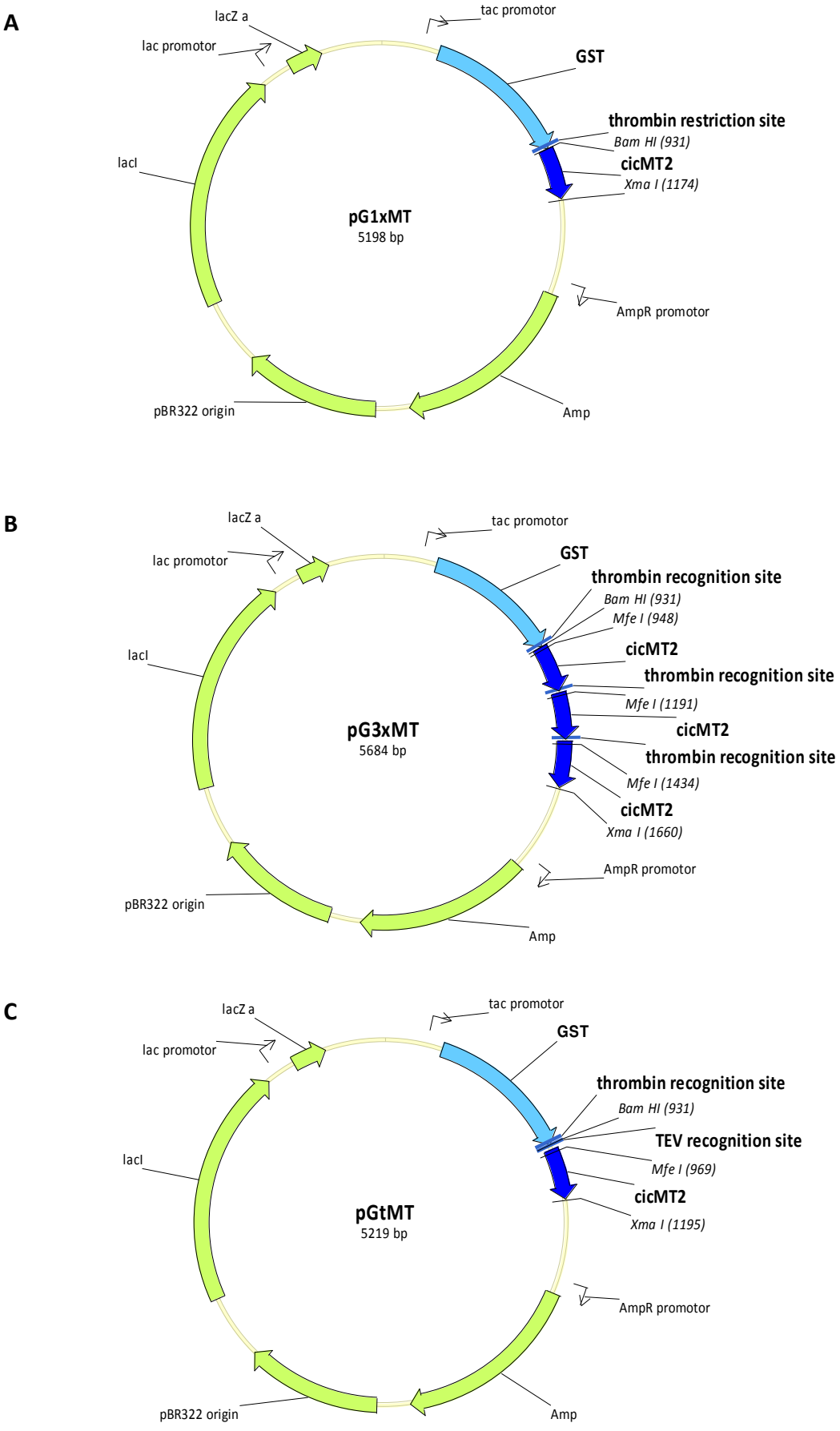

Fig. 9 Vector map of **(A)** pG1xMT, **(B)** pG3xMT, **(C)** pGtMT.

Tab. 3 cicMT2 constructs used in this work. The protein sequence of interest is highlighted in bold and italics, the rest are additional amino acids and accompanying tags. Underlined amino acids show the recognition sequences for the proteases thrombin and TEV, with the cleavage site indicated as ↓.

Plasmid	Encoded protein with	Encoded amino acid sequence	Inducibility, Resistance	Size	Origin
pTYB2 cicMT2	cicMT2-intein	***MSCCGGNCGCGSSCKCGSGCGGCKMYPDMSYTEQTTSETLVMGVASGKTQFEGAEMGFGAEN DGCKCGSNCTCNPCTCK***PG↓CFAKGTNVLMADGSIECIENIEVGNKVMGKDGRPREVIKLPRGRET MYSVVQKSQHRAHKSDSSREVPELLKFTCNATHELVVRTPRSVRRLSRTIKGVEYFEVITFEMGQKKA PDGRIVELVKEVSKSYPISEGPERANELVESYRKASNKAYFEWTIEARDLSLLGSHVRKATYQTYAPILY ENDHFFDYMQKSKFHLTIEGPKVLAYLLGLWIGDGLSDRATFSVDSRDTSLMERVTEYAEKLNLCAE YKDRKEPQVAKTVNLYSKVVRGNGIRNNLNTENPLWDAIVGLGFLKDGVKNIPSFLSTDNIGTRETFL AGLIDSDGYVTDEHGIKATIKTIHTSVRDGLVSLARSLGLVVSVNAEPAKVDMNVTKHKISYAIYMSG GDVLLNVLSKCAGSKKFRPAPAAAFARECRGFYFELQELKEDDYYGITLSDDSDHQFLLGSQVVVHA CGGLTGLNSGLTTNPGVSAWQVNTAYTAGQLVTYNGKTYKCLQPHTSLAGWEPSNVPALWQLQ	IPTG inducible, ampicillin resistance	whole expressed protein: 598 aa, 65.62 kDa cleaved construct: 81 aa, 8.10 kDa	[135]
pGEX T4-1	GST-thrombin		IPTG inducible, ampicillin resistance		GE Healthcare
pG1xMT	GST-thrombin-cicMT2	MSPILGYWKIKGLVQPTRLLLEYLEEKYEEHLYERDEGDKWRNKKFELGLEFPNLPYYIDGDVKLTQS MAIIRYIADKHNMLGGCPKERAEISMLEGAVLDIRYGVSRIAYSKDFETLKVDFLSKLPEMLKMFEDR LCHKTYLNGDHVTHPDFMLYDALDVVLYMDPMCLDAFPKLVCFKKRIEAIPQIDKYLKSSKYIAWPL QGWQATFGGGDHPPKSDLVPR↓G***SCCGGNCGCGSSCKCGSGCGGCKMYPDMSYTEQTTSETLV MGVASGKTQFEGAEMGFGAENDGCKCGSNCTCNPCTCK***	IPTG inducible, ampicillin resistance	whole expressed protein: 303 aa, 34.02 kDa cleaved construct: 79 aa, 7.87 kDa	this study
pG3xMT	GST-(thrombin-cicMT2)$_3$	MSPILGYWKIKGLVQPTRLLLEYLEEKYEEHLYERDEGDKWRNKKFELGLEFPNLPYYIDGDVKLTQS MAIIRYIADKHNMLGGCPKERAEISMLEGAVLDIRYGVSRIAYSKDFETLKVDFLSKLPEMLKMFEDR LCHKTYLNGDHVTHPDFMLYDALDVVLYMDPMCLDAFPKLVCFKKRIEAIPQIDKYLKSSKYIAWPL QGWQATFGGGDHPPKSDLVPR↓G***SCCGGNCGCGSSCKCGSGCGGCKMYPDMSYTEQTTSETLV MGVASGKTQFEGAEMGFGAENDGCKCGSNCTCNPCTCK***GR↓G***SCCGGNCGCGSSCKCGSGCGGCKMYPDMSYTEQTTSETLVMGVASGKTQFEGAEMGFGAENDGCKCGSNCTCNPCTCK***GR↓G***S CCGGNCGCGSSCKCGSGCGGCKMYPDMSYTEQTTSETLVMGVASGKTQFEGAEMGFGAENDG CKCGSNCTCNPCTCK***	IPTG inducible, ampicillin resistance	whole expressed protein: 465 aa, 50.14 kDa cleaved construct: 241 aa, 23.96 kDa ((cicMT2)$_3$), 81 aa, 8.09 kDa (1st, 2nd cicMT2), 79 aa, 7.87 kDa (3rd cicMT2)	this study
pGtMT	GST-thrombin-TEV-cicMT2	MSPILGYWKIKGLVQPTRLLLEYLEEKYEEHLYERDEGDKWRNKKFELGLEFPNLPYYIDGDVKLTQS MAIIRYIADKHNMLGGCPKERAEISMLEGAVLDIRYGVSRIAYSKDFETLKVDFLSKLPEMLKMFEDR LCHKTYLNGDHVTHPDFMLYDALDVVLYMDPMCLDAFPKLVCFKKRIEAIPQIDKYLKSSKYIAWPL QGWQATFGGGDHPPKSDLVPRGSENLYFQ↓***SCCGGNCGCGSSCKCGSGCGGCKMYPDMSYTEQ TTSETLVMGVASGKTQFEGAEMGFGAENDGCKCGSNCTCNPCTCK***	IPTG inducible, ampicillin resistance	whole expressed protein: 310 aa, 34.90 kDa cleaved construct: 78 aa, 7.82 kDa	this study
pRK793	His$_7$-TEV protease-Arg$_5$	HHHHHHH***GESLFKGPRDYNPISSTICHLTNESDGHTTSLYGIGFGPFIITNKHLFRRNNGTLLVQSLH GVFKVKNTTTLQQHLIDGRDMIIIRMPKDFPPFPQKLKFREPQREERICLVTTNFQTKSMSSMVSD TSCTFPSSDGIFWKHWIQTKDGQCGSPLVSTRDGFIVGIHSASNFTNTNNYFTSVPKNFMELLTNQ EAQQWVSGWRLNADSVLWGGHKVFMVKPEEPFQPVKEATQLMN***RRRRR	IPTG inducible, ampicillin resistance	whole expressed protein: 248 aa, 28.56 kDa	AddGene
pT7-7 NifS	NifS	***MADVYLDNNATTRVDDEIVQAMLPFFTEQFGNPSSLHSFGNQVGMALKKARQSVQKLLGAEHD SEILFTSCGTESDSTAILSALKAQPERKTVITTVVEHPAVLSLCDYLASEGYTVHKLPVDKKGRLDLEH YASLLTDDVAVVSVMWANNETGTLFPIEEMARLADDAGIMFHTDAVQAVGKVPIDLKNSSIHM LSLCGHKLHAPKGVGVLYLRRGTRFRPLLRGGHQERGRRAGTENAASIIGLGVAAERALQFMEHE NTEVNALRDKLEAGILAVVPHAFVTGDPDNRLPNTANIAFEYIEGEAILLLNKVGIAASSGSACTS GSLEPSHVMRAMDIPYTAAHGTVRFSLSRYTTEEEIDRVIREVPPIVAQLRNVSPYWSGNGPVED PGKAFAPVYG***

6.2.3. Plasmid generation for different plant MTs

Generation of yeast expression vectors coding for different plant MTs and a human MT2 for control (Fig. 10). Primers used are listed in Tab. 4, plasmids and their characteristics in Tab. 5.
The DNA coding sequences of the MTs were amplified with primers introducing *Bam*HI restriction sites on both ends with the corresponding pTYB2 vector as a template for PCR. The resulting construct was cloned into the pRS416 expression vector using the *Bam*HI restriction enzyme. The construct identity and its direction were subsequently verified by colony PCR and DNA sequencing.

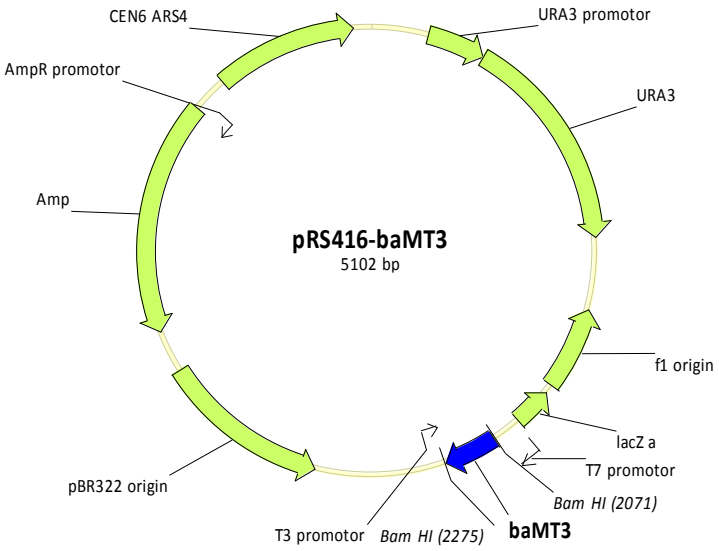

Fig. 10 Vector map of pRS416-baMT3 as an example for all the pRS416-MT vectors.

Tab. 4 Primers used for yeast plasmids. Indicated sequences are in the direction 5' to 3'. *Bam*HI restriction sites are underlined.

Primer	DNA Sequence 5'-3'	used for
EAP001 Sc_cicMT1_F	ATTCGCGGATCCATGTCTGGCTGCAACTGTGGC	PCR for pRS416-cpMT1
EAP003 Sc_cicMT2_F	ATTCGCGGATCCATGTCTTGCTGTGGCGGC	PCR for pRS416-cpMT2
EAP004 Sc_cicMT2_R	AATGCGGGATCCTCATTTGCAGGTGCACGGATTGC	PCR for pRS416-cpMT2
EAP005 Sc_musMT3_F	ATTCGCGGATCCATGTCGACCTGTGGCAACTGC	PCR for pRS416-baMT3
EAP006 Sc_musMT3_R	AATGCGGGATCCTCAGTTGCCACACTTGCAATCGGTG	PCR for pRS416-baMT3
EAP007 Sc_Ec-1_F	ATTCGCGGATCCATGGGCTGTGATGACAAGTGC	PCR for pRS416-E_c1, pRS416-γE_c1
EAP008 Sc_Ec-1_R	AATGCGGGATCCTCAGGCGGTCGCCGAGC	PCR for pRS416-E_c1, pRS416-βE_c1
EAP009 Sc_gEc-1_R	AATGCGGGATCCTCACCTCGCCGAGGTGCATC	PCR for pRS416-γE_c1
EAP010 Sc_bEc-1_F	ATTCGCGGATCCATGGGGGAACATACGACGTGTGGG	PCR for pRS416-βE_c1
EAP011 Sc_humMT2_F	ATTCGCGGATCCATGGATCCCAACTGCTCC	PCR for pRS416-huMT2
EAP012 Sc_humMT2_R	AATGCGGGATCCTCAGGCGC	PCR for pRS416-huMT2
TH018 Sc_cicMT1_R	AATGCGGGATCCTCATTTGCAGTTGCAAGGGTCACAGG	PCR for pRS416-cpMT1
TH012 Seq pRS416-F	CGACGGTATCGATAAGCT	colony PCR on pRS416
TH013 Seq pRS416-R	AGGGAACAAAAGCTGGA	colony PCR on pRS416

Tab. 5 Name of the template and constructed plasmids with the amino acid sequence of the encoded MT.

Constructed plasmid	Template plasmid	Amino acid sequence of encoded MT	length MT
pRS416-w/o	pRS416		
pRS416-cpMT1	pTYB2-cicMT1 [138]	MSGCNCGSSCNCGDQCKCNKRSGLSYVEAGETTETVVLGVGPTKIHF EGAEMSVAAEDGGCKCGSSCTCDPCNCK	75 aa
pRS416-cpMT2	pTYB2-cicMT2 [135]	MSCCGGNCGCGSSCKCGSGCGGCKMYPDMSYTEQTTSETLVMGV ASGKTQFEGAEMGFGAENDGCKCGSNCTCNPCTCK	79 aa
pRS416-E_c1	pTYB2-E_c-1 [57, 139]	MGCDDKCGCAVPCPGGTGCRCTSARSGAAAGEHTTCGCGEHCGCN PCACGREGTPSGRANRRANCSCGAACNCASCGSATA	81 aa
pRS416-βE_c1	pTYB2-β_E-E_c-1 [29]	MGEHTTCGCGEHCGCNPCACGREGTPSGRANRRANCSCGAACNCA SCGSATA	52 aa
pRS416-γE_c1	pTYB2-γ-E_c-1 [55]	MGCDDKCGCAVPCPGGTGCRCTSAR	25 aa
pRS416-baMT3	pTYB2-baMT3 [140]	MSTCGNCDCVDKSQCVKKGNSYGIDIVETEKSYVDEVIVAAEAAEHD GKCKCGAACACTDCKCGN	65 aa
pRS416-huMT2	pEThMT2 [141]	MDPNCSCAAGDSCTCAGSCKCKECKCTSCKKSCCSCCPVGCAKCAQ GCICKGASDKCSCCA	62 aa

6.2.4. Bacterial cell manipulation

E. coli DH5α was used as a host for cloning and propagation of plasmids. Protease deficient *E. coli* strains were used as an expression host, *E. coli* BL21(DE3) for cicMT2 and NifS, *E. coli* BL21(DE3)-RIL for TEV protease (Tab. 6).

Tab. 6 *E. coli* strains used in this work.

***E. coli* strains**	**Characteristics**	**Origin**
DH5α	genotype: *fhuA2 Δ(argF-lacZ)U169 phoA glnV44 Φ80 Δ(lacZ)M15 gyrA96 recA1 relA1 endA1 thi-1* deoR nupG *hsdR17* (r_K- m_K-), λ-	Life Technologies
BL21(DE3)	genotype : F- ompT gal dcm lon hsdSB(r_B- m_B-) λ(DE3 [lacI lacUV5-T7 gene 1 ind1 sam7 nin5]) deficient in lon and ompT proteases	Stratagene
BL21(DE3)-RIL	same as BL21(DE3) containing an additional plasmid encoding argU, ileY, and leuW (allows expression of genes encoding tRNAs for rare argenine, isoleucine and leucine codons) and a chloramphenicol resistance	Stratagene

Bacteria were grown aerobically in Luria-Bertani (LB) medium at 37 °C, either in liquid culture while shaking at 220 rpm or on 2 % agar plates. For plasmid maintenance, ampicillin was added to growth medium at concentrations of 100 μg mL^{-1}, for BL21(DE3)-RIL cells, 34 μg mL^{-1} chloramphenicol was added in addition. Cells were stored as glycerol stocks in 22 % glycerol, 50 % LB, 10 % ddH_2O at -80 °C.

For the preparation of chemically competent cells for plasmid transformations an overnight preculture was diluted 1:400 into fresh LB medium with appropriate antibiotics (final volume of 200 mL).[142] The cells were grown at 37 °C, 200 rpm to an OD_{600} of 0.5, cells were pelleted by gentle centrifugation at 830 x g and resuspended in 15 mL chilled TBF1 buffer (30 mM KOAc, 100 mM RbCl, 50 mM $MnCl_2$, 10 mM $CaCl_2$, pH 5.8) and incubated for 1 h on ice. Cells were again pelleted and resuspended in 4 mL TBF2 (10 mM MOPS, 10 mM RbCl, 75 mM $CaCl_2$, 15 % glycerol,

pH 7.0). Aliquots of 50 µL were flash-frozen in liquid nitrogen and stored at -80 °C. Competent cells were thawn on ice and mixed with 10 µL ligation mix or 1 µL purified vector. After 30 min incubation on ice, they were heat shocked for 45 s at 42 °C, cooled down on ice for 2 min and diluted with 250 µL LB medium. In the following they were incubated for 1 h at 37 °C while shaking followed by plating on agar plates with appropriate antibiotics. The transformants were grown at 37 °C overnight and tested for correct plasmid uptake by colony PCR.[143]

6.3. Eukaryotic DNA manipulation

In *S. cerevisiae*, yeast metallothioneins and metal ion transporter proteins (Tab. 7) were replaced by marker sequences. To complement the deleted proteins, plasmids coding for plant MTs were inserted and the mutated yeast cells where tested for metal resistance.

Tab. 7 *S. cerevisiae* genes of S288C strain deleted in the mutations.[144]

gene	function	protein sequence (of strain S288C)
cup1-1 (YHR053C) ***cup1-2*** (YHR055C)	Metallothionein, binds copper and mediates resistance to high concentrations of copper and cadmium. It is inducible by cooper.	MFSELINFQNEGHECQCQCGSCKNNEQCQKSCSCPTGCNSDDKC PCGNKSEETKKSCCSG(K)
crs5 (YOR031W)	Copper-binding metallothionein, required for wild-type copper resistance.	MTVKICDCEGECCKDSCHCGSTCLPSCSGGEKCKCDHSTGSPQCKS CGEKCKCETTCTCEKSKCNCEKC
zrc1 (YMR243C)	Vacuolar membrane zinc transporter, transports zinc from the cytosol into the vacuole for storage; also has a role in resistance to zinc shock resulting from a sudden influx of zinc into the cytoplasm.	MITGKELRIISLLTLDTVFFLLEITIGYMSHSLALIADSFHMLNDIISLLV ALWAVDVAKNRGPDAKYTYGWKRAEILGALINAVFLIALCFSIMIE ALQRLIEPQEIQNPRLVLYVGVAGLISNVVGLFLFHDHGSDSLHSHS HGSVESGNNDLDIESNATHSHSHASLPNDNLAIDEDAISSPGPSGQ IGEVLPQSVVNRLSNESQPLLNHDDHDHSHESKKPGHRSLNMHG VFLHVLGDALGNIGVIAAALFIWKTEYSWRYYSDPIVSLIITIIIFSSAL PLSRRASRILLQATPSTISADQIQREILAVPGVIAVHDFHVWNLTESI YIASIHVQIDCAPDKFMSSAKLIRKIFHQHGIHSATVQPEFVSGDVN EDIRRRFSIIAGGSPSSSQEAFDSHGNTEHGRKKRSPTAYGATTASS NCIVDDAVNCNTSNCL
cot1 (YOR316C)	Vacuolar transporter that mediates zinc transport into the vacuole; over expression confers resistance to cobalt and rhodium.	MKLGSKQVKIISLLLLDTVFFGIEITTGYLSHSLALIADSFHMLNDIISL VVALWAVNVAKNRNPDSTYTYGWKRAEILGALINAVFLIALCVSILI EALQRIIAPPVIENPKFVLYVGVAGLISNTVGLFLFHDNDQEHGHGH GHSHGGIFADHEMHMPSSHTHTHAHVDGIENTTPMDSTDNISEI MPNAIVDSFMNENTRLLTPENASKTPSYSTSSHTIASGGNYTEHNK RKRSLNMHGVFLHVLGDALGNIGVMLSAFFIWKTDYSWKYYTDPL VSLIITGIIFSSALPLSCKASKILLQATPSTLSGDQVEGDLLKIPGIIAIHD FHIWNLTESIFIASLHIQLDISPEQFTDLAKIVRSKLHRYGIHSATLQP EFITREVTSTERAGDSQGDHLQNDPLSLRPKTYGTGISGSTCLIDDA ANCNTADCLEDH

S. cerevisiae ZnWT (CM100) with the genotype *MATα, can1-100, his3-11, 15, leu2-3, 112, trp1-1, ura3-52* and *S. cerevisiae* Zn2MUT (CM137) with the genotype *MATα, can1-100, his3-11, 15, leu2-3, 112, trp1-1, ura3-52, Δzrc::HIS3, Δcot1::KAN^R* were used for testing the methods for the yeast complementation assays.[145] The strains were a kind gift of Peter Goldsbrough[92].
S. cerevisiae CUP1^S (DTY3) with the genotype *MATα, leu2-3, 112, his3Δ1, trp1-1, ura3-50, gal1, CUP1^S* containing a single copy of the *cup1* gene was used as a wild-type for the deletion mutants of yeast copper binding metallothioneins and zinc transporters (Tab. 7).[146] This strain was a kind gift of Sílvia Atrian.[133] In this yeast strain the iteration of *cup1* was replaced by a 5.2 kb fragment of genomic *cup1^S* DNA that includes the complete reiteration unit together with 0.8 kb of single-copy 5' flanking DNA and 2.4 kb of single-copy 3' flanking DNA (Fig. 11).

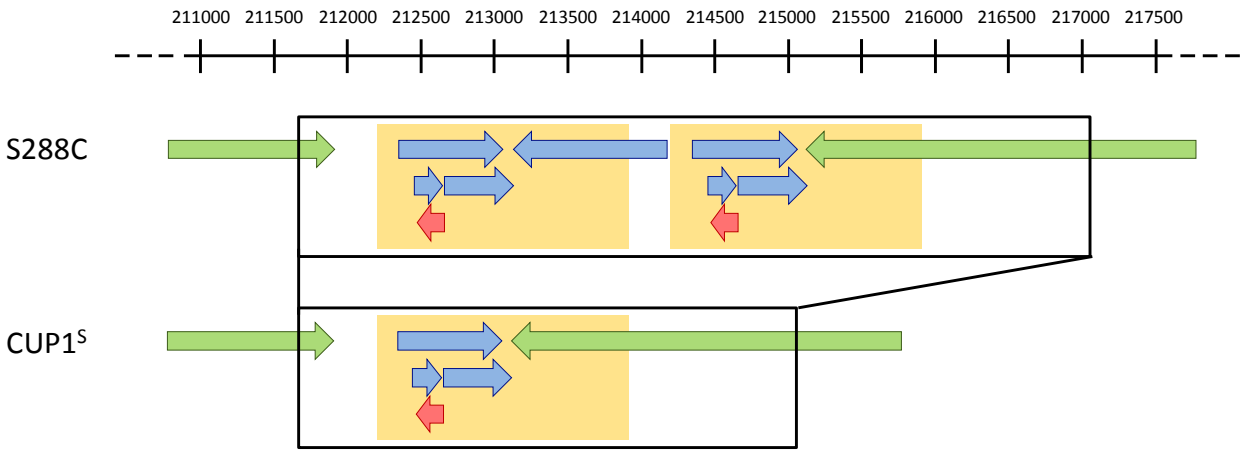

Fig. 11 Scheme of part of the chromosome VIII of the yeast strains *S. cerevisiae* S288C and CUP1^S. On top the region on the chromosome is indicated (numbering of S288C), green arrows show other essential proteins, blue arrows show other ORFs or replication origins, red arrows show the DNA coding for the protein Cup1, yellow highlighted parts the iteration units, and black squares the part with two iterations in S288C which was replaced in CUP1^S with only one iteration unit.

For cloning purposes it was assumed that the wild-type CUP1^S strain has an identical DNA sequence as the completely sequenced S288C strain in the yeast genome database.[144, 147] Two variations were expected: 1) the deletion of multiple copies of *cup1* replaced by one iteration unit; 2) the nonsense mutation (TAA) in codon nine of the *crs5* gene in S288C as an original glutamic acid (GAA).[144]

6.3.1. Growth of yeast cells

Yeast cells were grown aerobically at 30 °C, either in liquid culture while shaking at 250 rpm or on 2 % agar plates. The medium used was dependent on the strains. Wild-type CUP1^S and ZnWT cells were grown in rich medium YPD (1 % yeast extract, 2 % peptone, 2 % dextrose). Cells containing a newly introduced marker sequence were grown in selective media for selection of marker containing cells or maintaining of the plasmid. Strains with an antibiotic marker were grown in rich medium YPD supplemented with 200 µg mL^{-1} geneticin (G418). Strains with an auxotroph marker for histidine or uracil were grown in the minimal medium SD, either SD-His or SD-Ura. The composition of the SD medium was 0.67 % bacto yeast nitrogen base (YNB-AA), 2 % dextrose, 0.4 % adenine hemisulfate, 0.2 % L-arginine, 1 % L-aspartic acid, 1 % L-glutamic acid monosodium salt, 0.6 % L-leucine, 0.3 % L-lysine, 0.2 % L-methionine, 0.5 % L-phenylalanine, 3.75 % L-serine, 2.0 % L-threonine, 0.4 % L-tryptophan, 0.3 % tyrosine (dissolved in 30 mM NaOH), 1.5 % L-valine, and dependent on SD-His or SD-Ura 0.2 % uracil or 0.2 % L-histidine.
Cells were stored as glycerol stocks in 22 % glycerol, 50 % appropriate medium, 28 % ddH_2O at -80 °C.

6.3.2. Partial sequencing of genomic DNA

For sequencing of genomic *S. cerevisiae* DNA genomic DNA had to be purified and fragments for sequencing had to be amplified for the sequencing reaction.

6.3.2.1. Genomic DNA purification

Genomic DNA purification was done by ethanol precipitation.[148] *S. cerevisiae* was grown aerobically overnight in the appropriate medium at 30 °C in liquid culture (see 6.3.1) and 1.5 mL were harvested by centrifugation. Cells were washed twice with 0.5 mL water and supernatant was discarded. The pellet was resuspended in 0.2 mL TSENT (5 mM Tris-HCl, pH 8.0, 1 % Triton X-100, 0.5 % SDS, 0.5 mM EDTA, 50 mM NaCl) at 4 °C and approximately the same amount of glass beads (425-600 μm) were added. Thereon, 200 μL phenol-chloroform-isoamyl alcohol mixture (49.5:49.5:1) was added and the solution was vortexed for 2 min in a tightly closed tube. The phases were separated by centrifugation at 4 °C and to the upper aqueous phase were added 100 mM NaOAc and 65 % ethanol (final concentration). To precipitate the DNA the mixture was incubated for 15 min at -20 °C and the pellet was retrieved by centrifugation. The pellet was washed twice with 500 μL 70 % ethanol at 4 °C, dried for 1 h at room temperature, and resuspended in 50 μL water.

6.3.2.2. Amplification of fragment of genomic DNA and its sequencing

The fragment of genomic DNA, which was the target for sequencing had to be amplified first with PCR to obtain higher amounts of material. DNA amplification was performed in a Mastercycler personal or a Thermocycler T1. PCR was performed with a three times three step protocol with increasing annealing temperatures and decreasing annealing times. The rest was done as described by the Phusion polymerase supplier. The PCR primers were designed with Vector NTI and were synthesized by Microsynth (Tab. 8).

Tab. 8 Primers used for PCR reaction for sequencing of genomic DNA fragments.

Primer	DNA Sequence 5'-3'	used for
TH019 crs5 F	ATGCGAGAGGGCTGTGAA	sequencing crs5 gene, control HR crs5
TH020 crs5 control up	GTGACTGTTAAGGCGAATGTTG	sequencing crs5 gene, control HR crs5
TH021 crs5 control dn	CGTCCATCTTACCGAGCC	sequencing crs5 gene, control HR crs5
TH033 jo098 His F	CGATTTGGGATTAAAGCGTG	control HR crs5, zrc1
TH047 cup1 seq F	GAGGTACCACGTTGAATGTCCATTTGGG	sequencing cup1 gene, control HR cup1
TH048 cup1 seq Rw	GTCCTTCATTCTCAACGGTCGATCTTCC	sequencing cup1 gene, control HR cup1
TH052 crs5 up F	ACCAACATTATTTTAGTCCGACGTTCAG	control HR crs5
TH053 crs5 up R	GACATTGTAGTGTTCAGTGTAATATCGC	control HR crs5
TH054 crs down F	ACCCCTACTCTTTACTTATCATAAATACAT	control HR crs5
TH055 crs down R	CAAAATGTTTCAACACGACAGATAAAAC	control HR crs5

PCR products were separated by an agarose gel electrophoresis and the excised fragments were purified with the Wizard SV Gel and PCR Clean-Up System. In most cases, a consequent PCR had to be run with the previous PCR product as DNA template to yield sufficient amounts. The new

PCR product was purified directly using Wizard SV Gel and PCR Clean-Up System and the DNA sequence was verified by DNA sequencing. The resulting sequencing chromatograms were analyzed with the Sequence Scanner software and were aligned with the expected sequence using pDRAW32 and Vector NTI.

6.3.3. Homologous recombination

The deletion of DNA sequences of the target proteins was done by homologous recombination. To achieve this, a marker sequence flanked by homologous sequences up- and downstream of the target sequence was prepared by PCR and introduced by transformation into the *S. cerevisiae* cells. Once introduced into the cell, the homologous recombination of the marker and the target sequence was processed automatically by the cell.

6.3.3.1. Fragment generation for homologous recombination

Homologous sequences were designed 50 bp up- and downstream of the target protein and were connected to a 20 bp long sequence from the 5'-, and 3'-end of the marker sequence. The final 70 bp long primers were synthesized by Microsynth (Tab. 9) and were used for marker amplification. PCR was performed with a three times three step protocol with increasing annealing temperatures and decreasing annealing times. As templates were used plasmids coding for a histidine marker, pYM44, or a geneticin marker, pFA6a-kanMX6, both with an additional ampicillin resistance for amplification in *E. coli*.[149-151] PCR products were purified directly using Wizard SV Gel and PCR Clean-Up System.

Tab. 9 Primers used for production of fragments for homologous recombination.

Primer	DNA Sequence 5'-3'	used for
TH022 crs5D dn	TAAAATATGATGATGTATTTATGATAAGTAAAGAGTAGGGGTCACCTAATCGA TGAATTCGAGCTCG	Δcrs5 with His
TH023 crs5D up	GCGATATTACACTGAACACTACAATGTCAAATAGTACTCAATAAATATGCGTA CGCTGCAGGTCGAC	Δcrs5 with His
TH028 cup1D dn	CAGCAAATAGTTAGATGAATATATTAAAGACTATTCGTTTCAATCGATGAATT CGAGCTCG	Δcup1 with G418
TH029 cup1D up	GAAAAACAAACTGTACAATCAATCAATCAATCATCACATAAAATGCGTACGCT GCAGGTCGAC	Δcup1 with G418
TH035 HR zrc1 F	TTTCCCTATCGATATCCGTCAGGAATACCAGGAAACTAATAGAGTCATGCGTA CGCTGCAGGTCGAC	Δzrc1 with His
TH036 HR zrc1 R	CTTTATATCTTTATTACAGGCAATTGGAAGTATTGCAGTTTACAGCGTCAATCG ATGAATTCGAGCTCG	Δzrc1 with His
TH038 HR cot1 F	AGCTATAGAAAGAAAGTTAACACAAAGTACGGAAAGATTGAGTAAATATGCG TACGCTGCAGGTCGAC	Δcot1 with G418
TH039 HR cot1 R	TTTTTAAAAGTATTTAATTCTTCACGCTTTTTCGTTATAAAGTCCTTTTAATCGA TGAATTCGAGCTCG	Δcot1 with G418

6.3.3.2. Transformation for homologous recombination

The transformation of the fragments for homologous recombination was performed using the LiAc/SS carrier DNA/PEG method.[152] The appropriate medium was inoculated with yeast cells from a plate and cells were grown overnight at 30 °C, 250 rpm. Cells were harvested gently by centrifugation and the cell pellet was washed three times with water. For the transformation mixture, long single stranded salmon sperm DNA (SS-DNA) was denatured for 5 min at 95 °C. Transformation mix was prepared (36 % PEG 4000, 110 mM LiAc, 300 μg mL^{-1} denatured SS-DNA, 1.5-5 ng mL^{-1} DNA to be transformed) and the cell pellet was gently resuspended in transformation mix (1/3 of the initial cell culture volume). The cell solution was incubated at 42 °C for 40 min and 250 rpm agitation and cells were pelleted by centrifugation. The pellet was resuspended in water (1/4 of the initial cell culture volume) and plated on selective media plates. The transformants were grown at 30 °C for three days and were tested via genomic DNA sequencing (6.3.2).

6.3.4. Transformation of plasmid

The transformation of plasmids into *S. cerevisiae* was performed chemically.[153-154] YPD rich medium was inoculated with yeast cells from a plate and they were grown overnight at 30 °C, 250 rpm. The preculture was diluted to an OD_{600} of 0.3 in 8 mL fresh medium, and was grown to an OD_{600} of 0.6 at 30 °C and 250 rpm. Cells were harvested gently by centrifugation, the cell pellet was washed twice with water and finally resuspended in 100 μL ice cold 1x LiAc/TE buffer (10 mM Tris-HCl pH 7.5, 1 mM EDTA, 100 mM LiAc). For the transformation mix, single stranded herring sperm DNA (HS-DNA) was denatured for 10 min at 95 °C. The transformation mix (10 mM Tris-HCl pH 7.5, 1 mM EDTA, 40 % PEG 4000, 100 mM LiAc, 70 μg mL^{-1} denatured HS-DNA, 1.4 μg mL^{-1} DNA to be transformed) was prepared on ice and the cell pellet was resuspended in 710 μL transformation mix by vortexing. The cell solution was incubated at 30 °C for 30 min with 1200 rpm agitation and heat shocked for 15 min at 42 °C shaking at 1200 rpm in a thermomixer. Cells were pelleted by centrifugation, resuspended in 80 μL water and plated on selective media plates. The transformants were grown at 30 °C for three days and were tested for correct plasmid uptake by colony PCR.[143]

6.4. Protein expression and purification

6.4.1. cicMT2 purification

cicMT2 was over-expressed in the form of the glutathione *S*-transferase (GST)-MT fusion protein according to the GST purification manual.[155]

6.4.1.1. Protein expression and cell lysis

An overnight preculture of BL21(DE3) cells containing either pG1xMT, pG3xMT, or pGtMT was diluted 1:80 in fresh ampicillin supplemented (100 μg mL^{-1}) LB medium (final volume 800 mL). The cells were grown at 37 °C, 220 rpm until OD_{600} of 1.0 was reached. The expression of GST-cicMT2 was induced with 1 mM isopropyl-β-D-thiogalactopyranoside (IPTG) and the temperature changed to 30 °C. Cells were supplemented with each 100 μM $ZnCl_2$ 30 min and 1:30 h after induction and harvested after 6-8 h expression by centrifugation for 30 min at 8300 x g at 4 °C. Cells from 1.6 L cell culture were resuspended in 40 mL phosphate-buffered saline (PBS, 10 mM Na_2HPO_4, 1.8 mM KH_2PO_4, 140 mM NaCl, 2.7 mM KCl, pH 7.3), lysed by ultrasonication with a Brandson Sonifier 250 and cell debris was removed by centrifugation at 28'400 x g at 4 °C for 20 min.

6.4.1.2. GST affinity chromatography

Soluble cell lysate (supernatant after centrifugation) was filtered through a syringe filter MWCO 0.22 μM and loaded on a PBS equilibrated affinity column GSTPrep FF 16/10 connected to an automated FPLC system. After washing, the protein, which should be cleaved afterwards with thrombin protease, was additionally washed with 50 mM ethylenediaminetetraacetic acid (EDTA) in PBS to remove the metal ions and make the recognition sequence for the protease accessible. For cleavage with TEV protease, this additional step was not necessary. In the following the fusion protein was stripped from the column using 50 mM reduced glutathione dissolved in 10 mM Tris-HCl, 50 mM NaCl, pH 7.3 and the fractions with increased absorption at 254 nm were combined.

6.4.1.3. Thrombin cleavage of GST-thrombin-cicMT2 and GST-(thrombin-cicMT2)$_3$

Protein concentration of GST-thrombin-cicMT2 and GST-(thrombin-cicMT2)$_3$ eluted from the affinity chromatography was measured by absorption measurement at 280 nm with the corresponding extinction coefficient (for GST-thrombin-cicMT2 ε_{280} = 46'403 M^{-1} cm^{-1}, for GST-(thrombin-cicMT2)$_3$ ε_{280} = 50'141 M^{-1} cm^{-1}). The fusion protein was cleaved with 1 U thrombin protease per 30 nmol cicMT2 (per 1 mg GST-thrombin-cicMT2 or 1.5 mg GST-(thrombin-cicMT2)$_3$) for 36 h at 4 °C.

6.4.1.4. TEV cleavage of GST-thrombin-TEV-cicMT2

Protein concentration of GST-TEV-cicMT2 eluted from the affinity chromatography was determined by absorption measurement at 280 nm with the corresponding extinction coefficient (ε_{280} = 47'896 M^{-1} cm^{-1}) and was cleaved with 1 mg TEV protease per 40 mg of fusion protein for 12 h at 4 °C in presence of 0.5 mM EDTA and 1 mM dithiothreitol (DTT).[156]

6.4.1.5. Size exclusion chromatography (SEC)

Slightly precipitated and oxidized cleaved fusion protein was reduced for 1 h with 25 mM DTT at room temperature and concentrated with ultrafiltration using a regenerated cellulose filter (MWCO 1 kDa). Residual precipitate was removed by centrifugation and the supernatant was subjected to size exclusion chromatography to separate GST-tag and protease from cicMT2. Depending on the construct, the column was chosen. In general, for the GST-thrombin-cicMT2 and GST-thrombin-TEV-cicMT2 a Hiload 16/60 Superdex 75 prep grade column was used. The size exclusion column was run with 10 mM Tris-HCl, 50 mM NaCl, pH 7.3 connected to an automated FPLC system. The fractions of the second peak with increased absorption at 254 nm were combined (for Hiload 16/60 Superdex 75 prep grade column at around 70 mL). The protein was concentrated by ultrafiltration (1 kDa MWCO) and the oxidized cicMT2 was reduced with 100 mM DTT for 1 h at room temperature.

6.4.1.6. Zn_5/Cd_5-cicMT2 remetallation

Reduced protein of 6.4.1.5 was incubated with an excess of 5 equivalent $ZnCl_2$/$CdCl_2$ (total 10 equivalent) and incubated for 15 min. A final purification of Zn_5/Cd_5-cicMT2 was performed by size exclusion chromatography using a Hiload 16/60 Superdex 75 prep grade column in 10 mM Tris-HCl, 10 mM NaCl, pH 7.3. The fractions of the peak around 70 mL elution volume with increased absorption at 254 nm were combined.

6.4.1.7. apo-cicMT2 production

Reduced protein of 6.4.1.5 was acidified to pH 2.0 with 1 M HCl. The sample was applied under oxygen free conditions to a Hiload 16/60 Superdex 75 prep grade size exclusion column pre-equilibrated with 10 mM HCl to remove the metal ions. The fractions of the first peak at around 90 mL with increased absorption at 220 nm were combined.

6.4.1.8. Metal-sulfide-cicMT2 production

Apo-cicMT2 (6.4.1.7) or Zn_5-cicMT2 (6.4.1.6; for Cd^{2+}-, Ag^{+}-, and Cu^{+}-form) was used for reconstitution of a sulfide ion containing form. A solution of 20 μM Zn_5-cicMT2, 10 mM Tris-HCl pH 7.3, 10 mM NaCl, and 200 μM Na_2S was incubated 10 min before the addition of 200 μM $CdCl_2$. The sample was applied inside the anaerobic chamber to a HiTrap desalting column, equilibrated in the same buffer. The fractions with increased absorption at 220 nm were combined.

6.4.1.9. Metal-sulfide-cicMT2 production with the help of NifS

Zn_5-cicMT2 (6.4.1.6) was used for reconstitution of a sulfide ion containing form with the help of NifS.[157] A solution of 10 μM Zn_5-cicMT2, 10 mM Tris-HCl pH 7.3, 10 mM NaCl, 100 μM L-cysteine and 150 μg/μL NifS was incubated 5 min before the addition of 150 μM $CdCl_2$. After 2.5 h incubation an UV/Vis spectra was taken to detect incorporated CdS clusters in cicMT2 at 280 nm.

6.4.2. TEV protease purification

Tobacco etch virus (TEV) protease was over-expressed in the form of a fusion protein with a *N*-terminal His_7-tag and a *C*-terminal Arg_5-tag.[156] For a better survival of the host cells, the protease is expressed as maltose binding protein propeptide, which is cleaved already in the cells.

6.4.2.1. Expression and cell lysis

An overnight preculture of BL21(DE3)-RIL cells containing pRK793 was diluted 1:80 in fresh ampicillin supplemented (100 μg mL^{-1}) LB medium (final volume 800 mL). The cells were grown at 37 °C, 220 rpm until OD_{600} of 0.5 was reached. The expression of TEV protease was induced with 1 mM IPTG and the temperature changed to 30 °C. Cells were harvested after 4 h expression by centrifugation at 8300 x g at 4 °C. Cells from 1.6 L cell culture were resuspended in 40 mL 46.6 mM Na_2HPO_4, 3.4 mM NaH_2PO_4, 200 mM NaCl, 10 % glycerol, 25 mM imidazole, pH 8.0, lysed by ultrasonication with a Brandson Sonifier 250 and cell debris was removed by centrifugation at 28'400 x g at 4 °C.

6.4.2.2. Nickel affinity chromatography

Soluble cell lysate (supernatant) was filtered through a syringe filter MWCO 0.22 μM and loaded on a gravity flow nickel loaded nitrilotriacetic acid (NTA) agarose column, equilibrated in 46.6 mM Na_2HPO_4, 3.4 mM NaH_2PO_4, 200 mM NaCl, 10 % glycerol, 25 mM imidazole, pH 8.0. After washing, the TEV protease was stripped from the column by increasing the imidazole concentration to 500 mM. The protein concentration of the fractions was measured by Nanodrop 2000 at 280 nm with an extinction coefficient of ε_{280} = 31'970 M^{-1} cm^{-1} and fractions with high protein concentrations were combined.

6.4.2.3. Desalting chromatography

TEV protease was immediately applied to a 10 mL HiTrap desalting column connected to an automated FPLC system to prevent precipitation in high imidazole concentration. The column was equilibrated in 23.3 mM Na_2HPO_4, 1.7 mM NaH_2PO_4, 100 mM NaCl, 10 % glycerol, pH 8.0, and the sample was separated in 1.5 mL fractions to load to the column. Fractions with high absorption at 280 nm were combined. TEV protease concentration was determined by absorption measurement at 280 nm with an extinction coefficient of ε_{280} = 31'970 M^{-1} cm^{-1}. Aliquots were flash-frozen in liquid nitrogen and stored at -80 °C.

6.4.3. NifS purification

NifS was over-expressed without a tag and was purified via protein precipitation.[137, 158]

6.4.3.1. Expression and cell lysis

An overnight preculture of BL21(DE3) cells containing pT7-7 NifS was diluted 1:80 in fresh ampicillin supplemented (100 μg mL^{-1}) LB medium (final volume 800 mL). The cells were grown at 30 °C, 220 rpm until OD_{600} of 1.2 was reached. The expression of NifS was induced with 1 % lactose. Cells were harvested after 2 h expression by centrifugation at 8300 x g at 4 °C. In 25 mM Tris-HCl pH 7.4 were resuspended 1 g cells. Cell lysis was done by ultrasonication with a Brandson Sonifier 250 and cell debris was removed by centrifugation at 28'400 x g at 4 °C.

6.4.3.2. Nucleic acid precipitation by streptomycin sulfate

Soluble cell lysate (supernatant) was cooled down to 0 °C and powdered streptomycin sulfate were added to a final concentration of 1 % over 30 min while gently mixing. After another 15 min incubation the precipitate was removed by centrifugation at 28'400 x g at 4 °C.

6.4.3.3. Protein precipitation by ammonium sulfate

Supernatant was saturated to a final concentration of 25 % ammonium sulfate, added during 30 min at 0 °C while gently mixing.[159] The slightly cloudy solution was stirred for another 30 min and the precipitate was removed by centrifugation at 28'400 x g at 4 °C. To precipitate the NifS, 45 % ammonium sulfate was added to the supernatant and the solution was gently mixed for 15 min. Supernatant was removed by centrifugation at 28'400 x g at 4 °C. Pellet was dried and 50 mg protein was redissolved in 1 mL 25 mM Tris-HCl, pH 7.4. NifS concentration was determined by absorption measurement at 280 nm using an extinction coefficient of ε_{280} = 21'025 M^{-1} cm^{-1}. Aliquots were flash-frozen in liquid nitrogen and stored at -80 °C.

6.4.3.4. NifS activity test

For testing the activity of NifS the turnover rate of L-cysteine to sulfide ions was measured. A sample of 0.5 mM L-cysteine in 20 mM Tris-HCl, pH 8.0, 1 mM DTT was prepared in a N_2 purged glove-box, followed by the addition of 2 mg/mL NifS. The sample was incubated at room temperature for 2.5 h before measuring the amount of produced sulfide ions with the methylene blue assay.

6.4.4. Rabbit liver MT2A purification

Isolated rabbit liver MT2A was used for native analysis. The rabbit liver MT2A was isolated from its native source by the group of Prof. Milan Vašák (Institute of Inorganic Chemistry, University of Zurich, Switzerland).[87, 160]

For quantification of metal ions as well as potentially sulfide ions the isolated lyophilized protein was dissolved in 10 mM Tris-HCl, 10 mM NaCl, pH 8.3 and purified via size exclusion chromatography using a Hiload 16/60 Superdex 75 prep grade column.

For the reconstitution of the Zn^{2+}-form of rabbit liver MT2A the lyophilized protein was dissolved in 10 mM Tris-HCl, 10 mM NaCl, 10 mM DTT, pH 8.3 and incubated for 12 h to assure complete reduction of thiolate groups. Bound metal ions were removed by acidification of the protein solution to pH 2.0 with 1 M HCl and subsequent size exclusion chromatography applying a Hiload 16/60 Superdex 75 prep grade size exclusion column in 10 mM HCl in an anaerobic chamber followed. In a last step, 10 equivalents of $ZnCl_2$ were added to the apo-form, the pH was increased to pH 7.3 with NaOH and the protein was concentrated and free metal ions were removed via ultrafiltration (MWCO 1 kDa).

6.5. Protein titrations

6.5.1. Preparation of $[Cu(CH_3CN)_4]BF_4$

The synthesis of $[Cu(CH_3CN)_4]BF_4$ was done with 1 g $Cu(BF_4)_2$ and 2 g elemental Cu in 20 mL CH_3CN stirred for 3 h under reflux at 30 °C under nitrogen atmosphere.[161] The solution was filtrated and recrystallized from CH_3CN under nitrogen atmosphere at room temperature. The colorless crystalline product was stored under argon atmosphere.

6.5.2. Metal ion titration

Metal titrations were done either with apo-MT in case of Zn^{2+}, Cd^{2+}, Ag^+, or Cu^+ ion titrations or also Zn_5-MT for Cd^{2+}, Ag^+, or Cu^+ ion titration, both in the absence and presence of sulfide ions. Metal ions were added from 2 mM stocks, Zn^{2+} ions were added as $ZnCl_2$, Cd^{2+} ions as $CdCl_2$, Ag^+ ions as $AgNO_3$ and Cu^+ ions as $[Cu(CH_3CN)_4]BF_4$ in 4 % acetonitrile. The solutions were prepared in a N_2 purged glove-box and if not otherwise indicated, the titration was done with the following concentrations: 10 μM MT2, 10 mM Tris-HCl pH 7.3, 10 mM NaCl, and if desired 100 μM Na_2S. For Ag^+ ion titration, perchlorate was used as an anion (Tris-$HClO_4$ and $NaClO_4$).
Depending on the sequence of component addition, two different procedures were applied (6.5.2.1 and 6.5.2.2).

6.5.2.1. Standard metal ion titration with the order MT–(S^{2-})–metal ion

Standard metal titrations were done in one solution, where the metal ions were added as the last component. For each titration, 1.5 mL of 10 μM MT solution in 10 mM Tris-HCl, 10 mM NaCl, pH 7.3 was transferred into a septum-sealed cuvette with a path length of 1 cm inside an anaerobic chamber. If required 5-30 equivalents of S^{2-} were added in form of Na_2S and the protein solution was incubated for at least 10 min. The respective metal ion solution was filled into a Hamilton glass syringe, and the metal ion solution was added to the cuvette through the septum. Concentration changes due to dilution were negligible. UV, CD, and/or MCD spectra were recorded after each metal ion addition and incubation for approximately 2 min.

6.5.2.2. Metal ion titration with the order MT–Cd^{2+}–S^{2-} or Cd^{2+}–S^{2-}–MT

In case of an altered sequence of component addition, it was not possible to perform the experiments using a single solution, but rather a separate sample had to be prepared for each titration step. Each step was prepared as 120 μL sample buffered with 10 mM Tris-HCl, 10 mM NaCl, pH 7.3 in a N_2 purged anaerobic chamber.
For the order MT–Cd^{2+}–S^{2-}, 10 μM Zn_5-cicMT were mixed with the required equivalents of Cd^{2+} ions, incubated for 2 min and then 10 equivalent of S^{2-} ions were added, which are incubated for at least 10 min before the recording of the spectra.

For the order Cd^{2+}–S^{2-}–MT, 100 µM S^{2-} were mixed with the required equivalent of Cd^{2+}, incubated for at least 10 min and then 10 µM Zn_5-cicMT2 were added, which are incubated for 2 min before the recording of the spectra. The concentrations were stated as final concentrations in the 120 µL sample.

6.5.2.3. Sample purification

After titration, free metal ions and sulfide ions were removed by size exclusion chromatography using a Superdex 75 10/300 GL analytical column in 10 mM Tris-HCl, 10 mM NaCl, pH 7.3. The major peak around 13.5 mL corresponding to the monomeric protein species was collected and used for the determination of protein, metal ion and sulfide ion concentrations.

6.5.3. pH titration

cicMT2 used for pH titration was purified and loaded with metal ions or metal and sulfide ions. The pH was increased with NaOH to pH 8.5 and a UV/Vis spectrum was recorded. In the following, the samples were titrated with increments of diluted HCl solutions under a constant flow of argon. Subsequently to each acid addition, the pH value of the solution was measured and a UV/Vis spectrum recorded. Plots of molar absorptivity at the position of the ligand-to-metal charge transfer (LMCT) bands against pH were fitted with Origin 7.0 using equations derived as described (Eq. 1 and Eq. 2).[140]

$$\mathrm{A_{total}} = \frac{\mathrm{A_{MT}} + \mathrm{A_{MTH_m}} \cdot 10^{\mathrm{m(pK-pH)}}}{1 + 10^{\mathrm{m(pK-pH)}}}$$

Eq. 1 Equation used for curve fitting of pH titration data with one pK_a value. $\mathrm{A_{MT}}$ is the absorptivity of the fully metal ion loaded protein (maximum absorption), $\mathrm{A_{MTH_m}}$ denote the value obtained for apo-cicMT2 after acidification (minimum absorption), and m is a measure for the slope of the curves.

$$\mathrm{A_{total}} = \frac{0.5\ \mathrm{A_{MTH_m}} + \left(\mathrm{A_{MTH_{m+n}}} - 0.5\ \mathrm{A_{MTH_m}}\right) \cdot 10^{\mathrm{m(pK_1-pH)}}}{1 + 10^{\mathrm{m(pK_1-pH)}}}$$

$$+ \frac{\mathrm{A_{MT}} - 0.5\ \mathrm{A_{MTH_m}} + 0.5\ \mathrm{A_{MTH_m}} \cdot 10^{\mathrm{n(pK_2-pH)}}}{1 + 10^{\mathrm{n(pK_2-pH)}}}$$

Eq. 2 Equation used for curve fitting of pH titration data two pK_a values. $\mathbf{A_{MT}}$ is the absorptivity of the fully metal ion loaded protein (maximum absorption), $\mathbf{A_{MTH_{m+n}}}$ denote the value obtained for apo-cicMT2 after acidification (minimum absorption), $\mathbf{A_{MTH_m}}$ is the absorptivity of the protein species obtained after the first protonation step characterized by $\mathbf{pK_2}$, and $\mathbf{m}$ and $\mathbf{n}$ are a measure for the slope of the curves.

6.6. Yeast complementation assay

6.6.1. Metal sensitivity test

For metal sensitivity tests of different yeast strains, the respective growth media was inoculated with yeast cells from an agar plate and they were grown at 30 °C, 250 rpm overnight. Growth media for the liquid culture was YPD for strains lacking a plasmid or SD-Ura media for strains hosting a plasmid coding for a protein necessary for uracil synthesis. The metal sensitivity test was either done in liquid culture or on agar plates, both supplemented with different metal ions in different concentrations. In general, metal ion concentrations in liquid cultures were half the concentration on agar plates, because of the cation binding capacity of agar.

6.6.1.1. Metal sensitivity test with yeasts grown in liquid culture

To determine the metal sensitivity of different yeast strains in liquid culture, the optical density of the overnight cultures were adjusted to OD_{600} of 0.1-1.0 with fresh growth medium supplemented with metal salts. Used metal salts and concentrations were 0.1-10 μM $CdSO_4$, 1-50 μM $ZnSO_4$, 1-50 μM $CuSO_4$, 1-50 μM $Co(NO_3)_2$, or 1-50 μM $Ni(NO_3)_2$. The cultures were prepared, and 150 μL of each was placed in a 96 well flat bottom plate for UV/Vis spectra scanning by Microplate Spectrophotometer Power Wave XS2. The plate with the cell cultures was incubated at 30 °C with continuous shaking with 1140 rpm in the plate reader, and each 10 min a measurement was performed with rapid read speed OD_{600} from each well over a time period of 30-72 h.

6.6.1.2. Metal sensitivity test with yeasts grown on agar plates

To determine the metal sensitivity of different yeast strains growing as colonies on agar plates, the optical density of the overnight cultures were adjusted to OD_{600} of 0.001-1.0 with fresh growth medium. 2 μL each of the final sample was spotted on agar plates supplemented with metal salts with the following concentrations: 1-50 μM $CdSO_4$, 10-100 μM $ZnSO_4$, 10-100 μM $CuSO_4$, 10-100 μM $Co(NO_3)_2$, or 10-100 μM $Ni(NO_3)_2$. The plates were incubated at 30 °C for 72 h and colonies were counted every 12 h.

6.6.2. Metal accumulation test

Measurements of total cellular metal accumulation were performed by cell lysis followed by F-AAS.[162] Yeast cells were grown as described (6.6.1.1) for 30 h to an OD_{600} of 0.5-1.0 as 5 mL cultures. Cells were harvested by centrifugation for 5 min at 1000 x g and washed twice at 4 °C with 1 mM EDTA and once with water to remove surface-bound metal ions. Cells were digested overnight at 70 °C in 5 mL 15 % H_2O_2, 40 % HNO_3. Acid-digested samples were diluted with water, homogenized well, and metal content was measured using F-AAS.

6.7. Analytical methods

6.7.1. Quantification

6.7.1.1. Quantification of reduced proteins and sulfide ions via 2-PDS assay

Concentration of thiol groups of cysteine and sulfide ions bound to protein were assessed with 2,2'-dithiodipyridine (2-PDS) based on the specific absorption of the formed 2-thiopyridinone (Fig. 12).[163] A protein or sulfide solution with a thiol or sulfide ion concentration of 20-75 μM was added to 180 mM NaOAc, pH 4.0 and 100 μM 2-PDS. After incubation for 20 min at room temperature, absorption at 343 nm was measured. With the extinction coefficient of 2-thiopyridone (ε_{343} = 7600 M^{-1} cm^{-1}), the concentration was calculated. For protein concentration determination, all 14 cysteine residues of the protein were assumed to be present in the reduced state.

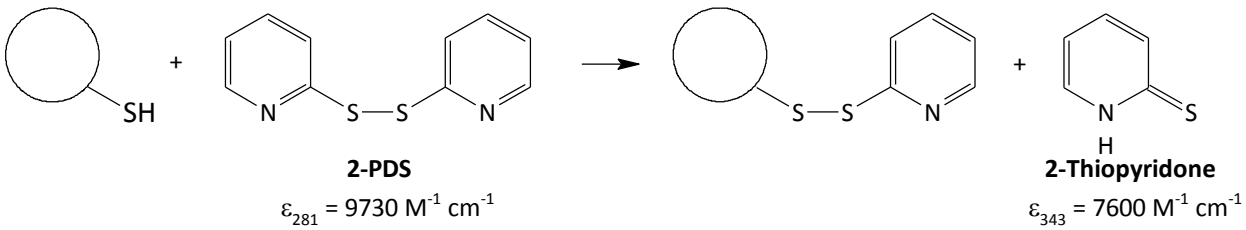

2-PDS
ε_{281} = 9730 M^{-1} cm^{-1}

2-Thiopyridone
ε_{343} = 7600 M^{-1} cm^{-1}

Fig. 12 Reaction scheme for 2-PDS assay.

6.7.1.2. Quantification of oxidized proteins via DTNB assay

The amount of oxidized protein was assessed by disulfide bond determination with 5,5'-dithiobis(2-nitro-benzoic acid) (DNTB) and sodium sulfite.[164-165] Three reactions take place in this assay (Fig. 13). 1) DNTB is reductively cleaved by sodium sulfite to 2-nitro-5-thiosulfo-benzoic acid (NTSB) and 2-nitro-5-thio-benzoic acid (NTB), NTB is reoxidized and converted again, 2) disulfide bonds are reduced by sodium sulfite, and 3) resulting thiol groups subsequently react with NTSB to NTB. For the first two reactions, 25 mM DTNB were dissolved in 1 M Na_2SO_3 at 38 °C and pH was adjusted to 7.5 with 1 M HCl. Solution was incubated in the dark at 38 °C for 45 min while sparging with air. The end of the reaction was followed via absorption measurement at 412 nm.

3) To measure the disulfide bridge concentration, a final assay mixture of ~4 μM protein, 500 μM NTSB, 100 mM Na_2SO_3, 3 mM EDTA, 2.6 M guanidinium thiocyanate, 200 mM Tris-HCl, pH 9.2 was prepared and reaction was developed in the dark for 25 min at room temperature. The specific absorption of the product NTB at 412 nm (ε_{412} = 13'600 M^{-1} cm^{-1}) was used for calculating the amount of oxidized protein. For each disulfide bond one molecule of NTB is produced.

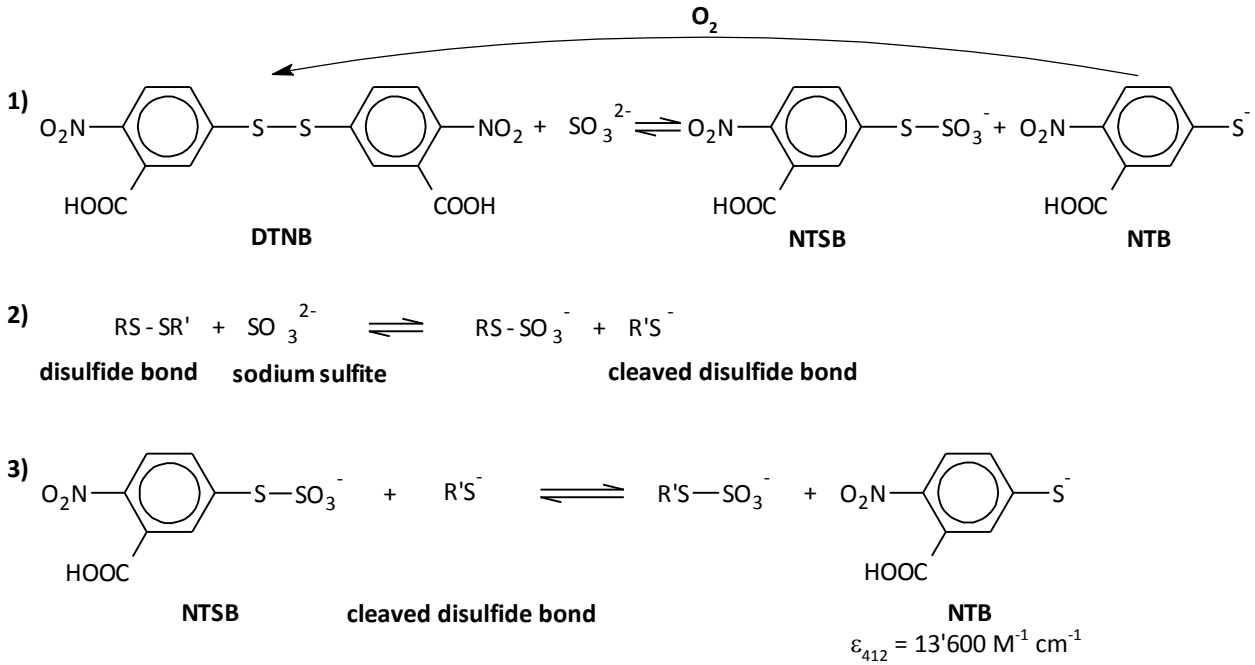

Fig. 13 Reaction scheme for DTNB assay.

6.7.1.3. Quantification of sulfide ions via methylene blue assay

Sulfide ions bound to the protein were quantified using the methylene blue assay (Fig. 14).[166] 15 µL of 20 mM *N*,*N*-dimethyl-*p*-phenylenediamine (DPD) in 7.2 M HCl was added to 150 µL of a solution containing a maximum concentration of 80 µM S^{2-} ions. 15 µL 30 mM $FeCl_2$ in 1.2 M HCl was added and vigorously mixed in the dark for 20 min. Concentrations were calculated with a standard curve of known Na_2S concentrations at the specific absorption of the formed methylene blue at 650 nm (ε_{650} = 19'000 M^{-1} cm^{-1}).

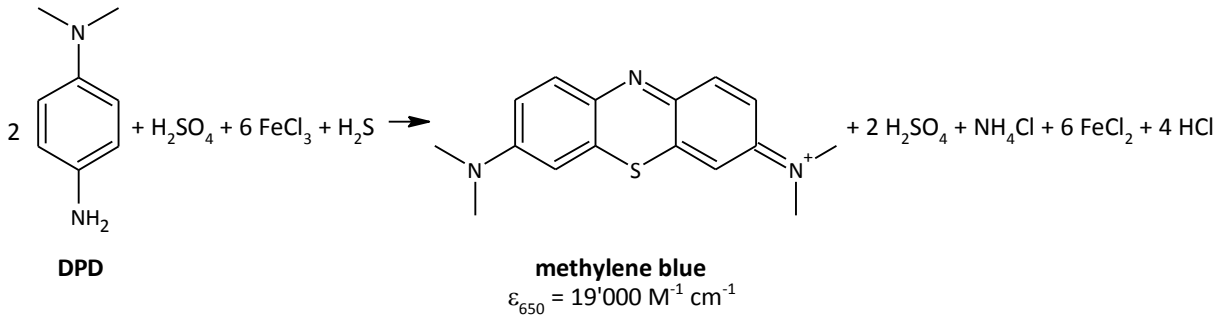

Fig. 14 Reaction scheme for methylene blue assay.

6.7.1.4. Quantification of sulfide ions via iodate assay

The concentration of the Na_2S solution was determined with a potassium iodate titration (Fig. 15).[167] KIO_3 was dried at 180 °C for 2 days and was dissolved in CO_2-free H_2O to an exact 10 mM solution. Solid KI was added in excess to a final concentration of 120 mM. The solution was acidified with 2 M HCl with a volume of approximately 25 times less than the final volume until the solution turned deep purple due to the stoichiometric formation of elemental iodine. To this solution an approximately 40 mM Na_2S solution was titrated until the transition to a light yellow color indicating consumption of all I_2. The exact S^{2-} ion concentration was calculated according to the reaction of I_2 with S^{2-} ions (Fig. 15).

$$6\ HCl + KIO_3 + 5\ KI \rightarrow 3\ I_2 + 3\ H_2O + 6\ KCl$$
$$S^{2-} + I_2 \rightarrow S + 2\ I^-$$

Fig. 15 Reaction scheme for iodate assay.

6.7.1.5. Quantification of metal ions via F-AAS

The metal ion concentration was analyzed with flame atomic absorption spectroscopy (F-AAS) using an AA240FS or an AA110 spectrometer equipped with a UltraAA high intensity boosted hollow cathode lamp for the metals Ag, Cd, Pb, and Zn or for the metals Co, Cu, Cr, Fe, Mn, and Ni. Standards were dissolved in 0.2 M HNO_3 for a lower background and were measured in a range of 0.1 – 1.0 ppm. Standards and samples were measured at least in triplicates.

6.7.2. UV/Vis, CD, MCD, and fluorescence spectroscopy

UV/Vis absorption spectra were recorded on a Cary 500 scan spectrophotometer using a scan speed of 600 nm min^{-1}. CD and MCD spectra were acquired with a J-810 spectropolarimeter equipped with a 1.5 T magnet over a spectral range of 180-500 nm with a scan speed of 50 nm min^{-1} and accumulation of four spectra. In general, cuvettes with a path length of 1 cm were used. For samples with a high ellipticity, rendering a to high voltage during measurement, a 1 mm path length cuvette was used for the range 180-300 nm and a 1 cm path length cuvette for 200-500 nm. The spectra were then merged based on the absorptivity at 250 nm. All spectra were recorded at room temperature. CD and MCD spectra were corrected with a FFT filter and are processed with Savitzky-Golay smoothing with a convolution width of nine.

In the UV/Vis spectra, the ligand-to-metal charge transfer bands were observed at the following wavelength: Zn^{2+}-thiolate at 230 nm, Zn^{2+}-sulfide at 260 nm, Cd^{2+}-thiolate at 250 nm, Cd^{2+}-sulfide at 280 nm, Ag^+-thiolate/sulfide at 251 nm, Cu^+-thiolate/sulfide at 255 nm.[41, 168-169]

Fluorescence spectra were recorded on a Cary Eclipse fluorescence spectrophotometer at room temperature. The scan rate was 600 nm/min, the slit width 5 nm. Excitation wavelengths were used between 200 nm and 500 nm, emission was measured depending on the excitation wavelength.

6.7.3. SDS-PAGE modified with mBBr

Analytical protein separation was performed under denaturing conditions with a Tris-based 14 % poly-acrylamide gel.[170] For correct estimation of the protein size with a protein marker, the thiols of the MTs had to be labeled with monobromobimane (mBBr). The protein solution containing not more than 2 mM cysteine SH groups was incubated with 4 mM mBBr at neutral pH for 30 min in the dark yielding the fluorescent mB-thioether (mBSR, Fig. 16).

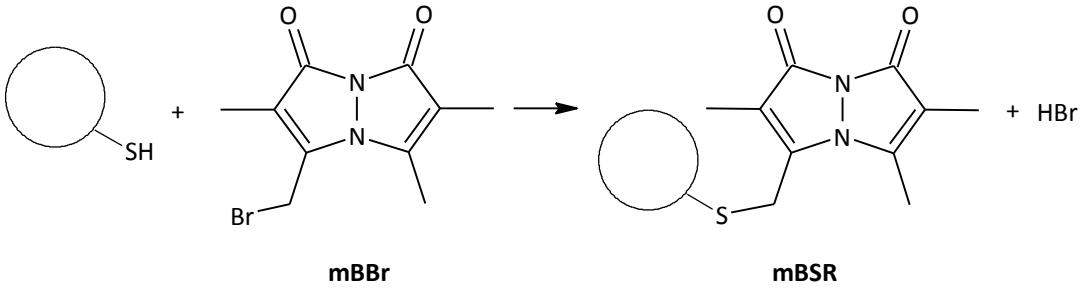

Fig. 16 Reaction scheme for fluorescence labeling with mBBr.

After modification, the protein solution was treated with Lämmli buffer and used for gel electrophoresis.[170] After this, unreacted mBBr was removed by incubation of the gel with 50 % methanol for 30 min. Fluorescence imaging of the mBBr labeled proteins was performed with a Bio Vision 3026 equipped with an EtBr filter. For staining the gels, standard procedures were chosen, either coomassie brilliant blue G 250 staining for GST containing proteins or silver staining for non-tagged MTs.[171-172]

6.7.4. Mass spectrometry

6.7.4.1. Electrospray ionization mass spectrometry (ESI-MS)

For ESI-MS analysis, the samples were either diluted with 0.2 % formic acid in 50 % acetonitrile (pH 2.5) or 5 mM ammonium acetate in 50 % methanol (pH 7.5). Samples containing salts were desalted prior to the analysis using C18 Zip Tips. Nano ESI-MS analysis of the samples was performed on a Q-TOF Ultima API mass spectrometer and the data were recorded with the MassLynx 4.1 software. The solutions were infused through a fused silica capillary (ID75μm) at a flow rate of 0.5 μL min^{-1} and sprayed through a PicoTips (ID30μm). Mass spectra were acquired in the positive-ion mode by scanning an m/z range from 600 to 3000 Da with a scan duration of 1 s and an interscan delay of 0.1 s. The spray voltage was set to 2.1 kV, the cone voltage to 50 V, the RF lens 1 energy to 50 V, and the collision to 10. The recorded m/z data were then deconvolved by applying the maximum entropy algorithm MaxEnt1 (MaxLynx).

6.7.4.2. Matrix-assisted laser desorption/ionization mass spectrometry (MALDI-MS)

MALDI-MS analysis was performed on an Autoflex mass spectrometer equipped with a nitrogen laser (337 nm). In order to keep the pH at 7-8, a solution of 2,4,6-trihydroxyacetophenone and ammonium citrate in 50 % acetonitrile (both 10 mg/μL, pH 7.5) was used as MALDI matrix. The sample solution was premixed on a steel target plate with the matrix and left to air-dry. The analysis was then performed in the positive-ion linear mode and the ions were accelerated at 20 kV with pulsed ion extraction time 300 ns.

6.7.5. Hydrodynamic radius measurement

Hydrodynamic radius of the protein was measured with diffusion ordered spectroscopy (DOSY) NMR and dynamic light scattering (DLS). Apo-cicMT2 was measured directly in 10 mM HCl pH 2.0, metal ion loaded protein used for both methods was reconstituted as ~100 μM cicMT2 in 5 mM d_{11}-Tris-HCl pH 7.9 and 95 % D_2O, protein measured only with DLS was reconstituted as 30 μM cicMT2 in 10 mM Tris-HCl pH 7.5, 10 mM NaCl. To remove the original buffer, the samples were washed via ultrafiltration (1 kDa MWCO) and the stoichiometry was verified by spectroscopic methods. Large particles were removed by filtering with a 0.2 μM Amicon filter and centrifugation for at least 30 min before measuring.

6.7.5.1. Diffusion ordered spectroscopy (DOSY) NMR

DOSY ^{1}H-NMR spectra were recorded on a Bruker AV700MHz spectrometer in 5-mm Shigemi NMR tubes with 300 μL sample volume.[173] Spectra were measured at 293 K with the standard Bruker plusprogram ledbpgp2s_es, which applies stimulated echoes using bipolar gradient pulses for diffusion. The diffusion time, the gradient length and the recovery delay after gradient pulses were set on 350 ms, 2 ms, 200 μs respectively, while the gradient strength was incremented from 14.4 to 45.3 G/cm in 60-82 steps. Hydrodynamic radius was calculated with the Stokes-Einstein equation for a spherical particle (Eq. 3).

$$r_H = \frac{k_B \cdot T}{6 \cdot \pi \cdot D \cdot \eta}$$

Eq. 3 Stokes-Einstein equation for the hydrodynamic radius r_H, with the Boltzmann constant k_B with $1.381 \cdot 10^{-23}$ N m K^{-1}, the temperature T with 293 K, and the dynamic viscosity η of the solvent with $1.247 \cdot 10^{-3}$ N s m^{-2} for 10 % D_2O, 90 % H_2O at 293 K, and D for the measured diffusion coefficient.

6.7.5.2. Dynamic light scattering (DLS)

DLS analysis was performed with a 20 μL protein solution using 10 acquisitions with 5-10 s acquisition time each, a laser power of 20-100 % and a temperature of 293 K. Each sample was measured at least five times. A DynaPro Titan instrument was used, the molecular weight of the

protein was calculated from the hydrodynamic radius based on a model for globular proteins implemented in the Dynamics software.

6.7.6. NMR spectroscopy

6.7.6.1. Proton NMR spectroscopy with cicMT2

To elucidate the structure of cicMT2 numerous samples of cicMT2 (oxidized apo-cicMT2, Zn_5-cicMT2, and Cd_5-cicMT2) were prepared starting either from the apo- or the Zn_5-form as described (6.4.1.6-6.4.1.8) as well as samples of GST-tagged cicMT2. Samples of GST-Zn_5-cicMT2 and GST-Cd_5-cicMT2 were purified with affinity chromatography and the partially oxidized protein was reduced with 200 mM DTT. The samples were then diluted with 10 mM Tris-HCl pH 7.5, 10 mM NaCl and were re-concentrated with ultrafiltration (5 kDa MWCO) to remove the reducing agent. At a GST-cicMT2 concentration of 10 μM, the protein was reconstituted with a slight excess of Zn^{2+} or Cd^{2+} ions added in form of 100 mM $ZnCl_2$ or $CdCl_2$. After reconstitution of the isolated or the fusion protein, the buffer was exchanged either by dialysis or ultrafiltration (for isolated cicMT2 with 1 kDa MWCO, for GST-cicMT2 with 5 kDa MWCO). The sample was concentrated by lyophilization or ultrafiltration to a final sample concentration of 50-200 μM for the single cicMT2 and 1-2 mM for the GST-tagged cicMT2 in 1-80 mM d_{11}-Tris-HCl pH 7.3-8.6, 0-50 mM NaCl, 90 % H_2O/10 % D_2O.

NMR spectra were recorded on a Bruker AV700 MHz spectrometer equipped with a TXI z-gradient CryoProbe® or on a Bruker AV600 MHz spectrometer equipped with a TCI z-gradient CryoProbe®. Samples were measured in 5-mm Shigemi NMR tubes with 300 μL sample volume. Simple 1D ^{1}H spectra were acquired to quickly check whether or not the samples were good enough for further investigations by NMR spectroscopy. If the samples showed relatively sharp proton resonances 2D ^{1}H-^{1}H TOCSY (mixing time of 100 ms) and 2D ^{1}H-^{1}H NOESY experiments (mixing time of 250 ms) at various temperatures (293-310 K) were recorded to allow the assignment of the proton resonances. All experiments were recorded with presaturation water suppression and the proton resonances were referenced to sodium 2,2-dimethyl-2-silapentane-5-sulfonate.

6.7.6.2. ^{1}H and ^{113}Cd NMR spectroscopy with rabbit liver MT2A

To analyze the metal-sulfide-thiolate cluster of the rabbit liver MT2A upon incorporation of sulfide ions ^{113}Cd NMR spectroscopy experiments were recorded on a Bruker DRX500 MHz spectrometer equipped with a BBI probehead in 5-mm Shigemi NMR tubes with 300 μL sample volume. $Cd_{6.7}$-MT2A and $Cd_{8.4}S_{3.0}$-MT2A were prepared with $^{113}CdCl_2$ as described (6.4.4) followed by buffer exchange accomplished either by dialysis or ultrafiltration (both 1 kDa MWCO). The final sample concentration was 500 μM MT2A in 20 mM d_{11}-Tris-HCl pH 7.0, 50 mM KCl, 90 % H_2O/10 % D_2O.[160] 2D ^{1}H-^{113}Cd HSQC NMR spectroscopy experiments were recorded with a coupling constant of 50 Hz and presaturation water suppression at 298 K. All ^{113}Cd chemical shifts were referenced to 0.1 M $Cd(ClO_4)_2$.

7. Results and Discussion

7.1. Production of cicMT2

For structural analysis of cicMT2 and the experiments for sulfide incorporation into cicMT2, it was desired to obtain a protein without tag and in a completely reduced state. The purification should be straight forward and preferably fast and inexpensive. Therefore different constructs and methods were used to optimize the purification procedure used before, which yielded rather low amount of cicMT2 with rather long purification times.[135]

7.1.1. Cloning of cicMT2

cicMT2 was previously expressed in the IMPACT^{TM}-CN system with low yield of purified protein (1-2 mg per L of cell culture). Therefore the DNA sequence of cicMT2, which was already previously optimized for *E. coli* codon usage, was inserted into a vector for its expression as a soluble GST fusion protein. Different constructs were tested to optimize the yield.

The plasmid pG1xMT encodes a cicMT2 construct with an *N*-terminal GST-tag and a thrombin cleavage site resulting in a GST-thrombin-cicMT2 fusion protein. This is a standard construct to produce a GST fusion protein. In the case of cicMT2, the target protein makes up only one fourth of the size of the entire fusion protein. To overcome this difference and to further increase the target protein yield, the plasmid pG3xMT was cloned. This fusion protein also consists of an *N*-terminal GST-tag and a thrombin cleavage site between the tag and cicMT2. However, two additional thrombin-cicMT2 sequences were inserted resulting in a GST-(thrombin-cicMT2)$_3$ construct. Mentionable is the slightly different DNA and amino acid sequence for the thrombin cleavage site directly after the GST and between the cicMT2 units. In the third construct, pGtMT, an additional TEV protease cleavage site was introduced into the pG1xMT vector between the thrombin cleavage site and the cicMT2 sequence giving GST-thrombin-TEV-cicMT2. The advantage of using TEV cleavage sites is that cicMT2 can be obtained with its native *N*-terminal residue. In addition, purification costs can be reduced as TEV protease can be rather easily over-expressed and purified in the lab.

The three constructs were transformed into chemically competent cells of the protease deficient expression host *E. coli* BL21(DE3) and the correctness was analyzed by DNA sequencing.

7.1.2. Expression of cicMT2

As a first step, the recombinant expression of the three different plasmids (pG1xMT, pG3xMT, and pGtMT) in *E. coli* BL21(DE3) was optimized by varying the cell density at the induction point, the expression time, the expression temperature, and different supplementation of the growth media with metal ions and sulfur.

Over-expression of the fusion proteins was analyzed with SDS-PAGE. The size of the fusion protein was estimated with a protein marker, and the intensity of the fusion protein bands was compared by eye, assuming equal protein material load in all gel chambers.

By comparing the yield of fusion protein at different induction points (OD_{600} of 0.4, 0.8, and 1.2) for all three constructs the one with the highest OD showed the most intense band at the size of the fusion protein. But comparing the intensities at OD_{600} of 0.8 and 1.2, not only the band at the size of the fusion protein was increased, but also the ones of other proteins. The ratio between fusion protein and other proteins was much more in favor at induction at OD_{600} of 0.8. To get a high amount of fusion protein and a low amount of other proteins, the middle value was chosen as an optimum (OD_{600} of 1.0).

The expression duration was tested for 0 h, 2 h, 4 h, 6 h, 8 h, and 20 h. For all three constructs the intensity of the band for the fusion protein increased with time. The increase was in the beginning larger than between 8 h and 20 h. The ratio between the fusion protein and the other proteins was higher for 8 h than for 20 h. Therefore, 8 h was chosen as optimal expression time.

Tested expression temperatures were 30 °C as standard expression temperature and 37 °C as optimal growth temperature of *E. coli*. Also here, the result for all plasmids showed the same picture. Decreasing the temperature to 30 °C after induction showed a much more pronounced band for the fusion protein, whereas keeping the temperature constant at 37 °C showed in general an increased expression of also the other proteins. Therefore, 30 °C was chosen as optimal expression temperature.

The desired proteins are cysteine-rich, and the production of cysteine is highly energy consuming for cells.[174] Additionally, MTs need metal ions to fold into their specific structure. To prevent aggregates and inclusion bodies, metal ions should be present for folding MTs after translation. Therefore, the bacterial cells were grown in Zn^{2+} ion and sulfur supplemented medium. Tested components were $ZnCl_2$, $ZnSO_4$, and L-cysteine, all in different concentrations (100 μM to 1000 μM final concentration in the growth media) and combinations. It turned out for all constructs, that sulfur supplementation ($ZnSO_4$ and L-cysteine) did not make a difference in the expression. Also Zn^{2+} supplementation played a minor role in increasing the intensity of the bands for the fusion protein. The slight increase of the intensity of the bands of the fusion protein detected with $ZnCl_2$ or $ZnSO_4$ supplemented media (200 μM Zn^{2+} compared to 0 μM) was still in the error range of the method. The chosen optimum was only supplementation with Zn^{2+} in the form of 200 μM $ZnCl_2$.

To summarize for all 3 constructs the same standard conditions for further expressions were chosen. These were induction at a cell density of OD_{600} = 1.0, an expression time of 8 h, an expression temperature of 30 °C, and a supplementation with 200 μM $ZnCl_2$.

The comparison of the cell growth of cells containing GST-thrombin-cicMT2, GST-(thrombin-cicMT2)$_3$, or GST-thrombin-TEV-cicMT2 at the same standard expression conditions showed a similar cell growth after expression up to OD_{600} = 5, yielding around 6 g cells per liter cell culture, except for the construct GST-(thrombin-cicMT2)$_3$, where a 20 % lower yield was achieved (Tab. 10). Also the previously used IMPACT^{TM}-CN system showed a yield in this range (Tab. 10).

7.1.3. Purification of cicMT2

The main optimization step of the purification of the three constructs (GST-thrombin-cicMT2, GST-(thrombin-cicMT2)$_3$, or GST-thrombin-TEV-cicMT2) was the cleavage procedure either with thrombin or TEV protease. Overall, the purification can be divided into four steps: first capture of the fusion protein with GST affinity chromatography, second the cleavage of the GST-tag with protease, third size exclusion chromatography to remove the cleaved tag, and fourth the reconstitution to a metal loaded or metal free, reduced, monomeric cicMT2 via another size exclusion chromatography step.

7.1.3.1. Purifying GST-thrombin-cicMT2 construct from pG1xMT

For the purification of the construct GST-thrombin-cicMT2 different procedures were tested for the affinity chromatography, the cleavage of the GST-tag and the polishing step with size exclusion chromatography. The proteolytic cleavage was performed when the fusion protein was bound to the GST column or with the fusion protein in solution and size exclusion chromatography was performed with columns of different separation ranges.

7.1.3.1.1. On-column and batch cleavage with thrombin

Cleared cell extract after cell lysis was applied to the GST column to capture the GST-thrombin-cicMT2 fusion protein from the cell lysate. Depending on the cleavage mode of the protease, different procedures are tested. To cleave the GST-tag from cicMT2 with thrombin protease, the bound protein was washed with EDTA to unfold cicMT2 by removing the Zn^{2+} ions. This step was crucial to allow the thrombin protease getting access to the protease recognition sequence. After an additional washing step, the uncleaved fusion protein was either eluted with reduced GSH for later batch cleavage or thrombin protease was applied to cleave the protein on the column.
For batch-mode cleavage, the concentration of the fusion protein was determined via its absorptivity at 280 nm. The yield was around 150 mg fusion protein of 1 L cell culture. The thrombin was added and incubated with 1 U thrombin per 1 mg fusion protein as described. To separate the monomeric cicMT2 from the uncleaved GST-thrombin-cicMT2, the cleaved GST-thrombin-tag, and the thrombin protease, size exclusion chromatography with a Hiload 16/60 Superdex 75 prep grade column was performed (Fig. 17 dashed line). For comparison, also an uncleaved sample was applied to the size exclusion column (Fig. 17 solid line). Apparently most of the fusion protein was cleaved, only a small shoulder originating from GST-thrombin-cicMT2 remained. The cleavage efficiency of the GST-MT constructs was also followed by a Coomassie stained SDS-PAGE (Fig. 18). On the stained gel, the shift of the bands caused by cleavage was clearly visible. The band of GST-thrombin-cicMT2 (34.0 kDa) in the uncleaved sample shifted in the cleaved sample to the size of GST-thrombin (28.2 kDa). Finally, the amount of eluted monomeric cicMT2 was determined by 2-PDS and DTNB assay and showed a yield of ~20 mg cicMT2 per L of cell culture.

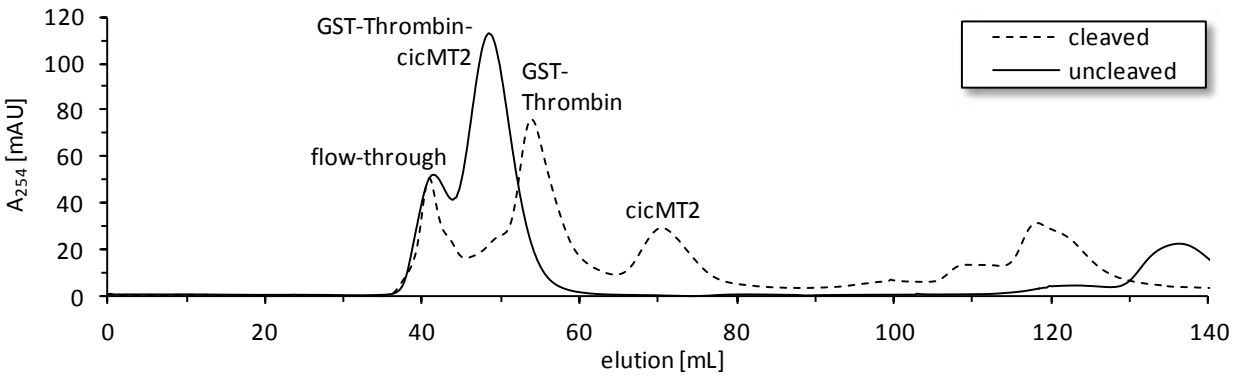

Fig. 17 Elution profiles of size exclusion runs with Hiload 16/60 Superdex 75 prep grade column of cleaved (dashed line) and uncleaved (solid line) GST-thrombin-cicMT2 (from 50 mL cell culture). Peak at 48 mL originates from GST-thrombin-cicMT2, peak at 54 mL from GST-thrombin, and peak at 71 mL from cicMT2.

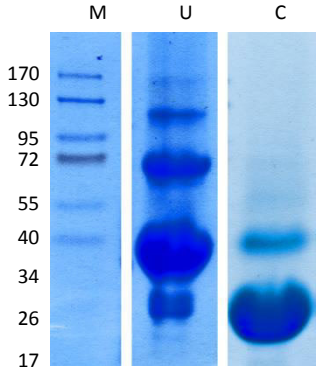

Fig. 18 Coomassie stained SDS-PAGE. First row (M) shows the protein marker with indicated protein size on the left size in kDa, middle row (U) shows the uncleaved GST-thrombin-cicMT2, and right row (C) shows the cleaved GST-thrombin-cicMT2. GST-thrombin-cicMT2 has a size of 34.0 kDa, GST-thrombin has a size of 28.2 kDa, and cicMT2 has a size of 7.9 kDa. The cicMT2 is not visible on the coomassie stained gel.

For on-column cleavage, the amount of the bound protein on the GST affinity column was assumed to be 150 mg per 1 L cell culture and thrombin was added in the same ratio as for batch cleavage (1 U thrombin per 1 mg fusion protein), dissolved in 20 mL buffer (equivalent to one column volume). Incubation with thrombin was performed for the same amount of time as for the batch cleavage, i.e. 36 h, and cleaved cicMT2 as well as thrombin were washed from the column with buffer and were collected. Uncleaved fusion protein and the cleaved GST-tag were later eluted with reduced GSH to clean the column and check the cleavage efficiency. Both samples, eluted with buffer and with reduced GSH, were applied consecutively to a Hiload 16/60 Superdex 200 prep grade size exclusion column (Fig. 19.). The elution profile of the buffer eluted sample shows a pronounced peak at 95 mL for the monomeric cicMT2. Compared to cleavage performed in batch-mode, on-column cleavage was approximately 50 % less efficient. The sample eluted with reduced GSH shows two major peaks at 74 mL for uncleaved GST-thrombin-cicMT2 and at 85 mL for cleaved GST-thrombin. The peak for uncleaved GST-thrombin-cicMT2 is even higher than the one for the cleaved tag, indicating a large amount of uncleaved fusion protein remaining on the column after cleavage. Therefore, the amount of thrombin was doubled to achieve higher cleavage rates, resulting in a 30 % lower GST-thrombin-cicMT2 peak after eluting with reduced GSH. The efficiency could not be remarkably increased by even higher thrombin

concentration taking also into account the high costs for twice the amount of protease. The amount of eluted monomeric cicMT2 was determined by 2-PDS and DTNB assay and showed a yield of ~10 mg monomeric cicMT2 when the same amount of thrombin was used as in batch mode cleavage.

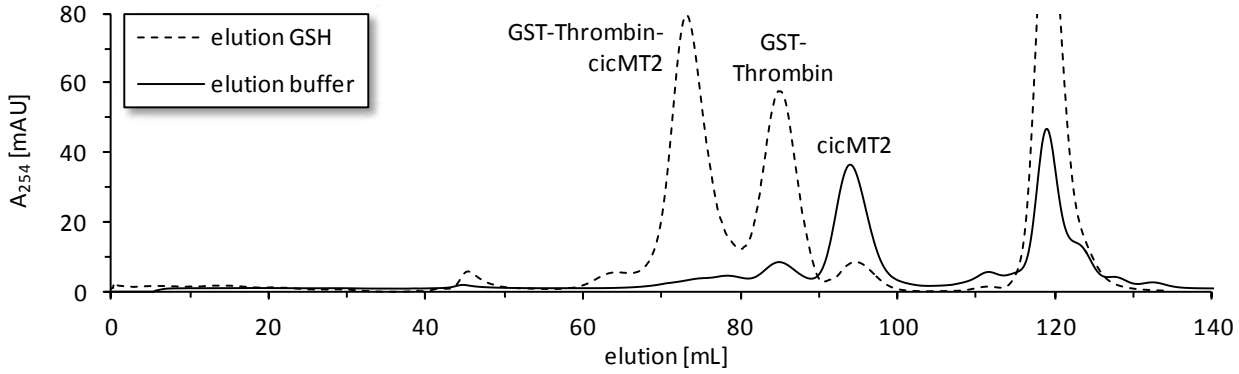

Fig. 19 Elution profiles of size exclusion runs with Hiload 16/60 Superdex 200 prep grade column of on-column cleaved GST-thrombin-cicMT2 (from 150 mL cell culture) directly after elution from GST affinity chromatography column. The solid line represents absorption profile of sample eluted with buffer from the affinity column, the dashed line represents absorption profile of GST-bound proteins eluted with reduced GSH after elution of cicMT2 with buffer. The peak at 74 mL originated from GST-thrombin-cicMT2, the peak at 85 mL from GST-thrombin, and the peak at 95 mL from cicMT2.

By comparing the efficiency of on-column and batch-mode cleavage, the batch-mode cleavage yielded twice the amount of monomeric cicMT2 after cleavage with the same amount of thrombin protease. Also with a higher concentration of thrombin protease, the on-column cleaved sample could not reach the yield of the sample cleaved in batch-mode. The advantage of fusion-protein cleavage and separation of the GST-tag in a single step via on-column cleavage was negligible compared to the lower yield and hence only batch-mode cleavage was used for protein production.

7.1.3.1.2. Polishing step of the monomeric cicMT2 with size exclusion columns

For the final polishing step in order to separate the uncleaved GST-thrombin-cicMT2, the GST-thrombin, and the cicMT2, a size exclusion chromatography step was performed. To evaluate for the most efficient separation, three different Hiload 16/60 Superdex prep grade size exclusion columns were compared. The Superdex 30 with a separation range of <10 kDa, Superdex 75 with a separation range of 3-70 kDa, and Superdex 200 with a separation range of 10-600 kDa. The elution profiles are shown in Fig. 20.

The elution profile of Superdex 30 shows a GST-thrombin peak at 45.0 mL and a monomeric cicMT2 peak at 52.6 mL. The elution profile of Superdex 75 shows a GST-thrombin peak at 53.9 mL and a monomeric cicMT2 peak at 70.6 mL. And the elution profile of Superdex 200 showed a GST-thrombin peak at 82.9 mL and a monomeric cicMT2 peak at 94.1 mL. As expected, the smaller the separation range of the used column, the smaller the elution volume of GST-thrombin and cicMT2. The difference in elution volume of the two peaks was largest with the Superdex 75 column, with a difference of 16.7 mL (Superdex 30 = 7.6 mL, Superdex 200 = 11.2 mL). The

Superdex 75 column shows the best separation results, what was also expected for proteins of the size 28.2 kDa (GST-thrombin) and 7.9 kDa (monomeric cicMT2). For all further separations of GST-thrombin and monomeric cicMT2 the Hiload 16/60 Superdex 75 prep grade column was used.

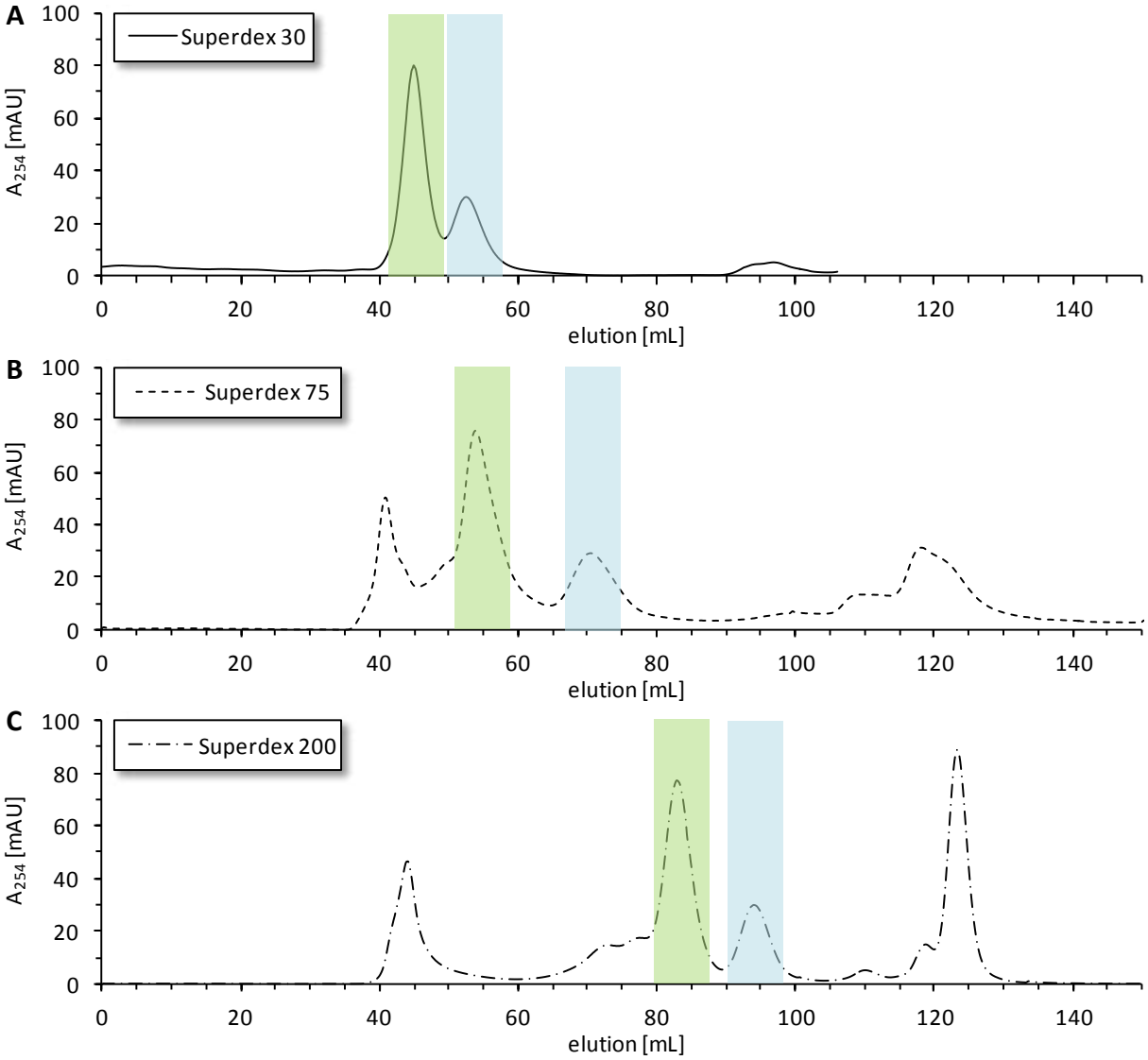

Fig. 20 Elution profiles of size exclusion runs after batch-mode cleavage of GST-thrombin-cicMT2 (from 150 mL cell culture) after cleavage with thrombin to separate GST-thrombin-cicMT2 (34.0 kDa), GST-thrombin (28.2 kDa, indicated with green square) and cicMT2 (7.9 kDa, indicated with blue square). **(A)** Hiload 16/60 Superdex 30 prep grade column with a separation range of <10 kDa, **(B)** Hiload 16/60 Superdex 75 prep grade column with a separation range of 3-70 kDa, and **(C)** Hiload 16/60 Superdex 200 prep grade column with a separation range of 10-600 kDa.

For the purification of cicMT2 starting from the construct GST-thrombin-cicMT2 different procedures were tested. The cleavage procedure with on- and off-column cleavage had a large impact, but also the final separation of the monomeric cicMT2 with size exclusion chromatography. The highest yields were found using off-column cleavage and subsequent separation of GST-thrombin and monomeric cicMT2 with the Hiload 16/60 Superdex 75 prep grade size exclusion column.

7.1.3.2. Purifying GST-(thrombin-cicMT2)$_3$ construct from pG3xMT

An increased yield of monomeric cicMT2 was expected to result from the GST-(thrombin-cicMT2)$_3$ construct because of a higher ratio of cicMT2 to GST-tag. The construct with three attached cicMT2 to one GST-tag was purified mainly in the same way as GST-thrombin-cicMT2. The cleared cell lysate was applied to the GST column and after washing with EDTA the fusion protein was eluted with reduced GSH. The protein concentration was determined via absorption measurement with the corresponding extinction coefficient. The yield was around 100 mg fusion protein per 1 L cell culture.

The thrombin protease was added and incubated as described. To separate the monomeric cicMT2, a size exclusion run with Hiload 16/60 Superdex 75 prep grade column was run, and for comparison, also uncleaved fusion protein was applied (Fig. 21).

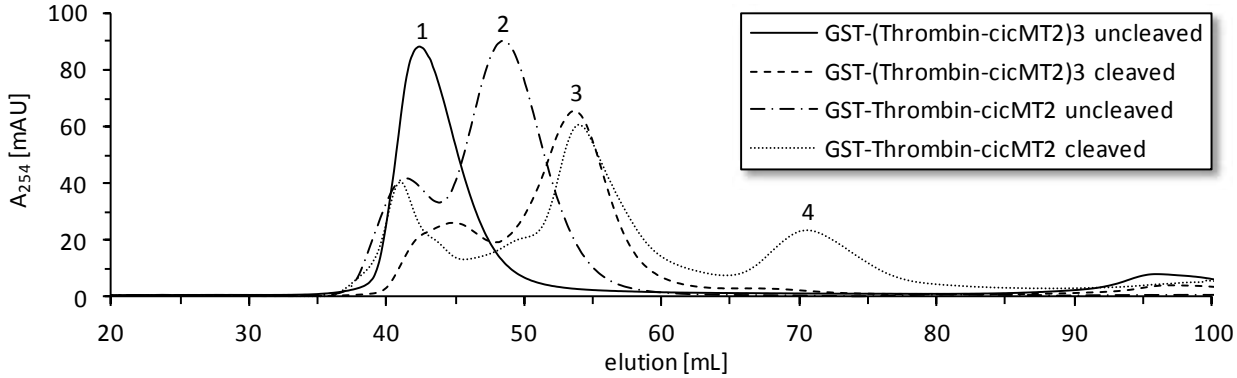

Fig. 21 Elution profiles of size exclusion runs with Hiload 16/60 Superdex 75 prep grade column of uncleaved (solid line) and cleaved (dashed line) GST-(thrombin-cicMT2)$_3$ (from 40 mL cell culture). For comparison also uncleaved (dashed dotted line) and cleaved (dotted line) GST-thrombin-cicMT2 were plotted. Peak at 42 mL (1) originates from GST-(thrombin-cicMT2)$_3$, peak at 48 mL (2) from GST-thrombin-cicMT2, peak at 54 mL (3) from GST-thrombin and cicMT2-thrombin-cicMT2-thrombin-cicMT2 (trimer), and peak at 71 mL (4) from cicMT2 (monomer).

The uncleaved sample shows a peak (1) at 42 mL elution volume. The flow-through and the GST-(thrombin-cicMT2)$_3$ were not separated with this column and eluted together. The cleaved sample showed two peaks, one at 45 mL and one at 54 mL (3) and no peak at 71 mL (4). As known from the construct GST-thrombin-cicMT2, GST-thrombin elutes at 54 mL with a size of 28.2 kDa. The GST-thrombin of the construct with three attached cicMT2 has the same size.

Unfortunately, if the protease only cleaves off the GST-tag, and the trimer cicMT2-thrombin-cicMT2-thrombin-cicMT2 stays intact, the trimer and the GST-tag show with 24.0 kDa (trimer) and 28.2 kDa (GST-tag) nearly the same size and accordingly coelute. It can hence be followed that only the first thrombin cleavage site was recognized and cleaved by the thrombin and the ones between the cicMT2 stretches not. There could be two reasons for this: First, the recognition sequence of the first and the two followings were slightly different (1st Leu-Val-Pro-Arg-↓-Gly, 2nd and 3rd Cys-Lys-Gly-Arg-↓-Gly), and might not be recognized with the same efficiency. Second, the tight packing of the cicMT2 might not give access to the recognition sequences. To overcome the

cleavage problem, different attempts were made and the cleavage efficiency was tested by size exclusion chromatography and SDS-PAGE.

1) To enhance the accessibility of the recognition sequence for the thrombin protease, the GST column bound fusion protein was washed longer with EDTA to release the metal ions and was also washed with 100 mM DTT to reduce formed disulfide bonds between the cysteines. After this treatment the cicMT2 stretches should be mainly in an unfolded form, however, no cleavage resulting in monomeric cicMT2 species was observed.

2) In another attempt to cleave the GST-(thrombin-cicMT2)$_3$ construct, the concentration of the thrombin protease was increased four times, but still no monomeric species was obtained. To increase the activity of thrombin a number of different additives were added to the cleavage solution, i.e. 0.01 % SDS, 1 M urea, 10 % glycerol, 2.5 mM $CaCl_2$, 0.1 mM EDTA pH 8.0, 10 mM DTT, and 200 mM imidazole. 0.01 % SDS, 1 M urea, and 10 mM DTT inhibited even thrombin cleavage of the first site in GST-(thrombin-cicMT2)$_3$, while 10 % glycerol and 200 mM imidazole had no influence. 2.5 mM $CaCl_2$ and 0.1 mM EDTA pH 8.0 increased the efficiency of cleavage of the first thrombin recognition sequence. In conclusion, additive addition had no effect on the cleavage rate of the 2nd and 3rd recognition sequence.

Due to the difficulties encountered with proteolytic cleavage, no further purification was performed with the construct GST-(thrombin-cicMT2)$_3$.

7.1.3.3. Purifying GST-thrombin-TEV-cicMT2 construct from pGtMT

To obtain cicMT2 with its native *N*-terminal amino acid residue as well as to enhance the efficiency of the cleavage between the GST-tag and the cicMT2 sequence, a TEV protease cleavage site was introduced between GST-thrombin and cicMT2. The construct GST-thrombin-TEV-cicMT2 was purified mainly in the same way as GST-thrombin-cicMT2 (7.1.3.1). The cleared cell lysate was applied to the GST column and was directly eluted with reduced GSH without washing with EDTA. The protein concentration was determined via absorption measurement with the corresponding extinction coefficient. The yield was around 150 mg fusion protein of 1 L cell culture, what is the same amount as for the GST-thrombin-cicMT2 construct.

The TEV protease was added, i.e. 1 mg TEV per 40 mg fusion protein, and incubation was performed as described. To separate the monomeric cicMT2, size exclusion chromatography with Hiload 16/60 Superdex 75 prep grade column was used. The elution profile of the cleaved protein was nearly identical with the one from GST-thrombin-cicMT2, but the shoulder for the uncleaved fusion protein was even lower. The amount of eluted monomeric cicMT2 was determined by 2-PDS assay and showed a yield of ~23 mg cicMT2, what was in the range of the one cleaved with thrombin (20 mg cicMT2).

7.1.3.4. Preparation of apo-cicMT2 and reconstitution to Zn_5-cicMT2

For the experiments with Cd^{2+}, Ag^{+}, and Cu^{+} ions a completely reduced and Zn^{2+} metallated cicMT2 form is required, for the experiments with Zn^{2+} ions a completely reduced apo-cicMT2 is needed. For apo-cicMT2, the monomeric cicMT2 form obtained from size exclusion chromatography after proteolytic cleavage was incubated with DTT, the pH was decreased to pH 2, and separation from released metal ions was achieved with size exclusion chromatography at pH 2 using a Hiload 16/60 Superdex 75 prep grade column under strictly anaerobic conditions. The monomeric apo-cicMT2 was collected and the protein and metal concentration measured with 2-PDS assay and F-AAS, respectively. For the thrombin cleaved construct (GST-thrombin-cicMT2) a yield of 4.2 mg apo-cicMT2 was obtained, while the TEV cleaved construct (GST-thrombin-TEV-cicMT2) gave a much higher yield of 18 mg apo-cicMT2.

For Zn_5-cicMT2, the monomeric cicMT2 obtained from size exclusion column was incubated with DTT, then six equivalents of Zn^{2+} ions in form of $ZnCl_2$ to form Zn_5-cicMT2 were added, and a size exclusion run with the Hiload 16/60 Superdex 75 prep grade column was performed under strictly anaerobic conditions. The monomeric Zn_5-cicMT2 was collected, and the stoichiometry was proven by measuring the protein concentration with 2-PDS assay, and the metal concentration with F-AAS. In this way, a Zn-form harboring 4.6 to 5.3 Zn^{2+} ions was obtained. Starting from GST-thrombin-cicMT2, average yields of 3.9 mg Zn_5-cicMT2 per liter cell culture were achieved, starting from GST-thrombin-TEV-cicMT2, average yields of 15 mg Zn_5-cicMT2 per liter cell culture were obtained. The higher yield of the construct GST-thrombin-TEV-cicMT2 might be due to the metal release with EDTA in the construct GST-thrombin-cicMT2 causing aggregation and precipitation of the unfolded protein.

7.1.3.5. Comparison of the three GST-cicMT2 constructs

Different attempts were conducted to increase the yield of cicMT2 and to reduce the time used for protein purification. To achieve this, different new constructs expressing cicMT2 as GST-tagged fusion proteins were cloned starting from the previously used pTYB2 IMPACT^{TM}-CN system. Three variants were constructed: 1) A construct with a *N*-terminal GST-tag and a thrombin cleavage site between the tag and cicMT2; 2) same construct as in 1) but with three cicMT2 sequences in a row separated by thrombin cleavage sites; 3) the same construct as in 1) but with an additional TEV cleavage site between the thrombin site and cicMT2. The target protein was purified with all the four systems, and the outcome was compared with respect to its advantages and drawbacks (Tab. 10).

Using the pTYB2 vector from the IMPACT^{TM}-CN system is an easy and straight forward method to obtain a protein completely reduced and metal-loaded. It is convenient concerning costs and handling as no protease is required to remove the self-cleavable intein-tag. However, the major drawback is the rather low protein yield of 1-2 mg per 1 L cell culture. Also the purification time was enormous (9.5 working days) involving also some time consuming methods for protein concentration and desalting, i.e. lyophilization and dialysis. The construct GST-(thrombin-cicMT2)$_3$ obtained from pG3xMT yielded higher amounts of fusion protein, but it was only

possible to cleave off the GST-tag and not the tri-repeat (cicMT2)$_3$ monomers. Therefore it was not suitable for the production of cicMT2. Expression and purification of cicMT2 from pG1xMT was relatively fast (5.5 working days) and the yield was increased (3.9 mg per 1 L cell culture) compared to the one obtained with the pTYB2 system, but the purification was expensive because of the thrombin protease. Production of cicMT2 from the pGtMT vector was slightly faster (5 working days, including TEV purification time), the yield was significantly higher (15 mg per 1 L cell culture), and the process was considerably less costly due to usage of recombinantly produced TEV protease for cleavage.

Tab. 10 Overview over yields after different purifications steps of fusion protein constructs. Concentration of fusion protein after affinity column was determined by A_{280} and the specific extinction coefficient, monomeric cicMT2 concentration after both gelfiltration steps was determined by 2-PDS assay and DTNB assay. Working days were counted from preculture of expression to 2nd size exclusion chromatography step where apo- or Zn_5-cicMT2 was obtained. * including purification time of TEV protease.

construct	pTYB2-cicMT2	pG1xMT	pG3xMT	pGtMT
cell culture	1 L	1 L	1 L	1 L
expressed wet cells	6.6 g	6.2 g	4.8 g	5.9 g
fusion protein after affinity column (≙ cicMT2)	-	150 mg, 4.4 μmol (34 mg, 4.4 μmol)	100 mg, 2.0 μmol (47 mg, 6.0 μmol)	150 mg, 4.3 μmol (34 mg, 4.3 μmol)
monomeric cicMT2 after 1st SEC	-	20 mg, 2.5 μmol	0 mg, 0 μmol	23 mg, 2.9 μmol
monomeric Zn_5-cicMT2 after 2nd SEC	1 mg, 0.1 μmol	3.9 mg, 0.5 μ.mol	-	15 mg, 1.9 μmol
monomeric apo-cicMT2 after 2nd SEC	-	4.2 mg, 0.5 μmol	-	18 mg, 2.3 μmol
total expression and purification time	9.5 working days	5.5 working days	-	5 working days*

The most important factor for successful and low-cost purification is the cleavage of the fusion protein from its tag. The three different cleavage agents differ notably. The DTT induced self-cleavage of the intein system is inexpensive, however the least efficient. Not all of the fusion protein was cleaved, and the incubation times needed were rather long. After cleavage, the intein precipitated easily lowering the yield. The cleavage with thrombin protease was efficient if high amounts, i.e. 1 U thrombin per 1 mg fusion protein, and long incubation times, i.e. 36 h, were used. This however results in two major drawbacks. On the one hand the thrombin protease is expensive, because it is produced *in vivo*. To lower the expenses, the incubation time was increased. But still then, not all the fusion protein could be cleaved. Longer incubation times let, on the other hand, to precipitation of the GST-tag, and partially also of the cicMT2. An additional disadvantage of the thrombin protease was the necessity of demetallation of the protein to gain access to the cleavage site. In this way, a not natively metallated form was obtained, and the production of the different metal-loaded forms always had to proceed via the apo-form. In case of the slightly altered recognition sequence in the tri-repeat sequence no cleavage was possible. To optimize the system further, TEV protease was used. This protease can be recombinantly purified in sufficient yield and therefore was less expensive. Accordingly, higher amounts of protease can be used, i.e. 1 mg TEV per 40 mg fusion protein, what increased the cleavage efficiency up to nearly 100 %. This also shortened the incubation times, i.e. 12 h, minimizing the possibility of protein precipitation. By including the time for TEV purification in the working time, the whole procedure was still faster than with the thrombin.

For successful, fast, and less expensive purification, also other factors were responsible. For concentration and separation of smaller molecules from cicMT2 more efficient methods were used then previously conducted ones. As example, ultrafiltration was used instead of lyophilization or dialysis, anaerobic size exclusion chromatography instead of Chelex™ resin treatment to remove excess of unbound metal ions. All this let to shorter purification times resulting in higher yields.
Comparing all these factors, the newly engineered construct GST-thrombin-TEV-cicMT2 of pGtMT was in all sections more successful than the formerly used cicMT2-intein construct of pTYB2-cicMT2. The yield could be increased 10-15fold, the purification time could be decreased more than roughly 50%, and the costs were comparable. Therefore, the new construct was used for the expression and purification of cicMT2 in this thesis.

7.1.4. Analysis of Zn_5-cicMT2 and apo-cicMT2

Stoichiometry and oxidation state of Zn_5-cicMT2 and apo-cicMT2 were determined to evaluate the quality of the proteins obtained with the new production pathway.
To determine the obtained stoichiometry, the metal concentration was measured with F-AAS and the protein concentration with 2-PDS assay, yielding a ratio of five Zn^{2+} ions to one cicMT2. This stoichiometry was confirmed by mass spectrometry (Fig. 22).

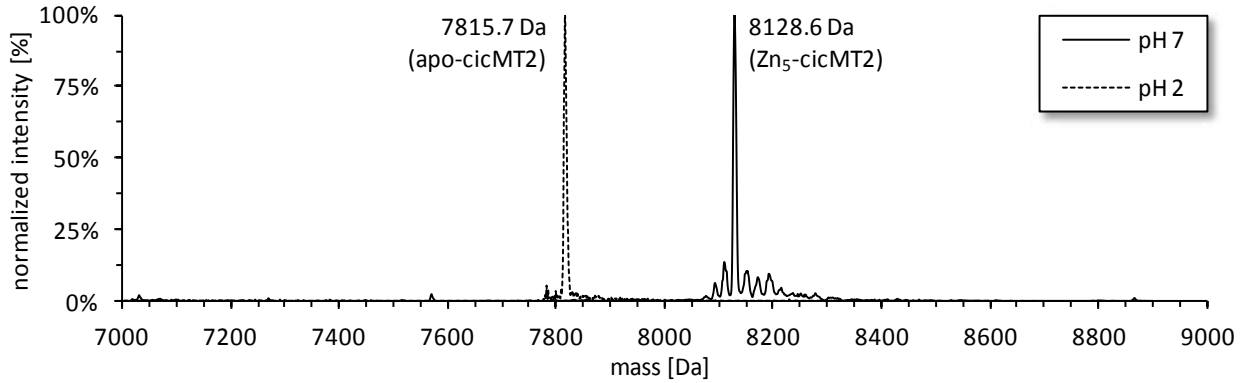

Fig. 22 Deconvoluted ESI^+-MS spectra of Zn_5-cicMT2 from GST-thrombin-TEV-cicMT2 cleaved with TEV protease measured at acidic pH (pH 2, dashed line) and neutral pH (pH 7, solid line), with a normalized intensity of 100 %. Acidic spectrum has a maximum intensity of 2149 counts s^{-1} and shows a single peak at 7815.7 Da for reduced apo-cicMT2 (calc. 7815.7 Da). Spectra taken at neutral pH revealed peaks with a maximum intensity of 13380 counts s^{-1} at 8128.5 Da for Zn_5-cicMT2 (calc. 8128.6 Da), at 8110.1 Da for Zn_4Na_2-cicMT2 (calc. 8109.2 Da), at 8151.5 Da for Zn_5Na_1-cicMT2 (calc. 8151.6 Da), at 8173.7 Da for Zn_5Na_2-cicMT2 (calc. 8174.6 Da), and at 8194.6 Da for Zn_5Na_3-cicMT2 (calc. 8197.6 Da).

The deconvoluted ESI^+-MS spectra of Zn_5-cicMT2 from GST-thrombin-TEV-cicMT2 cleaved with TEV protease showed the expected species, apo-cicMT2 with 7816.1 Da at pH 2 (calculated 7815.7 Da) and Zn_5-cicMT2 with 8128.5 Da at pH 7 (calculated 8128.6 Da). At neutral pH some additional peaks with low intensity appeared, at 8110.1 Da with 14 % intensity corresponding to Zn_4Na_2-cicMT2 (calculated 8109.2 Da), at 8151.5 Da with 10 % intensity corresponding to Zn_5Na_1-cicMT2 (calculated 8151.6 Da), at 8173.7 Da with 8 % intensity corresponding to

Zn_5Na_2-cicMT2 (calculated 8174.6 Da), and at 8194.6 Da with 9 % intensity corresponding to Zn_5Na_3-cicMT2 (calculated 8197.6 Da).
The oxidation of cicMT2 was analyzed with the DTNB assay, for all the samples the amount of disulfide bridges was lower than 5 % and hence within the detection limit of the method.
In conclusion, the quality and purity of the protein is in excellent agreement with results obtained with the IMPACT^{TM}-CN system previously used by our group.

7.1.5. Purification of TEV protease

For the GST-thrombin-TEV-cicMT2 cleavage, TEV protease had to be purified. The expression and purification was done as described by Tropea et al.[156] with only little changes. From 1 L cell culture 3.1 g wet cells were harvested, lysed and applied to a nickel affinity chromatography column. After elution with imidazole, the concentration of the TEV protease was determined via absorption measurement and an average yield of 20 mg TEV protease could be obtained. This value is slightly higher than the actual concentration, because the imidazole also absorbs at 280 nm. For removal of the high imidazole concentration in the enzyme solution and to prevent precipitation of the TEV protease a desalting column run was performed. The concentration determination with absorption measurement at 280 nm showed a final yield of 15 mg TEV per original 1 L cell culture.

7.2. Structural analysis of cicMT2

Previous structural studies of cicMT2 performed in our group delivered mainly information about the metal-thiolate cluster.[175] Spectroscopic methods revealed the stoichiometries of metal ions to protein, and showed the coordination of five divalent metal ions e.g. Zn^{2+}, Cd^{2+}, or Co^{2+} ions via the thiolate groups of its cysteine residues. Based on limited proteolytic digestion experiments strong evidence was provided for the presence of a single metal-thiolate cluster that connects the *N*-terminal with the *C*-terminal cysteine-rich region of Cd_5-cicMT2.[135] Information about the overall structure of cicMT2 is so far not available. In the following, we present our attempts to investigate the NMR solution structure of cicMT2.

7.2.1. NMR spectroscopy studies on cicMT2

Previous 3D structures of metallothioneins deposited in the protein database were to 94 % investigated by solution NMR spectroscopy.[46] NMR spectroscopy is the preferred tool to analyze such small and partially flexible proteins. Many of the deposited structures are from metallothioneins with two domains, e.g. the vertebrate forms. In these forms the two domains are connected by a short but flexible amino acid linker. As NMR spectroscopy experiments could not reveal any interactions, i.e. cross peaks, between the single domains, only the structures of the isolated domains could be determined and not of the full-length proteins. Having in mind, that cicMT2 seems to fold into a single metal-thiolate cluster, the long and presumably flexible linker part was not removed and the entire protein subjected to the NMR spectroscopy studies.
NMR spectroscopy samples of cicMT2 were prepared under the same conditions used to elucidate the structure of the β_E-domain and γ-domain of E_c-1 from *T. aestivum*, the only published structures of a plant metallothionein so far (15 mM d_{11}-Tris-HCl pH 6.9, 50 mM NaCl, 90 % H_2O/10 % D_2O).[29, 55] However, the concentration of the metallothionein was 150 µM instead 1 mM as used for E_c-1. Both 1D ^{1}H-NMR spectra of Cd_5-cicMT2 and Zn_5-cicMT2 measured at 298 K revealed resonances between 0 and 4 ppm and between 6.5 and 7.5 ppm, no resonances above 7.5 ppm could be detected. The resonances around 7 ppm were quite broad.
In general, the H^{α}, the protons of the aliphatic side-chains, and the methyl protons of the amino acids appear in the range of 0 to 6 ppm, whereas the H^N-protons of the backbone and the side-chains as well as the aromatic protons resonate in the range of 6 to 10 ppm.[176-177] These chemical shifts arise as a result of shielding the nucleus from the external magnetic field and therefore contain the majority of the information about the protein structure.[178] The ^{1}H chemical shift specifically depends on local geometry and on through-space interactions. Hence, in folded proteins a wide spectral dispersion is usually observed as amino acids in solely and rigid structures have a defined neighborhood, which creates a specific chemical shift.[179] By contrast, in unfolded proteins the resonances show a considerable degree of overlap and a lack of spectral dispersion as the amino acids can have several different neighborhoods at the same time resulting in different chemical shifts, which average out in the sum.[180] The chemical shift is therefore strongly dependent on the secondary and tertiary structure.

The small dispersion of resonances seen for Cd_5-cicMT2 and Zn_5-cicMT2 indicates a mostly disordered structure of cicMT2. In addition, the broadening of the low-field shifted peaks around 7 ppm implies also the existence of more than one species which interconvert with an intermediate-exchange rate ($k_{ex} \sim \nu_A - \nu_B$). In order to obtain a solution structure of a protein, it is however necessary that the resonances of the different amino acids are distinguishable from each other to assign them correctly.

To improve the quality of the 1D ^{1}H NMR spectra the sample and recording conditions were varied. First, the sample reconstitution was changed from reconstitution at high protein concentration to reconstitution at low protein concentration, and the exchange of the buffer from the slow method of dialysis to faster washing via ultrafiltration. Second, the protein concentration was raised in several steps up to 200 µM Cd_5-, Zn_5-cicMT2. Thereby it was difficult to balance between the highest concentrations possible in solution and protein precipitation. Third, the composition of the buffer was slightly changed using 1-80 mM d_{11}-Tris-HCl pH 7.3-8.6, 0-50 mM NaCl, 90 % H_2O/10 % D_2O. From these differently prepared samples 1D ^{1}H NMR spectra were measured at temperatures between 293 K and 310 K, but the improvements of the spectra were only marginal. The best spectrum was obtained from a 150 µM Zn_5-cicMT2 sample in 80 mM d_{11}-Tris-HCl pH 8.5, 80 mM NaCl, 90 % H_2O/10 % D_2O measured at 307 K (Fig. 23).

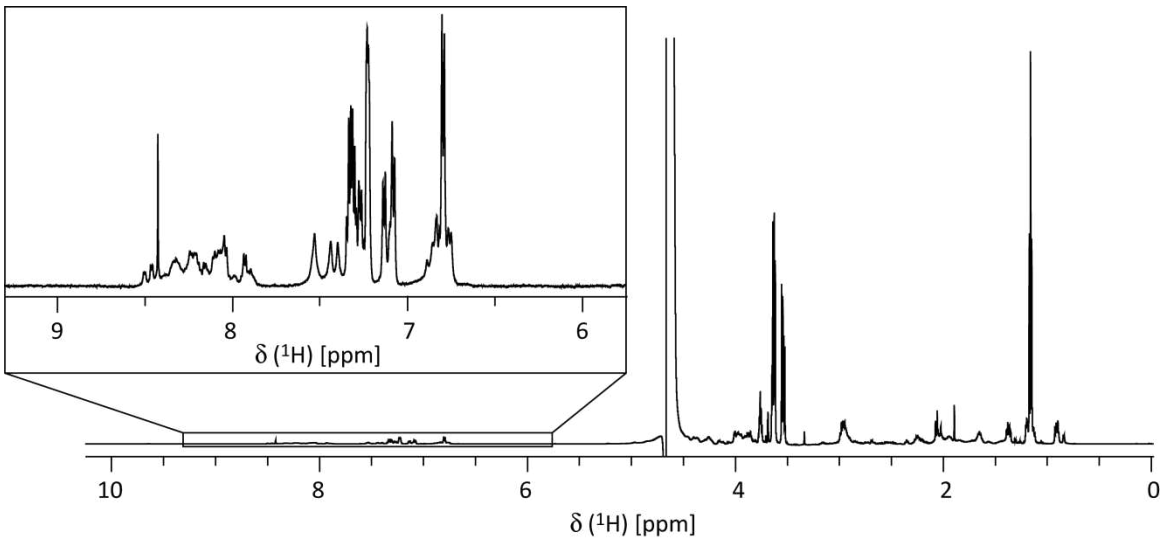

Fig. 23 ^{1}H-NMR spectra of 150 µM Zn_5-cicMT2 in 80 mM d_{11}-Tris-HCl pH 8.5, 80 mM NaCl, 90 % H_2O/10 % D_2O, pH 8.5, measured at 307 K. Inset shows the enlargement of the H^N backbone region, the most important part to solve a structure.

Nevertheless, also this spectrum shows no resonances higher than 8.5 ppm, indicating an unstructured or very flexible Zn_5-cicMT2. There are several reasons explaining this feature. First of all, it is possible that cicMT2 *in vivo* does not bind divalent metal ions such as Cd^{2+} or Zn^{2+} ions, but prefers monovalent metal ions like Cu^+ ions, or even exists in a metal-free form as oxidized or reduced apo-cicMT2. In this case, cicMT2 would not be evolutionary optimized for the binding of divalent metal ions and it would be very likely that Zn_5-cicMT2 forms a number of less structured and hence more flexible species. The high affinity of the Zn^{2+} and Cd^{2+} metal ions to the thiolates of the cysteines would still force the formation of some sort of metal-thiolate cluster, but

probably not in a defined and regular motif. Second, even if cicMT2 is coordinating divalent metal ions *in vivo* it is possible that Zn_5-cicMT2 still does not fold into a rigid structure, because its proposed function in metal homeostasis and detoxification of the cell requires a high flexibility for binding and releasing metal ions. The observed stoichiometry with five bound metal ions can be regarded as the maximum loading capacity of the protein, however, lower stoichiometries are as well feasible *in vivo* depending on the respective MT and metal ion concentrations in the cell. Third, cicMT2 was analyzed as the full-length protein and not as single domains as the other solved MT structures. Since cicMT2 was proposed to fold in a single metal-thiolate cluster, both domains were assessed together and the long floppy linker region was not removed.[135] Therefore, cicMT2 has the ability to host one big metal cluster, where the variety of possible connections is much higher than in a metal cluster with less cysteines/histidines residues. As shown for mammalian MTs, the long non-metal binding linker region can increase the flexibility dramatically. Such linkers between folded subunits in multi-domain proteins like MTs often occur as intrinsically disordered structures (IDS). They lack a well-defined tertiary structure and exist in a multitude of conformations that dynamically interconvert over time.[181-182] Although for the plant MTs was calculated a high content of β-sheets in the linker region it might be possible that their orientation varies due to a connection with flexible hinge regions.[183]

In another attempt NMR spectra of the oxidized apo-cicMT2 were recorded due to different advantages associated with oxidized apo-cicMT2. These are the possible existence of *in vivo* oxidized cicMT2, an expected reduction of cluster flexibility by stabilizing disulfide bonds, and the *in vitro* occurrence of monomeric oxidized cicMT2. The recorded NMR spectra look very similar to the ones obtained for the metallated forms. The dispersion of the resonances covered only the range between 0 and 4 ppm and between 6.5 and 8.5 ppm, and thus the spectra could also not be used to solve the protein structure of cicMT2.

No additional NOESY or TOCSY NMR spectra were recorded for any of the single cicMT2 samples necessary for structure determination, because it was not considered to be reasonable. However, further experiments of cicMT2 with Cu^+ or Ag^+ ions should be performed to investigate whether or not a preference for monovalent metal ions exist.

7.2.2. NMR spectroscopy studies of GST-tagged cicMT2

To overcome the above reported problems with the proposed high structural flexibility of cicMT2, a new approach was chosen. Recently, Liew et al.[78] showed the possibility to record conventional NMR spectra of small GST-fusion proteins. This has the advantage of efficient protein expression and purification without a cleavage step, resulting in higher yields and a decrease of purification time and costs. Additionally, the GST-tag can enhance the solubility and stability of the target protein. Observed resonances in the NMR spectra originate almost entirely form the target protein. This selectivity arises because the GST portion of the fusion protein forms a 52 kDa dimer in solution, resulting in significant broadening of the NMR signals from the GST component. The flexibility afforded by the linker between the GST and the target protein results in sharp NMR signals for the small target proteins (20-25 kDa).[184] Our research group already successfully

solved the solution structure of the plant MT γ-E_c-1 from a GST-tagged and GST-free system. The recorded NMR spectra show some noticeable differences, but the majority of the peaks are located at identical positions.[79] This allowed the structure solution of the target protein as part of the fusion protein yielding the same conformation as for the isolated protein.

To evaluate the use of this method for cicMT2, GST-cicMT2 was purified as described reaching a final fusion protein concentration of around 1.5 mM, and the stoichiometry of GST-Zn_5-cicMT2 and GST-Cd_5-cicMT2 was confirmed.

Like for the isolated cicMT2, 1D ^{1}H NMR spectra of GST-tagged cicMT2 were recorded. An example is shown in Fig. 24 for 1.7 mM GST-$Zn_{4.8}$-cicMT2 in 1 mM d_{11}-Tris-HCl pH 8.0, 90 % H_2O/10 % D_2O, measured at 307 K. The dispersions of the resonance in the spectra of the Cd^{2+}- and the Zn^{2+}-loaded form of GST-cicMT2 are similar, showing resonances between 0.5 and 4.5 ppm and between 6.5 and 8.5 ppm. The resonances with chemical shifts from 0.5 to 4.5 ppm were strongly influenced by the aliphatic side chains from the underlying GST spectra. The overall shape of resonances from 6.5 to 8.5 ppm is comparable to the one obtained for the isolated cicMT2, but the single resonances are even less resolved due to the broadening of the NMR signals from the large GST dimer. The intensity of the resonances is in general higher for the fusion protein than for the isolated protein as expected from the ten times higher concentration of the sample.

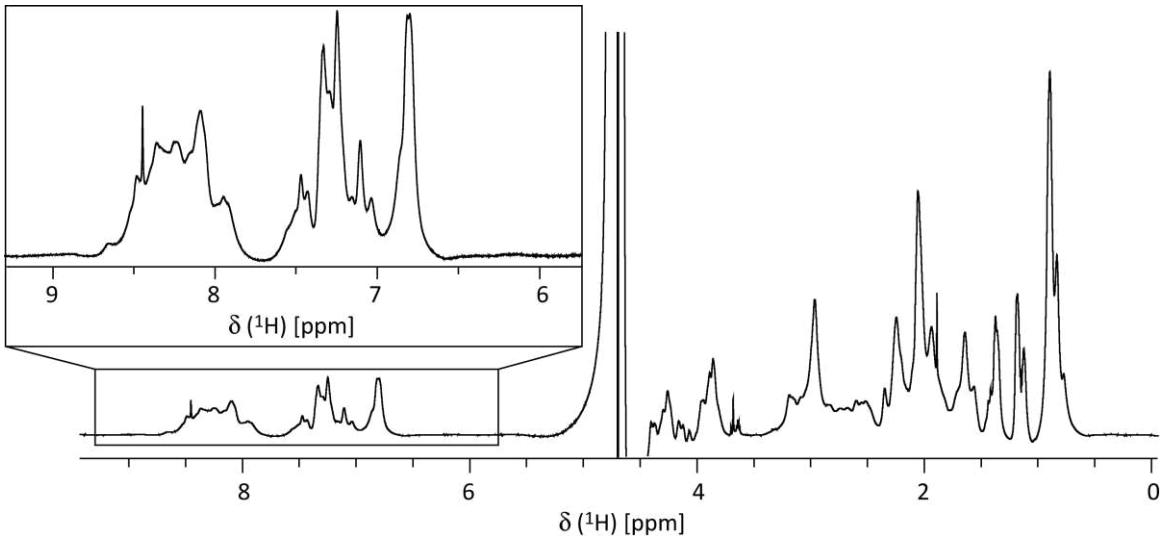

Fig. 24 ^{1}H-NMR spectra of 1.7 mM GST-$Zn_{4.8}$-cicMT2 in 1 mM d_{11}-Tris-HCl pH 8.0, 90 % H_2O/10 % D_2O, measured at 307 K. Inset shows the enlargement of the H^N backbone region, the most important part to solve a structure.

Nevertheless, 2D NMR spectroscopy experiments were performed with GST-Zn_5-cicMT2 and GST-Cd_5-cicMT2, i.e. ^{1}H-^{1}H NOESY NMR and ^{1}H-^{1}H TOCSY NMR, shown in Fig. 25 for the same sample as 1D ^{1}H NMR spectrum in Fig. 24 (1.7 mM GST-$Zn_{4.8}$-cicMT2 in 1 mM d_{11}-Tris-HCl, 10 % D_2O, pH 8.0, measured at 307 K). The ^{1}H-^{1}H NOESY NMR spectrum, where cross peaks appear for resonances from nuclei that are spatially close (through-space correlation), shows cross peaks in the region between 6.5 and 8.5 ppm. The ^{1}H-^{1}H TOCSY NMR spectrum, where cross peaks appear

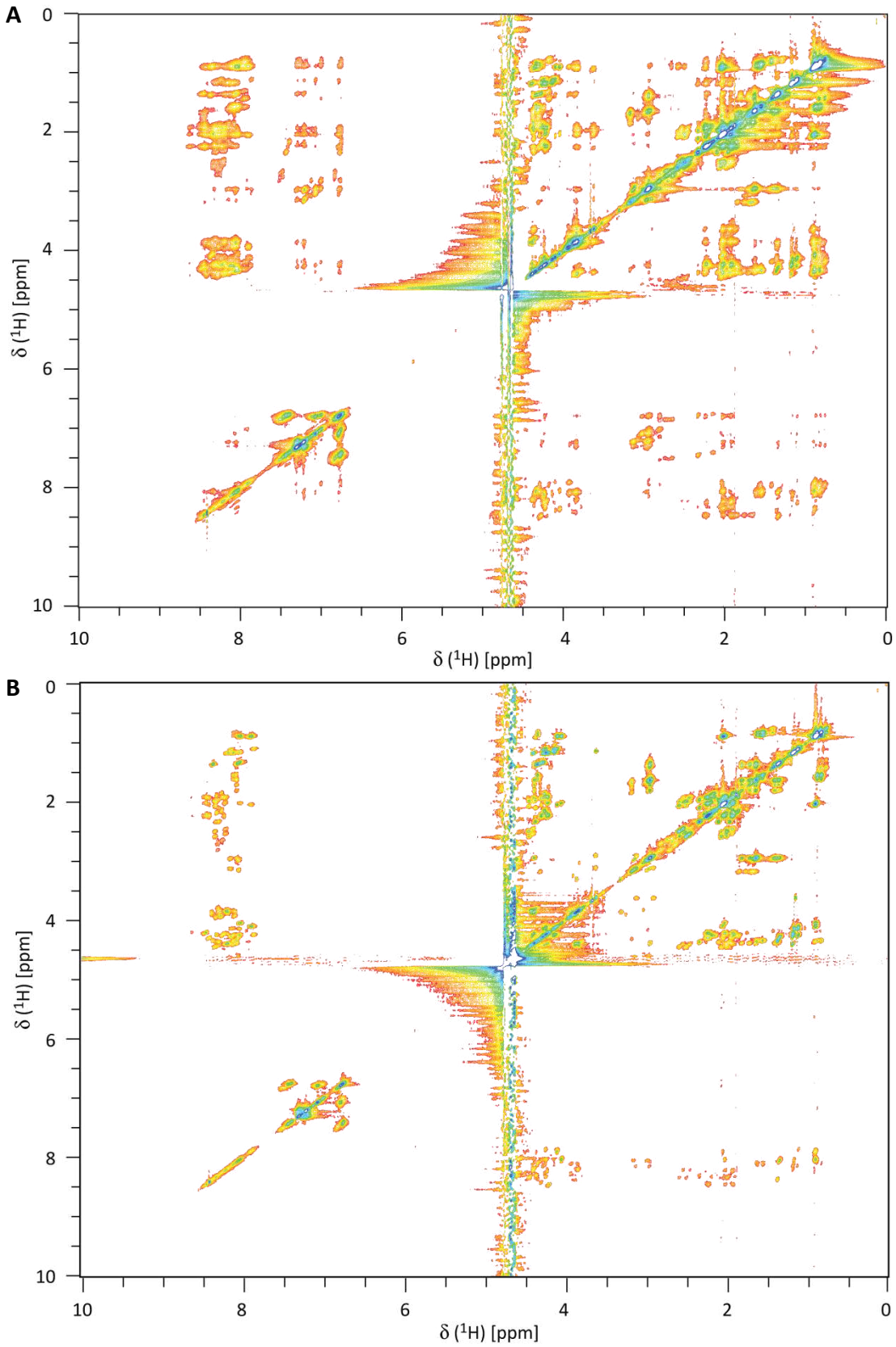

Fig. 25 **(A)** 2D ^{1}H-^{1}H NOESY-NMR spectrum and **(B)** 2D ^{1}H-^{1}H TOCSY NMR spectra of 1.7 mM GST-$Zn_{4.8}$-cicMT2 in 1 mM d_{11}-Tris-HCl, pH 8.0, 90 % H_2O/10 % D_2O, measured at 307 K.

for nuclei which are directly connected (through-bond correlation), shows cross peaks in the region between 7.5 and 8.5 ppm. The absence of resonance between 6.5 and 7.5 ppm in the

TOCSY NMR spectrum compared to the NOESY NMR spectrum originates from the lack of through-bond coupling of the side chain protons. The resonances of the NOESY and TOCSY spectra are well defined, but they show a low signal dispersion caused by the overlap of resonances as in the 1D ^{1}H NMR spectrum. With the available spectra, it is not possible to solve the 3D solution structure of the cicMT2 in its Cd^{2+}- and Zn^{2+}-loaded forms.

Several changes were applied to improve the quality of the NMR spectra. As already described for the isolated protein, the buffer composition was altered, but also the temperature during the spectra acquiring process. The different conditions could not enhance the spectra resolution. As described in Loebus[79] an improvement was expected by the heating of the final samples overnight at 37 °C to force the gelation process which sharpen the peaks, but this even decreased the quality of the signals. Surprisingly, the measuring of the oxidized apo-cicMT2 yielded in nearly the same spectra as recorded from metallated cicMT2.

As already mentioned in 7.2.1, reasons for the low resonance dispersions can be the possibly preferred binding of cicMT2 to monovalent metal ions, the need for a flexible structure for the function of binding and releasing metal ions, and the high flexibility induced by the long, non-metal binding linker region of cicMT2.

So far, the overall 3D structure determination of cicMT2 failed so far with the common methods. It has to be further investigated at least to get an insight into the function of this protein. For addressing the structural properties of IDS by NMR spectroscopy new computational methods were developed. Those might be helpful for the overall structure determination of cicMT2.[185-190]

7.3. Sulfide ion incorporation into the metal-thiolate clusters of cicMT2

Previous studies from our group have shown the incorporation of sulfide ions into the Cd^{2+}-thiolate cluster of cicMT2 *in vitro*.[136] Presuming that incorporation of sulfide ions has *in vivo* relevance for the function of cicMT2, we analyzed in detail the incorporation of mono- and divalent metal ions in presence of sulfide ions, the sulfide-induced stabilization and structural changes accompanying the cluster formation.

7.3.1. Cd^{2+} ion incorporation into cicMT2 in absence and presence of sulfide ions

7.3.1.1. Formation of Cd- and Cd,S-cicMT2 during Cd^{2+} titration

Recently, we reported that titration of Zn_5-cicMT2 with Cd^{2+} ions in the presence of sulfide ions leads to the formation of a complex with the composition Cd_9S_7-cicMT2.[136]

The experiments were performed via titration of 10 μM Zn_5-cicMT2, which was pre-incubated with 100 μM S^{2-} ions with increasing equivalents of Cd^{2+} ions (Fig. 26). During Cd^{2+} ion titration in absence of S^{2-} ions, an absorption band is evolving at 250 nm indicative for the ligand-to-metal charge transfer band of the thiolate groups of the cysteines to the coordinated Cd^{2+} ions (Fig. 26 A, B). In presence of sulfide ions, the band is shifted to 280 nm visualizing the LMCT band of the sulfide ions to the Cd^{2+} ions (Fig. 26 C, D). The band is increasing in intensity until a maximum of metal ion equivalents are incorporated. Further addition of metal ions does not lead to a change of the spectra. The equivalent, with which the increase at the LMCT stops, shows the amount of incorporated Cd^{2+} ions. Cd^{2+} ion titration to Zn_5-cicMT2 leads to the newly formed complexes $Cd_{5.0\pm0.1}$-cicMT2 and $Cd_{9.1\pm0.3}S_x$-cicMT2, respectively.

For the titration in absence of sulfide ions, it was shown, that the final stoichiometry is the same as for the titration of Zn_5-cicMT2 with Cd^{2+} ions as well as for the titration of apo-cicMT2 with Cd^{2+} ions. To evaluate, if this is also true for the sulfide ion containing form, and to test, if an already formed existent metal-thiolate cluster of the cicMT2 as a pre-fold structure is necessary to incorporate the sulfide ions, the same experiments were performed with the apo-cicMT2 (Fig. 27). In absence of additional sulfide ions, a band at 250 nm is evolving for the LMCT band of Cd^{2+} ions to the thiolate groups of the cysteines, until five equivalents of Cd^{2+} ions were added. In presence of sulfide ions, the LMCT bands cover a larger spectral range up to 280 nm for the LMCT band of the sulfide ions to the Cd^{2+} ions, and the increase of extinction coefficient stops after nine equivalents of Cd^{2+} ions. The final stoichiometries calculated from the metal titrations with the apo-form are $Cd_{5.1\pm0.2}$-cicMT2 and $Cd_{8.8\pm0.2}S_x$-cicMT2, respectively. These stoichiometries are the same as for the cadmium-forms starting from Zn_5-cicMT2.

Comparing the spectra of both variants, Cd_5-cicMT2 and Cd_9S_x-cicMT2, obtained from apo-cicMT2 or Zn_5-cicMT2, it is obvious, that they are mostly overlapping (Fig. 27 C). The small deviations do not have a large influence on the overall shape of the final spectra.

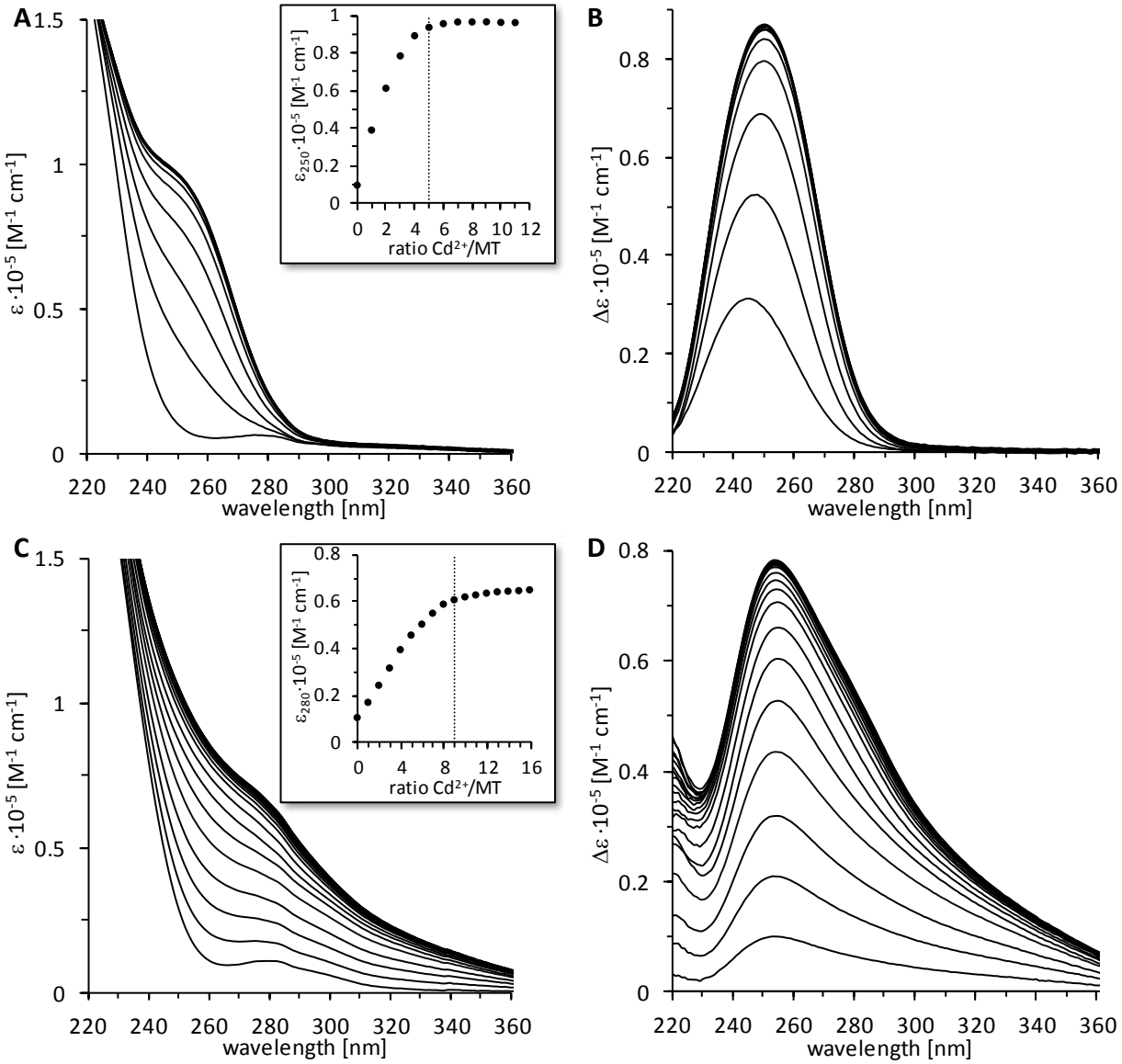

Fig. 26 UV spectra of Cd^{2+} ion titration to Zn_5-cicMT2 in absence **(A, B)** and presence **(C, D)** of additional sulfide ions. **(A, C)** shows the UV spectra, **(B, D)** the difference plot, where the spectra with 0 equivalent of Cd^{2+} ions is subtracted from the spectra where Cd^{2+} ions were added. Zn_5-cicMT2 (10 μM) was titrated (in presence of 100 μM Na_2S) with increasing equivalents of metal ions (10-200 μM) in 10 mM Tris-HCl, 10 mM NaCl, pH 7.5. Insets show the plot of the molar absorptivity at the LMCT bands (250 nm or 280 nm) of the specific form against the number of equivalents of Cd^{2+} ions added to Zn_5-cicMT2.

Both of the Cd_9S_x-cicMT2 forms show a bathochromic broadening of the absorption bands, indicative for sulfide ion incorporation into metal-thiolate clusters. The additional LMCT bands at higher wavelength or even red-shifted transitions were observed for Cd,S-cicMT2 species, upon titration of mammalian Cd-MTs with sulfide ions, and for the sulfide ion containing PC complexes in *S. pombe*.[83, 85, 136] The origins of the observed shifts of the LMCT transitions have been attributed to decreasing HOMO-LUMO gaps with increasing cluster size. A major influence is also

ascribed to the transition to structures with highly coordinated sulfur atoms, e.g. μ_3- or even μ_4-S^{2-} ions.[191-194]

To test that the change of absorption is not originating from Cd,S-clusters in solution, Cd^{2+} ions were titrated to S^{2-} ions under the same conditions as the cicMT2 titrations were performed (Fig. 28 A). The solution with S^{2-} ions shows an absorption below 250 nm, but the spectra are not changing upon the addition of Cd^{2+} ions. This indicates that changes in the absorption spectra of the Cd^{2+} ion titration to S^{2-} ion supplemented Zn_5-cicMT2 originate from the interaction with the metallothionein.

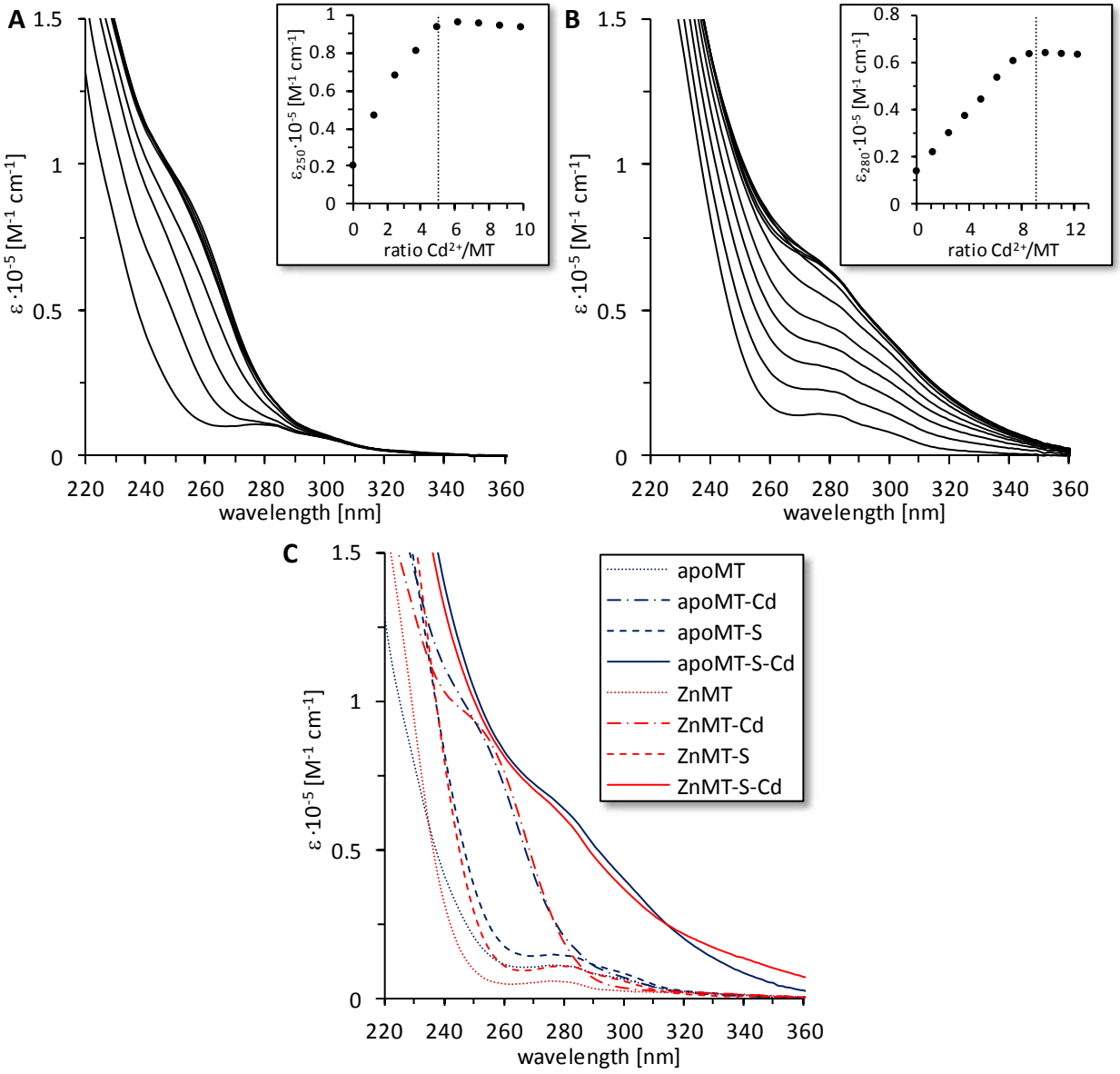

Fig. 27 UV spectra of Cd^{2+} ion titration to apo-cicMT2 in absence **(A)** and presence **(B)** of additional sulfide ions. Apo-cicMT2 (10 μM) was titrated (in presence of 100 μM Na_2S) with increasing equivalents of Cd^{2+} ions (10-200 μM) in 10 mM Tris-HCl, 10 mM NaCl, pH 7.5. Insets show the plot of the molar absorptivity at the LMCT bands (250 nm or 280 nm) of the specific form against the number of equivalents of Cd^{2+} ions added to apo-cicMT2. **(C)** Overlay of UV spectra from Cd^{2+} ion titrations of apo-cicMT2 (black) und Zn_5-cicMT2 (red) in presence and absence of sulfide ions. Samples and amounts as described in Fig. 26 A, C and Fig. 27 A, B. Samples as indicated in legend, apoMT indicates apo-cicMT2, ZnMT indicates Zn_5-cicMT2, Cd indicates Cd^{2+} ions, and S indicates S^{2-} ions.

For further clarification, difference spectra were calculated, where the spectrum of Zn_5-cicMT2 was subtracted from Zn_5-cicMT2 + 10 S^{2-} ions (Fig. 28 B). The spectrum is not at all overlapping with the spectrum of S^{2-} ions alone in solution. The spectrum of Zn_5-cicMT2 + 9 Cd^{2+} ions was also subtracted from Zn_5-cicMT2 + 10 S^{2-} ions+ 9 Cd^{2+} ions. Just as the starting form, also the final form after titration is not overlapping with 10 S^{2-} ions + 9 Cd^{2+} ions. In fact a strong band is appearing at 280 nm. Performing the calculation the other way around, summing up the spectrum of Zn_5-cicMT2 and 10 S^{2-} and also summing up Zn_5-cicMT2 + 5 Cd^{2+} ions and 10 S^{2-} ions + 9 Cd^{2+} ions does not lead to the spectrum of Zn_5-cicMT2 + 10 S^{2-} ions or Zn_5-cicMT2 + 10 S^{2-} ions+ 9 Cd^{2+} ions, respectively. The calculated spectra support the conclusion, that the S^{2-} ions added to the Zn_5-cicMT2 interact with the metallothionein and are not independent in solution. The titration of Cd^{2+} ions in presence of S^{2-} ions leads to an interaction of the sulfide ions with the metallothionein and/or the metal ions.

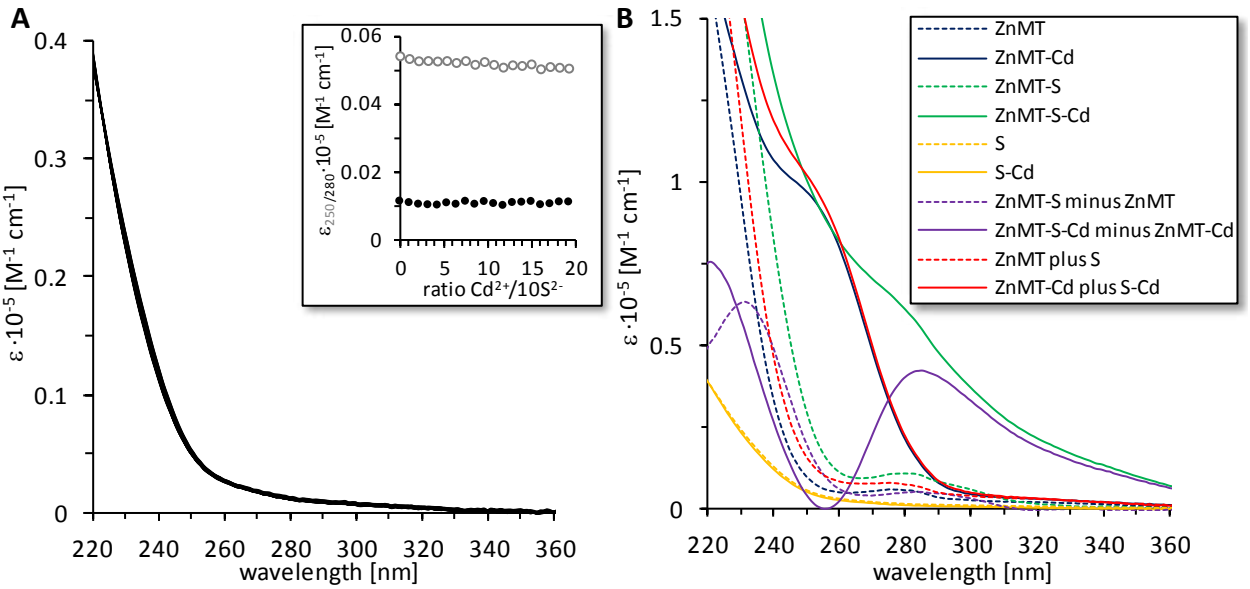

Fig. 28 **(A)** UV spectra of Cd^{2+} ion titration to S^{2-} ions. 100 µM Na_2S was titrated with increasing equivalents of $CdCl_2$ (10-250 µM) in 10 mM Tris-HCl, 10 mM NaCl, pH 7.5. Inset shows the plot of the molar absorptivity at the LMCT bands relevant for the Cd^{2+} ion titration with cicMT2 (250 nm in grey empty circles and 280 nm in black full circles) against the number of equivalents of Cd^{2+} ions added. **(B)** UV spectra and UV difference spectra for different forms of titrated samples. Measured forms are depicted with dotted lines, calculated forms are depicted with solid lines. Blue spectra show the Zn_5-cicMT2 and Zn_5-cicMT2 titrated with 5 equivalents of Cd^{2+} ions; green spectra show the Zn_5-cicMT2 supplemented with 10 equivalents of S^{2-} ions and Zn_5-cicMT2 titrated with 9 equivalents of Cd^{2+} ions in presence of 10 equivalents of S^{2-} ions; yellow spectra show the spectra of 10 equivalents of S^{2-} ions and the spectra of 10 equivalents of S^{2-} ions titrated with 9 equivalents of Cd^{2+} ions. The purple spectra show the subtraction of the green and blue spectra (Zn_5-cicMT2 + 10 S^{2-} minus Zn_5-cicMT2; Zn_5-cicMT2 + 10 S^{2-} + 9 Cd^{2+} minus Zn_5-cicMT2 + 9 Cd^{2+}), and the red spectra show the addition of the blue and yellow spectra (Zn_5-cicMT2 plus 10 S^{2-}; Zn_5-cicMT2 + 5 Cd^{2+} plus 10 S^{2-} + 9 Cd^{2+}).

To determine the sulfide ion content, excess metal and sulfide ions were removed via size exclusion chromatography from the titration solutions. The differently loaded cicMT2 eluted with a main monomeric peak at 13.5 mL, but the elution profiles also show minor peaks at an elution volume of 11.9 mL and 11.0 mL. All peaks were analyzed with a combination of F-AAS, 2-PDS assay and the methylene blue method.

The peaks at lower elution volume contain a very high amount of metal and sulfide ions, but only a low amount of protein. In terms of ratios this would result in 15-1900 metal ions per cicMT2 and 80-6000 sulfide ions per cicMT2. Due to the shift to smaller elution volume, they might show the occurrence of a small amount of dimers and trimers, and a high amount of Cd,S-clusters and Cd,S-aggregates. This is in contrast to the sulfide ion incorporation into PCs, where the Cd,S-cluster formation is accompanied by multimer formation of the short peptide chains.[130]

For the titration of Zn_5-cicMT2 with Cd^{2+} ions in absence of sulfide ions the main monomeric peak at 13.5 mL revealed a stoichiometric composition of $Cd_{5.0\pm0.6}S_{0.2\pm0.3}$-cicMT2 while the analogous titration in presence of ten equivalents of sulfide ions resulted in a stoichiometric composition of $Cd_{8.7\pm1.3}S_{7.4\pm1.2}$-cicMT2. The metal ion load of cicMT2 increased 1.7 ± 0.3 times in presence of sulfide ions showing a clear increase of the metal binding capacity in presence of ten equivalents of sulfide ions. The gain of equivalents of metal ions is the result of the additional incorporation of sulfide ions into the metal-thiolate cluster of the cicMT2 acting as additional anionic ligands for the metal ions.

The ratio of additionally added equivalent of Cd^{2+} ions per S^{2-} ions was calculated to 0.49 ± 0.11 meaning that for each additional metal ion roughly two sulfide ions were incorporated. The overall charge of S^{2-} ion lacking forms is -6 (charges: -2 Asp, -5 Glu, -14 Cys, +5 Lys), what increases further by two more negative charges for each additionally incorporated Cd^{2+} ion together with two S^{2-} ions. This is against expectations owing to the fact that such an increase in negative charge should destabilize the cluster assembly because of charge repulsion between the ligands and hence impede the formation of larger clusters. A solution for this controversy could be charge compensation in solution in form of counter ions such as Na^+ ions or by protonation of sites resulting in hydrogen sulfide, HS^-, acting as ligands, although this was never observed for "inorganic" Cd,S-clusters with additional organic thiolate ligands.[136] Nevertheless, similar ratios can be calculated based on the Cd^{2+} and S^{2-} ion contents given by Capdevila et al.[81] and hence seem to reflect a general trend. The structural implication of the cluster, however, remains unclear.

Examining the ratios between bound metal ions and the combined content of sulfide ions and cysteine thiolate groups (14 thiolates of cysteines and 8.7 sulfide ions) the calculated ratios are 0.35 ± 0.50 for $Cd_{5.0}S_{0.2}$-cicMT2 and 0.40 ± 0.09 for $Cd_{8.7}S_{7.4}$-cicMT2. These values agree well with those reported by Capdevila et al.[81] from cork oak, drosophila, yeast, sea urchin, chicken, and mammalian MTs.

7.3.1.2. Change in the cluster arrangement by sulfide ion incorporation

To evaluate, if sulfide ion incorporation and the accompanied increase in cluster size leads to changes of the cluster structure, CD and MCD spectra were recorded during the titration of Zn_5-cicMT2 with Cd^{2+} ions in presence of ten equivalents of sulfide ions (Fig. 29 B, D). The results were compared to spectra from the analogous titration without sulfide ions (Fig. 29 A, C).

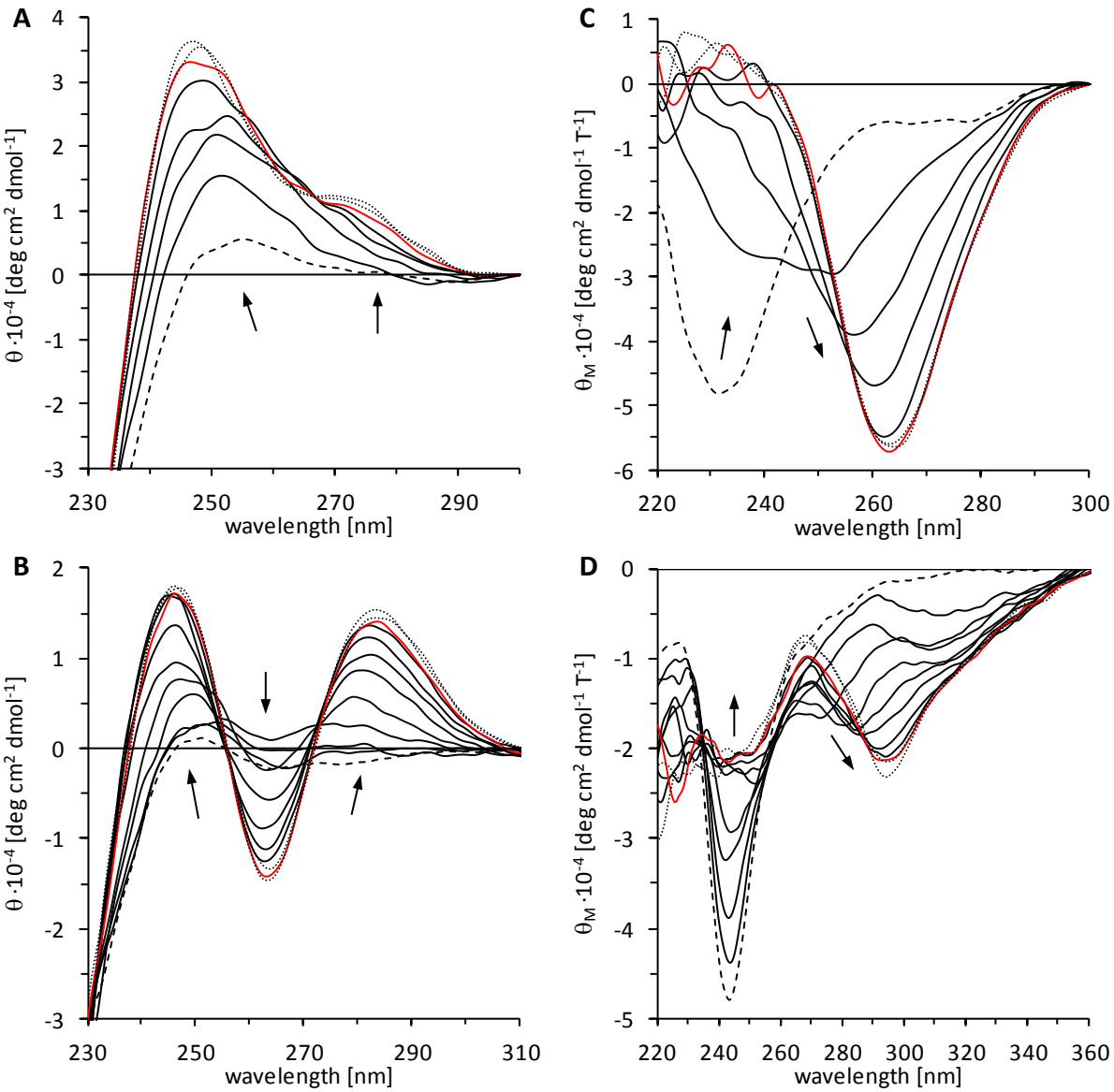

Fig. 29 CD **(A, B)** and MCD **(C, D)** spectra of the titration of Zn_5-cicMT2 in absence **(A, C)** and presence of S^{2-} ions **(B, D)** with Cd^{2+} ions. cicMT2 (10 µM) was titrated (in presence of 100 µM Na_2S) with increasing equivalents of Cd^{2+} ions (10-150 µM) in 10 mM Tris-HCl, 10 mM NaCl, pH 7.5. The dashed spectra belong to initial Zn_5-cicMT2, in **(B, D)** in presence of sulfide ions. Solid lines represent spectra of different equivalent of Cd^{2+} added. Red spectra indicate the respective titration points, at which additional Cd^{2+} ions do not cause further spectral changes, i.e. when the protein was saturated with Cd^{2+} ions. Dotted spectra show the spectra taken at higher equivalents of Cd^{2+} than the red spectra. Arrows show the evolution or disappearance of transitions with increasing amounts of Cd^{2+} ions added to the solution.

The pronounced CD bands in the spectra of Cd^{2+}-substituted MTs, which can be observed at higher wavelength than the bands of the peptide backbone, are proposed to originate from peptide-induced asymmetry of the binding sites within the cluster as well as from the chirality

introduced by bridging thiolate ligands.[195] The cluster formation, i.e. recruitment of bridging thiolate ligands, is often, but not always, accompanied by exciton splitting indicated by two oppositely signed CD bands with a cross-over point at the position of the absorption band around 250 nm. CD spectra of mammalian MTs typically show this feature.

For Cd_5-cicMT2 however, only a monophasic CD profile is observed as similarly seen, for example, in the spectrum of MtnE, one of the MTs from *Drosophila melanogaster*.[135, 196] Albeit this monophasic CD profile, the Cd^{2+} ions in Cd_5-cicMT2 are clearly coordinated in form of a metal-thiolate cluster as indicated by a red-shift of absorption bands during the titration of apo-cicMT2 with Cd^{2+} or Co^{2+} ions.[135] The CD spectra for the titration of Zn_5-cicMT2 with Cd^{2+} ions (Fig. 29 A) revealed a shift of the CD band, which is located around 255 nm in the Zn^{2+}-form, from 252 nm after addition of the first equivalent of Cd^{2+} ions to a final position at 248 nm after saturation of the protein with five Cd^{2+} ions. In addition, a broad band with low molar ellipticity evolved around 275 nm, again very similar to the spectrum reported for *D. melanogaster* MtnE. The CD spectra recorded for analogous titration in the presence of ten equivalent of sulfide ions look distinctively different (Fig. 29 B). Already after addition of four equivalents of Cd^{2+} ions evolution of a clearly biphasic CD profile is observed with extrema at (-)263.5 nm and (+)279.5 nm, the latter shifting to (+)284 nm after addition of ten equivalent of Cd^{2+} ions. The cross-over point is located at 272 nm. Hence the spectrum is clearly red-shifted with respect to spectra of mammalian Cd_7-MTs, which show extrema located around (-)240 nm and (+)260 nm. Results for cicMT2 can be well compared to the spectra of two MTs from *D. melanogaster*, i.e. MtnA ((-)261 nm and (+)279.5 nm) as well as the prior mentioned MtnE ((-)267.5 nm and (+) 281 nm), both in their sulfide ion containing forms.[196] The cross-over point at 272 nm mentioned above coincides with the position of the shoulder seen in the UV spectra, which is attributed to sulfide ion incorporation into cadmium-thiolate clusters as mentioned above, and hence the distinct CD profile is indicative for the presence of sulfide ions in the cluster of cicMT2.

Additionally, a spectrum of the final form of titrated sulfide ions with Cd^{2+} ions was recorded (Fig. 30 dotted line). The spectrum shows no extrema and only a small increase in negative chirality at low wavelength. This is an additional indication, that sulfide ions, in case of the cicMT2 titration with Cd^{2+} ions, are incorporated into the Cd^{2+}-thiolate cluster of cicMT2.

MCD spectra can be observed when the electronic states of a chromophore are influenced by an externally applied magnetic field causing differences in absorption of the left and right circularly polarized light.[195] While the MCD signal of the peptide backbone transitions is weak, a so-called *A*-term arises from tetrahedral Cd^{2+}-thiolate units, which shows a cross-over point at the maximum of the corresponding absorption band, i.e. again around 250 nm. In the MCD spectrum of mouse Cd_7-MT1 this cross-over point is located at 248 nm followed by a minimum at 258 nm.[195] The MCD spectra of the titration of Zn_5-cicMT2 with Cd^{2+} ions in absence of sulfide ions clearly show the evolution of an *A*-term indicative for tetrahedral CdS_4 sites. Additionally, this indicates cluster formation based on the shift of the respective cross-over points from roughly 246 nm after addition of two Cd^{2+} ions to 251 nm after five equivalents and saturation of the protein with metal ions (Fig. 29 C). The corresponding minima shifts from 257 nm to 263.5 nm. The MCD spectra for the titration of Zn_5-cicMT2 with Cd^{2+} ions in presence of ten equivalents of

sulfide ions show lower magnetic ellipticity values in the spectral range of the Cd^{2+}-thiolate cluster (Fig. 29 D). The minimum after addition of four Cd^{2+} ions is roughly located at 282 nm and shifts to 294.5 nm in the spectrum of the Cd^{2+}-saturated form. The cross-over point is located at 280 nm.

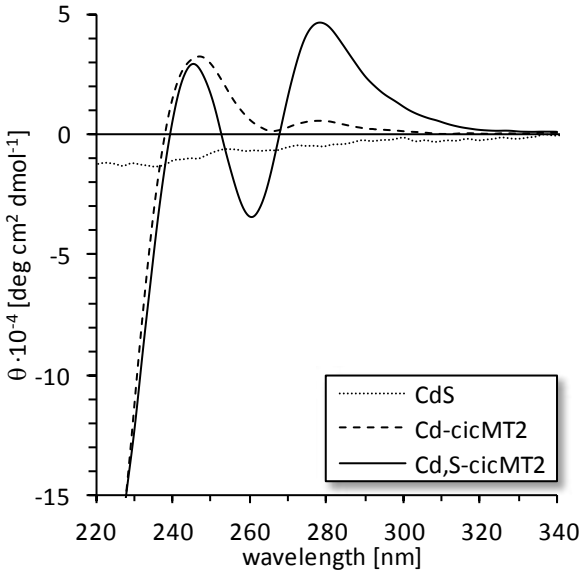

Fig. 30 CD spectra of the final forms of titrated Zn_5-cicMT2 with Cd^{2+} ions in absence (dashed line) and presence (solid line) of sulfide ions, and of the final form of titrated sulfide ions with Cd^{2+} ions in absence of cicMT2 (dotted line). Concentrations and conditions as in Fig. 29.

The distinctly different features of the UV, CD, and MCD spectra show clearly that the cluster structure in presence of sulfide ions differs from the cluster structure of Cd_5-cicMT2. In addition, very similarly shaped CD and MCD spectra were observed for the sulfide containing cadmium γ-glutamyl peptide complexes of the fission yeast *S. pombe*.[197] Interestingly, the sulfide ions seem to influence the cluster structure of Zn_5-cicMT2 already in absence of additional Cd^{2+} ions as evident from the UV and MCD spectra. The difference UV spectra obtained after subtraction of the Zn_5-cicMT2 absorption from the spectra of Zn_5-cicMT2 recorded in presence of 10 equivalents of S^{2-} ions reveals a peak around 232 nm, which is different from the spectra of a Zn^{2+}-S^{2-} ion mixture without cicMT2 at the experimental conditions used. This can be seen even more clearly in the MCD spectra: After addition of sulfide the spectrum entirely shifts to higher wavelength, i.e., from (-)232 nm to (-)243 nm, which cannot be explained by overlaying contributions from free sulfide ions or zinc sulfide particles in the mixture. But whatever the nature of this interaction is, it is apparently not thermodynamically stable, because, when the mixture of Zn_5-cicMT2 and sulfide ions is separated with size exclusion chromatography, analysis of the monomeric protein peak shows still 5 Zn^{2+} ions coordinated to the protein but no sulfide ions are detected. It is not surprising that the apparent interaction is not evident in the CD spectra as also the CD spectrum of Zn_5-cicMTs is rather featureless.

The distinctly different features of both the CD and MCD spectra of the titrations performed in presence of sulfide ions indicate that indeed sulfide ions are incorporated into the cluster and influence the cluster structure.

7.3.1.3. Increased pH stability of Cd,S-cicMT2 compared to Cd-cicMT2

To compare the pH stability of metal ion binding for the Cd^{2+}-thiolate and Cd^{2+}-sulfide-thiolate cluster, pH titrations were performed. First, metal loaded and metal-sulfide loaded cicMT2 were reconstituted and free ions were removed via a desalting column. The resulting cicMT2 species were analyzed for their metal and sulfide ion content to approve the designated stoichiometry. pH titrations were performed and the release of Cd^{2+} ions, which are competing with the increasing amount of protons was followed with UV spectroscopy at the specific LMCT bands (Fig. 31). The overall apparent pK_a value of the metal binding ligands, i.e. the cysteine thiolate groups together with S^{2-} ions, was determined from the single major drop of the absorption by curve fitting of the pH titration data as described (6.5.3).[140]

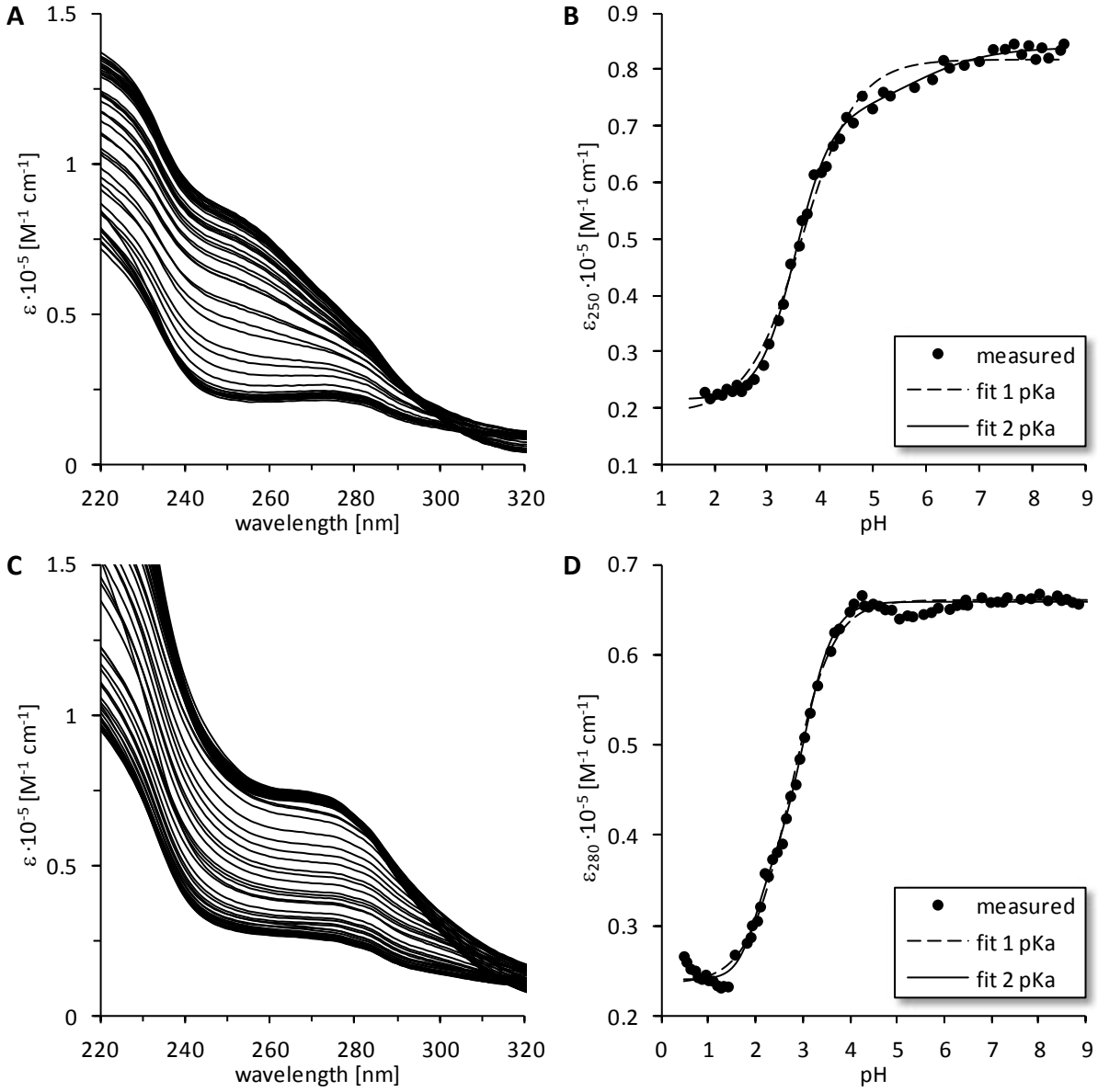

Fig. 31 UV spectra of HCl titrations to **(A)** Cd_5-cicMT2 and **(C)** Cd_9S_7-cicMT2 in 10 mM Tris-HCl, 10 mM NaCl showing the decreasing LMCT band indicative for Cd^{2+} ion release. **(B, D)** Plots of molar absorptivity against pH for HCl titration to **(B)** Cd_5-cicMT2 measured at 250 nm and to **(D)** Cd_9S_7-cicMT2 measured at 280 nm. Dots show the measured molar extinction coefficient, lines represent the fit for either one (dashed line) or two pK_a (solid line) calculated.

Tab. 11 Apparent pK_a values of cysteine residues in Cd_5-cicMT2 and Cd_9S_7-cicMT2. Data were obtained by curve fitting of pH titration data using two different equations (Tab. 11). $\mathbf{A_{MT}}$ is the absorptivity of the fully metal ion loaded protein (maximum absorption), $\mathbf{A_{MTH_m}}$ **(A)** and $\mathbf{A_{MTH_{m+n}}}$ **(B)** denote the value obtained for apo-cicMT2 after acidification (minimum absorption), $\mathbf{A_{MTH_m}}$ **(B)** is the absorptivity of the protein species obtained after the first protonation step characterized by $\mathbf{pK_2}$, and $\mathbf{m}$ **(A, B)** and $\mathbf{n}$ **(B)** are a measure for the slope of the curves.

	Cd_5-cicMT2	**Cd_9S_7-cicMT2 (at 280 nm)**	**Cd_9S_7-cicMT2 (at 250 nm)**
Eq. A			
A_{MT}	81822 ± 536	66066 ± 135	83110 ± 231
A_{MTH_m}	18941 ± 1077	23593 ± 263	29951 ± 376
pK	3.65 ± 0.03	2.73 ± 0.01	2.79 ± 0.01
m	0.85 ± 0.05	0.97 ± 0.03	1.03 ± 0.03
Adj. R^2	0.993	0.998	0.997
Eq. B			
A_{MT}	84019 ± 819	65856 ± 101	82857 ± 165
A_{MTH_m}	71352 ± 4161	36010 ± 2488	45392 ± 2971
$A_{MTH_{m+n}}$	21437 ± 481	24055 ± 203	30536 ± 280
pK_1	3.51 ± 0.02	1.97 ± 0.08	2.04 ± 0.07
pK_2	5.72 ± 0.51	3.03 ± 0.05	3.08 ± 0.05
m	1.27 ± 0.07	1.97 ± 0.37	2.35 ± 0.48
n	0.61 ± 0.29	1.38 ± 0.10	1.51 ± 0.13
Adj. R^2	0.998	0.999	0.998

The pH titration of Cd_5-cicMT2 shows a calculated pK_a of 3.65 ± 0.03 using a model with one deprotonation step, or a pK_a of 3.51 ± 0.02 using a model with two deprotonation steps (Fig. 31 A, B, Tab. 11). Both of the fitted curves are close together and indicate the pK_a for the major decrease of extinction. The fit with two deprotonation steps indeed shows the better fit parameters with an R^2 value of 0.998 compared to 0.993 (one pK_a). The value also agrees with the one reported in the literature with a pK_a of 3.44 ± 0.01 for two deprotonation steps.[136]

The pH titration of Cd_9S_7-cicMT2 evaluated at 280 nm revealed a pK_a of 2.73 ± 0.01 using a model with one deprotonation step, or a pK_a of 3.03 ± 0.05 using a model with two deprotonation steps (Fig. 31 C, D, Tab. 11). Also in this case, the fit with two deprotonation steps shows the better fit with an R^2 value of 0.999 compared to 0.998, although the difference is rather small. The same pH titration evaluated at 250 nm revealed a pK_a of 2.79 ± 0.01 using a model with one deprotonation step with an R^2 value of 0.997, or a pK_a of 3.08 ± 0.05 using a model with two deprotonation steps and an R^2 value of 0.998. For the sulfide containing form is no difference in pK_a for the evaluation at 250 nm or at 280 nm is detectable. Compared to previous published data with a pK_a of 2.95 ± 0.03 we obtained a similar result.[136]

The legitimation for using a model with more than one protonation step is discussed in detail in Freisinger[140] and Wan et al.[136]. In summary, different connection modes of the thiolate groups to the cadmium ions, i.e. bridging or terminal, reveal different energies resulting in different pK_a values. Additionally, the incorporated sulfide ions have an own pK_a. Therefore, the titration of the sulfide ion containing cluster should be fitted with three different pK_a values. But as the titration of Cd_9S_7-cicMT2 is well defined with only two pK_a values, two of the three pK_a values might overlap.

The main pK_a values fitted from titration with two pK_a values were 3.51 ± 0.02 for Cd_5-cicMT2 and 3.03 ± 0.05 for Cd_9S_7-cicMT2. The pK_a value of Cd_9S_7-cicMT2 is nearly 0.5 pH units lower than the one obtained for Cd_5-cicMT2, and hence Cd_9S_7-cicMT2 features a higher overall stability against pH-dependent metal ion loss. A higher thermodynamic stability accompanied by additional sulfide ion incorporation is already reported for phytochelatins, where the pK_a decreases from ~5.4 to ~3.9.[86] Accordingly, the pH stability of both forms of cicMT2 was significantly higher than for the corresponding complexes of fission yeast. Also compared to other plant MTs with pK_a values between 4.0 and 4.5, a pK_a of 3.51 of Cd_5-cicMT2 or 3.03 of Cd_9S_7-cicMT2 is rather low. Setting this values into relation with pH values occurring in plant cells, with a slightly alkaline pH in the cytoplasm (pH 7.4-7.5), and a pH of 4.5-6.0 in the vacuole, the pK_a of cicMT2 is lower excluding pH induced metal cluster release *in vivo*.[198]

7.3.1.4. Effect of sulfide ions on hydrodynamic radius of Cd-cicMT2

In order to evaluate the size of Cd_5-cicMT2 and Cd_9S_7-cicMT2, the hydrodynamic radii were determined with DLS and DOSY NMR.

Samples measured at a cicMT2 concentration of 100 μM show for both methods the same hydrodynamic radius in the range of the experimental error (Tab. 12, Fig. 32). In average, a hydrodynamic radius of 2.4 ± 0.2 nm was calculated for Cd_5-cicMT2. Slightly higher values were reached for Cd_9S_7-cicMT2 with a hydrodynamic radius of 2.7 ± 0.3 nm, what is an increase of 13 %. It is apparent, that the sulfide ions cause a change in the 3D shape and/or size of the molecule reflected in an altered hydrodynamic radius.

Samples measured at a cicMT2 concentration of 30 μM lead to a different result in the DLS measurement. The recording of DOSY NMR spectra was not possible at this concentration. For DLS was evaluated a hydrodynamic radius of 1.9 ± 0.1 nm for Cd_5-cicMT2 and 1.9 ± 0.2 nm for Cd_9S_7-cicMT2 (Tab. 12). At the lower concentration, no difference in the hydrodynamic radii in between the sulfide and non-sulfide containing cicMT2 species was observable.

Tab. 12 Hydrodynamic radii of Cd_5-cicMT2 and Cd_9S_7-cicMT2 measured by DOSY NMR and DLS at protein concentrations of 100 μM and 30 μM.

	DOSY NMR (100 μM cicMT2)	**DLS** (100 μM cicMT2)	**DLS** (30 μM cicMT2)
Cd_5-cicMT2	2.42 ± 0.15	2.38 ± 0.10	1.94 ± 0.07
Cd_9S_7-cicMT2	2.64 ± 0.04	2.70 ± 0.29	1.86 ± 0.16

It seems, that the hydrodynamic radius is strongly dependent on the protein concentration (Fig. 32). cicMT2 at concentrations of 100 μM seems to form weakly connected dimers or multimers, especially if sulfide ions are involved, whereat a concentration of 30 μM no difference occurs between the sulfide ion containing and lacking forms.

However, what remains unclear is the relation of the hydrodynamic radius to the molecular mass of the protein. The hydrodynamic radii expected for globular proteins assumed for Cd_5-cicMT2 with 8.4 kDa and Cd_9S_7-cicMT2 with 9.0 kDa would be 1.5 nm, what is much lower than the

measured one.[135-136] Even with the model of a linear polymer, sizes of 2.2-2.3 nm would be expected.

A similar phenomenon was observed by other empirical methods comparing the size of the cicMT2 to other proteins. By running a SDS-PAGE the Zn_5-cicMT2 appears at a size higher than 27 kDa, by running a size exclusion column it elutes with proteins of ~14 kDa with the analytical column (Superdex 75 10/300 GL), and even higher between 17 kDa and 43 kDa with the preparative column (Hiload 16/60 Superdex 75 prep grade)). Compared to this data, an average of ~30 kDa is expected, what fits to the hydrodynamic radius measurements with DLS and DOSY NMR. It could be concluded, that the cicMT2 exhibits a consistent behavior in different measurement methods of the hydrodynamic radius, while it shows a distinct different diffusion characteristic than other proteins with a similar molecular weight.

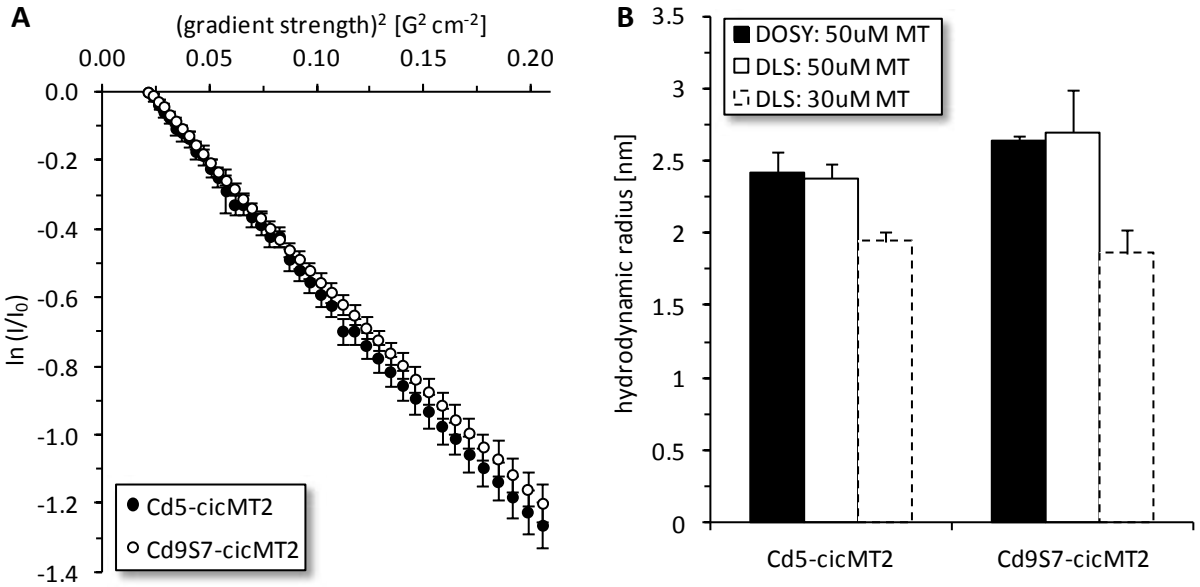

Fig. 32 Hydrodynamic radius measurements of Cd_5-cicMT2 and Cd_9S_7-cicMT2. **(A)** Plot of DOSY NMR measurements, intensity is plotted versus the gradient applied to evaluate the slope for calculating the diffusion coefficients. **(B)** Comparison of the results of DLS and DOSY NMR measurements for different hydrodynamic radii.

7.3.2. Zn^{2+} ion incorporation into cicMT2 in absence and presence of sulfide ions

7.3.2.1. Formation of Zn- and Zn,S-cicMT2 during Zn^{2+} titration

Previously we showed the incorporation of additional sulfide ions into the Cd^{2+}-thiolate cluster of cicMT2 (7.3.1).[136] To evaluate the formation of an analogous Zn,S-form apo-cicMT2 was titrated with Zn^{2+} ions in absence and presence of 10 equivalents of S^{2-} ions.[199]

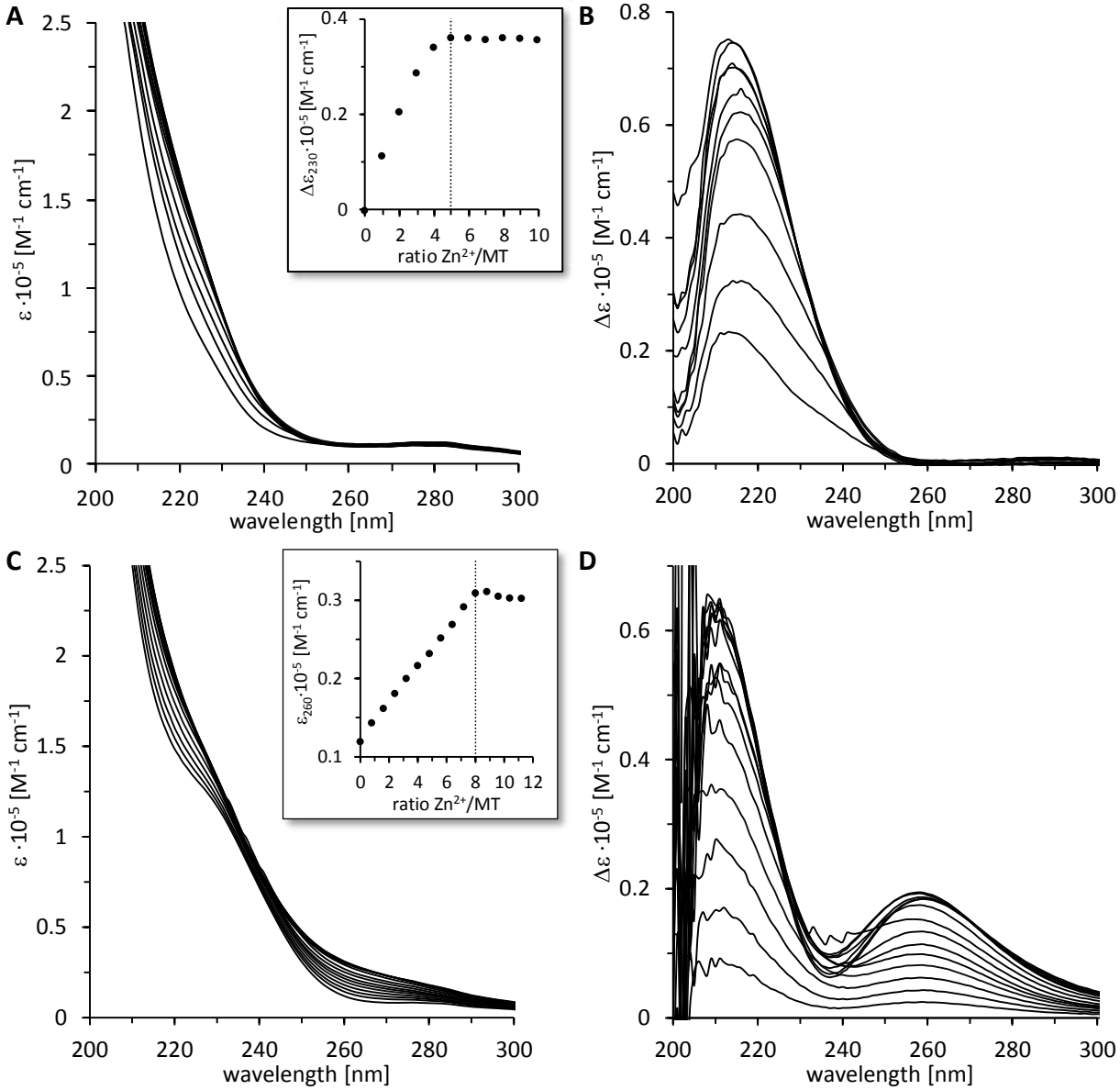

Fig. 33 UV spectra of Zn^{2+} ion titration to apo-cicMT2 in absence **(A, B)** and presence **(C, D)** of additional sulfide ions. **(A, C)** shows the UV spectra, **(B, D)** the difference plot, where the spectra with 0 equivalent of Zn^{2+} ions is subtracted from the spectra where Zn^{2+} ions were added. Apo-cicMT2 (10 μM) was titrated (in presence of 100 μM Na_2S) with increasing equivalents of metal ions (10-200 μM) in 10 mM Tris-HCl, 10 mM NaCl, pH 7.5. Insets show the plot of the molar absorptivity at the LMCT bands (230 nm and 260 nm) of the specific form against the number of equivalents of Zn^{2+} ions added to apo-cicMT2.

When titrating apo-cicMT2 in absence of sulfide ions with Zn^{2+} ions, the plot of molar absorptivity of the LMCT band at 230 nm, indicative of Zn^{2+} ion coordination to thiolate ligands, against the amount of Zn^{2+} ions added to the solution shows that the apo-protein is able to coordinate up to five Zn^{2+} ions (Fig. 33 A, B).This is as expected from the literature.[135, 175] The titration in presence of 10 equivalents of sulfide ions shows the evolution of an additional absorption band, or of multiple closely spaced bands, centered around 260 nm (Fig. 33 C, D). Analogous formation of LMCT bands in the spectral range between 260 and 280 nm has been observed during the titration of a solution containing Zn^{2+} ions and cysteine in a ratio of 1:2 with a Na_2S solution and was assigned to the formation of cysteine-capped ZnS nanocrystallites.[200] The plot of molar absorptivity at 260 nm against the equivalents of Zn^{2+} ions added shows an increase in Zn^{2+} equivalents of up to eight. As already observed in the titration with Cd^{2+} ions in presence of sulfide ions, a bathochromic shift of 30 nm of the absorption band occurs.

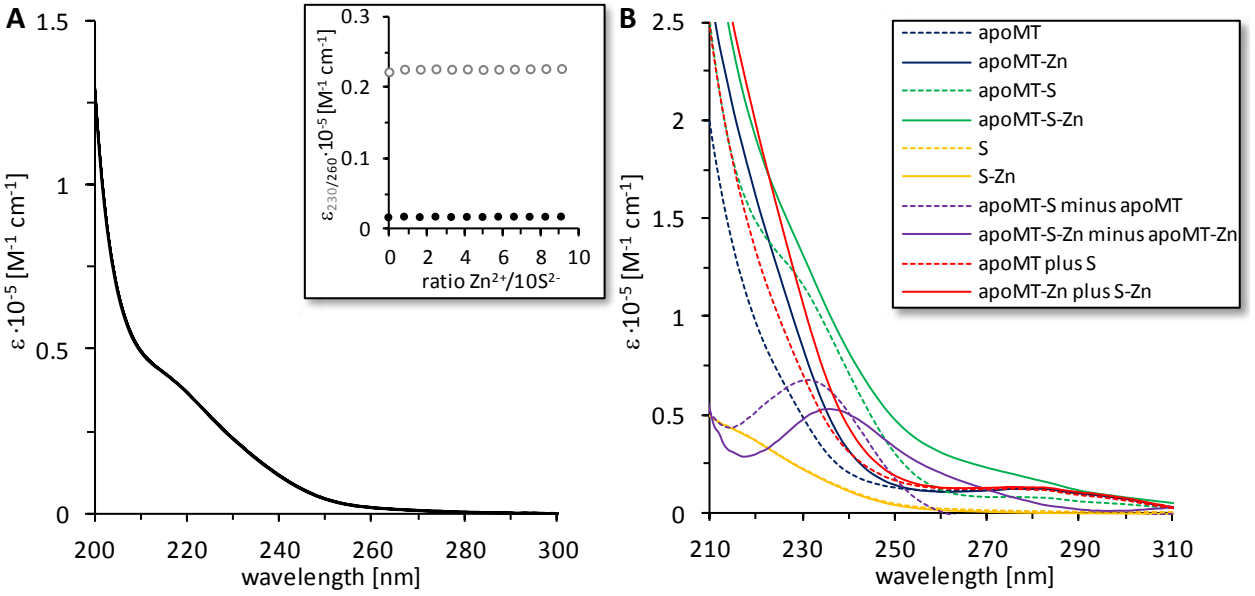

Fig. 34 **(A)** UV spectra of Zn^{2+} ion titration to S^{2-} ions. In a buffer containing 10 mM Tris-HCl, 10 mM NaCl, pH 7.5 100 µM Na_2S was added to which increasing equivalents of $ZnCl_2$ (10-90 µM) were titrated. Inset shows the plot of the molar absorptivity at the LMCT bands relevant for the Zn^{2+} ion titration with cicMT2 (230 nm and 260 nm) against the number of equivalents of Zn^{2+} ions added. **(B)** UV spectra and UV difference spectra for different forms of titrated samples are shown. Measured forms are depicted with dotted lines, calculated forms are depicted with solid lines. Blue spectra show the apo-cicMT2 and apo-cicMT2 titrated with 5 equivalents of Zn^{2+} ions; green spectra show the apo-cicMT2 supplemented with 10 equivalents of S^{2-} ions and apo-cicMT2 titrated with 8 equivalents of Zn^{2+} ions in presence of 10 equivalents of S^{2-} ions; yellow spectra show the spectra of 10 equivalents of S^{2-} ions and the spectra of 10 equivalents of S^{2-} ions titrated with 8 equivalents of Zn^{2+} ions. The purple spectra show the subtraction of the green and blue spectra (apo-cicMT2 + 10 S^{2-} minus apo-cicMT2; apo-cicMT2 + 10 S^{2-} + 8 Zn^{2+} minus apo-cicMT2 + 8 Zn^{2+}), and the red spectra show the addition of the blue and yellow spectra (apo-cicMT2 plus 10 S^{2-}; apo-cicMT2 + 5 Zn^{2+} plus 10 S^{2-} + 8 Zn^{2+}).

To verify that the change of the absorption profile does not originate from Zn,S-cluster formation in solution, Zn^{2+} ions were titrated to S^{2-} ions under the same conditions as the Zn^{2+} ions to cicMT2 titrations were performed (Fig. 34 A). The solution with S^{2-} ions only shows a band at 220 nm, however, this spectrum shows no changes when Zn^{2+} ions are added. This indicates that change

in the absorption spectra of the Zn^{2+} ion titration to S^{2-} ion supplemented apo-cicMT2 originates from the interaction of sulfide ions with the metallothionein.

For further clarification, difference spectra were calculated (Fig. 34 B). The spectra of apo-cicMT2 was subtracted from apo-cicMT2 + 10 S^{2-} ions. The spectrum is not at all overlapping with the spectrum of the S^{2-} ions alone in solution. The spectrum of apo-cicMT2 + 8 Zn^{2+} ions was also subtracted from the spectrum of apo-cicMT2 + 10 S^{2-} ion + 8 Zn^{2+} ions. Just as the starting form, also the final form after titration is not overlapping with 10 S^{2-} ions + 8 Zn^{2+} ions. In fact a strong band at 235-240 nm is appearing. Performing the test the other way around, i.e. summing up the spectra of apo-cicMT2 and 10 S^{2-} and also summing up apo-cicMT2 + 5 Zn^{2+} ions and 10 S^{2-} ions + 8 Zn^{2+} ions does not lead to the spectrum of apo-cicMT2 + 10 S^{2-} ions or apo-cicMT2 + 10 S^{2-} ions+ 8 Zn^{2+} ions, respectively. The calculated spectra support the conclusion, that the S^{2-} ions added to apo-cicMT2 interact with the metallothionein and are not independent in solution. The titration of Zn^{2+} ions in presence of S^{2-} ions leads to an interaction of the sulfide ions with the metallothionein and/or the metal ions.

Additional support for the changes in the cluster structure in presence of sulfide ions is provided by the measured CD spectra (Fig. 35 B). Under the same conditions as the UV spectra were measured, also the initial and final CD spectra of the titrations were recorded. By comparison of the Zn-cicMT2 form with the Zn,S-cicMT2 form, a general rearrangement of the cluster structure is visible.

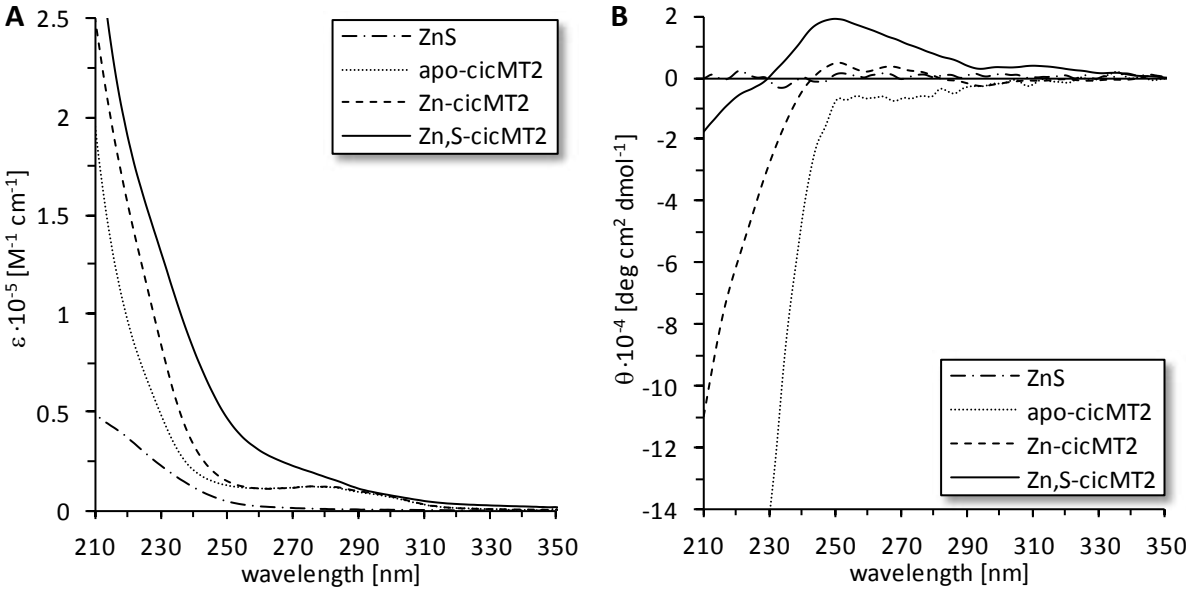

Fig. 35 UV **(A)** and CD **(B)** spectra of the final forms of titrated apo-cicMT2 (dotted line) with Zn^{2+} ions in absence (dashed line) and presence (solid line) of sulfide ions, and of the final form of titrated sulfide ions with Zn^{2+} ions in absence of cicMT2 (dashed-dotted line). Concentrations and conditions according to Fig. 33 and Fig. 34 A.

Zn-cicMT2 shows a similar spectrum as the Zn-form of SpMTA from sea urchin and the Zn-form of MTN from drosophila.[201-202] The sulfide ion containing form however shows a similarity to the Zn-form MT1 from mouse.[201, 203] Compared to the Zn-cicMT2 form, in the Zn,S-cicMT2 form a clear band at 250 nm is evolving. As shown with the CD spectrum of Zn^{2+} ion titrated S^{2-} ions, this

band at 250 nm cannot originate from ZnS-clusters in solution since they do not show any chirality. The rearrangement of the metal-thiolate cluster between Zn-cicMT2 and Zn,S-cicMT2 is not so clear as with Cd_5-cicMT2 and Cd_9S_7-cicMT2, but the CD spectra show a distinct difference.

7.3.2.2. Stoichiometry of the sulfide ion containing Zn^{2+}-form of cicMT2

To determine the sulfide ion content of the titrated Zn-form and Zn,S-form of cicMT2, excess metal and sulfide ions were removed via size exclusion chromatography. Both cicMT2 forms eluted in a main monomeric peak at 13.5 mL next to some minor peaks at lower elution volume (see 7.3.1.1). The monomeric peak was analyzed with F-AAS, 2-PDS assay and the methylene blue method and the stoichiometric composition was calculated. This resulted in $Zn_{5.8}$-cicMT2 in absence of sulfide ions and $Zn_{7.9\pm0.6}S_{7.4\pm1.2}$-cicMT2 titrated in presence of sulfide ions.

Surprisingly, similar metal and sulfide ion ratios were obtained for the titration with Cd^{2+} ions and Zn^{2+} ions in presence of S^{2-} ions. Previous literature reported that the Zn^{2+} and S^{2-} contents of Zn,S-MTs were usually around 50 % lower than the Cd^{2+} and S^{2-} ion contents of the respective Cd,S-MT.[58, 81, 83] It has to be noted however, that these literature values are for species directly isolated from *E. coli* and not obtained by systematic titration experiments as described here.

The calculated ratio of metal ion load of titrated cicMT2 in presence and absence of ten equivalents of sulfide ions for Zn^{2+} ions is 1.4 ± 0.1 showing a clear increase of the Zn^{2+} ion binding capacity in presence of sulfide ions. The gain of metal binding capacity is only 18 % lower than for the Cd^{2+}-form with 1.7 ± 0.3.

The ratio of additionally incorporated equivalent of Zn^{2+} ions per S^{2-} ions is 0.39 ± 0.07. This value is again 20 % lower than for the Cd^{2+}-form and equals roughly 2.5 S^{2-} ions for each additional Zn^{2+} ion added. The overall negative charge is therefore increasing even more than with the Cd^{2+}-form suggesting a destabilization of the system due to charge repulsion. Nevertheless it agrees with the general trend reported for the Cd^{2+}-forms.[81]

Examining the ratios between bound metal ions and the combined content of sulfide ions and cysteine thiolate groups the calculated ratios are 0.42 for $Zn_{5.8}$-cicMT2 and 0.37 ± 0.06 for $Zn_{7.9}S_{7.4}$-cicMT2. Again, these values are similar to the ones measured for the Cd^{2+}-form (0.35 and 0.40).

All in all the ratios obtained for Zn-cicMT2 and Zn,S-cicMT2 are comparable to the one of Cd-cicMT2 and Cd,S-cicMT2 and the difference between the two metal ions is marginal.

7.3.2.3. Increased pH stability of Zn,S-cicMT2 compared to Zn-cicMT2

To compare the pH stability of metal ion binding for the Zn^{2+}-thiolate and Zn^{2+}-sulfide-thiolate cluster, pH titrations were performed. First, metal loaded and metal-sulfide loaded cicMT2 was reconstituted and free ions were removed using desalting column. The resulting species of cicMT2s were analyzed regarding their metal and sulfide ion content to approve the designated stoichiometry. pH titrations were performed and the Zn^{2+} ion release was followed with UV spectroscopy at the specific LMCT bands (Fig. 36). The overall apparent pK_a value of the metal

binding ligands, i.e. the cysteine thiolate groups together with S^{2-} ions, was determined from the single major drop of the absorption by curve fitting of the pH titration data as described.[140]

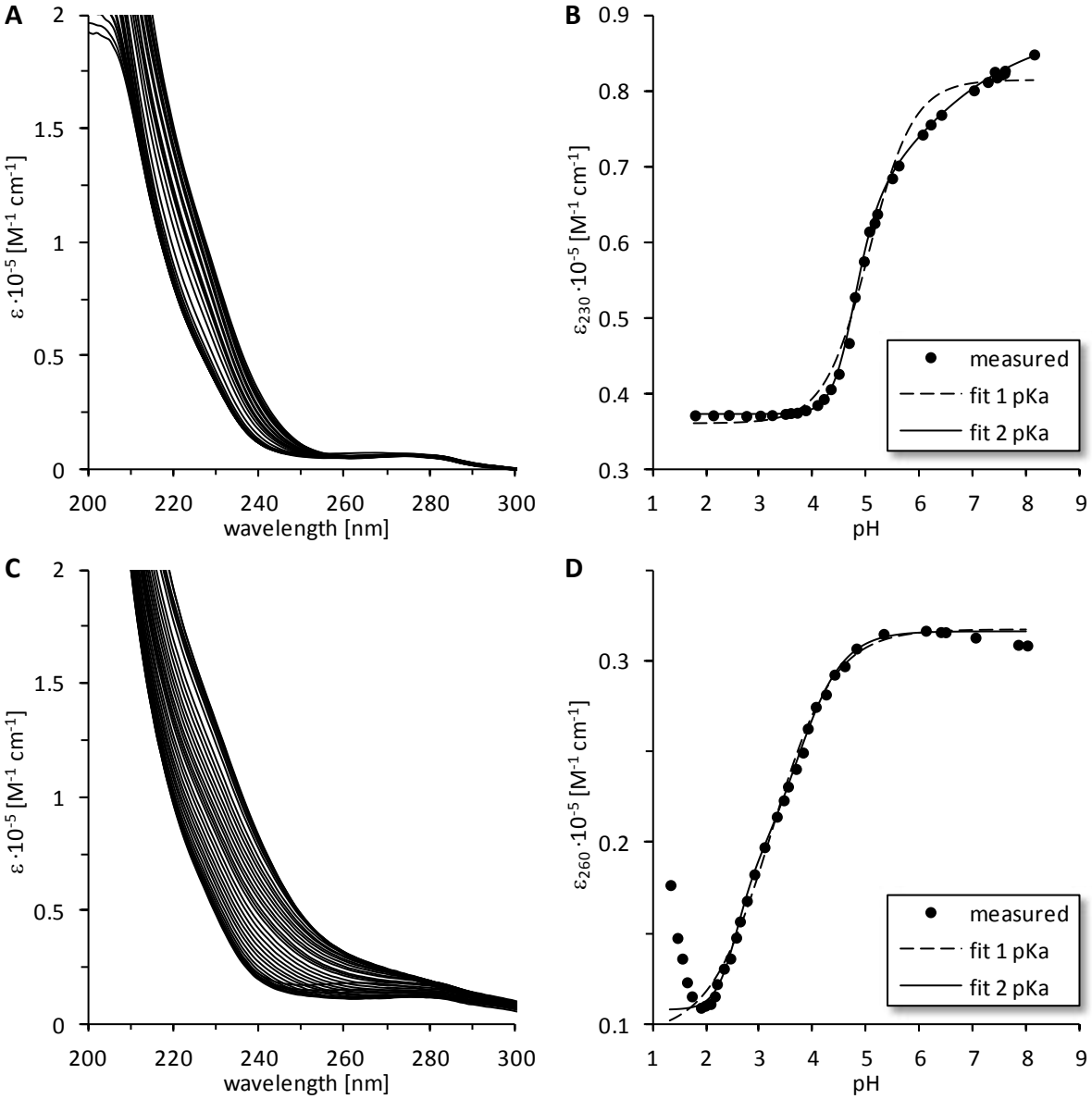

Fig. 36 UV spectra of HCl titration to **(A)** Zn_5-cicMT2 and **(C)** Zn_8S_7-cicMT2 in 10 mM Tris-HCl, 10 mM NaCl showing the decreasing LMCT band for Zn^{2+} ion release. **(B, D)** Plots of molar absorptivity against pH for HCl titration to **(B)** Zn_5-cicMT2 measured at 230 nm and to **(D)** Zn_8S_7-cicMT2 measured at 260 nm. Dots show the measured molar extinction coefficient, lines the fit for either one (dashed line) or two pK_a (solid line) calculated.

The pH titration of Zn_5-cicMT2 shows a calculated pK_a of 5.07 ± 0.03 using a model with one deprotonation step, or a main pK_a of 4.90 ± 0.16 using a model with two deprotonation steps (Fig. 36 A, B, Tab. 13). Both pK_a values are close together and indicate the pK_a for the major decrease of the molar extinction coefficient. Using the equation with two pK_a values a better fit with an R^2 value of 0.999 is obtained compared to 0.991 considering just a single pK_a value. The value is slightly higher than the one previously determined for two deprotonation steps (4.60 ± 0.01).[175]

The pH titration of Zn_8S_7-cicMT2 evaluated at 260 nm revealed a pK_a of 3.24 ± 0.03 using a model with one deprotonation step, or a main pK_a of 3.72 ± 0.06 using a model with two deprotonation steps (Fig. 36 C, D, Tab. 13). Also there, the fit with two deprotonation steps shows the better fit with an R^2 value of 0.999 compared to 0.997, although the difference is rather small. The same pH titration evaluated at 230 nm revealed a pK_a of 3.31 ± 0.06 using a model with one deprotonation step with an R^2 value of 0.997, or a pK_a of 3.86 ± 0.09 using a model with two deprotonation steps and an R^2 value of 0.999. For the sulfide containing form nearly no difference in pK_a for the evaluation at 230 nm or at 260 nm is detectable.

Tab. 13 Apparent pK_a values of cysteine residues in Zn_5-cicMT2 and Zn_8S_7-cicMT2. Data were obtained by curve fitting of pH titration data using two different equations (Tab. 11). $\mathbf{A_{MT}}$ is the absorptivity of the fully metal ion loaded protein (maximum absorption), $\mathbf{A_{MTH_m}}$ **(A)** and $\mathbf{A_{MTH_{m+n}}}$ **(B)** denote the value obtained for apo-cicMT2 after acidification (minimum absorption), $\mathbf{A_{MTH_m}}$ **(B)** is the absorptivity of the protein species obtained after the first protonation step characterized by $\mathbf{pK_2}$, and $\mathbf{m}$ **(A, B)** and $\mathbf{n}$ **(B)** are a measure for the slope of the curves.

	Zn_5-cicMT2	**Zn_8S_7-cicMT2 (at 260 nm)**	**Zn_8S_7-cicMT2 (at 230 nm)**
Eq. A			
A_{MT}	81433 ± 624	31719 ± 180	133131 ± 943
A_{MTH_m}	36137 ±660	9364 ± 322	32364 ± 2562
pK	5.07 ± 0.03	3.24 ± 0.03	3.31 ± 0.06
m	1.05 ± 0.08	0.75 ± 0.03	0.43 ± 0.02
Adj. R^2	0.991	0.997	0.997
Eq. B			
A_{MT}	88483 ± 3627	31641 ± 77	131871 ± 475
A_{MTH_m}	36690 ± 51634	17580 ± 950	58963 ± 4017
$A_{MTH_{m+n}}$	37290 ± 158	10785 ± 93	47332 ± 472
pK_1	4.90 ± 0.16	2.55 ± 0.04	2.27 ± 0.04
pK_2	4.70 ± 2.35	3.72 ± 0.06	3.86 ± 0.09
m	1.86 ± 0.10	2.12 ± 0.19	2.13 ± 0.27
n	0.31 ± 0.18	1.00 ± 0.06	0.56 ± 0.03
Adj. R^2	0.999	0.999	0.999

As already seen for the pH titration of the Cd- and Cd,S-form of cicMT2 (7.3.1.3) it is legitimate to use a model with two different protonation steps. Once for the different connection modes of the thiolate groups to the zinc ions, i.e. bridging or terminal, and second for the incorporated sulfide ions.[136, 140] As visible from the shape of the curve and the calculated m (Hill coefficient), the steepness of the fit with one pK_a is less pronounced and spread over a larger pH range for the sample with incorporated sulfide ions than for the sulfide ion lacking form. With two protonation steps, Zn_5-cicMT2 shows a clear step at a pK_a of 4.90 ± 0.16, indicated by the high m-value and the low standard deviation, whereat the one at 4.70 ± 2.35 is badly resolved (low n-value, high standard deviation). Zn_8S_7-cicMT2 however shows a larger steepness and a lower standard deviation for both pK_a values, meaning that both pK_a values are contributing to the overall pK_a. As the pK_a values at 3.7 and 3.9 are nearer to the one of Zn_5-cicMT2 (pK_a of 4.9), the one at 2.1 might originate from the additional sulfide ligands.

Taking the best fit for both forms, we calculated a pK_a of 4.90 ± 0.16 for Zn_5-cicMT2 and a pK_a of 3.72 ± 0.06 for Zn_8S_7-cicMT2. The pK_a value of Zn_8S_7-cicMT2 is nearly 1.2 pH units lower than the

one obtained for Zn_5-cicMT2, and hence Zn_8S_7-cicMT2 features a higher overall stability against pH-dependent metal loss. This stabilization is more than doubled compared to the Cd^{2+}-forms, where the difference in pH is 0.5 pH units. But it is in accordance with the tendency of a thermodynamic stabilization in presence of additional sulfide ions. Just as the Cd^{2+}-forms, also the Zn^{2+}-forms of cicMT2 have a pK_a value lower than the pH range occurring in the cell avoiding pH induced metal release.

7.3.2.4. Effect of sulfide ions on the hydrodynamic radius of Zn-cicMT2

In order to evaluate the size of Zn_5-cicMT2 and Zn_8S_7-cicMT2, the hydrodynamic radii were determined with DLS and DOSY NMR.

Tab. 14 Hydrodynamic radii of Zn_5-cicMT2 and Zn_8S_7-cicMT2 measured by DOSY NMR and DLS at protein concentrations of 65 μM and 30 μM.

	DOSY NMR (65 μM cicMT2)	**DLS** (65 μM cicMT2)	**DLS** (30 μM cicMT2)
Zn_5-cicMT2	2.43 ± 0.30	2.53 ± 0.09	1.86 ± 0.08
Zn_8S_7-cicMT2	-	-	1.53 ± 0.18

Zn_5-cicMT2 was measured at a protein concentration of 65 μM with both methods and an average hydrodynamic radius of 2.5 ± 0.3 nm was calculated (Tab. 14). At a cicMT2 concentration of 30 μM the sample revealed a 26 % lower hydrodynamic radius of 1.9 ± 0.1 nm according to DLS measurements. As already seen for the Cd^{2+}-form, the evaluated hydrodynamic radius is smaller with lower protein concentrations (7.3.1.4). Nevertheless, the results are comparable to the values obtained for Cd_5-cicMT2, with a hydrodynamic radius of 2.4 ± 0.2 nm with 100 μM cicMT2 and one of 1.9 ± 0.1 nm with 30 μM cicMT2. The hydrodynamic radius of cicMT2 seems to depend more on the protein concentration than on the metal ions incorporated. As already discussed for the Cd^{2+}-form (7.3.1.4), the obtained values are much higher than the expected one of 1.5 nm for a globular protein with a weight of 8.1 kDa. This leads to the conclusion, that cicMT2 is either not a globular protein but rather a linear polymer or cicMT2 appears as multimer for higher protein concentrations than used for mass analysis.

The sulfide ion containing form Zn_8S_7-cicMT2 was measured at a protein concentration of 30 μM with DLS and yielded a hydrodynamic radius of 1.5 ± 0.2 nm, what is remarkably lower than the corresponding Zn_5-cicMT2 of 1.9 ± 0.1 nm. The obtained value for Zn_8S_7-cicMT2 corresponds to the hydrodynamic radius of other proteins with a size of 8.5 kDa what is in contrast to the other measurements of Cd_5-cicMT2, Cd_9S_7-cicMT2, and Zn_5-cicMT2.

In summary, the hydrodynamic radius is strongly dependent on the sample concentration and is not comparable with other similar sized proteins.

7.3.3. Ag^+ ion incorporation into cicMT2 in absence and presence of sulfide ions

7.3.3.1. Formation of Ag- and Ag,S-cicMT2 during Ag^+ titration

So far, in cicMT2 only the formation of metal-thiolate clusters with divalent metals ions as Zn^{2+} and Cd^{2+} ions is reported, and accordingly the incorporation of sulfide ions with these metal ions (7.3.1, 7.3.2). To evaluate the formation of an analogous sulfide containing form with monovalent metal ions metal titrations of Zn_5-cicMT2 were performed with Ag^+ ions in absence and presence of 10 equivalents of S^{2-} ions.

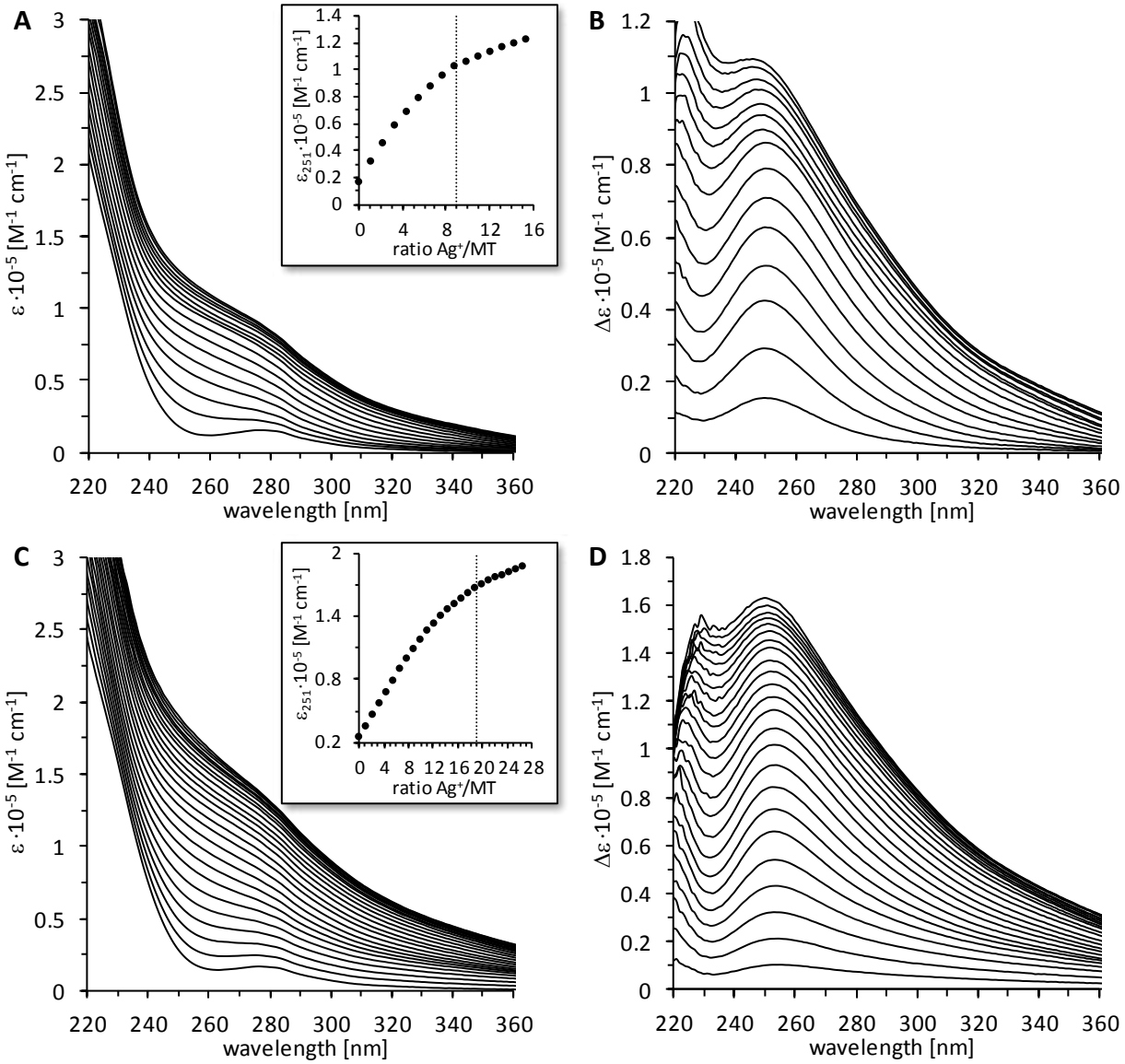

Fig. 37 UV spectra of Ag^+ ion titration to Zn_5-cicMT2 in absence **(A, B)** and presence **(C, D)** of additional sulfide ions. **(A, C)** shows the UV spectra, **(B, D)** the difference plot, where the spectrum with 0 equivalent of Ag^+ ions is subtracted from the spectra where Ag^+ ions were added. Zn_5-cicMT2 (10 μM) was titrated (in presence of 100 μM Na_2S) with increasing equivalents of metal ions (10-300 μM) in 10 mM Tris-HCl, 10 mM NaCl, pH 7.5. Insets show the plot of the molar absorptivity at the LMCT bands at 251 nm against the number of equivalents of Ag^+ ions added to Zn_5-cicMT2.

By titrating Zn_5-cicMT2 in absence of sulfide ions with Ag^+ ions, the plot of molar absorptivity of the LMCT band at 251 nm, indicative for Ag^+ ion coordination to thiolate ligands, against the amount of Ag^+ ions added to the solution shows an unclear picture (Fig. 37 A, B). One might suggest, that cicMT2 is coordinating nine Ag^+ ions due to the fact, that the plot of molar absorptivity against the ratio of Ag^+ ions to cicMT2 shows a clear change in the slope at nine equivalent of Ag^+ ions added (Fig. 39). Yet, the molar absorptivity after nine equivalents (10-20 equivalents) still has a slope higher than zero, but the increase in molar absorptivity is much smaller than for the first part of the titration (0-9 equivalents).

Repeating the same Ag^+ ion titration in presence of sulfide ions, the LMCT band was evolving at the same wavelength as witnessed without sulfide ions (Fig. 37 C, D). There is no bathochromic shift of the absorption envelope observable as shown for Zn^{2+} or Cd^{2+} ions in presence of sulfide ions. Also for this combination, the plot of molar absorptivity against the equivalents of added Ag^+ ions shows an unclear picture. In the first part of the titration (0-~11 equivalents) a constant slope is visible followed by a reduction of the slope, which converts again into a static slope (~19-28 equivalent), as displayed in Fig. 39. A transition phase is located between the 11th and 19th equivalent where a change in coordination takes place. A possible interpretation is, that 19 equivalent of Ag^+ ions are incorporated, and the following increase in molar absorptivity is caused by other effects.

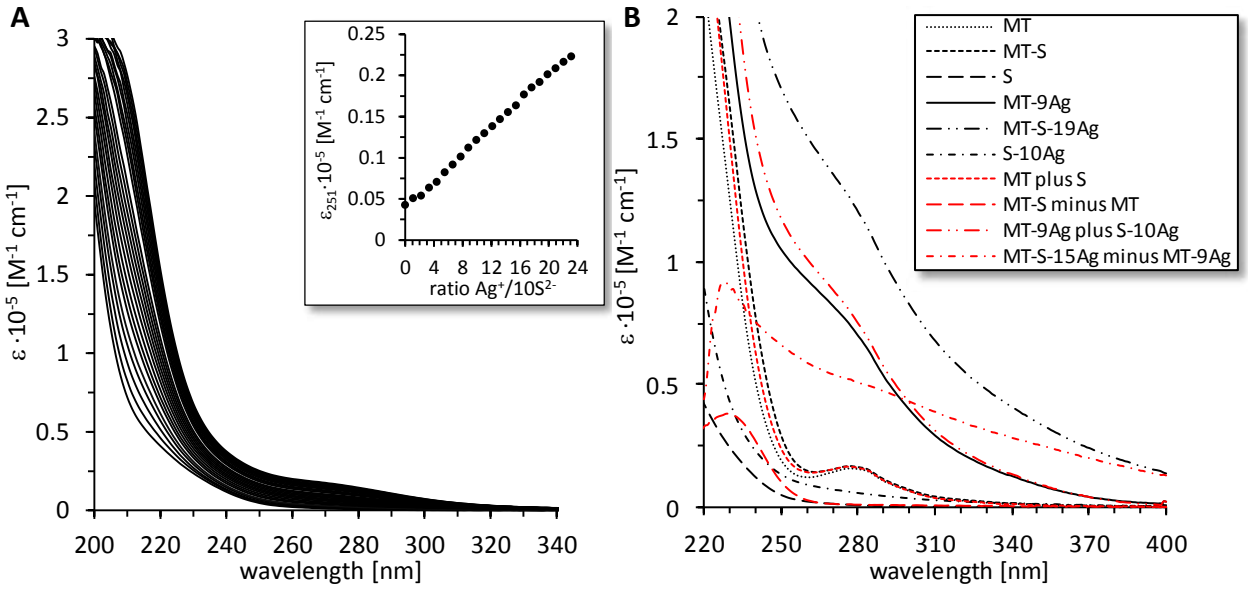

Fig. 38 **(A)** UV spectra of Ag^+ ion titration to S^{2-} ions. 100 µM Na_2S was titrated with increasing equivalents of $AgNO_3$ (10-250 µM) in 10 mM Tris-HCl, 10 mM NaCl, pH 7.5. Insets show the plot of the molar absorptivity at the LMCT band relevant for the Ag^+ ion titration with cicMT2 (251 nm) against the number of equivalents of Ag^+ ions added. **(B)** UV spectra (black) and UV difference spectra (red) for different forms of titrated samples as indicated in legend. MT corresponds to 1 equivalent Zn_5-cicMT2, S corresponds to 10 equivalent S^{2-} ions, Ag corresponds to indicated equivalents of Ag^+ ions. Compounds of mixed samples are separated by hyphen. Sort of lines for the red spectra correspond to the expected black ones, if sulfide ions are not interacting with cicMT2 and are solely in solution.

For titration with silver ions, it is difficult to determine precise numbers of incorporated Ag^+ ions. But it is clearly visible, that in presence and absence of sulfide ions the plot of molar absorptivity

against the ratio of Ag^+ ions to cicMT2 varies. To exclude, that this variation originates from Ag,S-clusters formed in solution, but rather from an interaction of sulfide ions with the metal cluster of the metallothionein, a titration of 10 equivalents of S^{2-} ions with Ag^+ ions is performed under the same conditions as the protein titrations were done (Fig. 38 A). At the wavelengths of 210 nm and 270 nm bands are evolving, as well as at 251 nm where the LMCT band of Ag^+ ions to the sulfide ions and thiolates appears. Here a constant increase of the absorption is evidenced. This constant increase however, has a more than tenfold lower slope than the slope of the titrated cicMT2. The increase in the absorption spectra of Ag,S-cicMT2 can therefore not originate from Ag,S-clusters in solution.

For further clarification, difference spectra were calculated in order to show the interaction of the sulfide ions with the metal-thiolate cluster of cicMT2 (Fig. 38 B). If an independent formation of Ag,S-clusters in solution would occur, the calculated spectra should overlap with the measured spectra. The addition of the spectra of 10 μM Zn_5-cicMT2 and of 100 μM S^{2-} ions should result in 10 μM Zn_5-cicMT2 + 100 μM S^{2-} ions; the subtraction of the spectra of 10 μM Zn_5-cicMT2 from 10 μM Zn_5-cicMT2 + 100 μM S^{2-} ions should result in the same spectra as 100 μM S^{2-} ions alone; the addition of the spectra of 10 μM Zn_5-cicMT2 + 90 μM Ag^+ ions and 100 μM S^{2-} ions + 100 μM Ag^+ ions should result in 10 μM Zn_5-cicMT2 + 100 μM S^{2-} + 190 μM Ag^+ ions; and the subtraction of the spectra of 10 μM Zn_5-cicMT2 + 90 μM Ag^+ ions from 10 μM Zn_5-cicMT2 + 100 μM S^{2-} ions + 190 μM Ag^+ ions should result in 100 μM S^{2-} ions + 100 μM Ag^+ ions. But none of the spectra are overlapping with the expected ones presuming an independent formation of Ag,S-clusters indicating the interaction of the sulfide ions with Ag-cicMT2.

A

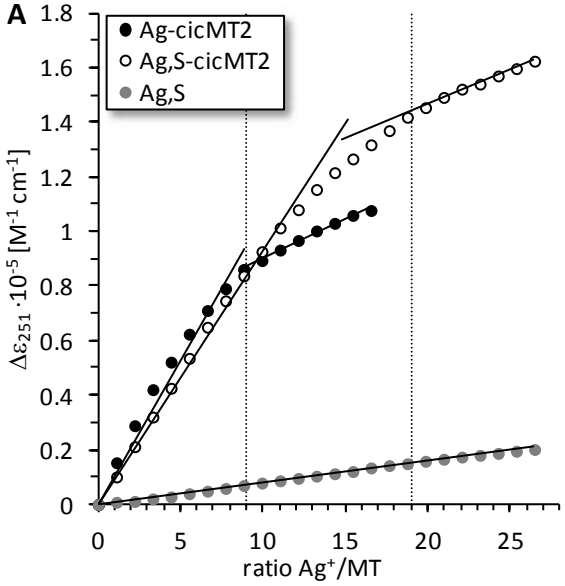

B

	region of analysis	slope [M^{-1} cm^{-1} per equivalent]
Ag-cicMT2	0-9 equivalents	10'625
	10-17 equivalents	7532
Ag,S-cicMT2	0-11 equivalents	9333
	19-28 equivalents	6629
Ag,S	0-27 equivalents	782

Fig. 39 **(A)** Plot of molar absorptivity at the LMCT band at 251 nm against the number of equivalents of Ag^+ ions added to Zn_5-cicMT2 (black circles of Fig. 37 A), to Zn_5-cicMT2 + S^{2-} ions (empty circles of Fig. 37 C), and to S^{2-} ions (grey circles of Fig. 38 A). Slopes and points of change of the slope are indicated. (B) List of calculated slopes for the specific region of analysis.

The assumption of sulfide ion incorporation into the silver-thiolate cluster of cicMT2 is also supported by the steepness of the slopes of the molar absorptivity plotted against the number of equivalents of Ag^+ ions added to Zn_5-cicMT2 (Fig. 39). The slopes of the initial increase of

Ag-cicMT2 is 10'625 M^{-1} cm^{-1} per equivalent of Ag^+ ions and of Ag,S-cicMT2 with 9333 M^{-1} cm^{-1} per equivalent of Ag^+ ions added. At this stage, the slopes are comparable, and also during excess addition of Ag^+ ions, the increase of molar absorptivity of Ag-cicMT2 with 7532 M^{-1} cm^{-1} per equivalent of Ag^+ ions and Ag,S-cicMT2 with 6629 M^{-1} cm^{-1} per equivalent of Ag^+ ions are similar. The slope of Ag^+ ions titrated to only S^{2-} ions shows an increase of molar absorptivity of 782 M^{-1} cm^{-1} per equivalent of Ag^+ ions, however, it is ten times lower than the increase during addition of excess of Ag^+ ions to cicMT2. This is an additional indication for the incorporation of sulfide ions into the Ag^+-thiolate cluster of cicMT2.

Additional support for the changes in the cluster structure in presence of sulfide ions comes from the measured CD spectra (Fig. 40 B). Initial and final CD spectra of the titrations were measured using the same conditions as for the UV spectra. By comparison of the Ag-cicMT2 with the Ag,S-cicMT2, a general rearrangement of the cluster structure is visible.

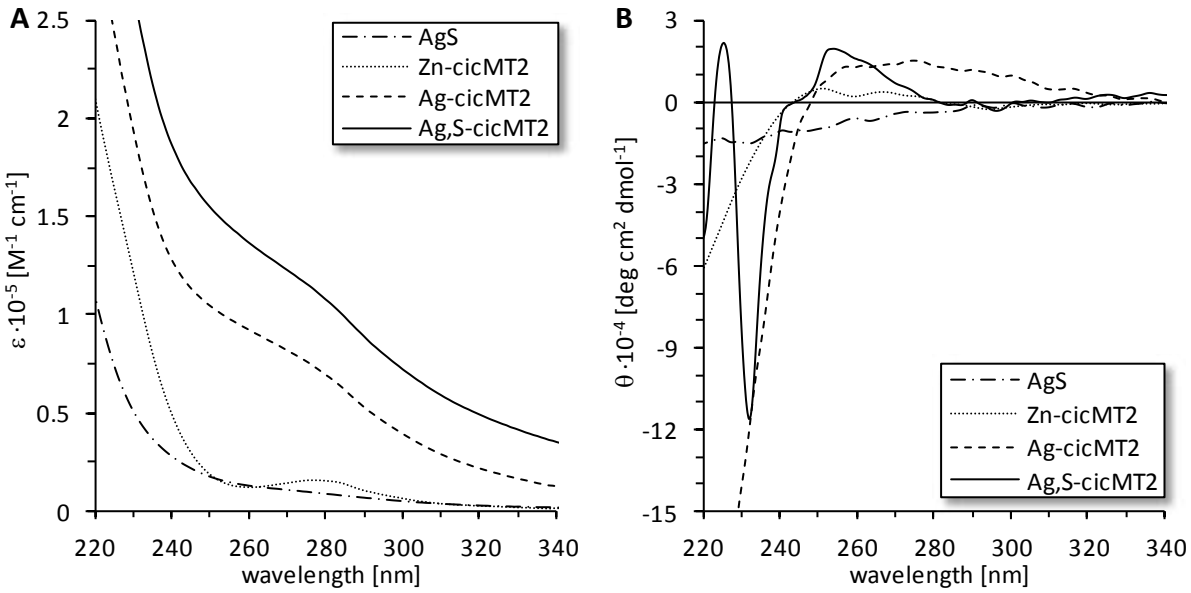

Fig. 40 UV **(A)** and CD **(B)** spectra of the final forms of titrated Zn_5-cicMT2 (dotted line) with Ag^+ ions in absence (dashed line) and presence (solid line) of sulfide ions, and of the final form of titrated sulfide ions with Ag^+ ions in absence of cicMT2 (dashed-dotted line). Concentrations and conditions as indicated in Fig. 37 and Fig. 38.

Ag-cicMT2 shows a monophasic CD profile with a maximum around 280 nm with a cross-over point at 248 m. Compared to the distinct bands observed for the Ag^+-thiolate cluster of mammalian MT1 titrated at pH 2.5 the profile of Ag-cicMT2 is relatively broad.[45, 204] Comparing Ag-cicMT2 with mammalian Ag-MT1 titrated both at neutral pH the spectra show similar broad, overlapping bands. The difference observed may arise from the initial spectra of the MTs: the pre-fold Zn-MT titrated at pH 7.5 and the unstructured apo-MT titrated at pH 2.5. From the shape of the CD band, it seems that Zn-MT folds differently than Ag-MT. By titrating Zn-MT with Ag^+ ions, the structure might not completely change to the structure of Ag-MT as observed for the titration with apo-MT resulting in a broad spectrum. The different connectivities of monovalent metal ions compared to divalent metal ion coordination to metallothioneins have already been shown.[205]

Monovalent metal ions coordinate mainly in trigonal or even diagonal modes, whereas the divalent metal ions show a dominant tetrahedral coordination.

The CD spectrum of Zn_5-cicMT2 titrated with Ag^+ ions in presence of sulfide ions shows a clear biphasic profile with extrema located at (+)225 nm, at (-)232 nm, and at (+)254 nm. The bands are well defined and cover a narrow wavelength region. Compared to the spectrum of Cd,S-cicMT2 (Fig. 30) the bands are clearly blue shifted probably caused by the more open structure of the larger metal-sulfide-thiolate cluster. Comparing the CD spectra of Ag-cicMT2 and Ag,S-cicMT2 a clear rearrangement of the cluster can be observed.

The CD spectrum of Ag^+ ion titrated S^{2-} ions shows no chirality. Therefore, the newly observed bands in the CD spectrum of Ag,S-cicMT2 are not originating from Ag,S-clusters in solution. They rather have to arise from sulfide ions incorporated into the metal-thiolate cluster of cicMT2.

7.3.3.2. Stoichiometry of Ag-cicMT2 and Ag,S-cicMT2

For further analysis of the amount of sulfide ions bound to cicMT2, excess metal and sulfide ions were removed via size exclusion chromatography from titrated Ag-cicMT2 and Ag,S-cicMT2. Both cicMT2 forms eluted in a main monomeric peak at 13.5 mL next to minor peaks at lower elution volume (see 7.3.1.1). The monomeric peak was analyzed with F-AAS, 2-PDS assay and the methylene blue method and the stoichiometric composition was calculated. Results showed a stoichiometry of $Ag_{10.6\pm0.5}S_{0.3}$-cicMT2 in absence of sulfide ions and $Ag_{18.3\pm2.8}S_{1.5\pm0.2}$-cicMT2 in presence of sulfide ions. These values for the Ag^+:cicMT2 ratios are in the same range as the ones obtained from titration with stoichiometries of Ag_9-cicMT2 and $Ag_{19}S_x$-cicMT2, respectively. The reliability of these values is however uncertain. Due to the low pK_a values of Ag-MTs the pH has to be decreased below pH 2 to release the Ag^+ ions completely from cicMT2. Under such conditions it is not clear, if the reaction with the 2-PDS used for the cysteine and sulfide ion content determination works properly, or if part of the thiolate groups of the cysteines and the sulfide ions are still blocked by Ag^+ ions and are not available for the reaction with the 2-PDS.

Apart from this problem, we were able for the first time to report the sulfide ion incorporation in presence of monovalent metal ions such as Ag^+ ions. The low amount of incorporated S^{2-} ions and also the missing bathochromic shift in the absorption spectra might be the reason for the absence of *in vitro* Ag,S-MTs in previous literature. Additionally, isolated Zn- and Cd-forms of *E. coli* showed a lower amount of incorporated S^{2-} ions than *in vitro* reconstituted forms, what would decrease the low level of sulfide ion incorporated even more, making it impossible to detect the S^{2-} ions anymore.[81, 83]

Nevertheless, the calculated ratios of metal ion load of titrated cicMT2 in presence and absence of ten equivalent of sulfide ions for Ag,S-cicMT2:Ag-cicMT2 is 1.7 ± 0.3. This is exactly the same as measured for the Cd^{2+}-form and shows a clear increase of the Ag^+ ion binding capacity in presence of sulfide ions.

The ratio of additionally added equivalent of Ag^+ ions per S^{2-} ions is 5.62 ± 1.11. This value is significantly higher than the one measured for divalent metal ions with an average ratio 0.44 ± 0.13 (0.49 ± 0.11 of Cd^{2+} ions and 0.39 ± 0.07 of Zn^{2+} ions). For divalent metal ions the overall charge is increasing by two more negative charges for each additionally incorporated

metal ion destabilizing the cluster assembly by charge repulsion. A different picture is evidenced by complexes with monovalent metal ions incorporated. The overall charge of -6 of sulfide ion lacking forms decreases slightly to -4 in sulfide ion containing forms. The lower charge compared to divalent metal ion complexes should stabilize monovalent metal-sulfide clusters and make them preferable over divalent metal-sulfide complexes.

Examining the ratios between bound metal ions and the combined content of sulfide ions and cysteine thiolate groups the calculated ratios are 0.74 ± 0.04 for $Ag_{10.6}S_{0.3}$-cicMT2 and 1.18 ± 0.26 for $Ag_{18.3}S_{1.5}$-cicMT2. Again these values are much higher than the ones measured for the divalent metal ions. Although the values for the divalent metal ions agree well with the one reported by Capdevila et al.[81], the ones of monovalent metal ion complexes with and without sulfide ions are higher than all the previous reported values. These high values indicate that monovalent metal ion containing cicMT2 could be a strong actor for metal ion detoxification in cells.

7.3.3.3. Effect of sulfide ions on the hydrodynamic radius of Ag-cicMT2

In order to evaluate the size of $Ag_{10.6}S_{0.3}$-cicMT2 and $Ag_{18.3}S_{1.5}$-cicMT2, the hydrodynamic radii were determined with DLS at a protein concentration of 30 μM. For $Ag_{10.6}S_{0.3}$-cicMT2 a hydrodynamic radius of 1.8 ± 0.2 nm was measured. This value is in line with the one measured at the same concentration for the Cd^{2+}- and Zn^{2+}-form but still higher than compared to other proteins with a comparable molar mass.

The sulfide ion containing form was also measured, but revealed no concise data. The polydiversity of $Ag_{18.3}S_{1.5}$-cicMT2 was more than 20 %, and the deviation between the single measurements was >50 %. The sulfide containing Ag^{+}-sample seems to aggregate much faster than the Cd^{2+}- and Zn^{2+}-form and do not appear as a single species.

7.3.4. Cu^+ ion incorporation into cicMT2 in absence and presence of sulfide ions

7.3.4.1. Formation of Cu- and Cu,S-cicMT2 during Cu^+ titration

To complement the dataset of the sulfide ion incorporation with monovalent metal ions apo-cicMT2 was titrated with the naturally more relevant Cu^+ ions in presence and absence of ten equivalents of S^{2-} ions, and for comparison ten equivalent of S^{2-} ions were titrated with Cu^+ ions in absence of protein.

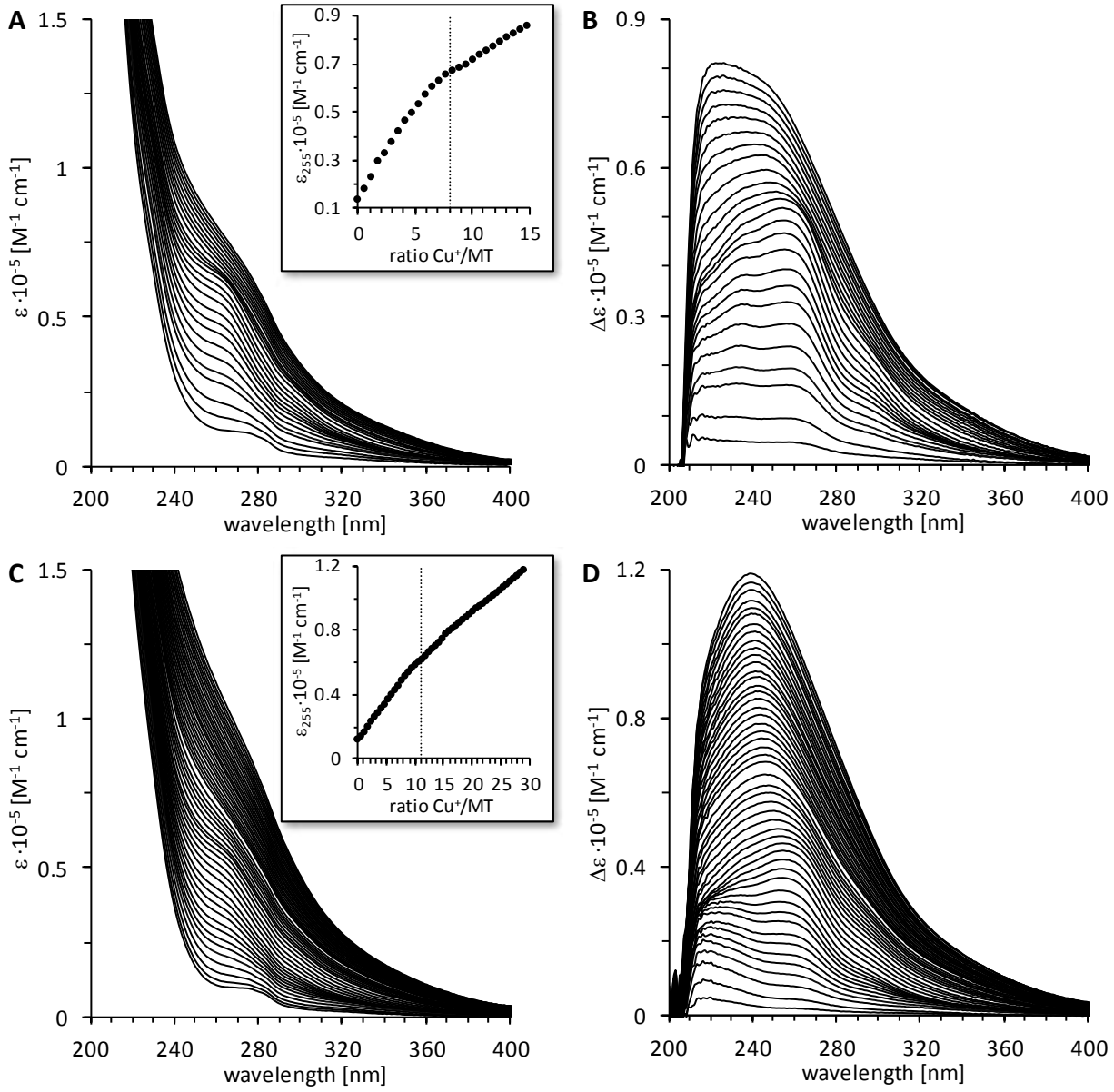

Fig. 41 UV spectra of Cu^+ ion titration to apo-cicMT2 in absence **(A, B)** and presence **(C, D)** of additional sulfide ions. **(A, C)** shows the UV spectra, **(B, D)** the difference plot, where the spectrum with 0 equivalent of Cu^+ ions is subtracted from the spectra where Cu^+ ions were added. Apo-cicMT2 (10 μM) was titrated (in presence of 100 μM Na_2S) with increasing equivalents of metal ions (10-300 μM) in 10 mM Tris-HCl, 10 mM NaCl, pH 7.5. Insets show the plot of the molar absorptivity at 255 nm against the number of equivalents of Cu^+ ions added to apo-cicMT2.

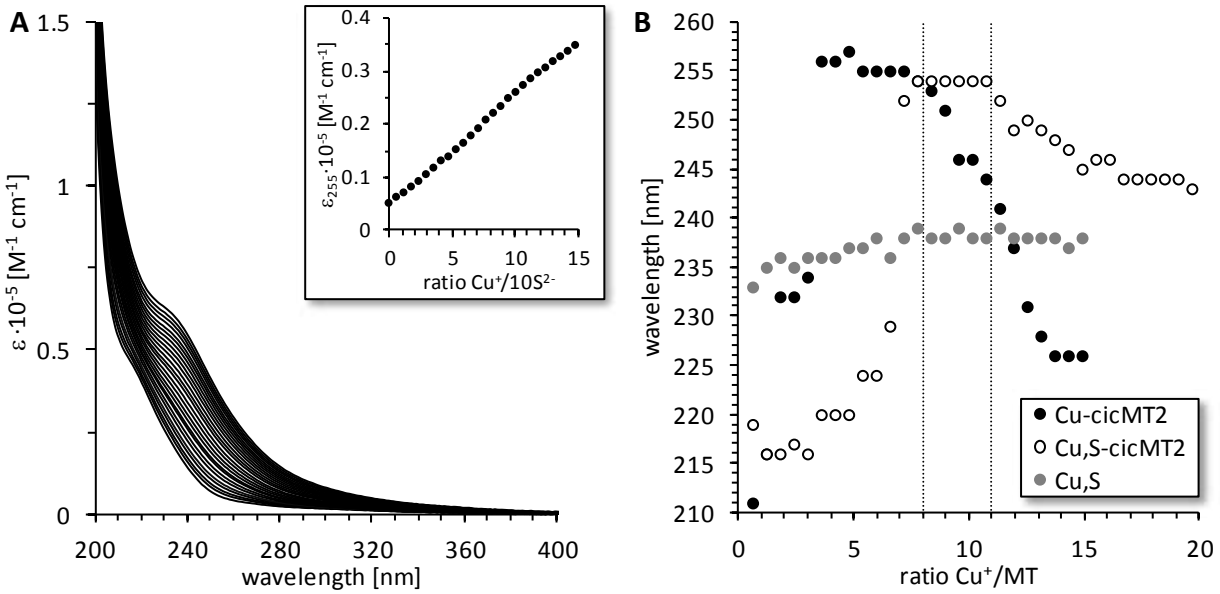

Fig. 42 **(A)** UV spectra of Cu^+ ion titration to S^{2-} ions. 100 µM Na_2S was titrated with increasing equivalents of $[Cu(CH_3CN)_4]BF_4$ (10-150 µM) in 10 mM Tris-HCl, 10 mM NaCl, pH 7.5. Inset shows the plot of the molar absorptivity at 255 nm relevant for the Cu^+ ion titration with cicMT2 against the number of equivalents of Cu^+ ions added. **(B)** Plot of the wavelength of the absorption maxima against the number of equivalents of Cu^+ ions added, taken from Fig. 41 B, D.

During the titration of apo-cicMT2 in absence of sulfide ions with increasing equivalents of Cu^+ ions the corresponding UV spectra exhibit prominent absorption shoulders around 260 nm, which are characteristic for LMCT bands of Cu^+ ion coordination to thiolate ligands (Fig. 41 A, B).[175] A closer look at the absorption maxima displays a shift in the wavelength from 211 nm to 255 nm and back to 226 nm (Fig. 42 B). This is typical for the interaction of Cu^+ ions with thiolate ligands of cysteines and indicates the change of high- and low-energy transitions. The plot of molar absorptivity of the LMCT band at 255 nm against the amount of Cu^+ ions added to the solution shows the coordination of around eight Cu^+ ions to cicMT2. The subsequent addition of more than eight equivalents of Cu^+ ions resulted in a progressive slight increase in absorption and disappearance of the pronounced shoulder. The UV spectra show the formation of Cu_8-cicMT2. This is in contrast to previous results, where Cu_{10}-cicMT2 and Cu_{12}-cicMT2 were found.[175] The difference in the stoichiometry is originating from the starting protein. The here reported Cu_8-cicMT2 was titrated with initial apo-cicMT2, formerly reported Cu_{10}-cicMT2 was titrated from Zn_5-cicMT2, and Cu_{12}-cicMT2 was titrated from Cd_5-cicMT2. As already shown for the Ag-cicMT2, the Cu-cicMT2 form is strongly dependent on the starting protein, its metal load and prefold. The much higher binding capacity of monovalent metal ions compared to divalent metal ions can be explained with trigonal or even diagonal coordination modes. In contrast, divalent metal ions show a dominant tetrahedral coordination.[49, 75, 206-207] The co-existence of multiple coordination geometries of Cu^+ ions even in one single protein molecules makes it difficult to predict exact stoichiometries from UV titration. As Cu^+ ions bind even stronger to the thiolate ligands of the cicMT2 than Ag^+ ions, it was not possible to determine the cicMT2 concentration by quantification of sulphydryl groups and hence it was not possible to determine the Cu^+ ion to cicMT2 ratio in this way. Reported ratios of Cu^+ ions to cysteinyl sulfur are between 1:1 to 1:2, the obtained ratio

of 1.8 for Cu_8-cicMT2 is therefore in accordance with the ratios found in other Cu^+-thiolate complexes.[208-210]

Repeating the Cu^+ ion titration in presence of sulfide ions (Fig. 41 C, D), the LMCT band was evolving at the same wavelength as evidenced without sulfide ions. This has already been seen for the titration with Ag^+ ions (7.3.3.1). Similar to the Cu^+ ion titration in absence of sulfide ions, the plot of the absorption maxima against the equivalent of Cu^+ ions added shifts in the wavelength from 216 nm over 254 nm to 244 nm (Fig. 42 B). The plot of molar absorptivity at 255 nm against the amount of Cu^+ ions added shows nearly a static increase over the whole range of added equivalents. If one however, calculates the slope of the initial and the final equivalents, a slight change can be detected (Fig. 43). The intercept of the initial (equivalent 0-11) and final slope (equivalent 11-30) occurs at eleven equivalent of Cu^+ ions. Differently to the titration with Ag^+ ions in presence of sulfide ions, no transition phase can be detected by titrating Cu^+ ions in presence of sulfide ions. Therefore it was assumed, that eleven Cu^+ ions are incorporated into the sulfide-thiolate cluster of cicMT2.

Interestingly, the absolute molar absorptivity values of the samples titrated in absence (67'413 $M^{-1}cm^{-1}$) and presence of sulfide ions (62'245 $M^{-1}cm^{-1}$) are rather similar. From this findings, two interpretations are possible. Either the structure is altered in the way, that the additional sulfide ions give rise to a lower extinction coefficient per single incorporated Cu^+ ion, or the Cu^+ ions are captured by the S^{2-} ions in solution, so that less than the expected equivalent of Cu^+ ions are available for the cicMT2 (0.73 equivalent instead of one equivalent), and the insertion proceeds until eight equivalent of Cu^+ ions are incorporated into cicMT2.

A

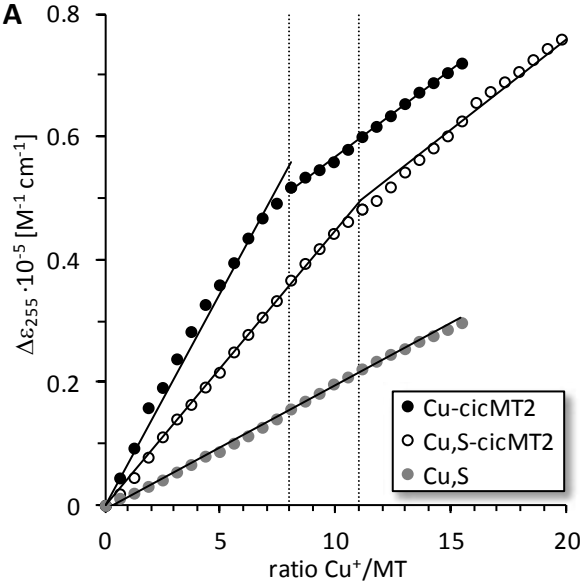

B

	region of analysis	slope [M^{-1} cm^{-1} per equivalent]
Cu-cicMT2	0-8 equivalents	6970
	8-15 equivalents	5176
Cu,S-cicMT2	0-11 equivalents	4467
	11-30 equivalents	3693
Cu,S	0-15 equivalents	1950

Fig. 43 **(A)** Plot of molar absorptivity at 255 nm against the number of equivalents of Cu^+ ions added to apo-cicMT2 (Fig. 41 A, C, Fig. 42 A) with indicated slopes and points of change of the slope. For clarity, only the first twenty equivalent of Cu^+ ions added are shown. **(B)** List of calculated slopes for the specific region of analysis.

To answer the question, if the sulfide ions are incorporated into the Cu^+-thiolate cluster of cicMT2, or if they compete in solution for the Cu^+ ions, the slopes of the titrations were compared to the one of S^{2-} ion titration with Cu^+ ions in absence of cicMT2 (Fig. 43).

The steepness of the slope of Cu-cicMT2 for the first eight equivalents is 6970 M^{-1} cm^{-1} per equivalent of Cu^+ ions followed by 5176 M^{-1} cm^{-1} per equivalent of Cu^+ ions for the equivalent eight to fifteen. The slope for Cu,S-cicMT2 is initially 4467 M^{-1} cm^{-1} per equivalent of Cu^+ ions (up to eleven equivalent) and proceeds with 3693 M^{-1} cm^{-1} per equivalent of Cu^+ ions for the equivalent eleven to thirty. Adding to the initial slope of Cu,S-cicMT2 the slope of the Cu,S-cluster (1950 M^{-1} cm^{-1} per equivalent of Cu^+ ions), a slope of 6417 M^{-1} cm^{-1} per equivalent of Cu^+ ions can be calculated reaching nearly the slope of Cu-cicMT2. This shows a likelihood of Cu^+-sulfide cluster formation in solution, which is independent of the protein. However, the formation of independent clusters would not explain the steepness of the slope after the eighth or eleventh equivalent of Cu^+ ions added, respectively. There, the decrease of the slope from Cu-cicMT2 to Cu,S-cicMT2 is around 70 %. Taking in account, that Cu,S-clusters in solution also show a certain absorption (Fig. 42 A), the second part of the plot for Cu,S-cicMT2 would be expected to be higher than the one of Cu-cicMT2 (calculated 5643 M^{-1} cm^{-1} per equivalent of Cu^+ ions). It seems, that the sulfide ions are interacting with the cicMT2, and are not staying solely in solution.

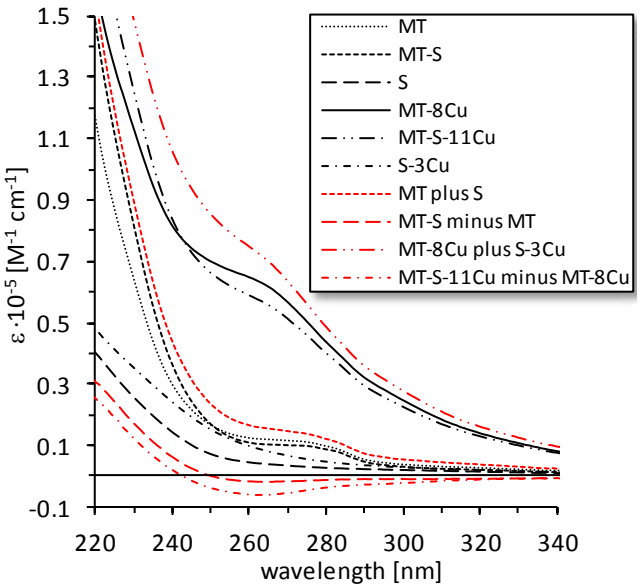

Fig. 44 UV spectra (black) and UV difference spectra (red) for different forms of titrated samples as indicated in the legend. MT corresponds to 1 equivalent apo-cicMT2, S corresponds to 10 equivalent S^{2-} ions, Cu corresponds to indicated equivalents of Cu^+ ions. Compounds of mixed samples are separated by hyphen. Sort of lines for the red spectra correspond to the expected black ones, if sulfide ions are not interacting with cicMT2.

To emphasize the sulfide ion incorporation during Cu^+ ion titration difference spectra were calculated (Fig. 44). With an independent formation of Cu,S-clusters in solution some calculated spectra should overlap with the measured spectra. The addition of the spectra of 10 µM apo-cicMT2 and of 100 µM S^{2-} ions should result in 10 µM apo-cicMT2 + 100 µM S^{2-} ions; the subtraction of the spectra of 10 µM apo-cicMT2 from 10 µM apo-cicMT2 + 100 µM S^{2-} ions should result in the same spectra as 100 µM S^{2-} ions alone; the addition of the spectra of 10 µM apo-cicMT2 + 80 µM Cu^+ ions and 100 µM S^{2-} ions + 30 µM Cu^+ ions should result in 10 µM apo-cicMT2 + 100 µM S^{2-} + 110 µM Cu^+ ions; and the subtraction of the spectra of 10 µM

apo-cicMT2 + 80 μM Cu^+ ions from 10 μM apo-cicMT2 + 100 μM S^{2-} ions + 110 μM Cu^+ ions should result in 100 μM S^{2-} ions + 30 μM Cu^+ ions. Owing to the fact, that none of the spectra are overlapping with the expected ones presumes no independent formation of Cu,S-clusters. This indicates the interaction of the sulfide ions with Cu-cicMT2.

In conclusion, we show a lot of indications suggesting the sulfide ion incorporation into Cu-cicMT2 or independent Cu,S-cluster formation. The result is ambiguous and only based on titrations followed by UV spectroscopy. Other methods as used for Zn^{2+}-, Cd^{2+}-, and Ag^+-forms were not suitable for the Cu-cicMT2 and Cu,S-cicMT2 evaluation.

7.3.4.2. Hydrodynamic radius of Cu-cicMT2 and Cu,S-cicMT2

In order to evaluate the size of Cu-cicMT2 and Cu,S-cicMT2, the hydrodynamic radii were determined with DLS at a protein concentration of 30 μM. For Cu-cicMT2 a hydrodynamic radius of 2.0 ± 0.1 nm was measured, for Cu,S-cicMT2 one of 1.9 ± 0.1 nm was determined. The Cu,S-cicMT2 is slightly smaller than the Cu-cicMT2, but the difference is in the error range of the measurement.

A

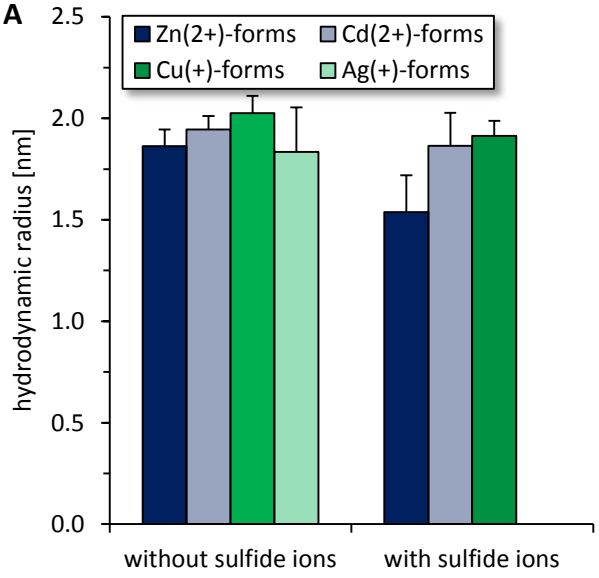

B

	sample	hydrodynamic radius [nm]	M,S-cicMT2: M-cicMT2
Zn^{2+}	Zn_5-cicMT2	1.86 ± 0.08	83 %
	Zn_8S_7-cicMT2	1.54 ± 0.18	
Cd^{2+}	Cd_5-cicMT2	1.94 ± 0.07	96 %
	Cd_9S_7-cicMT2	1.86 ± 0.16	
Cu^+	Cu_8-cicMT2	2.03 ± 0.09	95 %
	$Cu_{11}S_x$-cicMT2	1.91 ± 0.07	
Ag^+	Ag_9-cicMT2	1.83 ± 0.22	-
	$Ag_{19}S_x$-cicMT2	-	

Fig. 45 Hydrodynamic radii of different sulfide ion containing and lacking forms of cicMT2 titrated with Zn^{2+}, Cd^{2+}, Cu^+, and Ag^+ ions. Protein concentration was 30 μM, buffer was 10 mM Tris-HCl, 10 mM NaCl, pH 7.3. **(A)** Data shown as histogram with indicated standard deviations, **(B)** absolute values of hydrodynamic radii shown with percental decrease of the hydrodynamic radius in presence of additional sulfide ions.

As already seen for the other metallated forms, the expected radius of 1.5 nm for a protein with a size ~8.5 kDa was exceeded. The hydrodynamic radii of all metallated forms measured at 30 μM protein concentration are comparable with average radii of around 1.85 nm (Fig. 45).

Interestingly, at lower protein concentration the cicMT2s reconstituted in presence of sulfide ions are slightly smaller (4-15 %) than the form without additional sulfide ions. These contraction might be caused by a structural change of the linker region of the protein. As shown in the model (Fig. 46), two different structures are predicted for the linker region.[183] In one scenario, the entire

linker sequence forms a single long antiparallel β-sheet structure and hence a rather rigid scaffold for the cluster formation. In the other scenario, the amino acids of the linker region form a more flexible structure with four shorter β-sheets. The structure with one long β-sheet might be suitable for a tight cluster packing in absence of sulfide ions and for the calculation of the hydrodynamic radius would better fit a model for a linear polymer. The structure with four short β-sheets would allow a more versatile cluster necessary for the incorporation of additional sulfide ions and a calculation model for a globular protein would be appropriate. Calculating both structures with a globular protein model, the more spherical protein would result in a smaller radius than the one with the more elongated linker.

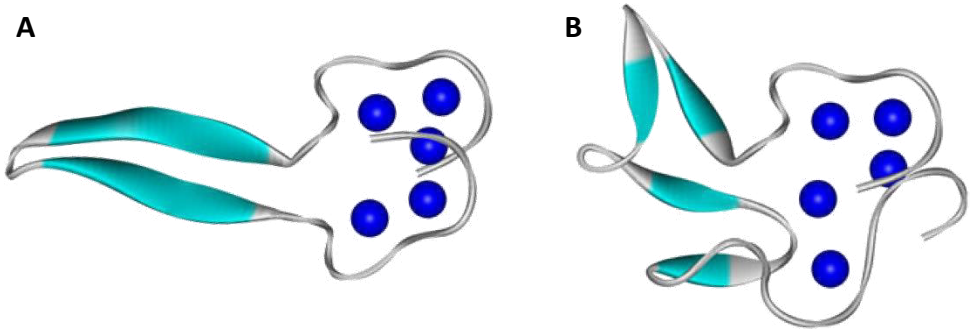

Fig. 46 Model for structural features for the linker region of plant MTs.[183] **(A)** The entire linker sequence forms a single long antiparallel β-sheet structure (cyan) and hence a rather rigid scaffold to bring the cysteine-rich regions (long, grey terminal tubes) into proximity for the joint cluster formation (metal ions are depicted as blue spheres). **(B)** The amino acids of the linker region form a more flexible structure with four shorter β-sheets, which allow different sizes of clusters.

7.4. Characterization of the Cd^{2+}-S^{2-}-thiolate clusters of MTs

Our previous studies showed the *in vitro* incorporation of sulfide ions with the divalent d^{10} metal ions Cd^{2+} and Zn^{2+} as well as with the monovalent d^{10} metal ions Ag^{+} and Cu^{+} into the metal-thiolate cluster of cicMT2 (7.3). The metal ion titrations and protein reconstitutions in presence of sulfide ions were all performed with initially ten equivalents of sulfide ions and resulted in a specific overall stoichiometry depending on the chemical identity of the metal ion. Further investigations were done to analyze in more detail the dependency of the stoichiometry on the sulfide ion supply. Furthermore, the impact of enzymatic support for the cluster formation was analyzed. Finally, the distinct pathway of successful sulfide ion incorporation was examined, and the transfer of these findings to other MTs was demonstrated.

7.4.1. The flexibility of the Cd,S-clusters in cicMT2

7.4.1.1. Sulfide ions as modulators of Cd,S-cluster size

It was shown already 30 years ago that the PC complexes of *S. pombe* can contain variable amounts of sulfide ions, and the Cd^{2+}-binding capacity of the PC complexes depends on the concentration of sulfide ions in the reaction system.[86, 211-214] It is hence possible that also plant MTs, e.g. cicMT2, might have the ability to host different sizes of metal-thiolate clusters depending on the metal ion concentration and the cellular supply of sulfide ions.

To evaluate this further, Zn_5-cicMT2 was titrated with Cd^{2+} ions in presence of 0, 5, 10, 20, 30, and 50 equivalents of sulfide ions and the evolution of the LMCT bands was monitored with UV/Vis spectroscopy (Fig. 47).[199] As apparent from the overlay of the initial spectra (Fig. 48 A), i.e. Zn_5-cicMT2 incubated with the respective amount of S^{2-} ions, the S^{2-} ions have an influence on the absorption spectra below 270 nm. Accordingly, the maximum Cd^{2+} ion binding capacity of the protein was accessed by plotting the molar absorptivity at a higher wavelength, i.e. 280 nm, against the equivalent of Cd^{2+} ions added to the solution (Fig. 48 B). This is also in agreement with the bathochromic shift reported in 7.3.1.1. As expected, in absence of S^{2-} ions a Cd_5-cicMT2 species was observed, with the more S^{2-} ions are provided, the more Cd^{2+} ions can be bound resulting in 26 equivalenta of Cd^{2+} ions in presence of 50 equivalents of S^{2-} ions (Fig. 48 A, Tab. 15 [a]). By plotting the number of bound Cd^{2+} against the initial provided sulfide ions a linear increase could be observed (Fig. 48 D). Additionally to the increase at 280 nm with higher amounts of sulfide ions, a broad shoulder at 360 nm occurred and a change from a colorless to a distinct yellow solution could be observed, indicating the independent generation of Cd,S-clusters in solution. Centrifugation of the samples resulted in a yellow precipitate of independent Cd,S-clusters due to the 270 times higher solubility of Na_2S (solubility at 20 °C = 2.4 M) compared to CdS (solubility at 20 °C = 9.0 μM). The UV/Vis spectra indeed did not change denoting that the band at 360 nm was solely caused by the Cd,S-cicMT2.

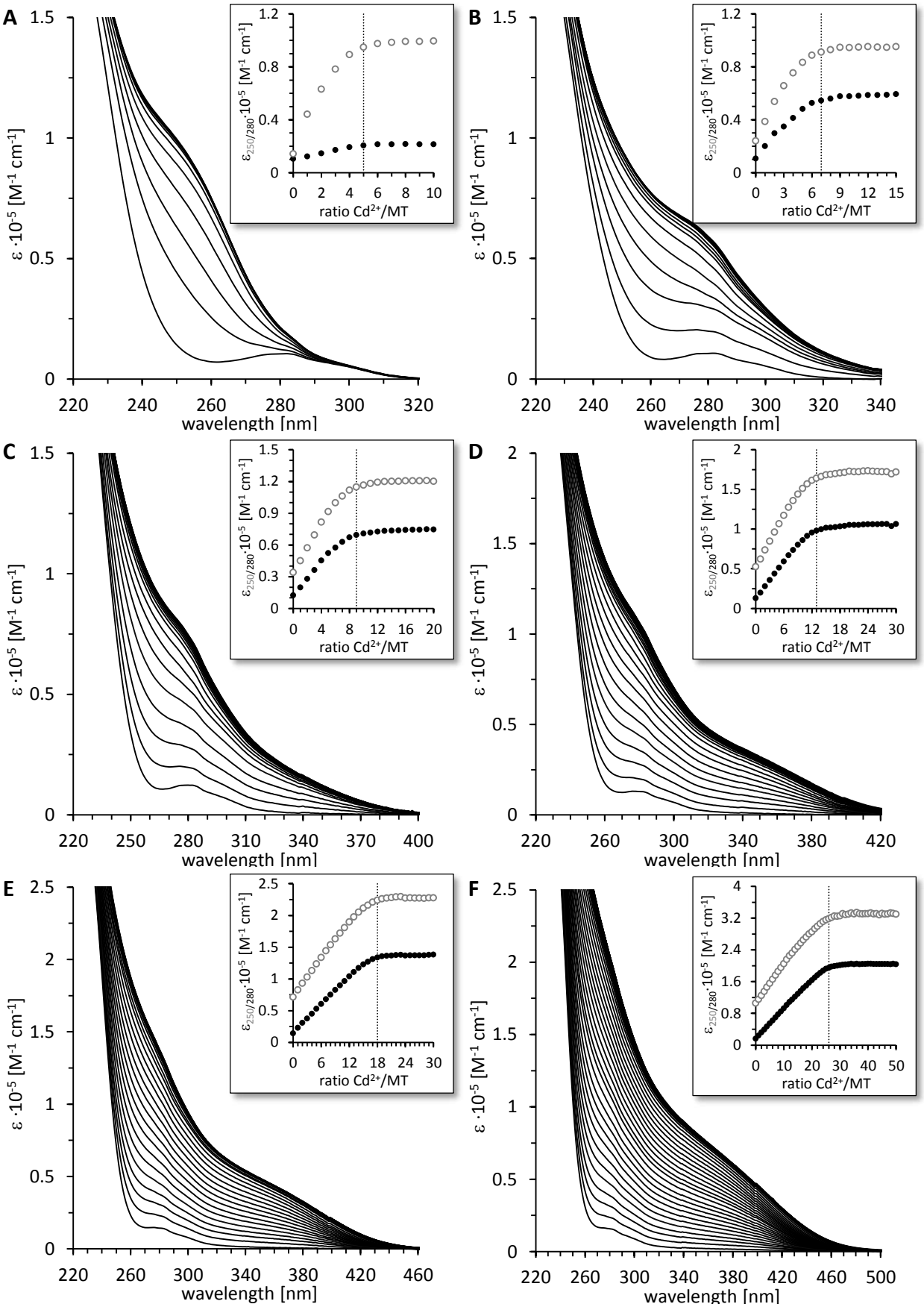

Fig. 47 UV/Vis spectra of Cd^{2+} ion titration (10-500 μM) to 10 μM Zn_5-cicMT2 in presence of Na_2S in 10 mM Tris-HCl, 10 mM NaCl, pH 7.5. Concentrations of Na_2S were **(A)** 0 μM, **(B)** 50 μM, **(C)** 100 μM, **(D)** 200 μM, **(E)** 300 μM, and **(F)** 500 μM. Insets show the plot of the molar absorptivity at the LMCT bands (250 nm for Cd^{2+}-thiolate, 280 nm for Cd^{2+}-S^{2-}) against the number of equivalents of Cd^{2+} ions added to cicMT2.

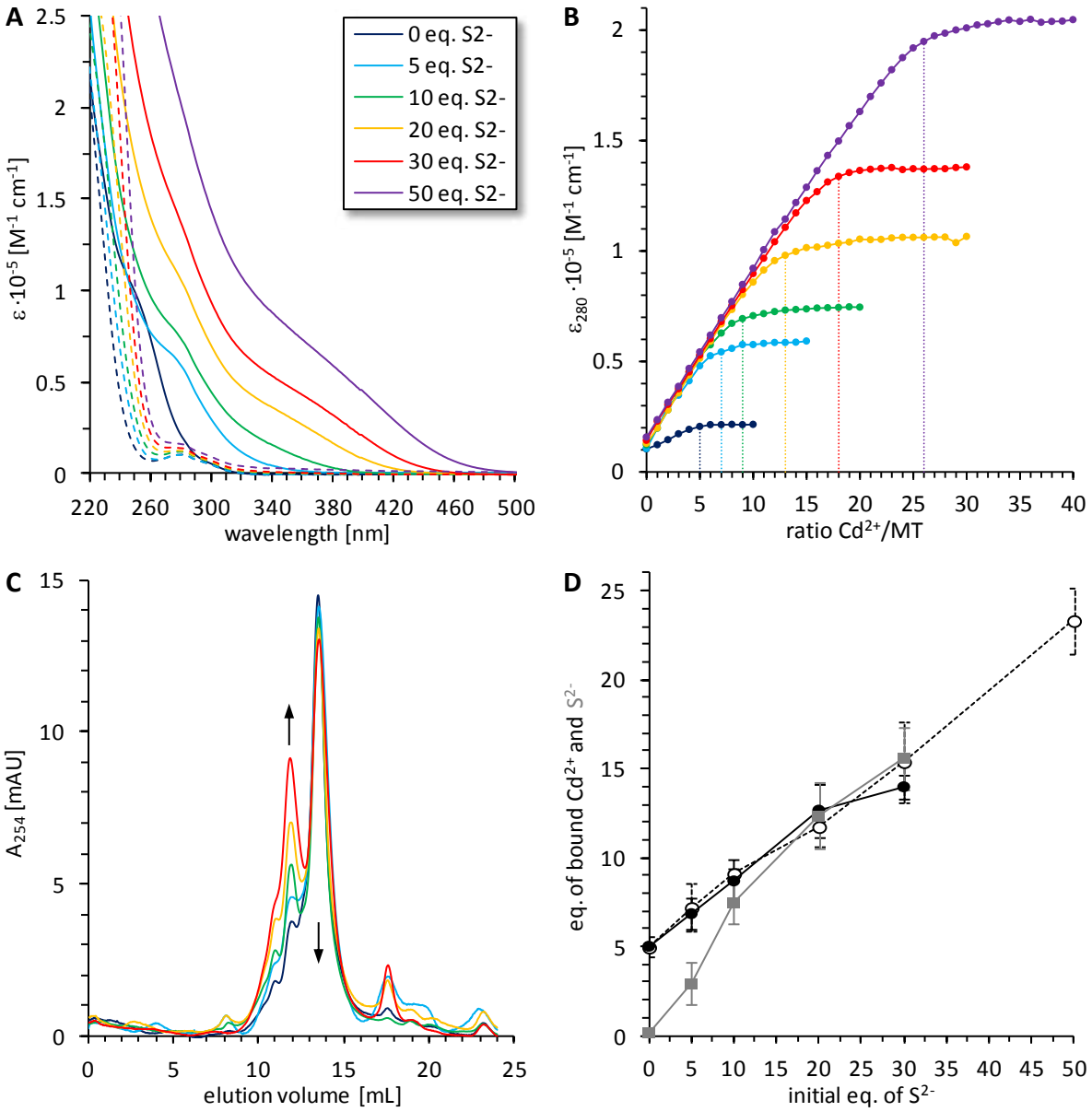

Fig. 48 **(A)** Overlay of UV/Vis spectra of Cd^{2+} titration to Zn_5-cicMT2 in presence of different equivalents of Na_2S (Fig. 47). Dashed spectra show the Zn_5-cicMT2 with different equivalents of Na_2S before the addition of Cd^{2+} ions. Solid spectra show the final Cd,S-cicMT2 spectra in presence of different equivalents of Na_2S, where additional Cd^{2+} ions do not cause further spectral changes. **(B)** shows an overlay of the plots of molar absorptivity at 280 nm against the number of equivalents of Cd^{2+} ions added to cicMT2 performed in presence of different Na_2S concentrations (Fig. 47). Legend as in **(A)**. **(C)** Elution profiles of the final titration mixtures of Cd,S-cicMT2 complexes when applied to an analytical size exclusion chromatography column (Superdex 75 10/300 GL). The peaks at 13.5 mL belong to the monomeric protein species, decreasing with higher sulfide ion concentrations (arrow). The peaks at 11.8 mL and lower elution volumes are increasing with increasing initial S^{2-} ions (arrow). Legend as in **(A)**. **(D)** Plot of final amounts of bound Cd^{2+} and S^{2-} ions against the equivalent of S^{2-} ions initially added to the solution. Circles represents the bound Cd^{2+} ions, empty ones evaluated from titration, black ones measured with F-AAS after purification, grey squares indicate the bound S^{2-} ions, measured with methylene blue assay after purification.

To further analyze, if the observed changes of the absorption spectra originate from additional protein bound Cd^{2+} and S^{2-} ions and not from Cd,S-aggregates in solution, the final titration mixtures were applied to an analytical size exclusion chromatography column (Fig. 48 C). The elution profiles were dominated by a peak at 13.5 mL corresponding to the monomeric protein

species. Apparently, the structure of the protein can be expanded to accommodate the growing cluster without a major alteration of the overall protein size, or more precisely its hydrodynamic radius. With increasing amounts of sulfide ions present in the initial titration solution, peaks with lower elution volumes rise in intensity corresponding most likely to protein dimers, trimers, and higher aggregates.

Tab. 15 Content of incorporated Cd^{2+} and S^{2-} ions per cicMT2 molecule in dependency of the S^{2-} ion equivalents initially supplied.

initial S^{2-}	$Cd^{2+}/MT^{[a]}$	$Cd^{2+}/MT^{[b]}$	$Cd^{2+}/MT^{[c]}$	$S^{2-}/MT^{[d]}$	$Cd^{2+}_{add}/S^{2-[e]}$	$Cd^{2+}/S_{tot}^{[f]}$
0	5.0 ± 0.1	5.0 ± 0.6	5.0 ± 0.4	0.2 ± 0.3	0.15 ± 0.22	0.35 ± 0.50
5	7.2 ± 1.3	6.9 ± 0.9	7.1 ± 1.2	2.9 ± 1.2	0.64 ± 0.28	0.41 ± 0.17
10	9.1 ± 0.3	8.7 ± 1.2	8.9 ± 1.0	7.4 ± 1.2	0.50 ± 0.11	0.41 ± 0.09
20	11.8 ± 1.1	12.7 ± 1.5	12.1 ± 1.3	12.4 ± 1.8	0.62 ± 0.12	0.48 ± 0.09
30	15.4 ± 2.2	14.0 ± 0.7	15.0 ± 2.0	15.6 ± 1.8	0.58 ± 0.07	0.47 ± 0.06
50	23.3 ± 1.9					

[a] eq. of Cd^{2+} ions added until no further changes were observed in the UV/Vis spectra
[b] eq. of Cd^{2+} ions measured with F-AAS after purification of titration mixture with SEC
[c] average of eq. of Cd^{2+} ions of [a] and [b]
[d] eq. of S^{2-} ions measured with 2-PDS and methylene blue assays after purification of titration mixture
[e] eq. of additional added Cd^{2+} per S^{2-} ions ([b] minus 5 eq. Cd^{2+} ions of titration without S^{2-} ions, divided by [d])
[f] eq. of added Cd^{2+} ions per total thiolate sulfide ion content ([b] divided by ([d] + 14 S_{Cys} of MT))

The respective peak at 13.5 mL of the monomeric protein was collected and analyzed for protein, metal and sulfide ion content by F-AAS and colorimetric assays, i.e., 2-PDS and methylene blue assay (Tab. 15 [b, d]). The Cd^{2+} ion contents in the purified protein fractions agreed very well with the values obtained from the titration experiments, although the Cd^{2+} ion content of the purified sample was slightly lower, caused by the loss of some weakly bound ions on the competing column material. Hence it can be concluded that all of the Cd,S-bonds that contributed to the detected absorption at 280 nm indeed belonged to the monomeric protein complex formed and did not originate from Cd,S-aggregates in solution. In addition the amounts of bound Cd^{2+} and S^{2-} ions showed a nearly linear dependency on the number of sulfide ion equivalents initially supplied (Fig. 48 D). The analysis of the first pronounced peak at 11.8 mL elution volume showed as main components Cd^{2+} and S^{2-} ions originating from independent Cd,S-clusters. The incomplete separation of the monomer and multimer peaks by the used column explains the rather high standard deviation for the values listed in Tab. 15. Experiments with higher initial amounts of sulfide ions than 30 equivalents were not successful due to increased precipitation of Cd,S-clusters and observation of large fractions of protein aggregates during size exclusion chromatography.

The calculated ratios between additionally incorporated Cd^{2+} ions (Cd^{2+}_{add}) and bound S^{2-} ions are around 0.58 for all samples (Tab. 15 [e]). The ratios are consistently in the range of 0.50 and 0.64 and independent on the initial sulfide ion supplement. The values are slightly higher than determined for divalent metal ion complexes, which showed a ratio near 0.49. Nevertheless, as already discussed in 7.3.1.1, the ratio of additionally incorporated Cd^{2+} and S^{2-} ions is following a general trend.[81]

The ratios between bound Cd^{2+} ions and the combined content of sulfide ions and thiolate groups of cysteines are 0.42 (Tab. 15 [f]) as already determined for divalent Cd^{2+} ion complexes (0.40, 7.3.1.1). The ratio Cd^{2+}:S_{tot} in absence of sulfide ions amounts to 0.35 and hence agrees well, e.g., with the value of 0.5 obtained for mammalian Cd_7-MT. In presence of 20 or 30 equivalent of sulfide ions this ratio was rising to 0.48 and 0.47, which is closer to the value of the sulfide ion containing higher molecular mass PC complex of yeast, i.e. 0.42. The ratios calculated from the data of Capdevila et al.[81] show a less clear picture with values ranging between 0.20 and 0.41. This lead to the conclusion, that these ratios are dependent on the metal ion (7.3.1.1, 7.3.2.1, 7.3.3.1, 7.3.4.1), the species investigated, and the origin of the species, either *in vivo* isolated, recombinantly expressed protein or *in vitro* titrated reconstituted protein.[81, 83, 136, 213]

To assess the Cd,S-cluster size of cicMT2 in an alternative way, we attempt to exploit the quantum size effect. The quantum size effect is a phenomena of quantum dots (QDs) of CdS and ZnS nanocrystals.[215] The emission wavelength of their intrinsic fluorescence is dependent on their size, the absorbance onset and emission maximum shift to higher energy with decreasing particle size (quantum size effect).[216-217] The QDs can be excited efficiently at any wavelength shorter than the emission peak yet will emit with a narrow (20-30 nm), symmetric spectrum regardless of the excitation wavelength. It was tried to use of this feature to determine the size of the metal-sulfide-thiolate clusters incorporated into cicMT2.
First, test samples (200 μM L-cysteine; 200 μM $CdCl_2$; 200 μM Na_2S; 200 μM L-cysteine + 200 μM $CdCl_2$; and 200 μM Na_2S + 200 μM $CdCl_2$) were measured to designate the excitation wavelength. Only the samples L-cysteine + $CdCl_2$ and Na_2S + $CdCl_2$ show (with an excitation wavelength of 300 nm in the emission spectra) a peak at 350 nm with a width of ~65 nm. According to our expectations, the other samples were silent in the fluorescence spectra.
To measure the metal loaded and metal-sulfide loaded cicMT2, they were reconstituted and free ions were removed via desalting column. The resulting cicMT2s were analyzed for their metal and sulfide ion content to verify the designated stoichiometry. Measured emission fluorescence spectra of 290 μM apo-cicMT2, of 50 μM Cd_5-cicMT2, or of 110 μM Cd_9S_7-cicMT2, all in 10 mM Tris-HCl, pH 7.3, 10 mM NaCl show no increased intensity for an excitation wavelength of 300 nm. By scanning the excitation wavelength from 200-500 nm in 10 nm increment steps, all samples show with an excitation at 410 nm a band in the emission spectra at 430 nm. Since the band occurs in all spectra, the fluorescence cannot originate from the Cd,S-clusters, but it might originate from the two tyrosines of the cicMT2.[218] In summary, it can be said, that the Cd,S-cluster incorporated into cicMT2 does not feature any fluorescence as reported for CdS QD.

7.4.1.2. Reduced flexibility of Cd,S-clusters with the help of NifS?

NifS from *Azotobacter vinelandii* is a cysteine desulfurase and belongs to the class-V pyridoxal-phosphate-dependent aminotransferase family Nif which consists of 15 proteins associated with the fixation of atmospheric nitrogen. Besides the subunits for the nitrogenase, the *nif* genes encode proteins involved in assembly and incorporation of the Fe and Mo into the nitrogenase subunits, proteins related to electron transfer taking place in the reduction process, and proteins regulating the *nif* gene expression.[219-221] The NifS participate in biosynthesis of the nitrogenase metalloclusters by providing the inorganic sulfur required for the Fe,S-core formation. The inorganic sulfur is produced by the reaction L-cysteine + acceptor to L-alanine + S-sulfanyl-acceptor.[222] In this function, the NifS was used for the incorporation of Fe,S-clusters in different proteins as e.g. the Na^+-translocating NADH:Quinone Oxidoreductase from *Vibrio cholerae*.[157] By the NifS, the metal-sulfide-cores are built in a more uniform structure with a stepwise supply of inorganic sulfur than by the simple addition of sulfide ions.[137]
Previous experiments with cicMT2 have shown a high flexibility in their Cd,S-cluster size. For solving the protein structure, it is however necessary to gain a uniform Cd,S-cicMT2 present in solution. To achieve this, it was tried to incorporate the Cd,S-cluster into cicMT2 with the help of the enzyme NifS.

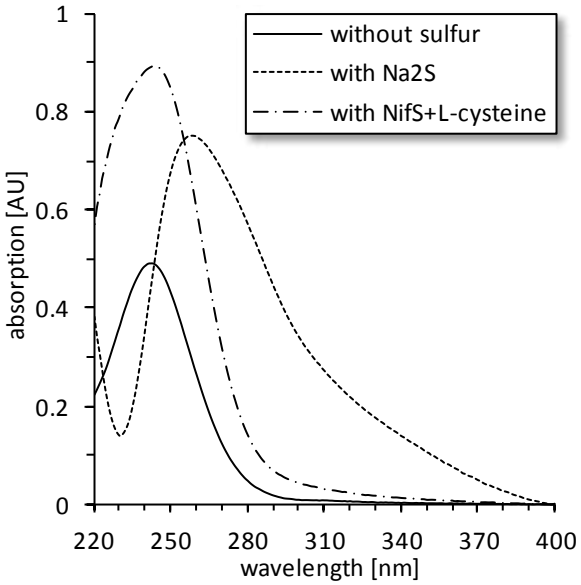

Fig. 49 UV spectra of metal cluster reconstitutions. Zn_5-cicMT2 (10 μM) in 10 mM Tris-HCl, 10 mM NaCl, pH 7.5 was supplemented with 150 μM $CdCl_2$ (solid spectra), with 100 μM Na_2S and 150 μM $CdCl_2$ (dashed spectra), or with 100 μM L-cysteine, 1 mM DTT, 150 g/L NifS and 150 μM $CdCl_2$ (dashed-dotted spectra). The mixtures before the addition of $CdCl_2$ were subtracted as baseline.

NifS was expressed and purified as described and its activity was tested. The ability to incorporate sulfide ions into the Cd,S-clusters was measured with 10 μM Zn_5-cicMT2 in 10 mM Tris-HCl, 10 mM NaCl, pH 7.5, supplemented with 100 μM L-cysteine, 1 mM DTT, and 150 g/L NifS. As a final component, 150 μM $CdCl_2$ was added, after 2.5 h incubation an absorption spectrum was recorded (Fig. 49), and the sulfide ion concentration was determined by methylene blue assay.

For comparison, references with sulfide ion supplementation (10 μM Zn_5-cicMT2 in 10 mM Tris-HCl, 10 mM NaCl, pH 7.5, 100 μM Na_2S and 150 μM $CdCl_2$) and without any sulfur supplementation (10 μM Zn_5-cicMT2 in 10 mM Tris-HCl, 10 mM NaCl, pH 7.5, 150 μM $CdCl_2$) were recorded (Fig. 49).

The absorption spectrum of the reference without sulfur supplementation shows an absorption maximum of 0.49 AU at 242 nm, and the spectrum of the one containing sulfide ions has a red-shifted maximum of 0.75 AU at 258 nm. The absorption spectrum of the sample containing NifS shows a maximum of 0.89 AU at 243 nm. This clearly overlaps with the sample without sulfur supplementation and not with the one of Cd,S-cicMT2. The measured sulfide ion concentration also points out the lack of sulfide ion formation. The 1.8 times increased absorption at 242 nm of the sample with NifS compared to the sample without sulfur supplementation can be explained by the additional cysteines present in solution also binding to the free Cd^{2+} ions in solution what increases the absorption at the LMCT band of Cd^{2+}-thiolate. The ratio of the cysteine content of the NifS sample to Cd-cicMT2 is 1.7 fitting to the increased absorption ratio of 1.8 (the sample without sulfur supplementation contains 140 μM cysteines of cicMT2, the one with NifS 240 μM cysteines in total (140 μM cysteines of cicMT2 and 100 μM of L-cysteines)). The binding of Cd^{2+} ions to the L-cysteines might be the reason for the failure of sulfide ion formation. NifS is presumably not able to catalyze the reaction with Cd^{2+} ions bound to L-cysteines.

In summary, it can be said, that there is no formation of sulfide ions in the sample containing NifS, L-cysteine, cicMT2 and Cd^{2+} ions, and therefore also no incorporation of sulfide ions into the metal-thiolate-cluster of cicMT2 takes place.

7.4.2. Successful sulfide ion incorporation follows a distinctive pathway

Up to this point, all experiments were performed adhering to a specific sequence of component addition, i.e. protein was first incubated with the required amount of sulfide ions and only then Cd^{2+} ions were added (ZnMT–S–Cd). This way it was possible to incorporate different amounts of sulfide ions. But the mechanism of incorporation remained unclear.

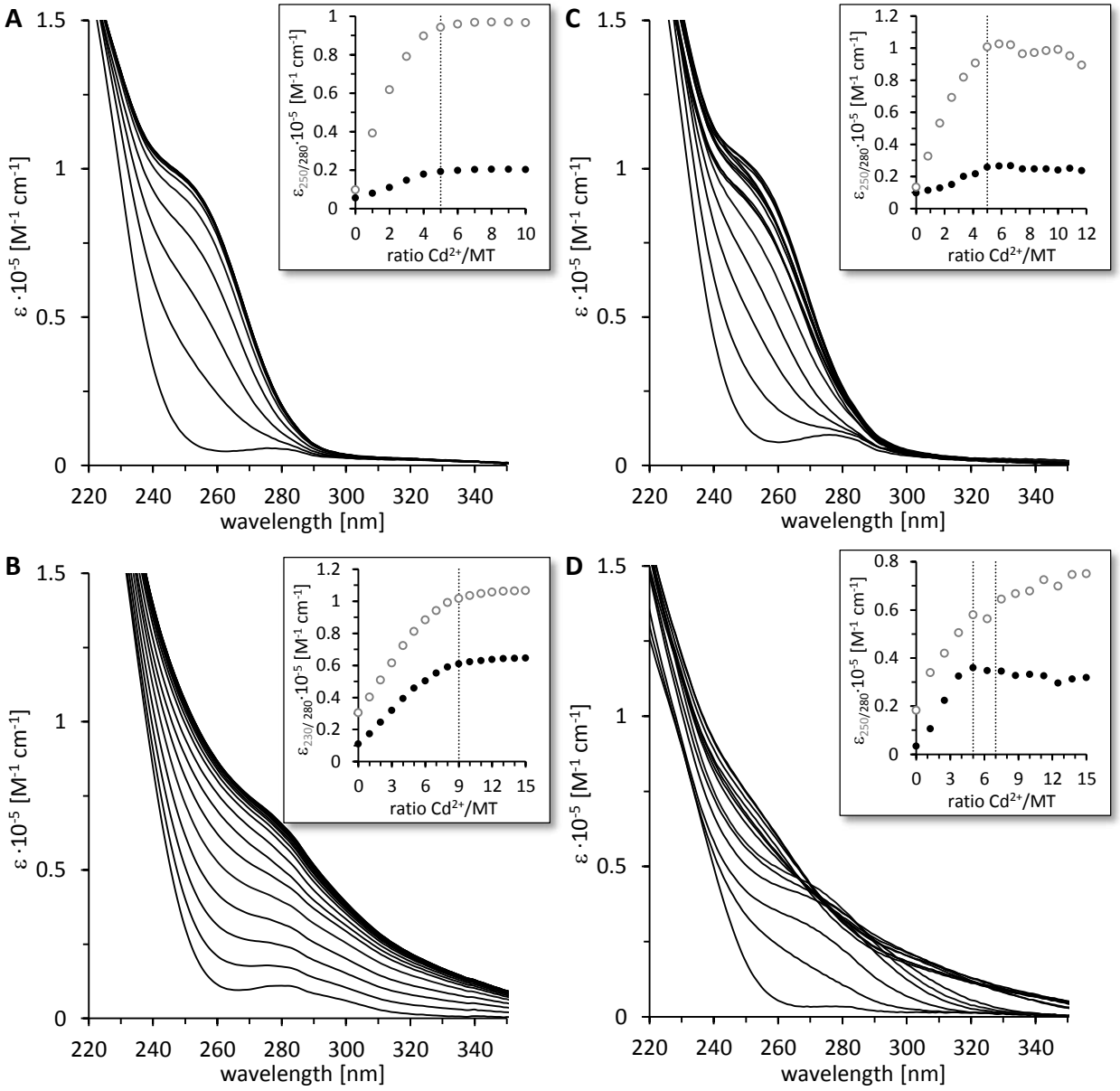

Fig. 50 UV spectra of titration of 10 μM Zn_5-cicMT2 in a buffer containing 10 mM Tris-HCl, 10 mM NaCl, pH 7.3 with Cd^{2+} ions in presence of 10 equivalents of S^{2-} ions (100 μM) varying the order of component addition. **(A)** shows the titration in absence of sulfide ions for comparison (ZnMT–Cd), **(B)** shows the standard titration with the order ZnMT–S–Cd, **(C)** shows the titration with the order Cd–S–ZnMT, and **(D)** shows the titration with the order ZnMT–Cd–S. Insets show the plot of the molar absorptivity at the LMCT bands (250 nm for Cd^{2+}-thiolate, 280 nm for Cd^{2+}-S^{2-}) against the number of equivalents of Cd^{2+} ions added to cicMT2.

To evaluate the importance of this procedure for the efficiency of sulfide ion incorporation and accordingly for the formation of larger clusters the order of addition was varied.[199]

In one experiment, Zn_5-cicMT2 was first incubated with the required amount of Cd^{2+} ions, i.e. 0-18 equivalents, and only then ten equivalents of S^{2-} ions were added (ZnMT–Cd–S). In the second experiment, the required amount of Cd^{2+} ions, i.e. 0-15 equivalents, was first mixed with ten equivalents of S^{2-} ions followed by the addition of Zn_5-cicMT2 as the last component (Cd–S–ZnMT). The progress of all titrations was followed with UV (Fig. 50, Fig. 51), CD, and MCD spectroscopy (Fig. 51).

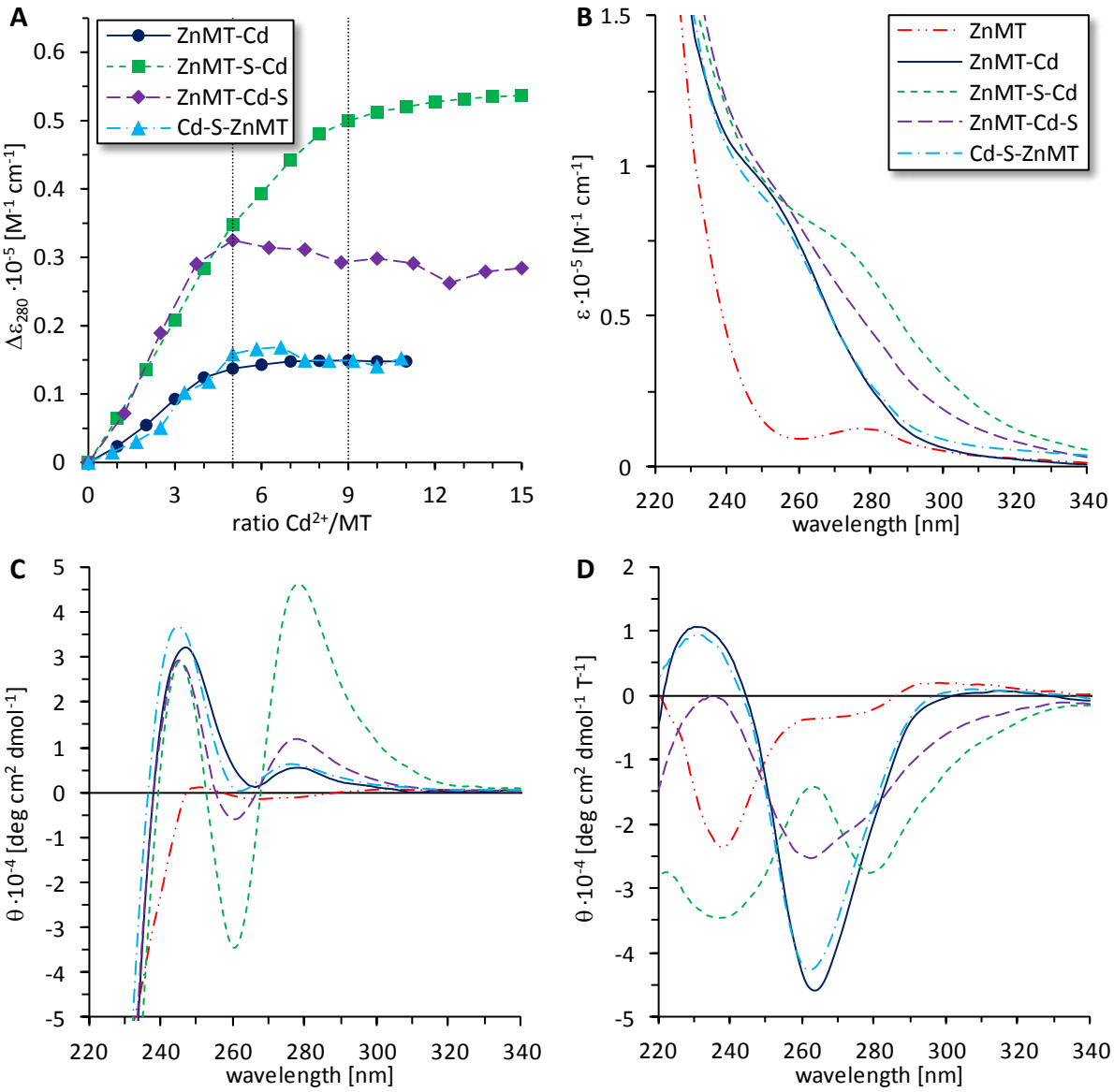

Fig. 51 **(A)** shows an overlay of the plot of molar absorptivity at 280 nm against equivalents of Cd^{2+} ions added to Zn_5-cicMT2 (Fig. 50) leading to the final spectra shown in **(B)**. **(B)** UV, **(C)** CD, and **(D)** MCD spectra of the endpoints of titration of 10 μM Zn_5-cicMT2 in a buffer containing 10 mM Tris-HCl, 10 mM NaCl, pH 7.3 with Cd^{2+} ions in presence of 10 equivalents of S^{2-} ions (100 μM) varying the order of component addition. For comparison, the spectra of Zn_5-cicMT2 and of Cd^{2+} ion titrated Zn_5-cicMT2 are also shown. The color code is for all spectra the same.

The UV spectra of the titration endpoints (Fig. 51 B), i.e. the points, at which additional equivalent of Cd^{2+} ions do no lead to further changes of the spectra, show as previously observed that the formation of sulfide ion containing Cd^{2+}-thiolate-clusters leads to an evolution of the absorption bands around 280 nm and higher. This is clearly visible comparing the spectra of the Cd_5-cicMT2 (ZnMT–Cd) and the Cd_9S_7-cicMT2 forms (ZnMT–S–Cd). When the sequence of addition was altered, the sequence, which first allowed the formation of a Cd,S-cluster, which is then added to Zn_5-cicMT2 (Cd–S–ZnMT) overlapped nearly identical with the sulfide-free form. The sample, where S^{2-} ions are added last (ZnMT–Cd–S) shows a molar absorptivity in the spectral range above 250 nm, which is situated between the two spectra of the sulfide-free and sulfide ion containing species.

To analyze the maximum binding capacity for Cd^{2+} ions, for each titration the molar absorptivity at 280 nm was plotted against the number of Cd^{2+} ions added (Fig. 51 A). Just as expected, for the titration in absence of sulfide ions the maximum absorptivity is reached with five equivalent Cd^{2+} ions. For the titration, in which incubation of the protein with sulfide ions occurred prior to Cd^{2+} addition, around nine Cd^{2+} ions were required to reach the maximum binding capacity. When components were mixed in the order ZnMT–Cd–S, saturation was achieved after addition of five Cd^{2+} ions as in the experiment without sulfide ions. For the sequence Cd–S–ZnMT seven equivalents of Cd^{2+} ions were required. It should be recalled at this point that for the titration experiments, in which Cd^{2+} ions were added as the last component, i.e. ZnMT–Cd and ZnMT–S–Cd the same basic solution was used and only the amount of Cd^{2+} ions was increased for each step. This was not possible for the two titrations with the addition order ZnMT–Cd–S and Cd–S–ZnMT, and accordingly for each titration point a separate solution with the respective amount of Cd^{2+} ions had to be prepared. This explains the larger variations in absorptivity evident in the plot shown in Fig. 51 A.

As seen in 7.3.1.2, the CD spectrum of Cd_9S_7-cicMT2 was distinctively different from the one of sulfide-free Cd_5-cicMT2 species and can be used as a reliable marker for the presence of a sulfide ion containing cluster (Fig. 51 C). While the final CD spectrum of the titration Cd–S–ZnMT was again closely similar to the one of Cd_5-cicMT2, the spectrum for the experiment ZnMT–Cd–S showed bands with ellipticity values between the sulfide-free and the sulfide-containing form.

A similar relation could also be obtained from the MCD spectra (Fig. 51 D). While the UV and CD spectra for the titration ZnMT–Cd–S seem to indicate the formation of a certain amount of sulfide ion containing cluster, the magnetic ellipticity envelope seen in the MCD spectrum is more similar to the sulfide-free Cd_5-cicMT2. Only a minor shoulder at roughly (-)277 nm is observed next to the most intense band at (-)262 nm, which might, on a hypothetical basis, indicate a low fraction of a protein form hosting a cluster with a low amount of sulfide ions.

From the combined results of UV, CD, and MCD spectra it is obvious that no sulfide ions are incorporated when Zn_5-cicMT2 was added as the last compound (Cd–S–ZnMT). The seemingly higher binding capacity for Cd^{2+} ions compared to the sulfide-free Cd_5-cicMT2 form might arise from additional unbound or only loosely bound Cd,S-aggregates in solution. It is however clear that Cd^{2+} ions were indeed incorporated into Zn_5-cicMT2 although the prior incubation of free Cd^{2+} ions with S^{2-} ions leads to significant precipitation of Cd,S-aggregates as expected from the

low solubility product of the compound. Nevertheless, the affinity of the protein for Cd^{2+} ions seems to be high enough to compete with Cd,S-formation and to recruit sufficient Cd^{2+} ions for the saturation of all thiolate binding sites of the cysteines.

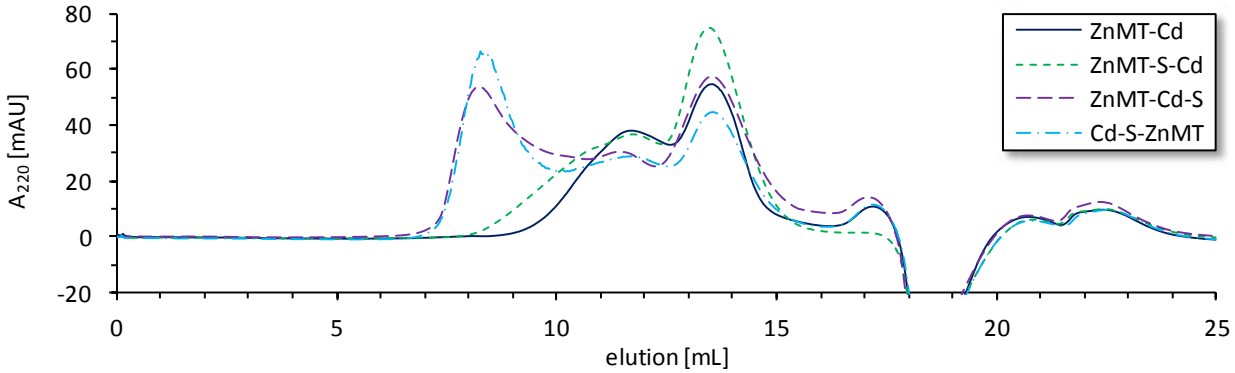

Fig. 52 Elution profiles of the final titration mixtures applied to an analytical size exclusion chromatography column (Superdex 75 10/300 GL). The peaks at 13.5 mL belong to the monomeric protein species, the one at 11.8 mL and lower elution volumes to multimeric species and aggregates. The color code is the same as for Fig. 51.

To characterize the final formed products in more detail the titration mixtures were purified with size exclusion chromatography to remove unbound Cd^{2+} and S^{2-} ions as well as protein aggregates (Fig. 52). UV spectra recorded from the fractions at 13.5 mL, i.e. of the monomeric protein, showed the same features as witnessed before the purification. Thus, all absorption bands are belonging to monomeric cicMT2. Analysis of the fractions regarding their Cd^{2+} and S^{2-} ion contents revealed that only the titration ZnMT–S–Cd was leading to the well-characterized $Cd_{9.1\pm0.3}S_{7.4\pm1.2}$-cicMT2 species with incorporated sulfide ions. For the titration ZnMT–Cd–S a final stoichiometry of $Cd_{5.0\pm1.2}S_{0.3\pm0.6}$-cicMT2 was found and for Cd–S–ZnMT the final composition of $Cd_{5.4\pm0.5}S_{0.4\pm0.1}$-cicMT2 was evidenced. Apparently, variation of the sequence of component addition does not enable sulfide ion incorporation into the cluster. However, the exchange of the bound Zn^{2+} ions with Cd^{2+} ions in all variants is remarkable.

Similar experiments were performed with apo-cicMT2 and Cd_5-cicMT2 (Fig. 53). For apo-cicMT2, the results are even more unambiguous than with Zn_5-cicMT2. Only when apo-cicMT2 is first incubated with sulfide ions before Cd^{2+} ions are added sulfide ion incorporation is observed. All other sequences of Cd^{2+} and S^{2-} ion addition result in UV spectra that are nearly identical to the one obtained for Cd_5-cicMT2. In case of Cd_5-cicMT2, no sulfide ions are incorporated by solely adding S^{2-} ions, and also not by the addition of S^{2-} ions and subsequent addition of Cd^{2+} ions.

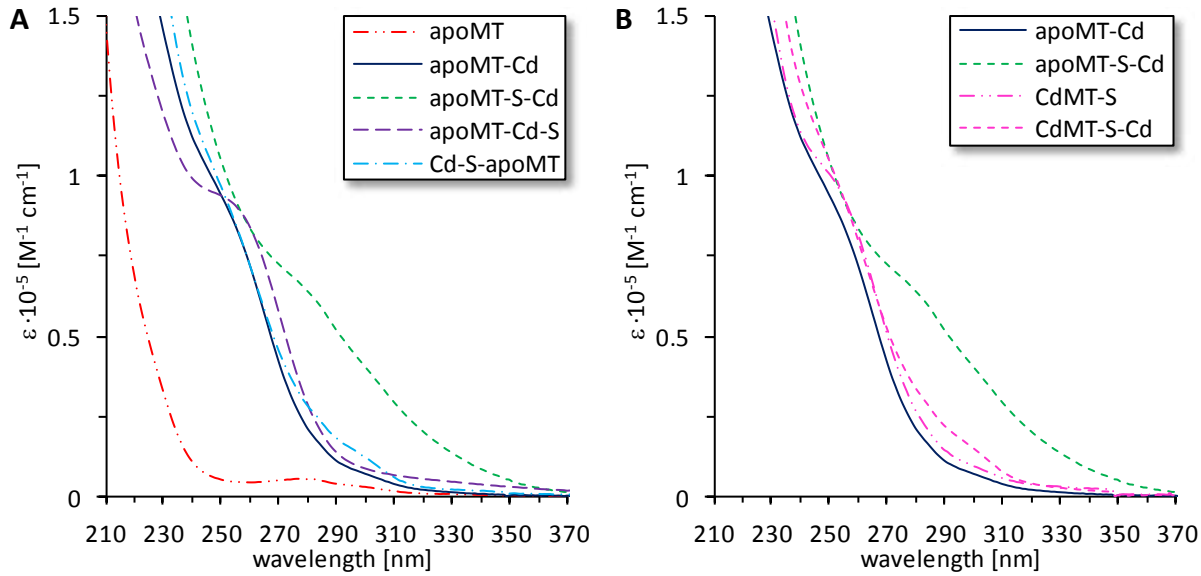

Fig. 53 UV spectra of the endpoints of titration of 10 µM apo-cicMT2 **(A)** and Cd_5-cicMT2 **(B)** in a buffer containing 10 mM Tris-HCl, 10 mM NaCl, pH 7.3 with Cd^{2+} ions in presence of 10 equivalents of S^{2-} ions (100 µM) varying the order of component addition. The color code is the same than for Fig. 51.

These experiments lead to the conclusion that the metal-thiolate cluster has to be opened before the sulfide ions can incorporate. However, so far it is not understood, if the sulfide ions remove the initial present Zn^{2+} ions from Zn_5-cicMT2 to incorporate themselves. To address this point in more detail we incubated Zn_5-cicMT2 with 20 equivalent of sulfide ions and purified the mixture with size exclusion chromatography. We performed the same with a twin sample without sulfide ions. After purification, in both samples still five equivalents of Zn^{2+} ions and no sulfide ions were detected. Hence clearly, sulfide ions do not remove Zn^{2+} ions from the protein. However, also no sulfide ions were incorporated. On the other hand, both the UV and MCD spectra of Zn_5-cicMT2 after incubation with ten equivalent of sulfide ions differ significantly from the spectra of Zn_5-cicMT2, which cannot be explained by spectral contributions of free sulfide ions or ZnS under the conditions and at the concentrations used here.

To sum up, we could show, that the sequence of metallothionein, Cd^{2+} and S^{2-} ions addition is crucial for the formation of Cd^{2+}-S^{2-}-thiolate clusters (Fig. 54).
It is intriguing that when first Cd^{2+} ions are added to apo- or Zn_5-cicMT2 and then sulfide ions are provided no sulfide ions are incorporated into the cluster. Hence, it appears that the sulfide ions must be already coordinated to the Cd^{2+} ions for successful incorporation. On the other hand, if first Cd^{2+} and sulfide ions are incubated in the absence of cicMT2, also no incorporation of sulfide ions is observed. It has been reported in the literature that the formation of the mineral ZnS from aqueous solution proceeds first via neutral complexes with 1:1 stoichiometry and additional aqua ligands that subsequently aggregate to larger negatively charged complexes, e.g. $Zn_4S_6^{4-}$.[223] Hence it might be mechanistically feasible that initially formed analogous neutral 1:1 Cd,S-complexes can be bound by the protein, while the aggregated negatively charged higher molar mass complexes are not incorporated. Consequently, it would be the kinetically controlled formation of Cd,S-aggregates that determines if sulfide ion incorporation into the MT takes place.

However, as mentioned above, Cd^{2+} ions are incorporated into the protein even after pre-incubation with sulfide ions. This suggests that cicMT2 must be able to compete with the preformed Cd,S-aggregates for Cd^{2+} ions.

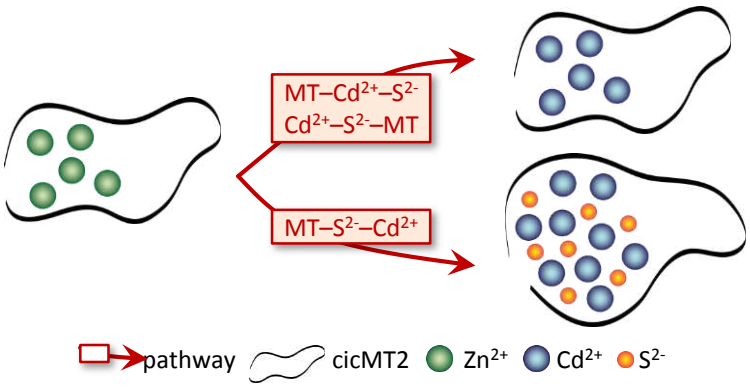

Fig. 54 Scheme of proposed pathways of Cd^{2+}-S^2-thiolate cluster formation in cicMT2 in dependence of the sequence of metallothionein, cadmium and sulfide ion addition.

7.4.3. Sulfide ion incorporation as a general feature of MTs

7.4.3.1. Native sulfide ion content of rabbit liver MT2A

In previous reports, occurrence of sulfide ions in MTs was only analyzed in recombinantly expressed proteins isolated from *E. coli* or in MTs from yeast, both grown in metal supplemented growth media.[81, 84, 213] Due to the difficulties in isolation of native plant MTs, the native sulfide ion content of MTs was accessed by rabbit liver MT2A.[60, 169, 224-225]

To investigate the presence of sulfide ions in mammalian MTs *in vivo* the native form of rabbit liver MT2A, isolated from Cd^{2+}-supplemented animals by the group of Prof. Milan Vašák (Institute of Inorganic Chemistry, University of Zurich),[87, 226] was analyzed with a combination of F-AAS, 2-PDS, and the methylene blue assay.[199] The native content of sulfide ions was below 0.2 equivalent of S^{2-} ions per MT2A, and thus within the error range of the method. The general formula $Zn_{2.4}Cd_{4.6}$-MT2A was determined, being in line with previous investigations that so far never revealed the occurrence of any sulfide ions in mammalian MTs.[227] It has to be considered however, that although the native protein was never exposed to acidic conditions during the purification procedure, which self-evidently would release any sulfide ions present in form of H_2S, it was exposed to ion exchange chromatography with DEAE cellulose, which has been proposed to remove sulfide ions from MT preparations.[84] Accordingly, the experiment could not finally prove the absence of sulfide ions from native preparations of mammalian MTs.

7.4.3.2. *In vitro* sulfide ion incorporation into rabbit liver MT2A

The analysis of *in vitro* sulfide ion incorporation abilities of mammalian MTs was attempted in more detail.[199] Natively purified protein was demetallated and remetallated with Zn^{2+} ions and titrated analogously to Zn_5-cicMT2. For this, 10 μM rabbit liver Zn_7-MT2A were titrated with Cd^{2+} ions in absence and presence of ten equivalent of S^{2-} ions and the progress of Cd^{2+} ion incorporation was monitored with UV spectroscopy (Fig. 55). Clearly, the titration of Zn_7-MT2A with Cd^{2+} ions in presence of sulfide ions led to the evolution of additional transitions red-shifted from the intense LMCT bands around 250 nm indicative for Cd^{2+}-thiolate cluster formation. Yet, the intensity of these additional transitions was considerably weaker compared to the titration of Zn_5-cicMT2. As expected, the absorptivity at 250 nm reached a maximum value after addition of seven equivalents of Cd^{2+} ions for the titration of rabbit liver Zn_7-MT2A in absence of sulfide ions. In presence of sulfide ions, the Cd^{2+} binding capacity seems to be increased resulting in saturation with metal ions after approximately 10 equivalents of Cd^{2+} ions.

To analyze the formed complexes further, both samples were purified with size exclusion chromatography and the content of Cd^{2+} and S^{2-} ions was determined (Fig. 55 D). The elution profiles of the size exclusion chromatography showed single peaks at 14 mL elution volume without any minor peaks resulting from aggregates. The final composition obtained this way was $Cd_{6.7\pm0.4}S_{0.2\pm0.2}$-MT2A for the titration performed in absence of sulfide ions and $Cd_{8.4\pm0.4}S_{3.0\pm0.3}$-MT2A for the form obtained after titration with Cd^{2+} ions in presence of sulfide ions.

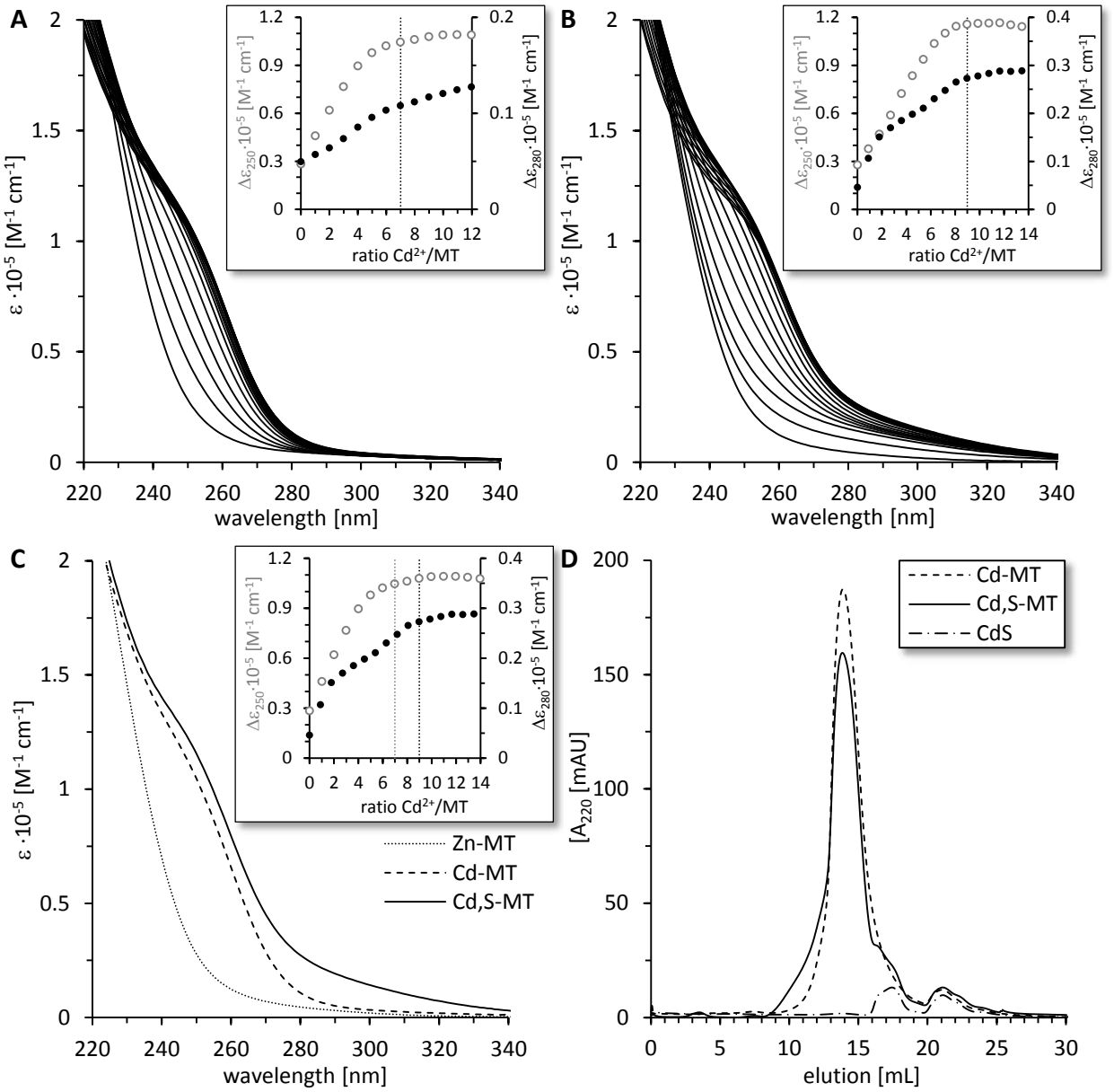

Fig. 55 **(A-C)** UV spectra of the titration of 10 μM rabbit liver Zn_7-MT2A in a buffer containing 10 mM Tris-HCl, 10 mM NaCl, pH 7.5 with increasing amounts of Cd^{2+} ions. **(A)** shows the titration in absence of additional S^{2-} ions, **(B)** in presence of 100 μM Na_2S. Insets show the plot of the molar absorptivity at the LMCT bands (250 nm and 280 nm) against the number of equivalent of Cd^{2+} ions added to MT2A. **(C)** Overlay of Zn_7-MT2A and Cd_7-MT2A from **(A)** and Cd_9S_x-MT2A from **(B)**. **(D)** shows the elution profiles of the final titration mixtures when applied to an analytical size exclusion chromatography column. The peaks at 14 mL belong to the monomeric protein species.

It is hence obvious that sulfide ions can only marginally increase the Cd^{2+} ion binding capacity of rabbit liver MT2A in comparison to cicMT2. In addition, the efficiency of Cd^{2+} ion binding is reflected in the ratio between additionally coordinated Cd^{2+} ions and incorporated sulfide ions. The ratio amounts to 0.47 ± 0.05 and is thus in the same range than the value of 0.49 obtained for cicMT2 (7.3.1.1). The ratio between the total amount of bound Cd^{2+} ions and the combined number of cysteine thiolate and sulfide ion ligands remained constant with 0.37 ± 0.04 compared to 0.35 in the sulfide-free Cd_7-MT2A form.

To validate the metal ion and sulfide ion content, both forms were subjected to ESI^+-MS and MALDI-MS (Fig. 56).

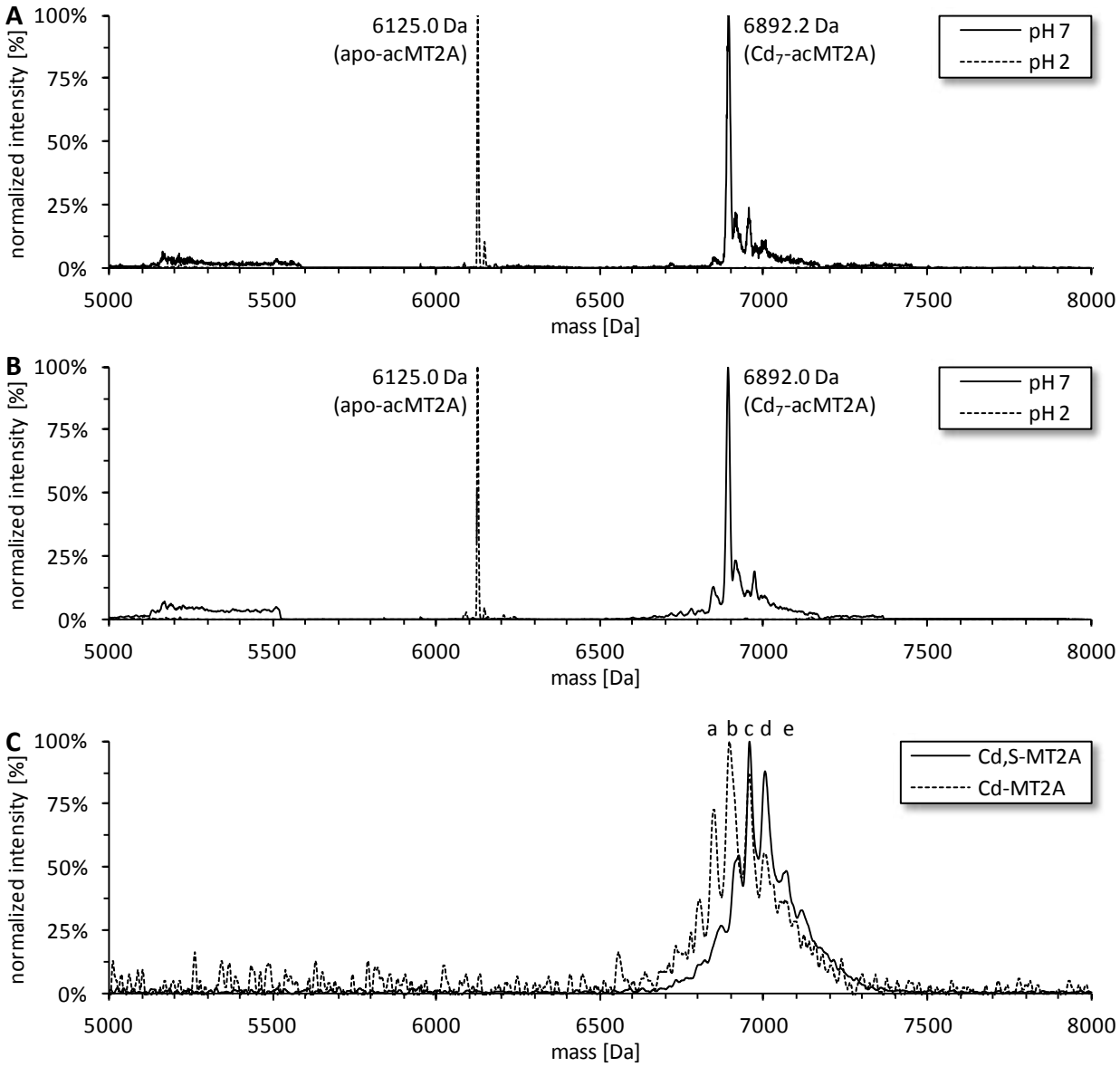

Fig. 56 Deconvoluted mass spectra with normalized intensities of 100%. **(A)** ESI^+-MS spectra of Cd_7-MT2A measured at acidic pH (pH 2, dashed line) and neutral pH (pH 7, solid line). Acidic spectrum has a maximum intensity of 26'200 counts s^{-1} and shows a single peak at 6125.0 Da for reduced acetylated apo-MT2A (calc. 6125.1 Da). Spectra taken at neutral pH revealed a main peak with a maximum intensity of 2630 counts s^{-1} at 6892.2 Da for acetylated Cd_7-MT2A (calc. 6891.8 Da). **(B)** ESI^+-MS spectra of Cd_8S_3-MT2A measured at acidic pH (pH 2, dashed line) and neutral pH (pH 7, solid line). Acidic spectrum has a maximum intensity of 107'000 counts s^{-1} and shows a single peak at 6125.0 Da for reduced acetylated apo-MT2A (calc. 6125.1 Da). Spectra taken at neutral pH revealed a main peak with a maximum intensity of 2220 counts s^{-1} at 6892.0 Da for acetylated Cd_7-MT2A (calc. 6891.8 Da). **(C)** MALDI-MS spectra of Cd_7-MT2A (dashed line) and Cd_8S_3-MT2A (solid line). Spectrum of Cd_7-MT2A has a maximum intensity of 115 counts s^{-1} and shows four main peaks (indicated a-d), (a) at 6847.3 Da for acetylated Cd_6-MT2A + 3 Na^+ (calc. 6848.4 Da), (b) at 6895.4 Da for acetylated Cd_7-MT2A (calc. 6891.9 Da), (c) at 6955.6 Da for acetylated Cd_7-MT2A + 3 Na^+ (calc. 6960.9 Da), and (d) at 7003.3 Da for acetylated Cd_8-MT2A (calc. 7004.3 Da). Spectrum of Cd_8S_3-MT2A has a maximum intensity of 695 counts s^{-1} and shows four main peaks (indicated b-e), (b) at 6923.0 Da for acetylated Cd_7S_1-MT2A (calc. 6923.9 Da), (c) at 6955.9 Da for acetylated Cd_7S_2-MT2A (calc. 6956.0 Da), (d) at 7003.8 Da for acetylated Cd_8-MT2A (calc. 7004.3 Da), and (e) at 7067.6 Da for acetylated Cd_8S_2-MT2A (calc. 7068.4 Da).

In the deconvoluted ESI^+-MS spectra Cd_7-MT2A shows at neutral pH a peak at 6892.2 Da for the metal loaded form (calculated 6892.2 Da), and at acidic pH one peak at 6125.0 Da for the apo-MT2A (calculated 6125.1 Da). Both ESI^+-MS spectra showed the acetylated MT2A, what is

typical for an isolated protein. In case of the sulfide ion containing form, the apo-MT2A is visible as well in the deconvoluted ESI^+-MS spectrum taken at acidic pH. But the ESI^+-MS spectrum recorded at neutral pH shows again the acetylated Cd_7-MT2A at 6892.0 Da (calculated 6892.2 Da). No sulfide containing form can be detected. The MALDI-MS shows a different picture, both sulfide containing and sulfide absent Cd-MT2A forms show four main peaks. For Cd_7-MT2A peaks are visible for acetylated Cd_6-MT2A + 3 Na^+ at 6847.3 Da (calculated 6848.4 Da), for acetylated Cd_7-MT2A at 6895.4 Da (calculated 6891.1 Da), for acetylated Cd_7-MT2A + 3 Na^+ at 6955.6 Da (calculated 6960.9 Da), and for acetylated Cd_8-MT2A at 7003.3 Da (calculated 7004.3 Da). The measured Cd_8S_3-MT2A shows masses of 6923.0 Da for acetylated Cd_7S_1-MT2A (calculated 6923.9 Da), of 6955.9 Da for acetylated Cd_7S_2-MT2A (calculated 6956.0 Da), of 7003.8 Da for acetylated Cd_8-MT2A (calculated 7004.3 Da), and of 7067.6 Da for acetylated Cd_8S_2-MT2A (calculated 7068.4 Da). The expected size of 7100.0 Da for the Cd_8S_3-MT2A is not detectable. But the peaks of the designated Cd_8S_3-MT2A in the deconvoluted MALDI-MS spectrum are clearly shifted to higher mass than those of Cd_7-MT2A. However, the metal-sulfide-thiolate-cluster of MT2A was not stable enough for the measurement conditions.

A more gentle method than mass spectrometry to obtain information about the sulfide ion incorporation into the metal-thiolate cluster of rabbit liver MT2A is ^{113}Cd-NMR spectroscopy. Zn_7-MT2A was loaded with $^{113}Cd^{2+}$ ions and, if required, with sulfide ions, and was analyzed with NMR spectroscopy. 1D ^{1}H NMR and 2D ^{1}H-^{113}Cd HSQC NMR spectra were recorded and compared to 2D ^{1}H-^{113}Cd COSY NMR spectra measured 25 years ago by Vašák et al.[160] using the same conditions, except a lower protein concentration.

For $Cd_{6.7}$-MT2A, the recorded 2D ^{1}H-^{113}Cd HSQC NMR spectrum shows nine different chemical shifts in the cadmium dimension at 606, 613, 616, 626, 632, 642, 645, 668, and 673 ppm (Fig. 57 B). Expected would have been seven different signals, for each bound Cd^{2+} ion one, as shown by Vašák et al.[160] in the 2D ^{1}H-^{113}Cd COSY NMR spectra with chemical shifts of 613, 626, 632, 650, 661, 670, and 673 ppm (Fig. 57 A). Different from the literature are additional cross peaks at 606, 616, 642, and 645 ppm, and one disappeared peak at 661 ppm. The spectra of Vašák et al. does not show the region below 610 ppm, therefore we could not figure out, if the cross peaks at 606 nm originated just from our sample or were simply not shown in the past. One of the other peaks at 616, 642, and 645 ppm is probably a substitution for the one we could not detect at 661 ppm most likely caused by the different NMR spectroscopy methods used. COSY and HSQC are both correlation spectroscopy NMR methods for identifying nuclei sharing a scalar coupling. In the COSY spectra typical couplings over three bonds were detected, in the HSQC spectra couplings between nuclei separated by only one bond are preferred, while J^3 and J^4 couplings are sometimes also observed. Subtracting one of the three additional cross peaks, still two new peaks were visible in the spectrum, indicating two or three different species present in solution. This might be due to different reconstitution methods used. Vašák et al. performed size exclusion runs to ensure size homogeneity before each NMR spectroscopy recording, while in this work the sample was only washed via ultrafiltration due to the low quantity of sample available.

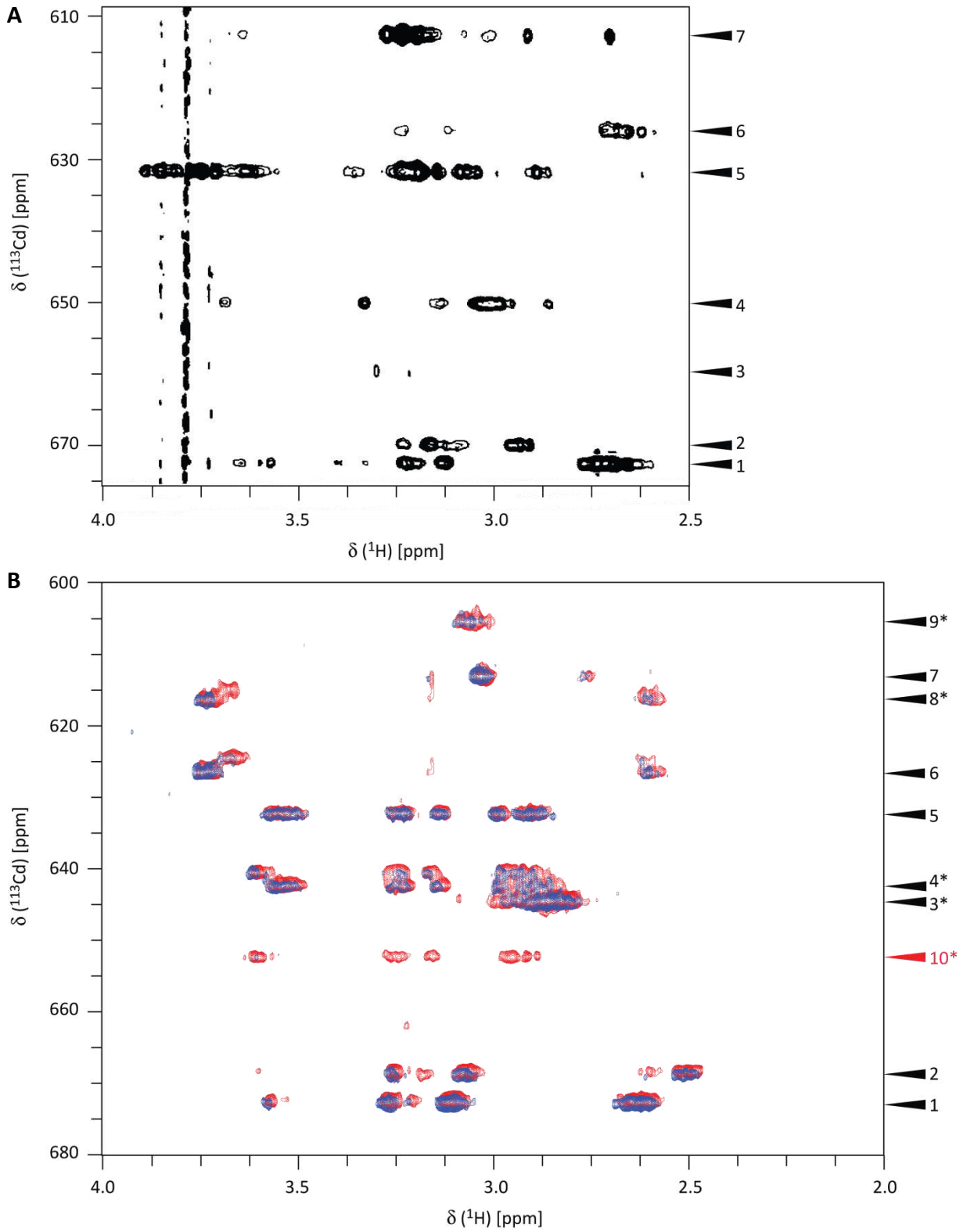

Fig. 57 NMR spectra **(A)** of Cd_7-MT2A of Vašák et al.[160] and **(B)** overlay of $Cd_{6.7}$-MT2A (blue) and $Cd_{8.4}S_{3.0}$-MT2A (red). **(A)** Section of 2D ^{1}H-^{113}Cd COSY NMR spectra of 10 mM Cd_7-MT2A in 20 mM deuturated Tris-HCl pH 7.0, 50 mM KCl, D_2O, measured at 298 K. **(B)** Overlay of a section of the 2D ^{1}H-^{113}Cd HSQC NMR spectra from 500 µM $Cd_{6.7}$-MT2A (blue) or 500 µM $Cd_{8.4}S_{3.0}$-MT2A (red) in 20 mM deuturated Tris-HCl pH 7.0, 50 mM KCl, 10 % D_2O, measured at 298 K. The locations of the ^{113}Cd resonances are indicated on the right side of the spectra. They correspond for **(A)** and **(B)**, the changed one are marked with a *, the red colored one is only appearing for the form containing sulfide ions.

Just as for $Cd_{6.7}$-MT2A, a 2D ^{1}H-^{113}Cd HSQC NMR spectrum was recorded of $Cd_{8.4}S_{3.0}$-MT2A (Fig. 57 B). An overlay of the NMR spectra of both forms shows additional resonances for the sulfide containing form with a chemical shift for cadmium to 652 ppm, what is in accordance with 1.4 additional Cd^{2+} ions bound to MT2A in presence of sulfide ions. The additional resonances with a distinct chemical shift indicate a change in the cluster arrangement of the protein, although the cluster structure seems to change only slightly, as most of the resonances overlap with the ones of Cd_7-MT2A. The clear appearance of only one additional resonance indicate the favored incorporation of only one additional cadmium ion into one of the metal-thiolate clusters or as a connection between two clusters which maintains a well-defined structure.[228] With this, we could clearly show the influence of the sulfide ions on the metal-thiolate cluster of rabbit liver MT2A.

Different methods could show the incorporation of a small amount of sulfide ions into the metal-thiolate clusters of rabbit liver MT2A. The metal-thiolate cluster of cicMT2 is able to host much larger metal-sulfide-thiolate clusters compared to the metal-thiolate clusters of MT2A. An explanation for this can, again on a hypothetical basis, be found in the specific amino acid structure of cicMT2. Plant MTs from the MT1, MT2, and MT3 subgroups in general feature a long cysteine-free amino acid stretch between the *N*- and *C*-terminal cysteine-rich regions. Cd_5-cicMT2 as well as Cd_9S_7-cicMT2 were shown to presumable form a hairpin-like single cluster structure. In a single cluster even larger cluster structures can be easily envisioned to be hosted in such an arrangement with the linker region functioning as an adjustable hinge not unlike the ends of an accordion (Fig. 58).[135-136] However, the amino acid sequences of mammalian MTs enclose two separate metal-thiolate clustesr and do not contain longer linker regions within the amino acid stretches forming a cluster. With this dumbbell like shape, steric reasons can be envisioned that prevent expansion of these clusters. A view that would nicely explain the finding that incorporation of sulfide ions only marginally increases the cluster size of rabbit liver MT2A.

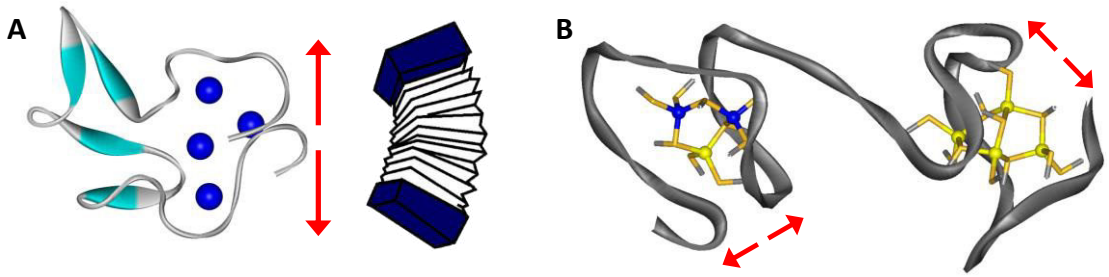

Fig. 58 **(A)** Scheme of proposed structure of Cd_5-cicMT2. The arrows indicate the possibility of cluster expansion due to the long cysteine free linker region similar to the movement of an accordion. **(B)** The absence of cysteine free linker regions within the two domains in mammalian MTs inhibits significant expansion of the clusters as illustrated by the shorter arrows. Structure is prepared using the coordinates of rat Zn_2Cd_5-MT2 (PDB ID: 4MT2).[62]

7.5. Functional analysis of plant MTs

So far, no conclusive data about the function of plant metallothioneins are available and also the roles proposed for other metallothioneins are still under discussion. With their high affinity to metal ions, MTs are supposed to play a role in metal homeostasis and detoxification, e.g. the yeast *S. cerevisiae* has two protection systems against high metal ion concentration, i.e. scavenging and transporter proteins. These two opinions present also a possible role for the plant MTs. Therefore their function was investigated by yeast complementation assays. The protection systems of the yeast are knocked out and are replaced by vectors coding for plant MTs. It was supposed, that the plant MTs take over the function of the missing protection systems in yeast when grown in a metal enriched environment.

7.5.1. Cloning of the yeast deletion strains

Defense mechanisms of *S. cerevisiae* against high metal concentrations are Cu^{+} scavenging proteins such as Cup1 and Crs5, as well as Zn^{2+} transporter proteins as Zrc1 and Cot1.[92, 131] These defense mechanisms are knocked out in yeast complementation assays and are replaced by a DNA coding for another protein supposed to have a similar function. Former studies already showed such yeast complementation assays with MTs, but they were performed with diverse wild-type strains for the different deletion mutations. It is however important to use the same wild-type for all experiments, because the optical density can differ substantially depending on the employed strain.[229] The yeast strain used in this work as wild-type was specifically chosen based on the number of existing *cup1* repetitions on the chromosome, since the number of repetitions defines the sensitivity to Cu^{+} ions.[230] In general, yeast strains, as the completely sequenced S288C strain from the yeast genome database, have two or multiple copies of *cup1* sequences in a row.[144, 231] These multiplications developed when the budding yeast was widely used in fermentation and brewing industries, and the environmental changes, e.g. the use of copper vessels for brewing, let to changes of the complex biological networks in order to gain resistance.[232-234] The Cu^{+}-binding protein Cup1 was already investigated in the past and for this purpose the *cup1* repetition was replaced by a single unit resulting in the $CUP1^{S}$ strain.[146] This $CUP1^{S}$ strain is more sensitive to high metal ion concentration in the environment and therefore was used in this work as a wild-type strain.

7.5.1.1. DNA sequence verification of the strain $CUP1^{S}$

To be sure, that the used haploid wild-type strain contains only one copy of the *cup1* gene and had not undergone a spontaneous mutation in the meantime, the chromosomal DNA sequence of *cup1* with an up- and downstream part was amplified by PCR and then sequenced. For this, the genomic DNA of the $CUP1^{S}$ strain was purified, and a standard PCR was performed with the primers TH047 cup1 seq F and TH048 cup1 Rw. The PCR product was purified and used as template for a second identical PCR. This second step was necessary to improve the yield. The gained fragment was purified and sequenced. The sequence result shows the same DNA sequence

as S288C in the database, but with one deleted iteration unit, and some point mutations not affecting the *cup1* gene (Fig. 70). It was shown, that the CUP1^S strain still contains one single copy of the *cup1* gene.

The completely sequenced S288C *S. cerevisiae* strain showed a nonsense point mutation (stop codon TAA) in the ninth codon of the *crs5* gene, which originally was a glutamic acid (GAA).[144] To ensure a complete *crs5* gene encoded on the genomic DNA, the chromosomal DNA sequence of *crs5* with an up- and downstream part was amplified by PCR and sequenced. For this, the genomic DNA of the CUP1^S strain was purified, and a standard PCR was performed with the primers TH019 crs5 F and TH021 crs5 R. The obtained fragment (900 bp) was purified and sequenced. The sequence result shows the same DNA sequence as S288C in the database, but without point mutation in the 9th codon and with the original glutamic acid encoded (Fig. 72).

We could show that the CUP1^S strain contains one single copy of the *cup1* gene and the full-length *crs5* gene. Therefore, the CUP1^S strain can be further used for the production of the deletion mutants.

7.5.1.2. Knock out of Zn transporters and MTs from the yeast chromosome

7.5.1.2.1. General strategy

For the yeast complementation assays, the defense mechanism of *S. cerevisiae* against high metal ion concentration had to be knocked out. As we work with a haploid strain, the deletion of the desired gene can be performed singly by homologous recombination, and no further strain crossing, sporulation, tetrades dissection and spore analysis is necessary. Homologous recombination is a widely used technique for gene targeting and was already used for the production of the wild-type CUP1^S strain.[146, 235] To produce a mutant yeast strain by homologous recombination, two major elements are needed. A wild-type CUP1^S strain contributing to the germ line, and a targeting construct containing target-gene sequences with the desired mutation. Following the procedure, target gene sequences with homologous sequences for the up-, and downstream regions of the endogenous gene are transformed into the CUP1^S strain, and homologous recombination occurs, resulting in the introduction of the mutation from the targeting construct into the target gene.

Two possibilities exist for knocking out an endogenous gene. Either a sequence is inserted into a gene disrupting its functional sequence or a sequence replaces a gene deleting it completely. Our approach was to delete the original defense mechanisms completely with marker sequences facilitating the selection for mutant cells. Since four single mutants and two double mutants were planned, two different markers are sufficient. Chosen were the aminoglycoside antibiotic marker geneticin and the auxotrophic marker histidine. Due to the lack of the *his* gene in the genotype of CUP1^S it was possible to use an auxotrophic *his* marker. Cells with re-integrated marker are able to growth on media lacking histidine. G418 is an analogue of kanamycin, against which the yeast cells are resistant. The mode of action for both markers is the same. They block the polypeptide synthesis by interfering with ribosomal function and inhibiting protein elongation. By inserting the *kan^R* marker into the chromosomal DNA, the yeast cells can gain resistance against G418.

A scheme of the exact procedure for the replacement of *crs5* with *his* is shown in Fig. 59. From the template marker plasmid pYM44 the *his* gene is amplified with additional overhangs on the 5'- and 3'-ends, which are homologous of the up-, and downstream part from *crs5*. Afterwards, the PCR product is transformed into the CUP1^{S} strain which partially performs the homologous recombination of the PCR product with the chromosomal DNA via the homologous sequences. Finally, the transformants are selected by the growth media.

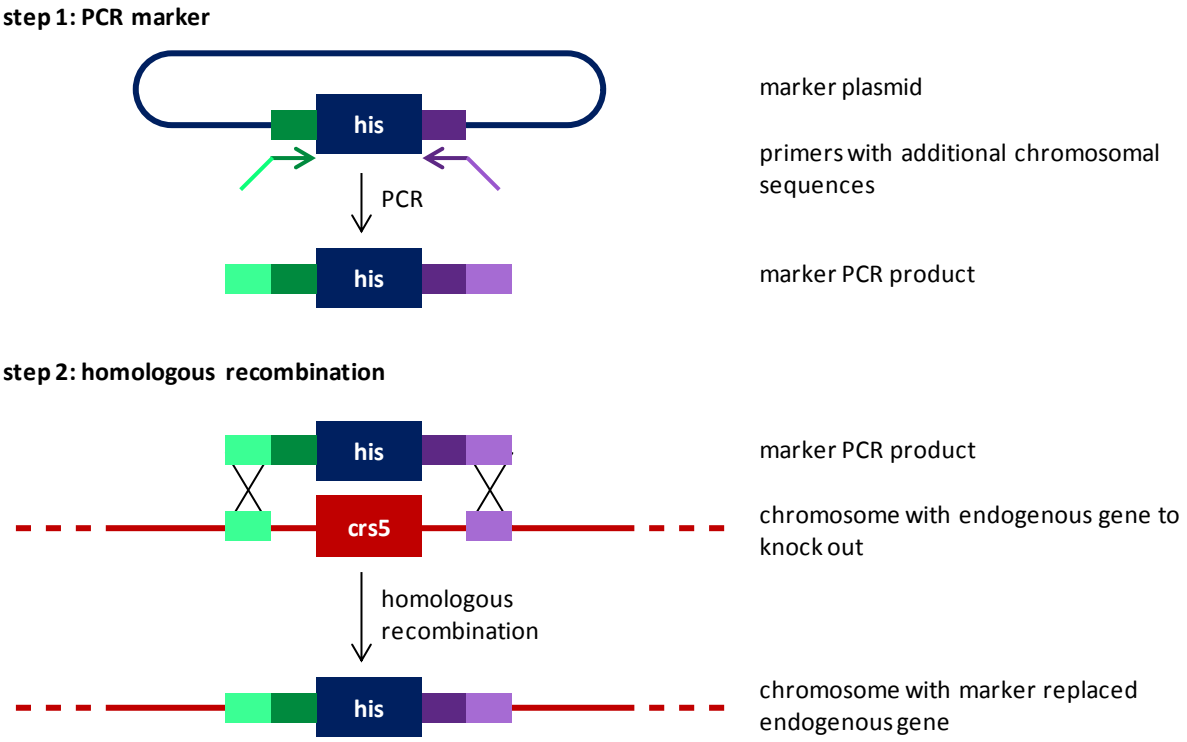

Fig. 59 Scheme of the strategy for the homologous recombination. In the first step, a PCR is performed, amplifying the marker sequence from a marker plasmid (pYM44). As primers were used 20 bp long marker sequences connected to 50 bp long chromosomal regions, yielding in 70 bp long primers. The 20 bp long sequences are complementary to the up-, and downstream region of the marker gene (*his*) from the marker plasmid. The connected 50 bp long sequences are complementary to the chromosomal DNA up-, and downstream of the deleting gene sequence (*crs5*). In a second step, the PCR product is transformed into the wild-type yeast strain (CUP1^{S}), which performs itself a homologous recombination of the PCR product with the chromosomal DNA via the homologous sequences. This results in a deletion of the *crs5* gene, which is replaced by the marker sequence *his*.

7.5.1.2.2. First trials

The target construct containing the target-gene sequences with the desired mutation and the additional homologous overhangs were produced by PCR as described (6.3.3.1). The genes *cup1* (Fig. 70) and *cot1* (Fig. 76) should be replaced by a *kan*^{R} sequence (Fig. 71, Fig. 77). Therefore the PCR was performed with a pFA6a-kanMX6 template and primers encoding the overhangs (TH028 cup1D dn and TH029 cup1D up for *cup1*, or TH038 HR cot1 F and TH039 HR cot1 R for *cot1*). The genes *crs5* (Fig. 72) and *zrc1* (Fig. 74) should be replaced by a *his* sequence (Fig. 73, Fig. 75). Therefore the PCR was performed with a pYM44 template and primers encoding the

overhangs (TH022 crs5D dn and TH023 crs5D up for *crs5*, or TH035 HR zrc1 F and TH036 HR zrc1 R for *zrc1*). All fragments could be amplified with a reasonable amount and as single products, except for some primer dimers running at 100-150 bp on the agarose gel (Fig. 60).

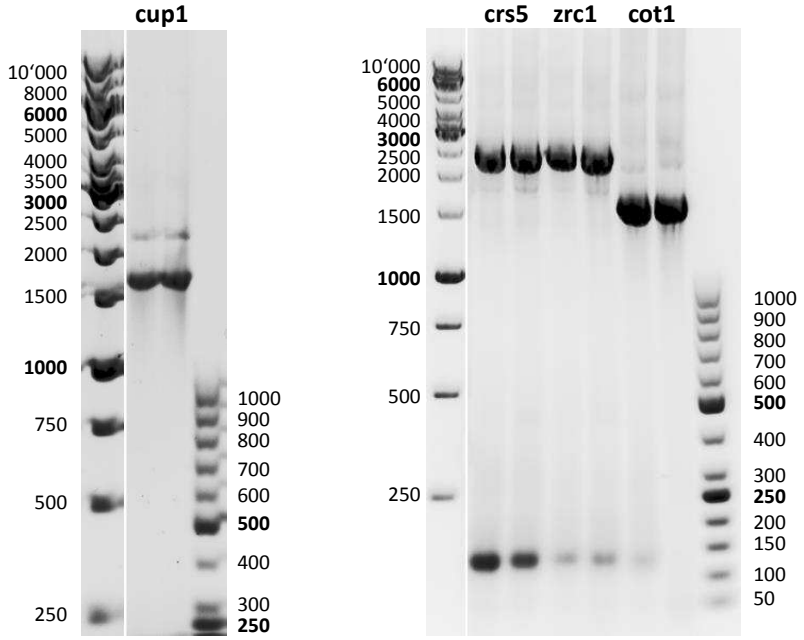

Fig. 60 Agarose gel of DNA marker fragments for homologous recombination amplified with PCR. Fragments coding for the *his/kan*^{R} sequence flanked by up-, and downstream DNA sequences of the target gene. The fragment cup1 encodes *kan*^{R} with *cup1* flanking sequences and has an expected size of 1503 bp. The fragment crs5 encodes *his* with *crs5* flanking sequences and has an expected size of 2411 bp. The fragment zrc1 encodes *his* with *zrc1* flanking sequences and has an expected size of 2413 bp. The fragment cot1 encodes *kan*^{R} with *cot1* flanking sequences and has an expected size of 1603 bp. Ladder sizes are indicated on the sides in bp.

The 1503-2413 bp long DNA fragments obtained from PCR (Fig. 60) were purified and transformed into freshly prepared competent wild-type CUP1^{S} yeast cells (6.3.3.2) and the cells were plated on selective media. After one week of growth, no yeast colonies could be detected containing the desired deletion mutations, despite the fact, that the positive and negative controls were growing. The two positive controls, one with the transformed plasmid pRS416 grown on SD-Ura medium, and the other transformed with the PCR products grown on rich medium, showed normal yeast growth. In the negative control, the cells were transformed with water. Here, no yeast growth could be detected on the selective plate. It seems, that either the transformation with linear DNA was not successful, or the homologous recombination after transformation was not taking place. Judging from the positive controls, the yeast cells seem to survive the transformation and transformed circular DNA is functional in the cells.

An additional problem was bacterial contamination. On all plates bacterial colonies could be detected. To prevent the overgrow of yeast colonies with bacterial colonies, the plates used for the following experiments were supplemented with 50 ng L^{-1} ampicillin stopping or at least lowering the bacterial grow without impact on the yeast growth. To verify this, wild-type CUP1^{S}

cells were grown on media with ampicillin supplementation and are compared to cells grown on media without ampicillin. Both plates showed a similar growth pattern after one week, however the one without ampicillin supplementation was growing slightly faster in the beginning of the experiment.

To improve the transformation efficiency of the $CUP1^S$ strain several changes were made stepwise in the protocol. 1) The concentration of the PCR product in the transformation mixture was increased from 1.5 ng mL^{-1} to 5 ng mL^{-1}. 2) The used SS-DNA was changed from short stranded herring sperm DNA to long stranded salmon sperm DNA, and the denaturation of the SS-DNA was performed directly before use. 3) The incubation of the cell solution was done in a cell shaker with a larger shaking radius than the thermoshaker. 4) The transformants were not directly plated after 40 min of incubation but were first grown for one day in liquid culture. 5) The transformants are not centrifuged and resuspended to reduce the plating volume, but they are directly plated with the whole liquid.

The changed conditions were tested in different combinations, but none of them led to growing transformants. Only the transformation of plasmids could be slightly improved. Due to the positive and negative controls the problem was either the transformation of linear DNA or the following homologous recombination in the cell. Since the $CUP1^S$ strain was already widely used for homologous recombination, this process should not be a principal problem.[80, 133, 236-237] Therefore, further protocol changes should be conducted for the production of the deletion mutants. Changes for increasing the transformation efficiency could be: Finding of the optimal cell density for transformation.[153] DNA purification by phenol extraction or by CsCl/ethidium bromide density gradients.[148, 238] The use of Difco agar to prepare the dropout plates. The Use of fresh PEG 3350 instead of PEG 8000 or PEG 1000.[152] Additionally, the homologous recombination is sensitive to the size of the homologous DNA sequences, and the sequence heterogeneity of the homologous DNA. To force the recombination events, the sequences can be prolonged with the wild-type DNA.[239]

7.5.1.2.3. Strategy for facilitating the homologous recombination process

As the transformation of circular DNA (positive controls) was successful, it was expected, that the homologous recombination presents the main problem. The occurrence of this event is dependent mainly on two factors. Once, the integration event is sensitive to small amounts of sequence heterogeneity, already single point mutations between the construct and the target genome can have a dramatic effect on the event rate.[239-241] Second, the homologous recombination is sensitive to the size of the homologous DNA sequences. The rate of homologous recombination may increase with increasing lengths of homologous DNA up to 15 kb for transgenic animals.[242-243] Ideally, the marker genes are flanked by >100 bp homologous sequences in yeast, which are exactly identical with the target strain.

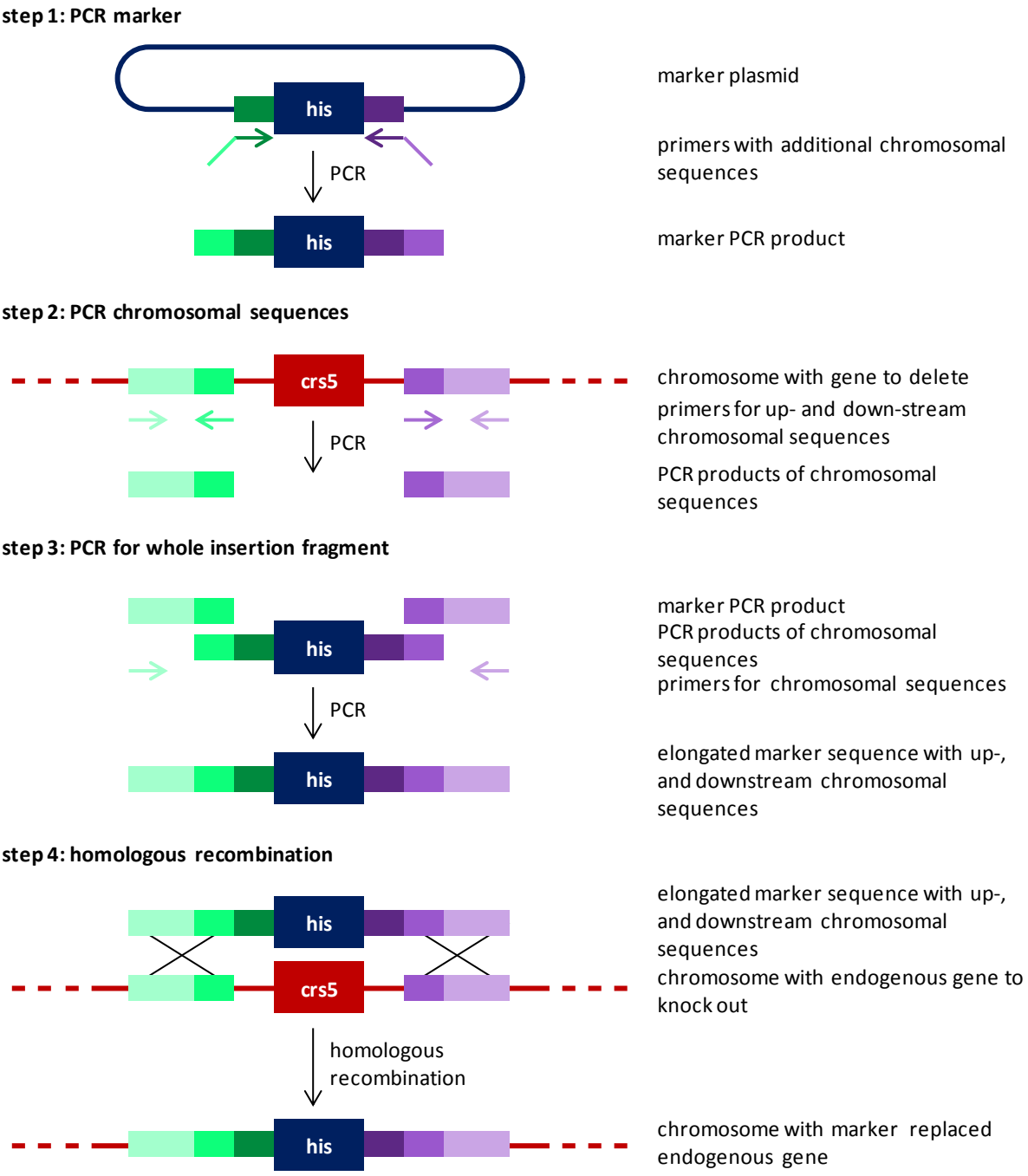

Fig. 61 Scheme of the strategy for the extended homologous recombination. In the first step, a PCR is performed, where the marker sequence is amplified from a marker plasmid (pYM44). As primers were used 20 bp long marker sequences connected to 50 bp long chromosomal regions, yielding in 70 bp long primers. The 20 bp long sequences are complementary to the up-, and downstream region of the marker gene (*his*) from the marker plasmid. The connected 50 bp long sequences are complementary to the chromosomal DNA up-, and downstream of the deleting gene sequence (*crs5*). For prolongation of the homologous sequences with the chromosomal DNA, two standard PCRs of a 350 bp long up-, and downstream sequence of the *crs5* gene are performed in a second step. These sequences contain a 50 bp long overlap with the first PCR product from the marker plasmid (*his*). In the third step, the up-, and downstream chromosomal sequences are combined with the first PCR product of the marker plasmid (*his*), and a further PCR is performed, resulting in a PCR product containing the marker sequence (*his*) with additional 350 bp long up-, and downstream homologous sequences of *crs5* gene from the chromosomal DNA. In a last step, the PCR product is transformed into the wild-type yeast strain (CUP1^{S}), which performs itself a homologous recombination of the PCR product with the chromosomal DNA via the homologous sequences. This results in a deletion of the *crs5* gene, which is replaced by the marker sequence *his*.

For facilitating the homologous recombination process, the homologous sequences flanking the *his* and *kan*^{R} genes are prolonged with wild-type sequence. For this, the same PCR products with 50 bp long homologous stretches are amplified as shown in 7.5.1.2.1 and afterwards elongated in two steps before the transformation (Fig. 61). For the prolongation, an up-, and downstream sequence of the target gene have to be produced. Their amplification directly from the used wild-type strain CUP1^{S} via PCR has the advantage, that possible point mutations compared to the S288C strain are non-relevant. The homologous long up-, and downstream sequences has to have an >20 bp overlapping sequence with the homologous sequence of the marker PCR from the first step. In the third step, the three PCR products from the first and second step, i.e. marker PCR product, upstream PCR product, and downstream PCR product, are combined with additional primers for the 5'- and the 3'-end and a fourth PCR is performed. During this fourth PCR, all three original elements are connected resulting in a marker gene flanked by long up-, and downstream homologous sequences. The final PCR product can be transformed into the wild-type yeast cells CUP1^{S} strain as described in Fig. 59. If the homologous recombination takes place, yeast colonies with a deleted defense mechanism should grow.

7.5.1.2.4. Trial for the deletion mutant CUP1^{S} Δcrs5

The new strategy with elongated homologous sequences was first tried for the CUP1^{S} Δcrs5 strain, because the up-, and down-stream part of the *crs5* gene was sequenced. Therefore, a heterologous sequence in the 50 bp long synthesized primer sequence can be excluded.
The first PCR product was produced by PCR as described and discussed in 7.5.1.2.2. The result was a purified and correct *his* gene flanked by 50 bp long homologous sequences to the up-, and downstream part of the chromosomal *crs5* gene (Fig. 73).
In the second step, ~350 bp of the up-, and downstream part of the chromosomal *crs5* gene were amplified from purified CUP1^{S} template DNA (Fig. 62 A). For the upstream part, the primers TH052 crs5 up F and TH053 crs5 up R were used to produce a 350 bp long DNA fragment, which has downstream a 28 bp long overlapping part with the marker PCR from the first step. For the downstream part, the primers TH054 crs5 down F and TH055 crs5 down R were used to produce a 334 bp long DNA fragment, which has upstream a 42 bp long overlapping part with the marker PCR from the first step. In the third step, the products of the first and second step were combined with additional primers for the amplification of the whole insert (TH052 crs5 up F and TH055 crs5 down R). In a single PCR, first the up- and downstream homologous sequences acted as primers for connecting them to the marker sequence and second the additional primers operated as primers to amplify the whole prolonged template (Fig. 62 B). In the last step, the PCR product was transformed into the wild-type yeast strain CUP1^{S} as described and discussed in 7.5.1.2.2. The CUP1^{S} performed homologous recombination of the complete PCR product with the chromosomal DNA allowing the growth of the transformants on selective histidine lacking media. After one week of growing, some single yeast colonies could be detected. It seemed, that the longer homologous sequences solved the problem of recombination, but still the efficiency is quite low. Maybe further improvements can be achieved by even longer homologous sequences.

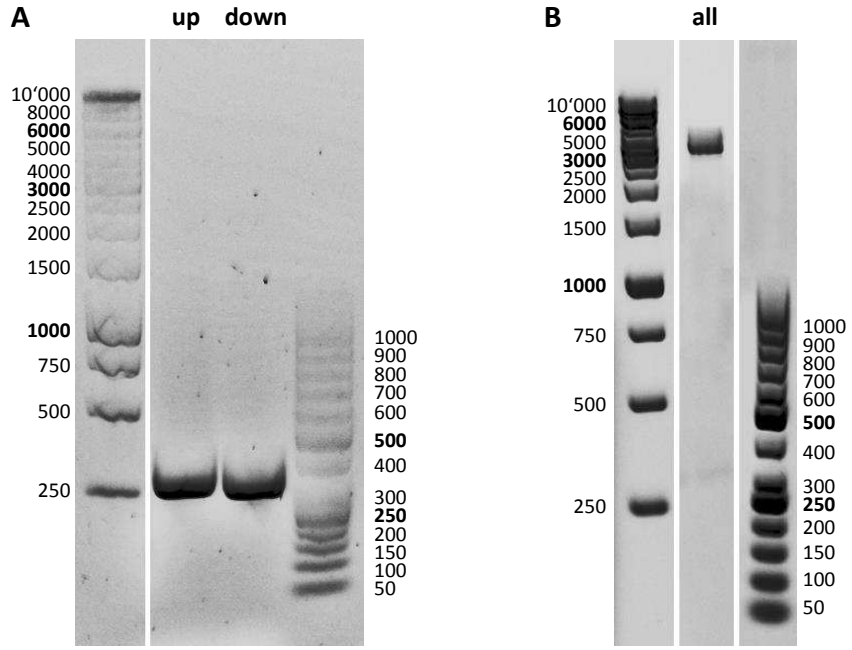

Fig. 62 Agarose gel of DNA *his* marker fragments for homologous recombination amplified with PCR. Fragments coding for the **(A)** upstream (up, expected 350 bp) and downstream (down, expected 334 bp) homologous DNA sequences of the *crs5* gene and **(B)** for the complete insertion fragment with up-, and downstream part connected to the *his* gene (all, expected 3025 bp). Ladder sizes are indicated on the side in bp.

The next step was to check the strain for the correct chromosomal DNA. Therefore, several transformed colonies of the CUP1^S Δcrs5 strain were grown in liquid culture and their DNA was purified to obtain a DNA template for PCR. The PCR was performed in two ways: Once a forward primer on the *his* gene (TH033 jo098 His F) and a reverse primer downstream of the *crs5* gene (TH021 crs5 control dn) was used, expecting a positive PCR product of 1059 bp. Second a forward primer on the *crs5* gene (TH020 crs5 control up) and a reverse primer downstream of the *crs5* gene (TH021 crs5 control dn) were employed, expecting a negative PCR product of 759 bp. The agarose gels showed several bands for both PCRs from different colonies. The result is ambiguous and cannot definitely state a correct CUP1^S Δcrs5 strain. Furthermore, changes in the protocol could not solve the problem.

For a final prove, the chromosomal region of the original *crs5* gene should be sequenced as described for the wild-type strain (7.5.1.1). The chromosomal region was amplified with primers up- and downstream of the *crs5* or inserted *his* gene (TH019 crs5 F and TH021 crs5 R) what should result in a 3010 bp long fragment, if the *his* gene is inserted, or a 900 bp long fragment for the original *crs5* gene. The agarose gel showed also for this PCR a very diverse output. Bands occurred at 3010 bp as well as at 900 bp and other sizes. To avoid the problem of unspecific annealing different primers were used. With the primers TH019 crs5 F and TH055 crs5 down R a 2782 bp long fragment for the mutant and a 672 bp long fragment for the wild-type was expected. With the primers TH033 jo098 His F and TH055 crs5 down R a 831 bp long fragment for the mutant and no fragment for the wild-type was expected. Finally, with the primers TH033 jo098 His F and TH021 crs5 control dn a 1059 bp long fragment for the mutant and no fragment for the wild-type

was expected. But none of the different combinations led to a single correctly sized band on the agarose gel. It was not possible to obtain a single PCR product for sequencing, concluding that the control approach failed.
It can be said, that the transformation and homologous recombination with the elongated PCR products seems to work, as the transformed cells gained the ability to survive in a histidine free medium. Nevertheless, it is not clear, if the recombination worked correctly, since it was not possible to gain an unambiguous control result for the replacement of the *crs5* gene by the *his* gene. For the yeast complementation assays it is crucial to have a *crs5* deletion mutant. Therefore, before using of the strains in any experiments further investigations need to be performed to ensure the correctness of their gene sequences. Another possibility is to change the production of the deletion mutants, either slightly e.g. by increasing the homologous sequences, or the complete strategy.

7.5.2. Plasmid preparation coding for plant MTs

For the yeast complementation assays, DNA of different plant MTs present on vectors for expression in bacteria had to be cloned on a vector suitable for expression in yeast cells. As vector the centromeric yeast vector pRS416 was chosen which encodes an ampicillin resistance for selection in bacteria, as well as the auxotrophic selection marker URA3 for selection in yeast. With its T7 promotor it is inducible with IPTG.[244-245] The vector allows its amplification in bacterial *E. coli* cells as well as its amplification and over-expression in yeast *S. cerevisiae*.
Already investigated plant MTs were chosen, i.e. MT1 and MT2 from chickpea (*C. arietinum*), MT3 from banana (*Musa acuminata*), and E_c-1 and its single domains γ-E_c-1 and β_E-E_c-1 from wheat (*T. aestivum*). Additionally, the well-studied human MT2 (*H. sapiens*) was chosen as a control (Tab. 5). The DNA of the plant MTs was copied via PCR from the bacterial vector pTYB2 and was introduced into the eukaryotic vector pRS416. The correctness was proven by sequencing. The final vectors contained the plant MTs without additional amino acids or tags and are named after the inserted plant MTs, i.e. pRS416-cpMT1 for MT1 and pRS416-cpMT2 for MT2 of chickpea, pRS416-baMT3 for MT3 of banana, pRS416-E_c1 for E_c-1, pRS416-γE_c1 for γ-E_c-1, and pRS416-βE_c1 for β_E-E_c-1 of wheat, and pRS416-huMT2 for huMT2 of human.
Finally, the constructed plasmids were amplified in *E. coli* and purified for the following insertion into the wild-type and mutant yeast strains. As the cloning of the deletion mutants was not possible to complete, only the wild-type $CUP1^S$ strain was transformed with the vectors coding for plant MTs.

7.5.3. Metal sensitivity pre-tests

Different methods are available for metal sensitivity tests, either cell growth in liquid cultures or cell growth on solid medium. Both of them have advantages and drawbacks. To find the most suitable one, trials were made with the wild-type and the mutant containing different plant MT vectors. As the production of the deletion mutants is not finished, the tests were performed with another yeast strain, which is similar to the $CUP1^S$ the wild-type strain, the ZnWT, containing all

DNA sequences for the defense proteins and its double deletion mutant for the zinc transporters Zrc1 and Cot1 (Zn2MUT). These strains were only used for testing the methods, because they contain an unknown repetition of the *cup1* gene.

The first experiments were done with 5 mL liquid yeast cultures with manually measured optical densities. For this, ZnWT, Zn2MUT–pRS416, Zn2MUT–pRS416-E_c1, and Zn2MUT–pRS416-cpMT2 cells were grown in a Zn^{2+} ion containing YPD media (100 µM $ZnSO_4$) and in metal ion lacking YPD media. The optical density of the cells was measured several times over a growth time of 30 h (Fig. 63 A). The yeast cells were harvested and the Zn^{2+} ion concentration in the cells was determined by F-AAS. The values were plotted together with the final reached OD_{600} in a histogram for comparison of the different strains (Fig. 63 B).

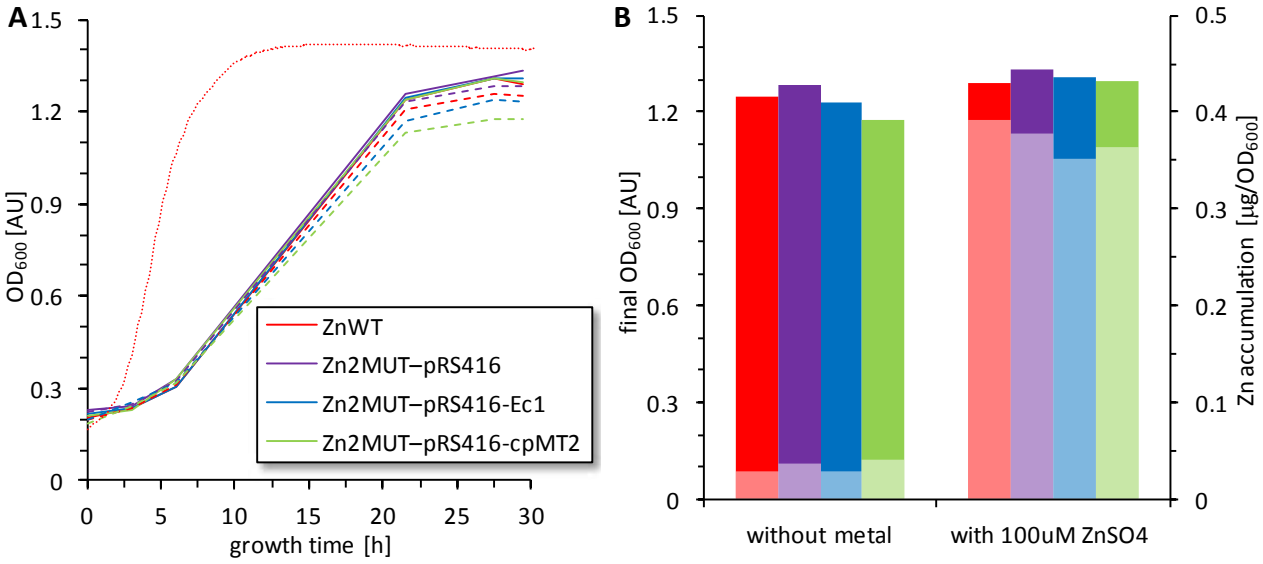

Fig. 63 Different *S. cerevisiae* strains were grown for 30 h at 30 °C in liquid growth media, once without additional metal ions, and once with 100 µM $ZnSO_4$ supplementation. The color code is the same for both diagrams. **(A)** Growth curves with plotted optical density at 600 nm against growth time. Solid lines represent the cells grown in $ZnSO_4$ supplemented media, dashed line in media without metal supplementation. Solid and dashed lines display cultures grown in 5 mL cultures and OD_{600} was measured manually. Dotted line represents an average of eight 150 µL cultures grown in a 96 well plate, and measured directly with the microplate reader. **(B)** Plotted final OD_{600} of yeast strains from **(A)** grown in 5 mL cultures (dark bars), and measured Zn content in the yeast strains after 30 h of growth (light bars).

The growth curves of all yeast strains show a similar behavior, only small differences in the final optical density can be detected. Surprisingly, the cells grown in $ZnSO_4$ supplemented media grow to a slightly higher optical density then the one without metal addition. As visualized in the histogram, the difference of Zn-accumulation in the supplemented media compared to standard YPD is rather high and thus significant. But these values have to be related to the optical cell density, and the time consuming manual measurement of the OD_{600} is quite imprecise because of the fast sedimentation of the cells and the interruption of the cell incubation when the cells stand without shaking at room temperature during measurement. To obtain values with low standard deviations the experiments have to be repeated many times.

This can be easier achieved by growing the yeast cells in a 96-well plate, where the shaking and reading of the OD_{600} is done by a microplate reader (Fig. 63 A). This has the advantages that the experiments are much less laborious making it possible to decrease the measurement interval, and the measurement itself is more precise, because the plate temperature is constantly set to 30 °C and the reading does only shortly interrupt the shaking. Hence it does not surprise, that the experiments with the 150 μL cultures look different form the ones manually measured. However, an important point is the relativity of the automatically measured optical densities. For absolute values it would be necessary to have a defined path length, but with the automated system the path length depends on the filling level of the wells. The advantage however is the additional information about the progress of the growth from the exact shape of the curve.

Both metal sensitivity tests performed in liquid cultures provide similar information, but they are not directly comparable because of the absolute/relative values and the different conditions during OD_{600} measurement. In general, the automated system has more advantages, but the larger volumes of the manual system are more beneficial for further downstream experiments. For measuring accumulated metal ions or quantifying the MT concentration, bigger volumes are necessary, what certainly also can be achieved by the use of microplates with less and larger wells. Both methods do not deliver information about the conditions of the cells, than the measured optical density only depicts data about the overall cell mass and not about the number of cells, meaning that many small colonies can have the same optical density than a few large colonies. Information about the conditions of the cells can be gained for example by microscopy, flow cytometry, or by growing the yeast cells on solid agar plates.

A short analysis of the number of cells was done by growing them on solid agar plates. Pre-cultures of Zn2MUT–pRS416, Zn2MUT–pRS416-E_c1, Zn2MUT–pRS416-βE_c1, Zn2MUT–pRS416-γE_c1, Zn2MUT–pRS416-cpMT2, Zn2MUT–pRS416-huMT2, and ZnWT were diluted to different optical densities and were applied to agar plates. One was supplemented with 2 μM $ZnSO_4$ and the other was without metal supplementation. The plates were incubated for 72 h and the cell colonies were manually counted (Fig. 64, Fig. 65).

The numbers of yeast colonies are for all different yeast strains in a similar range, whereat the experiment shows the tendency of a higher colony growth without metal supplementation. The differences may also originate from the inaccurate counting of the colonies by eye and by a high deviation caused by the low amount of colonies. For more reliable results, the experiment has to be repeated several times. Compared to liquid cultures a different information can be obtained, but an insight is only received on the number of colonies and not directly on the condition of the cells. Similar to the liquid cultures, colony counting on plates has its disadvantages in the high imprecision and in the time consuming manual counting.

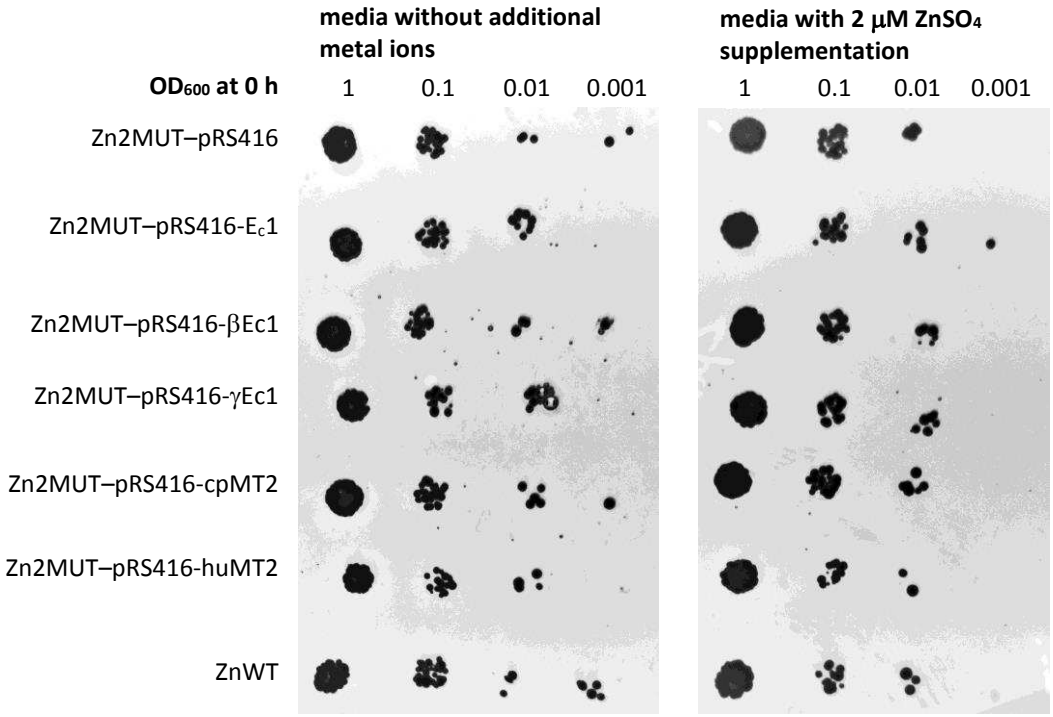

Fig. 64 Different *S. cerevisiae* strains were grown for 72 h at 30 °C on solid growth media, once without additional metal ions, and once with 2 µM $ZnSO_4$ supplementation. Yeast strains used were indicated on the left side (Zn2MUT–pRS416, Zn2MUT–pRS416-E_c1, Zn2MUT–pRS416-βE_c1, Zn2MUT–pRS416-γE_c1, Zn2MUT–pRS416-cpMT2, Zn2MUT–pRS416-huMT2, ZnWT), and they were plated with different initial cell densities (OD_{600} of 0.001-1).

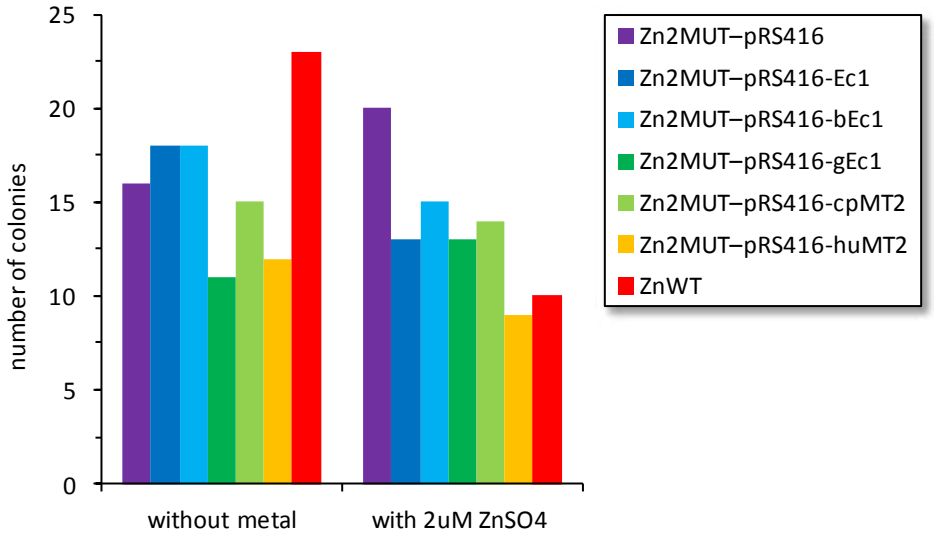

Fig. 65 Analysis of $ZnSO_4$ tolerance of different *S. cerevisiae* strains grown on solid growth media with and without 2 µM $ZnSO_4$ supplementation (Fig. 64). Numbers of colonies are counted from the initial OD_{600} of 0.1 after growing them for 72 h at 30 °C.

We could observe that all three tested methods are not directly comparable. One so far not addressed point is the different metal concentrations in the liquid and solid medium. As the agar in the solid cultures can form complexes with metal ions, the metal ion concentrations have to be

higher than in the liquid cultures. Hence, it is difficult to decide, which experiment in liquid culture correlates to the one on solid medium. Moreover, the different conditions during measurement and the varying growth times make it difficult to compare these data. It is therefore important, to conduct all experiments in the same system.

The best choice for this might be the liquid cultures in microplates, because they deliver most information and is least laborious. However, these experiments have to be complemented by other methods such as flow cytometry or microscopy. Flow cytometry is a laser based biophysical technology for simultaneous multiparametric analysis, e.g. cell counting, sorting, and biomarker detection. This method is already tested for MTs and the use of it would reduce the necessary downstream experiments to a minimum.[246-249]

8. Conclusion and Outlook

Up to now, only little information is published about plant metallothioneins. As they are almost omnipresent in nature, it is assumed that they play an important role in life. Therefore, we investigated the structure and function of the plant metallothioneins to shed light on these proteins.

A dominant structural component of the MTs are the metal-thiolate clusters. Secondary structural elements as α-helices and β-sheets are almost absent in these regions and only predicted for the linker regions connecting them. For these reasons, two aspects were investigated, on one hand the overall structure and on the other hand the formed metal-thiolate clusters. The subject of our structural investigations was the already partially analyzed MT2 of chickpea, which shows the binding of five divalent metal ions as Zn^{2+}, Cd^{2+}, and Co^{2+} ions and forms to a single metal-thiolate cluster.[135, 175]

The overall structure of cicMT2 was studied by NMR spectroscopy. The pattern of the chemical shifts in the NMR spectra indicates an unfolded or partially unfolded protein. The same behavior was observed for the apo- and for the holo-form of the protein, even when cicMT2 was stabilized by an *N*-terminal GST-tag. The two main explanations for this feature are the occurrence of intrinsically disordered structures and the choice of the metal ion bound to the protein.

Proteins showing IDS do not adopt unique and specific three-dimensional structures under physiological conditions, especially in the absence of essential binding partners.[189] They can undergo disorder-order transitions during or prior to their biological function, where they play key role in a remarkable range of cellular processes, including signaling, cell cycle control, molecular recognition, transcription, and replication.[186-187] Other IDS remain flexible, and sometimes act as linkers between structural domains.[189, 250] As the linker region of cicMT2 covers 53 % of the whole protein sequence, it depicts an eligible reason for the floppiness of the whole structure, although the linker region of the plant MTs are predicted to fold into β-sheets.[183]

Additionally, the type of metal ions bound to cicMT2 can influence the structure. As stated by Palacios et al.[36] MTs can be classified into Zn^{2+} or Cu^{+} ion binding proteins. If cicMT2 belongs to the monovalent metal ion binding proteins, the investigated Zn^{2+}- or Cd^{2+}-forms are not natural states and therefore might not fold to a unique structure. Nevertheless, the thiolate groups of cicMT2 have a high affinity for divalent metal ions although they do not lead to an ordered folding. For answering the question of classification into monovalent or divalent metal ion binding proteins, NMR spectroscopy experiments of Cu-cicMT2 or Ag-cicMT2 should be performed in further studies.

To have a look at the composition of the metal cluster, metal ion titrations of cicMT2 were performed. Titrations with divalent metal ions show a clear binding of five Zn^{2+} or Cd^{2+} ions to cicMT2, what was also confirmed by mass analysis. The stoichiometry of the monovalent metal ions is more complex indicating a less structured and more flexible fold. Nevertheless, the estimation of the ratio of metal ion to protein is almost double for monovalent metal ions disclosing stoichiometries of Ag_9-cicMT2 and Cu_8-cicMT2. The increase compared to divalent

metal ions can be explained by the charge compensation of the negatively loaded reduced apo-cicMT2 (charge of -16), which is compensated to a final charge of -6 to -8 with less divalent metal ions than monovalent metal ions.
The binding of monovalent as well as divalent metal ions was already shown for several plant MTs.
Some of them, including cicMT2, bind more monovalent metal ions than divalent metal ions, e.g. MT1 of *C. arietinum* binds 4 Zn^{2+}/Cd^{2+} ions or 6 Cu^{+} ions, MT2 of *Avicennia marina* binds 3 Zn^{2+}/Cd^{2+} ions or 4 Cu^{+} ions, or MT2 of *Q. suber* binds 3.5 Zn^{2+}/Cd^{2+} ions or 5.5 Cu^{+} ions. The other MTs show a contrary behavior with the binding of a higher amount of divalent metal ions than monovalent metal ions, e.g. MT1 of *P. sativum* binds 5.6 Zn^{2+}/Cd^{2+} ions or 2.3 Cu^{+} ions.[80, 138, 251-253]

Although the amount of incorporated metal ions differs, the hydrodynamic radii showed an average of 1.92 ± 0.26 nm for all four metal bound forms (Cd_5-cicMT2, Zn_5-cicMT2, Ag_9-cicMT2, Cu_8-cicMT2). The differences in size are in the range of the experimental error and do not correlate with the slight differences in the molecular masses of the differently loaded cicMT2. However, interesting is the difference of the hydrodynamic radii by varying the concentration of the proteins. With a three times increased concentration, the hydrodynamic radius of Cd_5-cicMT2 changes from 1.94 ± 0.07 nm to 2.38 ± 0.10 nm. It seems that cicMT2 forms transient dimers or multimers depending on the concentration. In any case, the hydrodynamic radii do not match the calculated molecular masses empirically determined of other proteins.

Previous studies of cicMT2 also have shown the additional incorporation of sulfide ions into the Cd^{2+}-thiolate cluster, accompanied by a higher pH stability.[136, 175] As additional sulfide ligands have an impact on the structure and function of cicMT2, the *in vitro* sulfide ion incorporation into metallothioneins was further investigated.
We show the *in vitro* incorporation of S^{2-} ions in combination with Zn^{2+}, Cd^{2+}, Ag^{+}, and Cu^{+} ions. This is in contrast to previous reports, where sulfide ions only together with divalent metal ions such as Zn^{2+} and Cd^{2+} are present in MTs, and not with monovalent metal ions such as Ag^{+} and Cu^{+}.[80, 202, 254-256] UV, CD, and MCD show clearly a difference in the absorption spectra of M-cicMT2 and M,S-cicMT2. In the UV spectra, typical red-shifted absorption bands arise for the divalent metal ions upon incorporation of sulfide ions. This is a known feature of Cd,S-MTs and sulfide ion containing PC complexes.[83, 85, 136] The origin of the observed shifts of the LMCT transitions was attributed to decreasing HOMO-LUMO gaps with increasing cluster size.[191-194] For monovalent metal ions, no shift is detected, but an increase of the respective LMCT band is observed.
Moreover, sulfide ion incorporation was shown via determining the stoichiometry of the obtained MT species after purification of the holo-form. For divalent metal ions, stoichiometries of Zn_8S_7-cicMT2 and Cd_9S_7-cicMT2 were evidenced.[136] Surprisingly, the ratios of Zn^{2+} and Cd^{2+} to S^{2-} are nearly identical, although previous literature reported for Zn^{2+}-loaded MTs around 50 % lower S^{2-} ion contents than for Cd^{2+}-forms.[58, 81, 83] Additionally, the sulfide to protein ratio itself was higher than the one detected in most other phyla. However, former work assessed the sulfide ion incorporation of proteins directly isolated from *E. coli* and not by systematic investigation by

in vitro experiments. Sulfide-complexes with monovalent metal ions show also an increased metal ion content compared to the sulfide ion lacking forms. The found stoichiometries are $Ag_{19}S_x$-cicMT2 and $Cu_{11}S_x$-cicMT2. The amount of incorporated sulfide ions could not be precisely assessed by colorimetric assays which were used for the divalent metal ion containing MT-forms, because the pK_a values of the thiolate groups of cysteines in presence of Cu^+ and Ag^+ ions are too low to release quantitatively the metal ions from cicMT2. Due to the fact that the sulfide ion containing complexes are not stable enough for mass spectrometry, methods such as inductively coupled plasma mass spectrometry (ICP-MS) might be more suitable to determine the sulfide ion to protein ratios.

Although the molecular masses of the sulfide ion containing forms increased, the hydrodynamic radii were decreasing by 4-15 % in the presence of additional sulfide ions. This contraction might be due to a rearrangement of the protein structure in order to gain more space for the enlarged cluster. For example a reduction of size could be envisioned by a change of the structure of the protein-linker region from a single long and relatively rigid antiparallel β-sheet to a structure with multiple shorter β-sheets yielding a more flexible cluster necessary for the incorporation of additional sulfide ions.[183]

Previous work already reported pK_a values for the sulfide lacking forms of cicMT2 and the occurrence of system stabilization by sulfide ion incorporation into the Cd^{2+}-thiolate cluster by decreasing the pK_a value by 0.5 pH units.[135-136] We could also show the tendency of a thermodynamic stabilization in presence of additional sulfide ions for the Zn^{2+}-form of cicMT2. The decrease of pK_a values from Zn_5-cicMT2 to Zn_8S_7-cicMT2 is even higher with 1.2 pH units. This is in accordance with data already reported for phytochelatins and denotes no pH induced metal cluster release *in vivo*.[86]

Additionally, we found a dependence of the metal:sulfide:protein stoichiometry regarding the sulfide ion supplementation. By varying the initial sulfide ion concentration a high diversity of isoforms can be produced with a nearly linearly dependence on the applied S^{2-} ion concentration. This further describes the tight relation of cicMT2 to the PCs where the metal and sulfide ion content is higher than previously reported for MTs.[130] The *in vitro* results of this work show a higher sulfide ion content than reported for *in vivo* incorporation of sulfide ions. It is the question, if the *in vivo* results are physiologically more relevant, or if the loosely bound sulfide ions are just lost during purification and therefore not detectable. This has to be further investigated.

An important factor for sulfide ion incorporation is the specific pathway observed. The sequence of MT, Cd^{2+}, and S^{2-} ion addition is crucial for the formation of larger Cd,S-thiolate clusters. On a hypothetical basis, it seems to be of utter importance that the Cd^{2+} ions are already bound to sulfide ions prior to incorporation into the cluster. But the Cd,S-aggregates may not be too large or even negatively charged. Once the Cd_5Cys_{14}-cluster of cicMT2 is formed no additional sulfide ions can be incorporated. This means that *in vivo* the incorporation of the sulfide ions has to take place before the metal ions can bind to the MT, or the metal ions are released first. The high stability of the metal-sulfide-thiolate cluster indicates a co-regulation of free sulfide ions in the cell with the expression of the MT. This would result in an effective way of metal ion capturing for heavy metal detoxification.

Another interesting observation is that cicMT2 is able to form a much larger Cd,S-thiolate cluster structure relative to its Cd^{2+}-thiolate cluster in absence of sulfide ions than observed for rabbit liver MT2A using the same *in vitro* experimental conditions. Again on a hypothetical basis, an explanation for this can be found in the cysteine-free linker region of plant MTs and in the formation of a single metal-thiolate cluster.[135-136, 183] The amino acid sequence of mammalian MTs encloses two separate metal-thiolate clusters in a dumbbell like shape, separated only by a very short three amino acids long linker.[60] Accordingly, steric reasons can be envisioned that prevent expansion of these clusters like in a single cluster with more space and flexibility for cluster rearrangement.
However, the remaining question is still if sulfide ion incorporation into MTs has any physiological relevance. It is evident that recruitment of sulfide ions as additional ligands is a rather cost-efficient way for an organism to increase the metal ion binding capacity of a protein, and the underlying concept has been already shown to be effective for the PC complexes of yeast and plants. The idea of expandable metal-thiolate clusters in response to physiological requirements would also shine light on a possible function of the enigmatic long cysteine-free linker regions observed in most plant MT-forms. Nevertheless, the final answer awaits further analysis of native MT-forms.

To further elaborate the general function of the plant MTs yeast complementation assays should be performed. To have a uniform basis for the comparison, it was planned to prepare the deletion mutants via homologous recombination and to introduce the plant MT DNA sequences with an inducible plasmid. So far, the mutation of the yeast strains are not finished, but trials for the metal sensitivity tests were done, concluding to proceed with the liquid cultures measured automatically with the microplate reader.
For the future, first tests should screen for the optimal assay condition in terms of cell density and metal ion concentration. If there is no difference appearing, the contrast might be boosted by over-expression of the plant MTs. Once a difference in growth appears, several further experiments have to be performed for more precise analysis of the function of MTs. One has to prove that the observed effects originate from plant MTs, e.g. by western blot analysis or flow cytometry. Additional, metal and sulfide ion content has to be determined, as well as the condition of the cells by flow cytometry or microscopy. An advantage would also be the insertion of the plant MTs into the chromosomal genome of the yeast strains to control their expression under natural promoters.

This work shed light on different aspects of plant metallothioneins. Structurally, the interaction of cicMT2 with different metal ions alone as well as in combination with additional sulfide ligands was elucidated. Functionally, the mechanism of the sulfide ion incorporation into differently metallated cicMT2 was analyzed, but also first steps were done for a general analysis of the plant metallothionein function.

9. Appendices

9.1. DNA sequences of plasmids

9.1.1. pG1xMT

acgttatcgactgcacggtgcaccaatgcttctggcgtcaggcagccatcggaagctgtggtatggctgtgcaggtcgtaaatcactgcataattcgt
gtcgctcaaggcgcactcccgttctggataatgttttttgcgccgacatcataacggttctggcaaatattctgaaatgagctgttgacaattaatca
tcggctcgtataatgtgtggaattgtgagcggataacaatttcacacaggaaacagtattc**atgtcccctatactaggttattggaaaattaa**gggcc
ttgtgcaacccactcgacttcttttggaatatcttgaagaaaaatatgaagagcatttgtatgagcgcgatgaaggtgataaatggcgaaacaaaaag
tttgaattgggtttggagtttcccaatcttccttattatattgatggtgatgttaaattaacacagtctatggccatcatacgttatatagctgacaa
gcacaacatgttgggtggttgtccaaaagagcgtgcagagatttcaatgcttgaaggagcggttttggatattagatacggtgtttcgagaattgcat
atagtaaagactttgaaactctcaaagttgattttcttagcaagctacctgaaatgctgaaaatgttcgaagatcgtttatgtcataaaacatattta
aatggtgatcatgtaacccatcctgacttcatgttgtatgacgctcttgatgttgttttatacatggacccaatgtgcctggatgcgttcccaaaatt
agtttgttttaaaaaacgtattgaagctatcccacaaattgataagtacttgaaatccagcaagtatatagcatggcctttgcagggctggcaagcca
cgtttggtggtggcgaccatcctccaaaatcggatctggttccgcgtgga**tcctgctgtggcggcaattgtgggtgtggaagcagctgcaaatgcggg**
agtggctgtggcggctgcaagatgtatccggacatgagctacacagagcagacgacgagcgaaaccctggtgatgggagtggcatctgggaagaccca
atttgaaggcgcggaaatgggttttggcgcggagaatgatggctgcaaatgtgggtcaaactgcacctgcaatccgtgcacctgcaaataatgacccg
ggtcgactcgagcggccgcatcgtgactgactgacgatctgcctcgcgcgtttcggtgatgacggtgaaaacctctgacacatgcagctcccggagac
ggtcacagcttgtctgtaagcggatgccgggagcagacaagcccgtcagggcgcgtcagcgggtgttggcgggtgtcggggcgcagccatgacccagt
cacgtagcgatagcggagtgtataattcttgaagacgaaagggcctcgtgatacgcctatttttataggttaatgtcatgataataatggtttcttag
acgtcaggtggcacttttcggggaaatgtgcgcggaacccctatttgtttatttttctaaatacattcaaatatgtatccgctcatgagacaataacc
ctgataaatgcttcaataatattgaaaaaggaagagtatgagtattcaacatttccgtgtcgcccttattccctttttgcggcattttgccttcctg
tttttgctcacccagaaacgctggtgaaagtaaaagatgctgaagatcagttgggtgcacgagtgggttacatcgaactggatctcaacagcggtaag
atccttgagagttttcgccccgaagaacgttttccaatgatgagcacttttaaagttctgctatgtggcgcggtattatcccgtgttgacgccgggca
agagcaactcggtcgccgcatacactattctcagaatgacttggttgagtactcaccagtcacagaaaagcatcttacggatggcatgacagtaagag
aattatgcagtgctgccataaccatgagtgataacactgcggccaacttacttctgacaacgatcggaggaccgaaggagctaaccgcttttttgcac
aacatgggggatcatgtaactcgccttgatcgttgggaaccggagctgaatgaagccataccaaacgacgagcgtgacaccacgatgcctgcagcaat
ggcaacaacgttgcgcaaactattaactggcgaactacttactctagcttcccggcaacaattaatagactggatggaggcggataaagttgcaggac
cacttctgcgctcggcccttccggctggctggtttattgctgataaatctggagccggtgagcgtgggtctcgcggtatcattgcagcactggggcca
gatggtaagccctcccgtatcgtagttatctacacgacggggagtcaggcaactatggatgaacgaaatagacagatcgctgagataggtgcctcact
gattaagcattggtaactgtcagaccaagtttactcatatatactttagattgatttaaaacttcatttttaatttaaaaggatctaggtgaagatcc
tttttgataatctcatgaccaaaatcccttaacgtgagttttcgttccactgagcgtcagaccccgtagaaaagatcaaaggatcttcttgagatcct
ttttttctgcgcgtaatctgctgcttgcaaacaaaaaaaccaccgctaccagcggtggtttgtttgccggatcaagagctaccaactctttttccgaa
ggtaactggcttcagcagagcgcagataccaaatactgtccttctagtgtagccgtagttaggccaccacttcaagaactctgtagcaccgcctacat
acctcgctctgctaatcctgttaccagtggctgctgccagtggcgataagtcgtgtcttaccgggttggactcaagacgatagttaccggataaggcg
cagcggtcgggctgaacgggggggttcgtgcacacagcccagcttggagcgaacgacctacaccgaactgagatacctacagcgtgagctatgagaaag
cgccacgcttcccgaagggagaaaggcggacaggtatccggtaagcggcagggtcggaacaggagagcgcacgagggagcttccagggggaaacgcct
ggtatctttatagtcctgtcgggtttcgccacctctgacttgagcgtcgatttttgtgatgctcgtcaggggggcggagcctatggaaaacgccagc
aacgcggccttttacggttcctggccttttgctggccttttgctcacatgttctttcctgcgttatcccctgattctgtggataaccgtattaccgc
ctttgagtgagctgataccgctcgccgcagccgaacgaccgagcgcagcgagtcagtgagcgaggaagcggaagagcgcctgatgcggtattttctcc
ttacgcatctgtgcggtatttcacaccgcataaattccgacaccatcgaatggtgcaaaacctttcgcggtatggcatgatagcgcccggaagagagt
caattcagggtggtgaatgtgaaaccagtaacgttatacgatgtcgcagagtatgccggtgtctcttatcagaccgtttcccgcgtggtgaaccaggc
cagccacgtttctgcgaaaacgcgggaaaaagtggaagcggcgatggcggagctgaattacattcccaaccgcgtggcacaacaactggcgggcaaac
agtcgttgctgattggcgttgccacctccagtctggccctgcacgcgccgtcgcaaattgtcgcggcgattaaatctcgcgccgatcaactgggtgcc
agcgtggtggtgtcgatggtagaacgaagcggcgtcgaagcctgtaaagcggcggtgcacaatcttctcgcgcaacgcgtcagtgggctgatcattaa
ctatccgctggatgaccaggatgccattgctgtggaagctgcctgcactaatgttccggcgttatttcttgatgtctctgaccagacacccatcaaca
gtattattttctcccatgaagacggtacgcgactgggcgtggagcatctggtcgcattgggtcaccagcaaatcgcgctgttagcgggcccattaagt
tctgtctcggcgcgtctgcgtctggctggctggcataaatatctcactcgcaatcaaattcagccgatagcggaacgggaaggcgactggagtgccat
gtccggttttcaacaaaccatgcaaatgctgaatgagggcatcgttcccactgcgatgctggttgccaacgatcagatggcgctgggcgcaatgcgcg
ccattaccgagtccgggctgcgcgttggtgcggatatctcggtagtgggatacgacgataccgaagacagctcatgttatatcccgccgttaaccacc
atcaaacaggattttcgcctgctggggcaaaccagcgtggaccgcttgctgcaactctctcagggccaggcggtgaagggcaatcagctgttgcccgt
ctcactggtgaaaagaaaaaccaccctggcgcccaatacgcaaaccgcctctccccgcgcgttggccgattcattaatgcagctggcacgacaggttt
cccgactggaaagcgggcagtgagcgcaacgcaattaatgtgagttagctcactcattaggcaccccaggctttacactttatgcttccggctcgtat
gttgtgtggaattgtgagcggataacaatttcacacaggaaacagctatgaccatgattacggattcactggccgtcgttttacaacgtcgtgactgg
gaaaaccctggcgttacccaacttaatcgccttgcagcacatcccccttcgccagctggcgtaatagcgaagaggcccgcaccgatcgcccttccca
acagttgcgcagcctgaatggcgaatggcgctttgcctggtttccggcaccagaagcggtgccggaaagctggctggagtgcgatcttcctgaggccg
atactgtcgtcgtcccctcaaactggcagatgcacggttacgatgcgcccatctacaccaacgtaacctatcccattacggtcaatccgccgtttgtt
cccacggagaatccgacgggttgttactcgctcacatttaatgttgatgaaagctggctacaggaaggccagacgcgaattatttttgatggcgttgg
aatt

Fig. 66 DNA sequence of pG1xMT. Bold colored part is transcribed and translated sequence, green part tag and overhang, blue part the target protein. Underlined parts are restriction sequences used for cloning.

9.1.2. pG3xMT

acgttatcgactgcacggtgcaccaatgcttctggcgtcaggcagccatcggaagctgtggtatggctgtgcaggtcgtaaatcactgcataattcgt
gtcgctcaaggcgcactcccgttctggataatgtttttgcgccgacatcataacggttctggcaaatattctgaaatgagctgttgacaattaatca
tcggctcgtataatgtgtggaattgtgagcggataacaatttcacacaggaaacagtattc**atgtcccctatactaggttattggaaaattaagggcc**
ttgtgcaacccactcgacttcttttggaatatcttgaagaaaaatatgaagagcatttgtatgagcgcgatgaaggtgataaatggcgaaacaaaaag
tttgaattgggtttggagtttcccaatcttccttattatattgatggtgatgttaaattaacacagtctatggccatcatacgttatatagctgacaa
gcacaacatgttgggtggttgtccaaaagagcgtgcagagatttcaatgcttgaaggagcggttttggatattagatacggtgtttcgagaattgcat
atagtaaagactttgaaactctcaaagttgattttcttagcaagctacctgaaatgctgaaaatgttcgaagatcgtttatgtcataaaacatattta
aatggtgatcatgtaacccatcctgacttcatgttgtatgacgctcttgatgttgttttatacatggacccaatgtgcctggatgcgttcccaaaatt
agtttgttttaaaaaacgtattgaagctatcccacaaattgataagtacttgaaatccagcaagtatatagcatggcctttgcagggctggcaagcca
cgtttggtggtggcgaccatcctccaaaatcggatctggttccgcgtggatcctgctgtggcggcaattgtgggtgtggaagcagctgcaaatgcggg
agtggctgtggcggctgcaagatgtatccggacatgagctacacagagcagacgacgagcgaaaccctggtgatgggagtggcatctgggaagaccca
atttgaaggcgcggaaatgggttttggcgcggagaatgatggctgcaaatgtgggtcaaactgcaccagcaatccgtgcacctgcaaaggccgtggct
cttgctgtggcggcaattgtgggtgtggaagcagctgcaaatgcgggagtggctgtggcggctgcaagatgtatccggacatgagctacacagagcag
acgacgagcgaaaccctggtgatgggagtggcatctgggaagacccaatttgaaggcgcggaaatgggttttggcgcggagaatgatggctgcaaatg
tgggtcaaactgcacctgcaatccgtgtacctgcaaaggccgcggatcttgctgtgggggcaattgtgggtgtggaagcagctgcaaatgcgggagtg
gctgtggcggctgcaagatgtatccggacatgagctacacagagcagacgacgagcgaaaccctggtgatgggagtggcatctgggaagacccaattt
gaaggcgcggaaatgggttttggcgcggagaatgatggctgcaaatgtgggtcaaactgcacctgcaatccgtgcacctgcaaataatgacccgggtc
gactcgagcggccgcatcgtgactgactgacgatctgcctcgcgcgtttcggtgatgacggtgaaaacctctgacacatgcagctcccggagacggtc
acagcttgtctgtaagcggatgccgggagcagacaagcccgtcagggcgcgtcagcgggtgttggcgggtgtcggggcgcagccatgacccagtcacg
tagcgatagcggagtgtataattcttgaagacgaaagggcctcgtgatacgcctatttttataggttaatgtcatgataatgtttcttagacgt
caggtggcacttttcggggaaatgtgcgcggaacccctatttgtttatttttctaaatacattcaaatatgtatccgctcatgagacaataaccctga
taaatgcttcaataatattgaaaaaggaagagtatgagtattcaacatttccgtgtcgcccttattcccttttttgcggcattttgccttcctgtttt
tgctcacccagaaacgctggtgaaagtaaaagatgctgaagatcagttgggtgcacgagtgggttacatcgaactggatctcaacagcggtaagatcc
ttgagagttttcgccccgaagaacgttttccaatgatgagcacttttaaagttctgctatgtggcgcggtattatcccgtgttgacgccgggcaagag
caactcggtcgccgcatacactattctcagaatgacttggttgagtactcaccagtcacagaaaagcatcttacggatggcatgacagtaagagaatt
atgcagtgctgccataaccatgagtgataacactgcggccaacttacttctgacaacgatcggaggaccgaaggagctaaccgcttttttgcacaaca
tgggggatcatgtaactcgccttgatcgttgggaaccggagctgaatgaagccataccaaacgacgagcgtgacaccacgatgcctgcagcaatggca
acaacgttgcgcaaactattaactggcgaactacttactctagcttcccggcaacaattaatagactggatggaggcggataaagttgcaggaccact
tctgcgctcggcccttccggctggctggtttattgctgataaatctggagccggtgagcgtgggtctcgcggtatcattgcagcactggggccagatg
gtaagccctcccgtatcgtagttatctacacgacggggagtcaggcaactatggatgaacgaaatagacagatcgctgagataggtgcctcactgatt
aagcattggtaactgtcagaccaagtttactcatatatactttagattgatttaaaacttcatttttaatttaaaaggatctaggtgaagatccttttt
tgataatctcatgaccaaaatcccttaacgtgagttttcgttccactgagcgtcagaccccgtagaaaagatcaaaggatcttcttgagatccttttt
ttctgcgcgtaatctgctgcttgcaaacaaaaaaaccaccgctaccagcggtggtttgtttgccggatcaagagctaccaactctttttccgaaggta
actggcttcagcagagcgcagataccaaatactgtccttctagtgtagccgtagttaggccaccacttcaagaactctgtagcaccgcctacatacct
cgctctgctaatcctgttaccagtggctgctgccagtggcgataagtcgtgtcttaccgggttggactcaagacgatagttaccggataaggcgcagc
ggtcgggctgaacgggggttcgtgcacacagcccagcttggagcgaacgacctacaccgaactgagatacctacagcgtgagctatgagaaagcgcc
acgcttcccgaagggagaaaggcggacaggtatccggtaagcggcagggtcggaacaggagagcgcacgagggagcttccagggggaaacgcctggta
tctttatagtcctgtcgggtttcgccacctctgacttgagcgtcgatttttgtgatgctcgtcaggggggcggagcctatggaaaaacgccagcaacg
cggccttttacggttcctggccttttgctggccttttgctcacatgttctttcctgcgttatcccctgattctgtggataaccgtattaccgccttt
gagtgagctgataccgctcgccgcagccgaacgaccgagcgcagcgagtcagtgagcgaggaagcggaagagcgcctgatgcggtattttctccttac
gcatctgtgcggtatttcacaccgcataaattccgacaccatcgaatggtgcaaaacctttcgcggtatggcatgatagcgcccggaagagagtcaat
tcagggtggtgaatgtgaaaccagtaacgttatacgatgtcgcagagtatgccggtgtctcttatcagaccgtttcccgcgtggtgaaccaggccagc
cacgtttctgcgaaaacgcgggaaaaagtggaagcggcgatggcggagctgaattacattcccaaccgcgtggcacaacaactggcgggcaaacagtc
gttgctgattggcgttgccacctccagtctggccctgcacgcgccgtcgcaaattgtcgcggcgattaaatctcgcgccgatcaactgggtgccagcg
tggtggtgtcgatggtagaacgaagcggcgtcgaagcctgtaaagcggcggtgcacaatcttctcgcgcaacgcgtcagtgggctgatcattaactat
ccgctggatgaccaggatgccattgctgtggaagctgcctgcactaatgttccggcgttatttcttgatgtctctgaccagacacccatcaacagtat
tattttctcccatgaagacggtacgcgactgggcgtggagcatctggtcgcattgggtcaccagcaaatcgcgctgttagcgggcccattaagttctg
tctcggcgcgtctgcgtctggctggctggcataaatatctcactcgcaatcaaattcagccgatagcggaacgggaaggcgactggagtgccatgtcc
ggttttcaacaaaccatgcaaatgctgaatgagggcatcgttcccactgcgatgctggttgccaacgatcagatggcgctgggcgcaatgcgcgccat
taccgagtccgggctgcgcgttggtgcggatatctcggtagtgggatacgacgataccgaagacagctcatgttatatcccgccgttaaccaccatca
aacaggattttcgcctgctggggcaaaccagcgtggaccgcttgctgcaactctctcagggccaggcggtgaagggcaatcagctgttgcccgtctca
ctggtgaaaagaaaaaccaccctggcgcccaatacgcaaaccgcctctccccgcgcgttggccgattcattaatgcagctggcacgacaggtttcccg
actggaaagcgggcagtgagcgcaacgcaattaatgtgagttagctcactcattaggcaccccaggctttacactttatgcttccggctcgtatgttg
tgtggaattgtgagcggataacaatttcacacaggaaacagctatgaccatgattacggattcactggccgtcgttttacaacgtcgtgactgggaaa
accctggcgttacccaacttaatcgccttgcagcacatccccctttcgccagctggcgtaatagcgaagaggcccgcaccgatcgcccttcccaacag
ttgcgcagcctgaatggcgaatggcgctttgcctggtttccggcaccagaagcggtgccggaaagctggctggagtgcgatcttcctgaggccgatac
tgtcgtcgtcccctcaaactggcagatgcacggttacgatgcgcccatctacaccaacgtaacctatcccattacggtcaatccgccgtttgttccca
cggagaatccgacgggttgttactcgctcacatttaatgttgatgaaagctggctacaggaaggccagacgcgaattatttttgatggcgttggaatt

Fig. 67 DNA sequence of pG3xMT. Bold colored part is transcribed and translated sequence, green part tag and overhang, blue part the target proteins. Underlined parts are restriction sequences used for cloning.

9.1.3. pGtMT

acgttatcgactgcacggtgcaccaatgcttctggcgtcaggcagccatcggaagctgtggtatggctgtgcaggtcgtaaatcactgcataattcgt
gtcgctcaaggcgcactcccgttctggataatgttttttgcgccgacatcataacggttctggcaaatattctgaaatgagctgttgacaattaatca
tcggctcgtataatgtgtggaattgtgagcggataacaatttcacacaggaaacagtattc**atgtcccctatactaggttattggaaaattaagggcc**
ttgtgcaacccactcgacttcttttggaatatcttgaagaaaaatatgaagagcatttgtatgagcgcgatgaaggtgataaatggcgaaacaaaaag
tttgaattgggtttggagtttcccaatcttccttattatattgatggtgatgttaaattaacacagtctatggccatcatacgttatatagctgacaa
gcacaacatgttgggtggttgtccaaaagagcgtgcagagatttcaatgcttgaaggagcggttttggatattagatacggtgtttcgagaattgcat
atagtaaagactttgaaactctcaaagttgattttcttagcaagctacctgaaatgctgaaaatgttcgaagatcgtttatgtcataaaacatattta
aatggtgatcatgtaacccatcctgacttcatgttgtatgacgctcttgatgttgttttatacatggacccaatgtgcctggatgcgttcccaaaatt
agtttgtttttaaaaaacgtattgaagctatcccacaaattgataagtacttgaaatccagcaagtatatagcatggcctttgcagggctggcaagcca
cgtttggtggtggcgaccatcctccaaaatcggatctggttccgcgtggatccgagaacctttacttccaatcctgctgtggcggcaattgtgggtgt
ggaagcagctgcaaatgcgggagtggctgtggcggctgcaagatgtatccggacatgagctacacagagcagacgacgagcgaaaccctggtgatggg
agtggcatctgggaagacccaatttgaaggcgcggaaatgggttttggcgcggagaatgatggctgcaaatgtgggtcaaactgcacctgcaatccgt
gcacctgcaaataatgacccgggtcgactcgagcggccgcatcgtgactgactgacgatctgcctcgcgcgtttcggtgatgacggtgaaaacctctg
acacatgcagctcccggagacggtcacagcttgtctgtaagcggatgccgggagcagacaagcccgtcagggcgcgtcagcgggtgttggcgggtgtc
ggggcgcagccatgacccagtcacgtagcgatagcggagtgtataattcttgaagacgaaagggcctcgtgatacgcctatttttataggttaatgtc
atgataataatggtttcttagacgtcaggtggcacttttcggggaaatgtgcgcggaacccctatttgtttatttttctaaatacattcaaatatgta
tccgctcatgagacaataaccctgataaatgcttcaataatattgaaaaaggaagagtatgagtattcaacatttccgtgtcgcccttattccctttt
ttgcggcattttgccttcctgtttttgctcacccagaaacgctggtgaaagtaaaagatgctgaagatcagttgggtgcacgagtgggttacatcgaa
ctggatctcaacagcggtaagatccttgagagttttcgccccgaagaacgttttccaatgatgagcacttttaaagttctgctatgtggcgcggtatt
atcccgtgttgacgccgggcaagagcaactcggtcgccgcatacactattctcagaatgacttggttgagtactcaccagtcacagaaaagcatctta
cggatggcatgacagtaagagaattatgcagtgctgccataaccatgagtgataacactgcggccaacttacttctgacaacgatcggaggaccgaag
gagctaaccgcttttttgcacaacatgggggatcatgtaactcgccttgatcgttgggaaccggagctgaatgaagccataccaaacgacgagcgtga
caccacgatgcctgcagcaatggcaacaacgttgcgcaaactattaactggcgaactacttactctagcttcccggcaacaattaatagactggatgg
aggcggataaagttgcaggaccacttctgcgctcggcccttccggctggctggtttattgctgataaatctggagccggtgagcgtgggtctcgcggt
atcattgcagcactggggccagatggtaagccctcccgtatcgtagttatctacacgacggggagtcaggcaactatggatgaacgaaatagacagat
cgctgagataggtgcctcactgattaagcattggtaactgtcagaccaagtttactcatatatactttagattgatttaaaacttcatttttaattta
aaaggatctaggtgaagatccttttgataatctcatgaccaaaatcccttaacgtgagttttcgttccactgagcgtcagaccccgtagaaaagatc
aaaggatcttcttgagatcctttttttctgcgcgtaatctgctgcttgcaaacaaaaaaaccaccgctaccagcggtggtttgtttgccggatcaaga
gctaccaactctttttccgaaggtaactggcttcagcagagcgcagataccaaatactgtccttctagtgtagccgtagttaggccaccacttcaaga
actctgtagcaccgcctacatacctcgctctgctaatcctgttaccagtggctgctgccagtggcgataagtcgtgtcttaccgggttggactcaaga
cgatagttaccggataaggcgcagcggtcgggctgaacgggggttcgtgcacacagcccagcttggagcgaacgacctacaccgaactgagatacct
acagcgtgagctatgagaaagcgccacgcttcccgaagggagaaaggcggacaggtatccggtaagcggcagggtcggaacaggagagcgcacgaggg
agcttccagggggaaacgcctggtatctttatagtcctgtcgggtttcgccacctctgacttgagcgtcgatttttgtgatgctcgtcaggggggcgg
agcctatggaaaaacgccagcaacgcggcctttttacggttcctggccttttgctggccttttgctcacatgttctttcctgcgttatcccctgattc
tgtggataaccgtattaccgcctttgagtgagctgataccgctcgccgcagccgaacgaccgagcgcagcgagtcagtgagcgaggaagcggaagagc
gcctgatgcggtattttctccttacgcatctgtgcggtatttcacaccgcataaattccgacaccatcgaatggtgcaaaacctttcgcggtatggca
tgatagcgcccggaagagagtcaattcagggtggtgaatgtgaaaccagtaacgttatacgatgtcgcagagtatgccggtgtctcttatcagaccgt
ttcccgcgtggtgaaccaggccagccacgtttctgcgaaaacgcgggaaaaagtggaagcggcgatggcggagctgaattacattcccaaccgcgtgg
cacaacaactggcgggcaaacagtcgttgctgattggcgttgccacctccagtctggccctgcacgcgccgtcgcaaattgtcgcggcgattaaatct
cgcgccgatcaactgggtgccagcgtggtggtgtcgatggtagaacgaagcggcgtcgaagcctgtaaagcggcggtgcacaatcttctcgcgcaacg
cgtcagtgggctgatcattaactatccgctggatgaccaggatgccattgctgtggaagctgcctgcactaatgttccggcgttatttcttgatgtct
ctgaccagacacccatcaacagtattatttttctcccatgaagacggtacgcgactgggcgtggagcatctggtcgcattgggtcaccagcaaatcgcg
ctgttagcgggcccattaagttctgtctcggcgcgtctgcgtctggctggctggcataaatatctcactcgcaatcaaattcagccgatagcggaacg
ggaaggcgactggagtgccatgtccggttttcaacaaaccatgcaaatgctgaatgagggcatcgttcccactgcgatgctggttgccaacgatcaga
tggcgctgggcgcaatgcgcgccattaccgagtccgggctgcgcgttggtgcggatatctcggtagtgggatacgacgataccgaagacagctcatgt
tatatcccgccgttaaccaccatcaaacaggattttcgcctgctggggcaaaccagcgtggaccgcttgctgcaactctctcagggccaggcggtgaa
gggcaatcagctgttgcccgtctcactggtgaaaagaaaaaccaccctggcgcccaatacgcaaaccgcctctccccgcgcgttggccgattcattaa
tgcagctggcacgacaggtttcccgactggaaagcgggcagtgagcgcaacgcaattaatgtgagttagctcactcattaggcaccccaggctttaca
ctttatgcttccggctcgtatgttgtgtggaattgtgagcggataacaatttcacacaggaaacagctatgaccatgattacggattcactggccgtc
gttttacaacgtcgtgactgggaaaaccctggcgttacccaacttaatcgccttgcagcacatccccctttcgccagctggcgtaatagcgaagaggc
ccgcaccgatcgcccttcccaacagttgcgcagcctgaatggcgaatggcgctttgcctggtttccggcaccagaagcggtgccggaaagctggctgg
agtgcgatcttcctgaggccgatactgtcgtcgtcccctcaaactggcagatgcacggttacgatgcgcccatctacaccaacgtaacctatcccatt
acggtcaatccgccgtttgttcccacggagaatccgacgggttgttactcgctcacatttaatgttgatgaaagctggctacaggaaggccagacgcg
aattatttttgatggcgttggaatt

Fig. 68 DNA sequence of pGtMT. Bold colored part is transcribed and translated sequence, green part tag and overhang, blue part the target proteins. Underlined parts are restriction sequences used for cloning.

9.1.4. pRS416-MT

tcgcgcgtttcggtgatgacggtgaaaacctctgacacatgcagctcccggagacggtcacagcttgtctgtaagcggatgccgggagcagacaagcc
cgtcagggcgcgtcagcgggtgttggcgggtgtcggggctggcttaactatgcggcatcagagcagattgtactgagagtgcaccataccacagcttt
tcaattcaattcatcatttttttttttattcttttttttgatttcggtttctttgaaatttttttgattcggtaatctccgaacagaaggaagaacgaa
ggaaggagcacagacttagattggtatatatacgcatatgtagtgttgaagaaacatgaaattgcccagtattcttaacccaactgcacagaacaaaaa
acctgcaggaaacgaagataaatcatgtcgaaagctacatataaggaacgtgctgctactcatcctagtcctgttgctgccaagctatttaatatcat
gcacgaaaagcaaacaaacttgtgtgcttcattggatgttcgtaccaccaaggaattactggagttagttgaagcattaggtcccaaaatttgtttac
taaaaacacatgtggatatcttgactgatttttccatggagggcacagttaagccgctaaaggcattatccgccaagtacaatttttttactcttcgaa
gacagaaaatttgctgacattggtaatacagtcaaattgcagtactctgcgggtgtatacagaatagcagaatgggcagacattacgaatgcacacgg
tgtggtgggcccaggtattgttagcggtttgaagcaggcggcagaagaagtaacaaaggaacctagaggccttttgatgttagcagaattgtcatgca
agggctccctatctactggagaatatactaagggtactgttgacattgcgaagagcgacaaagattttgttatcggctttattgctcaaagagacatg
ggtggaagagatgaaggttacgattggttgattatgacacccggtgtgggttagatgacaagggagacgcattgggtcaacagtatagaaccgtgga
tgatgtggtctctacaggatctgacattattattgttggaagaggactatttgcaaagggaagggatgctaaggtagagggtgaacgttacagaaaag
caggctgggaagcatatttgagaagatgcggccagcaaaactaaaaaactgtattataagtaaatgcatgtatactaaactcacaaattagagcttca
atttaattatatcagttattacccctatgcggtgtgaaataccgcacagatgcgtaaggagaaaataccgcatcaggaaattgtaaacgttaatatttt
gttaaaattcgcgttaaatttttgttaaatcagctcatttttttaaccaatagggccgaaatcggcaaaatcccttataaatcaaaagaatagaccgaga
tagggttgagtgttgttccagtttggaacaagagtccactattaaagaacgtggactccaacgtcaaagggcgaaaaaccgtctatcagggcgatggc
ccactacgtgaaccatcaccctaatcaagtttttttggggtcgaggtgccgtaaagcactaaatcggaaccctaaagggagcccccgatttagagcttg
acggggaaagccggcgaacgtggcgagaaaggaagggaagaaagcgaaaggagcgggcgctagggcgctggcaagtgtagcggtcacgctgcgcgtaa
ccaccacacccgccgcgcttaatgcgccgctacagggcgcgtcgcgccattcgccattcaggctgcgcaactgttgggaagggcgatcggtgcgggcc
tcttcgctattacgccagctggcgaaaggggggatgtgctgcaaggcgattaagttgggtaacgccagggttttcccagtcacgacgttgtaaaacgac
ggccagtgagcgcgcgtaatacgactcactatagggcgaattgggtaccgggccccccctcgaggtcgacggtatcgataagcttgatatcgaattcc
tgcagcccgggg

MT

gatccactagttctagagcggccgccaccgcggtggagctccagcttttgttccctttagtgagggttaattgcgcgcttggcgtaatcatggtcata
gctgtttcctgtgtgaaattgttatccgctcacaattccacacaacataggagccggaagcataaagtgtaaagcctggggtgcctaatgagtgaggt
aactcacattaattgcgttgcgctcactgcccgctttccagtcgggaaacctgtcgtgccagctgcattaatgaatcggccaacgcgcggggagaggc
ggtttgcgtattgggcgctcttccgcttcctcgctcactgactcgctgcgctcggtcgttcggctgcggcgagcggtatcagctcactcaaaggcggt
aatacggttatccacagaatcaggggataacgcaggaaagaacatgtgagcaaaaggccagcaaaaggccaggaaccgtaaaaaggccgcgttgctgg
cgtttttccataggctccgccccctgacgagcatcacaaaaatcgacgctcaagtcagaggtggcgaaacccgacaggactataaagataccaggcg
tttcccccctggaagctccctcgtgcgctctcctgttccgaccctgccgcttaccggatacctgtccgcctttctcccttcgggaagcgtggcgctttc
tcatagctcacgctgtaggtatctcagttcggtgtaggtcgttcgctccaagctgggctgtgtgcacgaaccccccgttcagcccgaccgctgcgcct
tatccggtaactatcgtcttgagtccaacccggtaagacacgacttatcgccactggcagcagccactggtaacaggattagcagagcgaggtatgta
ggcggtgctacagagttcttgaagtggtggcctaactacggctacactagaaggacagtatttggtatctgcgctctgctgaagccagttaccttcgg
aaaaagcggttagctccttcggtcctccgatcgttgtcagaagtaagttggccgcagtgttatcactcatggttatggcagcactgcataattctctt
actgtcatgccatccgtaagatgcttttctgtgactggtgagtactcaaccaagtcattctgagaatagtgtatgcggcgaccgagttgctcttgccc
ggcgtcaatacgggataataccgcgccacatagcagaactttaaaagtgctcatcattggaaaacgttcttcggggcgaaaactctcaaggatcttac
cgctgttgagatccagttcgatgtaacccactcgtgcacccaactgatcttcagcatcttttactttcaccagcgtttctgggtgagcaaaaacagga
aggcaaaatgccgcaaaaaagggaataagggcgacacggaaatgttgaatactcatactcttccttttttcaatattattgaagcatttatcagggtta
ttgtctcatgagcggatacatatttgaatgtatttagaaaaataaacaaatagggggttccgcgcacatttccccgaaaagtgccacctgggtcctttt
catcacgtgctataaaaatattataatttaaattttttaatataaatatataaattaaaaatagaaagtaaaaaaagaaattaaagaaaaaatagtt
tttgttttccgaagatgtaaaagactctagggggatcgccaacaaatactaccttttatcttgctcttcctgctctcaggtattaatgccgaattgtt
tcatcttgtctgtgtagaagaccacacacgaaaatcctgtgattttacattttacttatcgttaatcgaatgtatatctatttaatctgcttttcttg
tctaataaatatatatgtaaagtacgctttttgttgaaatttttttaaaccttgtttatttttttttcttcattccgtaactcttctaccttctttat
ttactttctaaaatccaaatacaaaacataaaaataaataaacacagagtaaattcccaaattattccatcattaaaagatacgaggcgcgtgtaagt
tacaggcaagcgatccgtcctaagaaaccattattatcatgacattaacctataaaaatagggcgtatcacgaggccctttcgtc

cpMT1

gatcc**atgtctggctgcaactgtggcagtagctgcaattgtggcgatcagtgcaaatgcaataagagatcagggttgagctatgtcgaagccggcgaa
accacagagacggtggttttaggcgtaggtccgaccaagatccattttgagggagcggaaatgagtgtggcagctgaagatggtggctgcaaatgtgg
gtcaagctgcacctgtgacccttgcaactgcaaa**tgag

cpMT2

gatcc**atgtcttgctgtggcggcaattgtgggtgtggaagcagctgcaaatgcgggagtggctgtggcggctgcaagatgtatccggacatgagctac
acagagcagacgacgagcgaaaccctggtgatgggagtggcatctgggaagacccaatttgaaggcgcggaaatgggttttggcgcggagaatgatgg
ctgcaaatgtgggtcaaactgcacctgcaatccgtgcacctgcaaa**tgag

baMT3

gatcc**atgtcgacctgtggcaactgcgattgcgttgacaaaagccagtgcgtgaaaaagggaaacagctacggtatcgatattgttgaaaccgaaaaa
agctacgtcgatgaggtgatcgttgccgcagaagctgccgaacatgacggcaaatgtaagtgcggcgccgcctgcgcctgcaccgattgcaagtgtgg
caac**tgag

E_c-1

gatccatgggctgtgatgacaagtgcgggtgtgccgtgccgtgccccggcggcacgggctgtagatgcacctcggcgaggagcggcgcggcggcgggg
gaacatacgacgtgtgggtgcggcgaacactgtgggtgcaatccgtgtgcgtgcgggcgcgaggggacgccgtccggtcgtgcgaataggagagccaa
ctgctcctgcggtgcagcctgcaactgcgcttcatgcggctcggcgaccgcctgag

γ-E_c-1

gatccatgggctgtgatgacaagtgcgggtgtgccgtgccgtgccccggcggcacgggctgtagatgcacctcggcgaggtgag

β_E-E_c-1

gatccatgggggaacatacgacgtgtgggtgcggcgaacactgtgggtgcaatccgtgtgcgtgcgggcgcgaggggacgccgtccggtcgtgcgaat
aggagagccaactgctcctgcggtgcagcctgcaactgcgcttcatgcggctcggcgaccgcctgag

huMT2

gatccatggatcccaactgctcctgcgccgccggtgactcctgcacctgcgccggttcctgcaaatgcaaagagtgcaaatgcacttcgtgcaagaaa
agctgctgctcctgctgccctgtgggctgtgccaagtgtgcccaaggctgcatctgcaaaggggcgtcggacaagtgcagctgctgcgcctgag

Fig. 69 DNA sequence of pRS416 with different MT inserts. MT is indicating the different plant MTs which are inserted in the pRS416. The sequences of the plant MTs are shown at the bottom. Blue part is transcribed and translated sequence of the target proteins. Underlined parts are restriction sequences used for cloning.

9.2. Sequences of yeast chromosomal DNA

9.2.1. Genomic sequence for *cup1* gene

gaggtaccacgttgaatgtccatttgggtaatttagaatggttaaggccagaagagtttgtagataacgttgaattaatttctgaacagttaatcaaa
gcataccaaatcagatccatttttatcaaaaccaataagtcgcccgtattgccattatactataaccaggacgttcttgatgaacttgaagctaaaaa
ggacaaaatcgaagaaacccacgaagatgacatggtcaccattgatggtgtacaagttcatttatctaccttcaacaagggtttgatggaaatcgcca
atccttccgaattgggttcaatttttctctaaacaaattaacaatgcaaaaaagagatcttctagcgagcttgaaaaagaatctagcgagtcagaagct
gtcaagaagactaaaagttaatttgtgtcctccttatctatcttttctctcatttttttcttgtgaagaaaaaaatttgaatttcatagagtgcggtg
catatgtatatatctatatatgtttgaagtgtatattaaaaataaagtcattatttgaatattggtttctcggtctaagagcttatacgttttagact
gatctgttgtactatccgcttcaaataaatagatcattgaaagtgacggggataacagcattttacctttaaaagacgttctcataatacattttagg
attaatacatatgctttttttttattcaaaatctggggattttatacagagttgtaagttaggcaaactagaatttggtaataatattttattcttgg
ggcgacatatggagatactttatttccttttcttaattattaacgtatacctataaattaacaaagtatctaaacaaaatacataagtgtactcaaac
tgagtagaatcgtcgattaaacttccttctccttttaaaattaaaaacagcaaatagttaaatgaatatattaaagactattcgttTTATTTCCCAGA
GCAGCATGATTTCTTGGTTTCTTCAGACTTGTTACCGCAGGGGCATTTGTCGTCGCTGTTACACCCCGTTGGGCAGCTACATGATTTTTGGCATTGTT
CATTATTTTTGCAGCTACCACATTGGCATTGGCACTCATGACCTTCATTTTGGAAGTTAATTAATTCGCTGAACATtttatgtgatgattgattgatt
gtacggtttgtttttgttaatatctatttcgatgacttctatatgatattgcactaacaagaagatattataatgcaattggtacaagacaaggagtt
atttgcttctcttttatatgattctgacaatccatattgcgttggtagtctttttgctggaacggttcagcggaaaagacgcatcgctcttttttgct
tctagaagaaatgccagcaaaagaatctcttgacagtgactgacagcaaaaatgtctttttctaactagtaacaaggctaagatatcagcctgaaata
aagggtggtgaagtaataattaaatcatccgtataaacctatacacatatatgaggaaaaaataatacaaaagtgttttaaatacagatacatacatg
aacatatgcacgtatagcgtccaaatgtcggtaatgggatcggcttactaattataaaatgcatcatagaaatcgttgaagtttgccgtagtaatacc
cagattatcagattccaaatccttgtcaataattatactcctttggaaaacttctctttccattaaaaaatctgaaatctccttaaatttaaataga
ttctgttcagttcactaacggggaatttcaagagaacatttttgttcttcgccgactgactataatctgtaacattattattatcagagtttctcgca
aaattttgtttttttcttgctaaatctcagcatatatttaatcagattcaaaaccttgttgaaacctttaatagatttgaaatttccgttgctattcat
ttcatcccgtaaaaaggatacgataatttctatttttttttaaaatttccaaaatcttgtcatgaatcaatagcaattgaacattaatctcctcatttg
aaagatttttgtaaaattcgtcatataatattacttcacaacgttggaaaatagcaaatgtgattgctataaaattctgtaagatttcaataaaatga
tttgcgaataaaaattctttaccattagaatgaaagcgattattgccgcttgaaaatgactttatcgactttatggggaagataaaattaaatgttac
tgagtaaaaaatgtgcatattagaaataattttcatcagatcctttgcacatctttcagagttcgaggtcttattgttgttagaagaatgctgaactg
ccatggacaaagaggattcgttttgaacaaaaaggaaaaaatttgtataaacaatggtattgataaaatttaaagtgtctttccattcttttctgact
tcgttgtcatgaaaatataagtctactgtattactcacgcccatagtcaaggtttctaacagactttcaattttggttaaatttactggcaagtagaa
aggaacatcttgcagaatatttatcaattttgcttgcgtttccagtaattttaaatcgttagcaattaaaggaatgtcgttcgtatcaatagaggcag
gtatcggagataggttttcagtagcgggtaccatgaatgaagactgacctagaagcgaatgtcttgagtaatacatttttttcaaaaaatggaataac
ttgaaatcttttatctggaagcttaagagacagctcaaatcttcgtctaaacttgatttatgatcatcatgcatgtacagagattcataaaatttttgt
gatggcaataaatttgattgtctcttggtcataatattccaggtttatcaatgtgatttggcttcgaatcaacctcaaattattcattaatgccgaaa
catggttattaatagcctgcttattgaatagggtcattgaatcgtttaacaacagcagaagcacagttaatcggcctagtttggtcagttgagataaa
ggaagatcgaccgttgagaatgaaggac

Fig. 70 DNA sequence of CUP1^S corresponding to S288C DNA sequence of chromosome VIII: 211‘568-216‘635 bp with a deleted iteration unit. Shown are the sequences 969 bp upstream and 1912 bp downstream of *cup1* gene (186 bp). Grey part is unsequenced DNA, black part is sequenced. Underlined part shows the iteration unit, green, bold part, written in capital letters shows the reverse *cup1* gene.

tcaatcgatgaattcgagctcgtttaaactggatggcggcgttagtatcgaatcgacagcagtatagcgaccagcattcacatacgattgacgcatga
tattactttctgcgcacttaacttcgcatctgggcagatgatgtcgaggcgaaaaaaaatataaatcacgctaacatttgattaaaatagaacaacta
caatataaaaaaactatacaaatgacaagttcttgaaaacaagaatctttttattgtcagtactgaTTAGAAAAACTCATCGAGCATCAAATGAAACT
GCAATTTATTCATATCAGGATTATCAATACCATATTTTTGAAAAAGCCGTTTCTGTAATGAAGGAGAAAACTCACCGAGGCAGTTCCATAGGATGGCA
AGATCCTGGTATCGGTCTGCGATTCCGACTCGTCCAACATCAATACAACCTATTAATTTCCCCTCGTCAAAAATAAGGTTATCAAGTGAGAAATCACC
ATGAGTGACGACTGAATCCGGTGAGAATGGCAAAAGCTTATGCATTTCTTTCCAGACTTGTTCAACAGGCCAGCCATTACGCTCGTCATCAAAATCAC
TCGCATCAACCAAACCGTTATTCATTCGTGATTGCGCCTGAGCGAGACGAAATACGCGATCGCTGTTAAAAGGACAATTACAAACAGGAATCGAATGC
AACCGGCGCAGGAACACTGCCAGCGCATCAACAATATTTTCACCTGAATCAGGATATTCTTCTAATACCTGGAATGCTGTTTTGCCGGGGATCGCAGT
GGTGAGTAACCATGCATCATCAGGAGTACGGATAAAATGCTTGATGGTCGGAAGAGGCATAAATTCCGTCAGCCAGTTTAGTCTGACCATCTCATCTG
TAACATCATTGGCAACGCTACCTTTGCCATGTTTCAGAAACAACTCTGGCGCATCGGGCTTCCCATACAATCGATAGATTGTCGCACCTGATTGCCCG
ACATTATCGCGAGCCCATTTATACCCATATAAATCAGCATCCATGTTGGAATTTAATCGCGGCCTCGAAACGTGAGTCTTTTCCTTACCCATggttgt
ttatgttcggatgtgatgtgagaactgtatcctagcaagattttaaaaggaagtatatgaaagaagaacctcagtggcaaatcctaacctttatatt
tctctacaggggcgcggcgtggggacaattcaacgcgtctgtgaggggagcgtttccctgctcgcaggtctgcagcgaggagccgtaatttttgcttc
gcgccgtgcggccatcaaaatgtatggatgcaaatgattatacatggggatgtatgggctaaatgtacgggcgacagtcacatcatgcccctgagctg
cgcacgtcaagactgtcaaggagggtattctgggcctccatgtcgctggccgggtgacccggcggggacgaggcaagctaaacagatctggcgcgcct
taattaacccggggatccgtcgacctgcagcgtacgcat

Fig. 71 DNA sequence (1509 bp) from pFA6a-kanMX6 replacing the *cup1* gene in the deletion mutant, with the reverse *kan*^{R} marker (810 bp, blue, bold capital letters).

9.2.2. Genomic sequence for *crs5* gene

ttacggagaagatttaggcaagcatttaagcgccataacgttaaacagggatttaaacactactaaaagtaacactacttcccacgattcatcaagtt
tagtaggatccccttcacccacctggaaatctccaatcgaaagaataagggacagaagaagaagacataagataatgaaaagtgagaataaatttggg
caaaatcccagttttggaagtaaatcgaatggcaaacctaatactaaaacgacattatccaaatatcgacagctattaaggaagcctaggcgaaaaac
caattcatatgaaccaaaaaatggcattggacagaataaagaaggctcaactgttagaccaggagccgacaaacatattagagattccaattatctag
ctacagacatcagtgacaacgaaagtatggaaaccgaacttcgaaccaaccacatttataattacgaaaatagtgattaaggcaggcccagtggacga
aaagacataactgcagaagtacagctgcctttatttcttgtggtcatttattgcttttattttcaagtcagatatacaagaaaatcaaatcccatcgt
caacgtcacgtataaacgattaatttacagtaataccatactctaccaacattattttagtccgacgttcagtcctgtaggtgttccaaatccttctg
gcattgacttctgtgcagaaacccttcaaaatgagttccacttacgtcagatcgcataacaaccggtcatatatttttttcttttgctaaaccccct
actgcaagcacttttaagaaaaagaacaataaatgcgtctttattgctgtgtggaagtgatttttgtctttcggacaaaaaaaggatagggatgcgag
agggctgtgaagtagtgatcaagcggggcctatataagaagggcgcacatcgtccccctaagaatagcgaagcgatattacactgaacactacaatg
tcaaatagtactcaataaatATGACTGTAAAAATATGTGACTGTGAAGGCGAATGTTGTAAGGACTCTTGTCATTGTGGGAGCACCTGCCTTCCAAGC
TGTTCTGGCGGTGAAAAGTGCAAATGTGATCACAGCACCGGAAGCCCTCAATGTAAGAGTTGTGGTGAAAAATGCAAATGCGAAACCACGTGCACTTG
TGAAAAGAGTAAATGCAATTGTGAAAAATGTTAGgtgacccctactctttacttatcataaatacatcatcatattttacccttaattaacaacattt
atttaactgcatgaactaaatataaggtatagtttcttttttcccggaatctttttttagatcgttattatttagacggcactaagagaaataaatta
aactaaattacggtgcggagctcaaggcatctgcgagtgtttactaacactaaaagagatgaataaaatagatttctcaatgcaaaattaaaattaca
atgttacgcatacacacaagtacagatttgtatatagtatttcttcttcgttttatctgtcgtgttgaaacattttgttgttcaagtattaaaagtct
cctgcgttgttaaaatccatatcatgtgaattgttggtgccgctcatgaggccgttttgatgtggaatattatattgaatgttatgcaatggttgttg
ttgtcgtggctgccgctgccgttggcgttggcagcttctggtttgcttttgtacttgttcactactactgttgtcactcaacggttgagatggctcgg
taagatggacgaaagaatcccgtgtgtcatttgataaatgttgattagccaagcttagctgtaggcactttctttctaaatgacaaatatattcaata
gatttcgttaaaatggacgccttattcaattttgttgctggctctaggccatctaagtctgctaggtctctagatgtaatgggaagatcgttacattt
tttatacgctactcgtagcgttgggacagttctccttaattgttcaatttttatcattaatattggaacggtatttcttttcaattatattgtgtgata
cccttcctgtcctcacccttgttattcttttgggtttaacatgaaaatgtttccgtataggtgaagtttttaacttgaagctcatactgtcagcattg
tcaatattctccaaattcaaagatgatttaatctcgtctgcagtaactaaggga

Fig. 72 DNA sequence of CUP1^S corresponding exactly to S288C DNA sequence of chromosome XV: 388'213-390'422 bp, except the original glutamic acid (GAA, underlined) instead of a stop codon (TAA) in S288C. Shown is the sequence 1000 bp up- and downstream of the forward oriented *crs5* gene (210 bp, green, bold part, written in capital letters). Grey part is unsequenced DNA, black part is sequenced.

atgcgtacgctgcaggtcgacggatccggagcaggtgctggtgctggtgctggagcaattctgtctaaaggtgaagaattattcactggtgttgtccc
aattttggttgaattagatggtgatgttaatggtcacaaatttttctgtctccggtgaaggtgaaggtgatgctacttacggtaaattgaccttaaaat
ttatttgtactactggtaaattgccagttccatggccaaccttagtcactactttcggttatggtgttcaatgttttgcgagatacccagatcatatg
aaacaacatgacttttttcaagtctgccatgccagaaggttatgttcaagaaagaactatttttttcaaagatgacggtaactacaagaccagagctga
agtcaagtttgaaggtgataccttagttaatagaatcgaattaaaaggtattgattttaaagaagatggtaacattttaggtcacaaattggaataca
actataactctcacaatgtttacatcatggctgacaaacaaaagaatggtatcaaagttaacttcaaaattagacacaacattgaagatggttctgtt
caattagctgaccattatcaacaaaatactccaattggtgatggtccagtcttgttaccagacaaccattacttatccactcaatctgccttatccaa
agatccaaacgaaaagacagaccacatggtcttgttagaatttgttactgctgctggtattacccatggtatggatgaattgtacaaataactgcgcg
ccacttctaaataagcgaatttcttatgatttatgatttttattattaaataagttataaaaaaaaataagtgtatacaaattttaaagtgactcttag
gttttaaaacgaaaattcttattcttgagtaactctttcctgtaggtcaggttgctttctcaggtatagtatgaggtcgctcttattgaccacacctc
taccggcagatccgctagggataacagggtaatatagatctgtttagcttgcctcgtccccgccgggtcacccggccagcgacatggaggcccagaat
accctccttgacagtcttgacgtgcgcagctcaggggcatgatgtgactgtcgcccgtacatttagcccatacatccccatgtataatcatttgcatc
catacattttgatggccgcacggcgcgaagcaaaaattacggctcctcgctgcagacctgcgagcagggaaacgctcccctcacagacgcgttgaatt
gtccccacgccgcgcccctgtagagaaatataaaaggttaggatttgccactgaggttcttctttcatatacttccttttaaaatcttgctaggatac
agttctcacatcacatccgaacataaacaaccATGGGTAGGAGGGCTTTTGTAGAAAGAAATACGAACGAAACGAAAATCAGCGTTGCCATCGCTTTG
GACAAAGCTCCCTTACCTGAAGAGTCGAATTTTATTGATGAACTTATAACTTCCAAGCATGCAAACCAAAAGGGAGAACAAGTAATCCAAGTAGACAC
GGGAATTGGATTCTTGGATCACATGTATCATGCACTGGCTAAACATGCAGGCTGGAGCTTACGACTTTACTCAAGAGGTGATTTAATCATCGATGATC
ATCACACTGCAGAAGATACTGCTATTGCACTTGGTATTGCATTCAAGCAGGCTATGGGTAACTTTGCCGGCGTTAAAAGATTTGGACATGCTTATTGT
CCACTTGACGAAGCTCTTTCTAGAAGCGTAGTTGACTTGTCGGGACGGCCCTATGCTGTTATCGATTTGGGATTAAAGCGTGAAAAGGTTGGGGAATT
GTCCTGTGAAATGATCCCTCACTTACTATATTCCTTTTCGGTAGCAGCTGGAATTACTTTGCATGTTACCTGCTTATATGGTAGTAATGACCATCATC
GTGCTGAAAGCGCTTTTAAATCTCTGGCTGTTGCCATGCGCGCGGCTACTAGTCTTACTGGAAGTTCTGAAGTCCCAAGCACGAAGGGAGTGTTGTAA
agagtactgacaataaaaagattcttgttttcaagaacttgtcatttgtatagttttttatattgtagttgttctattttaatcaaatgttagcgtg
atttatatttttttcgcctcgacatcatctgcccagatgcgaagttaagtgcgcagaaagtaatatcatgcgtcaatcgtatgtgaatgctggtcgc
tatactgctgtcgattcgatactaacgccgccatccagtttaaacgagctcgaattcatcgattaa

Fig. 73 DNA sequence (2320 bp) from pYM44 replacing the *crs5* gene in the deletion mutant, with the forward *his* marker (654 bp, blue, bold, capital letters).

9.2.3. Genomic sequence for *zrc1* gene

aaggaaatgatatgaaagtagttgcatttttataggtgaaaaaaagagaactagctaaaaagaaattaaatatcgttctcttattcaccgatacatcg
cccatgaaatcgactgagtagctaagtaagatgatgtagaaaaagaaaaagaaaaagaaaaagaataagaaaaagaataagaaaaagaataagaaaaa
gaataagaaataagaaataagaagaaatcaaaaaaaagaaacaataatgctttgcggacccgctgctactaaagcacttccacttgaaaaaagaaact
accgccgtggcactggtaggtttacagattcaaaaaaaaaaaaaaaaactgagatctttactacataaaaagaaagttatctcggtttgcagatcggt
gcaggtcccatgagataaacttttgcgttgagttctggactcttgatgtatctccggactacagtattcattctgctaaggggaaggcgtctggctaa
gttcagccagacttcctttctacaaccctttttactagctgagcctacttcccaggaagcaaaaaaaattcttgctactttctcttcatgacgcagcg
tagtgagtgcatttgtctttccctacctacgccgaaaatatatatgtcatataacggaagtcataaacggtgactccttttttgtttttgctggtcaac
cttaaagaaacaaaaactctaatatgatttcttggcatagacccacacaccctcggaaaacctcatttttcaaaagaaaaaaaatgccgtttttgttt
gcgaaaaataacgtccctccctctgttttccttcttcagatggccttgaaggtgaggaatgaggtggttgctgcatcagctaaaacttttcattgcaa
agtcatcagagctcaaagtttcataaaagaatataacattcaagatactttaaagggcttggcgcagtaatttttccctatcgatatccgtcaggaat
accaggaaactaatagagtc**ATGATCACCGGTAAAGAATTGAGAATCATCTCTCTTTTGACCTTAGACACGGTTTTTTTCCTATTGGAAATTACCATA**
GGTTATATGTCACATTCATTGGCCTTGATTGCCGATTCATTTCACATGTTGAATGATATCATCTCTCTTTTAGTGGCACTATGGGCTGTGGATGTGGC
CAAAAACAGGGGTCCAGACGCTAAATACACTTATGGATGGAAAAGAGCAGAAATTTTGGGTGCTTTAATCAATGCTGTTTTTCTTATTGCCCTGTGTT
TCTCTATTATGATTGAAGCTTTACAAAGATTGATTGAACCTCAAGAAATTCAAAACCCAAGGTTGGTTTTATACGTTGGTGTAGCAGGGTTAATTTCT
AATGTCGTAGGTTTATTTTTGTTCCACGATCATGGCAGCGATAGTCTGCACTCACACTCTCATGGCTCTGTGGAAAGCGGGAATAACGATTTGGACAT
AGAATCTAATGCGACTCATTCCCACTCTCATGCATCTCTTCCAAACGATAATTTGGCCATCGATGAAGATGCTATTTCGAGTCCTGGGCCCTCAGGGC
AAATTGGTGAAGTGTTGCCACAATCAGTAGTAAACAGATTATCAAACGAAAGCCAACCCTTATTGAACCACGATGATCATGACCACAGCCATGAATCG
AAGAAACCAGGTCATCGCTCTTTGAATATGCATGGTGTCTTCTTACATGTACTAGGTGATGCTCTGGGTAATATTGGTGTTATTGCAGCTGCTTTGTT
TATTTGGAAAACTGAATATTCTTGGAGATATTACTCGGATCCAATCGTTTCTTTAATCATCACCATTATTATTTTCTCTTCCGCTCTGCCCTTATCAC
GTAGAGCTTCAAGAATTTTACTACAGGCTACTCCTTCTACAATTTCTGCTGATCAGATTCAAAGAGAGATTTTGGCAGTACCTGGCGTGATAGCGGTC
CATGACTTCCACGTCTGGAACTTAACTGAATCAATATATATTGCATCTATCCACGTTCAAATAGACTGTGCACCTGATAAATTCATGAGCTCCGCCAA
GCTGATAAGAAAAATATTCCATCAACACGGTATTCATTCTGCAACTGTTCAACCAGAATTTGTTTCTGGAGATGTTAATGAGGATATTCGCAGAAGAT
TTTCTATCATAGCAGGTGGTTCACCATCTTCGTCTCAAGAAGCCTTTGACAGCCATGGAAACACTGAGCATGGTAGAAAAAAGCGTTCACCTACTGCC
TATGGTGCTACTACAGCATCATCTAATTGTATTGTAGATGAcgctgtaaactgcaatacttccaattgcctgtaataaagatataaagggctgaagcc
gtcggtgaatttatcccatggttctacagagaacataaactatatactatttacataattaattcttagacgtataggaagaaggcagttcttcctaa
ctcaagaactgcgttattcaatgtatgaatacgctatcttttagctataaatctccattaaaaatttgtatgcaatatgtgccacaatccttcctcat
ctttttttgagacttttaacccaaacataaaatacccccatacatccagaatagcgtttttatgtctcaaatagttaacttttttcagcgcgcgcag
agcaggaaacaaattaagctcacttcggtgtggtaccagcccaggaataccgcttctcaataagcgttcccctctaaaccctgctgcaatttactaag
tgcattgaggcagaatccagcgcacatttgatgctcttagcccaactctaagccgggcgcctgcttgttccctcctgtaccaaaatctgaccgtggca
aggtatcgccaaatttcattttaaacattgaggttgaagaatttggacaatcataagcatctatatagttcctcaagtcttttaaggaaaaacagtgc
ggaaaaagtgagtaaatacctactaaactatgccacaaaaatggaagagtaatgccatctacatcgcagaactaggctcggagcgatcatgaaatgaa
tgaccacactgcgtttaaaacttaagctactatcaccactaaaatagttcaactaggattacactctaaatatgtcaaggaaaacagcgagtttgtta
cgaccgaaaagaaatgaacgacgttaattgtaccatgctgaataatatgatcccatccatcctagaaatacgattgcaaaagaagtgtataggttctt
tttggttcaatgacgaaacacctgagttaaactttcatggatctttcaaatgtctaaaagg

Fig. 74 DNA sequence of CUP1^S corresponding to S288C DNA sequence of chromosome XIII: 753'837-757'132 bp. Shown is the sequence 1000 bp up- and downstream of the forward oriented *zrc1* gene (1295 bp, green, bold part, written in capital letters).

atgcgtacgctgcaggtcgacggatccggagcaggtgctggtgctggtgctggagcaatttctgtctaaaggtgaagaattattcactggtgttgtccc
aattttggttgaattagatggtgatgttaatggtcacaaatttttctgtctccggtgaaggtgaaggtgatgctacttacggtaaattgaccttaaaat
ttatttgtactactggtaaattgccagttccatggccaaccttagtcactactttcggttatggtgttcaatgttttgcgagatacccagatcatatg
aaacaacatgacttttttcaagtctgccatgccagaaggttatgttcaagaaagaactatttttttcaaagatgacggtaactacaagaccagagctga
agtcaagtttgaaggtgataccttagttaatagaatcgaattaaaaggtattgattttaaagaagatggtaacattttaggtcacaaattggaatacа
actataactctcacaatgtttacatcatggctgacaaacaaaagaatggtatcaaagttaacttcaaaattagacacaacattgaagatggttctgtt
caattagctgaccattatcaacaaaatactccaattggtgatggtccagtcttgttaccagacaaccattacttatccactcaatctgccttatccaa
agatccaaacgaaaagacagaccacatggtcttgttagaatttgttactgctgctggtattacccatggtatggatgaattgtacaaataactgcgcg
ccacttctaaataagcgaatttcttatgatttatgatttttattattaaataagttataaaaaaaaataagtgtatacaaattttaaagtgactcttag
gttttaaaacgaaaattcttattcttgagtaactctttcctgtaggtcaggttgctttctcaggtatagtatgaggtcgctcttattgaccacacctc
taccggcagatccgctagggataacagggtaatatagatctgtttagcttgcctcgtccccgccgggtcacccggccagcgacatggaggcccagaat
accctccttgacagtcttgacgtgcgcagctcaggggcatgatgtgactgtcgcccgtacatttagcccatacatccccatgtataatcatttgcatc
catacattttgatggccgcacggcgcgaagcaaaaattacggctcctcgctgcagacctgcgagcagggaaacgctcccctcacagacgcgttgaatt
gtccccacgccgcgcccctgtagagaaatataaaaggttaggatttgccactgaggttcttctttcatatacttccttttaaaatcttgctaggatac
agttctcacatcacatccgaacataaacaacc**ATGGGTAGGAGGGCTTTTGTAGAAAGAAATACGAACGAAACGAAAATCAGCGTTGCCATCGCTTTG**
GACAAAGCTCCCTTACCTGAAGAGTCGAATTTTATTGATGAACTTATAACTTCCAAGCATGCAAACCAAAAGGGAGAACAAGTAATCCAAGTAGACAC
GGGAATTGGATTCTTGGATCACATGTATCATGCACTGGCTAAACATGCAGGCTGGAGCTTACGACTTTACTCAAGAGGTGATTTAATCATCGATGATC
ATCACACTGCAGAAGATACTGCTATTGCACTTGGTATTGCATTCAAGCAGGCTATGGGTAACTTTGCCGGCGTTAAAAGATTTGGACATGCTTATTGT
CCACTTGACGAAGCTCTTTCTAGAAGCGTAGTTGACTTGTCGGGACGGCCCTATGCTGTTATCGATTTGGGATTAAAGCGTGAAAAGGTTGGGGAATT
GTCCTGTGAAATGATCCCTCACTTACTATATTCCTTTTCGGTAGCAGCTGGAATTACTTTGCATGTTACCTGCTTATATGGTAGTAATGACCATCATC
GTGCTGAAAGCGCTTTTAAATCTCTGGCTGTTGCCATGCGCGCGGCTACTAGTCTTACTGGAAGTTCTGAAGTCCCAAGCACGAAGGGAGTGTTGTAA
agagtactgacaataaaaagattcttgttttcaagaacttgtcatttgtatagttttttatattgtagttgttctattttaatcaaatgttagcgtg
atttatatttttttcgcctcgacatcatctgcccagatgcgaagttaagtgcgcagaaagtaatatcatgcgtcaatcgtatgtgaatgctggtcgc
tatactgctgtcgattcgatactaacgccgccatccagtttaaacgagctcgaattcatcgattga

Fig. 75 DNA sequence (2320 bp) from pYM44 replacing the *zrc1* gene in the deletion mutant, with the forward *his* marker (654 bp, blue, bold, capital letters).

9.2.4. Genomic sequence for *cot1* gene

ttcaccgcgcttagatcaagagggcatcatgaggctacctacaattgacatactaagtcaagaaaaataatagtgtatcgaatacgcgtggtagctac
attaaatactaaagtatggttttttttttaagtaggtttactcttcatattcttcattttcatttttccttttcttcccgttcttcatttttattcc
tagaaaaaaaaataaatatgtctatcgttaacctaaacataaacaaagtttagcccgcttatttaaatgatgcccagtacttttttcaaaactcata
taattatatatatcaagaatgctttccaaccaccgcttgtattaaggtgtagaaaggtggtttttgtattcaaaaagagtacaagcccattatagcta
acttaacagtccaccctactatatcccacgcatatctggttttaacttgtggcgggcgatatggaacgaatttttcaaagttaaccatagaaaaaagc
atgtgatcaaggcagagtgaacgagggaaaaagaaagtgtggagaaggccacctttgaaaagtttaccaatcgatcggtctctcagcactttctaca
tttaatctctttatagtgaacatcgctggctcatgctggttcccatgcataactcacccacggccgccaacggccgcttatcacttactgtcgccagc
tccggtcttagaaagggtaaaaaaaaccgggtgtatactatacactcatacatccgctcacccgtttccagtagtgaattttcatttttctgtacgaag
gcaatataagctgacgatccgcataaagcagaagactcatttgtaatgcagaatatccgtacaataaaggaatttattggtcttatatattctacgtg
ggagctcgaaaagcatttctggttctatttagtaaccaattattttcactttgctcagaatagttctgcatagctatagaaagaaagttaacacaaag
tacggaaagattgagtaaat**ATGAAACTCGGAAGCAAACAGGTAAAAATTATATCCTTGTTGCTGCTAGACACAGTGTTCTTCGGGATCGAGATAACT**
ACCGGGTACTTGTCTCACTCTTTGGCTCTAATCGCGGACTCATTCCATATGCTAAACGATATAATTTCTCTTGTGGTTGCACTTTGGGCCGTAAATGT
TGCCAAAAACAGAAATCCGGATTCAACGTACACTTATGGTTGGAAAAGGGCGGAGATTTTGGGTGCTCTGATTAACGCCGTCTTTTTGATTGCCTTAT
GTGTCTCAATTTTGATAGAAGCGCTACAAAGAATTATTGCTCCCCCCGTGATTGAAAATCCTAAGTTTGTGTTGTATGTGGGTGTCGCAGGGTTGATA
TCGAACACCGTTGGACTTTTCTTATTTCACGACAATGATCAAGAGCATGGACATGGACACGGACATTCCCATGGCGGTATCTTTGCCGACCATGAGAT
GCATATGCCATCATCCCACACACATACACATGCCCATGTTGATGGAATAGAGAATACTACACCAATGGATAGTACGGATAACATTAGTGAGATTATGC
CTAATGCTATAGTAGATAGTTTTATGAACGAAAATACTAGATTATTGACACCGGAAAATGCATCCAAGACGCCATCATACTCAACGTCAAGCCATACG
ATTGCCAGCGGCGGAAATTACACAGAACACAACAAGCGCAAGAGATCTTTAAATATGCATGGTGTGTTTCTTCACGTTTTGGGCGATGCTCTTGGCAA
CATCGGCGTTATGTTGTCTGCATTTTTCATTTGGAAGACCGACTATTCTTGGAAGTATTATACAGATCCGCTTGTCTCATTGATAATTACCGGTATAA
TTTTTTCCTCTGCGCTTCCTCTATCGTGCAAGGCTTCCAAAATATTGTTACAAGCGACACCTTCCACTTTATCCGGCGATCAAGTAGAAGGTGATCTT
TTGAAAATACCAGGAATAATAGCTATTCATGATTTCCATATTTGGAATTTAACAGAGTCTATTTTTATTGCATCTTTGCATATTCAACTAGATATCAG
CCCGGAACAATTTACTGACCTGGCCAAAATAGTTAGATCAAAACTTCACCGCTATGGCATTCACTCCGCTACTTTGCAACCTGAATTTATTACCAGAG
AGGTTACTTCAACCGAAAGAGCCGGAGACTCCCAAGGTGATCATCTACAAAATGACCCGCTTTCATTAAGGCCAAAGACATATGGTACTGGCATTTCA
GGTTCCACTTGTCTTATCGACGACGCTGCCAACTGCAACACAGCTGATTGCTTAGAGGATCATTAAaaggactttataacgaaaaagcgtgaagaatt
aaatacttttaaaaatcgttatacggtacatatacatacacacacacacatatatatagtcgtctataatgtttttatacaatgtttatcataaatttt
tgttacagtaagaagtataggagataatatataaaaaaagaggaaaagcgaaaacaggtgataataatgatgatcataataataatataataatagcaatagt
cttgcaaaacaacaacttgaggaaggaaaatagtaataatggtgtttagctttttttagattactccagcttctaaaaaagagtacaatacttagcac
aataatgctgttatctttttttcatttaattaaaaagaccagttgttaagaaataataaaaaaaaactcctttgtttagaattcaacaaattagaagaa
aaagaacctagttattgttctaaaacctttgcccactgaacttttttgtagtccttcgtactctgtagttcattacattgcgtcagctcatcgcgcct
tcctgactgaaattcgtaacctcttattactgccgcgtcgggaaggtcgtcttcattgtcttcttcattatcttcatcttcgccaaaattactagctt
gcccatatatttggtctttaagcttcttgtatttctccttaattgaagagtttactggaattgtgagcttctcccaaatactagaaattgctggtaat
ttgttttcttcattgctcaaagtagaatttatttcggtggcaaagatggtagcgtcatttaatgagcctcgcgacgaactgactatgagattcagaga
tttggctggtactgttagaattgatttttttgggcttcaatagacggtgagagggttcgtaccttgttggcttgaaggtcgatctgtttactggagata
acctttttttgagtttaggcaataaaagtggcacatcactgttggattccagtgggctcatcggaaacgaagaatgaatcattcgg

Fig. 76 DNA sequence of CUP1^{S} corresponding to S288C DNA sequence of chromosome XV: 905'233-908'552 bp. Shown is the sequence 1000 bp up- and downstream of the forward oriented *cot1* gene (1320 bp, green, bold part, written in capital letters).

atgcgtacgctgcaggtcgacggatccccgggttaattaaggcgcgccagatctgtttagcttgcctcgtccccgccgggtcacccggccagcgacat
ggaggcccagaataccctccttgacagtcttgacgtgcgcagctcaggggcatgatgtgactgtcgcccgtacatttagcccatacatccccatgtat
aatcatttgcatccatacattttgatggccgcacggcgcgaagcaaaaattacggctcctcgctgcagacctgcgagcagggaaacgctcccctcaca
gacgcgttgaattgtccccacgccgcgcccctgtagagaaatataaaaggttaggatttgccactgaggttcttctttcatatacttccttttaaaat
cttgctaggatacagttctcacatcacatccgaacataaacaacc**ATGGGTAAGGAAAAGACTCACGTTTCGAGGCCGCGATTAAATTCCAACATGGA**
TGCTGATTTATATGGGTATAAATGGGCTCGCGATAATGTCGGGCAATCAGGTGCGACAATCTATCGATTGTATGGGAAGCCCGATGCGCCAGAGTTGT
TTCTGAAACATGGCAAAGGTAGCGTTGCCAATGATGTTACAGATGAGATGGTCAGACTAAACTGGCTGACGGAATTTATGCCTCTTCCGACCATCAAG
CATTTTATCCGTACTCCTGATGATGCATGGTTACTCACCACTGCGATCCCCGGCAAAACAGCATTCCAGGTATTAGAAGAATATCCTGATTCAGGTGA
AAATATTGTTGATGCGCTGGCAGTGTTCCTGCGCCGGTTGCATTCGATTCCTGTTTGTAATTGTCCTTTTAACAGCGATCGCGTATTTCGTCTCGCTC
AGGCGCAATCACGAATGAATAACGGTTTGGTTGATGCGAGTGATTTTGATGACGAGCGTAATGGCTGGCCTGTTGAACAAGTCTGGAAAGAAATGCAT
AAGCTTTTGCCATTCTCACCGGATTCAGTCGTCACTCATGGTGATTTCTCACTTGATAACCTTATTTTTGACGAGGGGAAATTAATAGGTTGTATTGA
TGTTGGACGAGTCGGAATCGCAGACCGATACCAGGATCTTGCCATCCTATGGAACTGCCTCGGTGAGTTTTCTCCTTCATTACAGAAACGGCTTTTTC
AAAAATATGGTATTGATAATCCTGATATGAATAAATTGCAGTTTCATTTGATGCTCGATGAGTTTTTCTAAtcagtactgacaataaaaagattcttg
ttttcaagaacttgtcatttgtatagttttttttatattgtagttgttctattttaatcaaatgttagcgtgatttatatttttttttcgcctcgacatc
atctgcccagatgcgaagttaagtgcgcagaaagtaatatcatgcgtcaatcgtatgtgaatgctggtcgctatactgctgtcgattcgatactaacg
ccgccatccagtttaaacgagctcgaattcatcgattaa

Fig. 77 DNA sequence (1509 bp) from pFA6a-kanMX6 replacing the *cot1* gene in the deletion mutant, with the forward oriented *kan*^{R} marker (810 bp, blue, bold capital letters).

10. References

[1] M. Capdevila, S. Atrian, Metallothionein protein evolution: a miniassay. *J. Biol. Inorg. Chem.* **2011**, *16*, 977-989.

[2] D. H. Hamer, Metallothionein. *Annu. Rev. Biochem.* **1986**, *55*, 913-951.

[3] Y. Kojima, P.-A. Binz, J. H. R. Kägi, Metallothionein: molecular evolution and classification, in *Metallothionein IV*, Eds. C. Klaassen, Birkhäuser Verlag, Basel, Switzerland, **1999**, pp. 3-13.

[4] M. Margoshes, B. L. Vallee, A cadmium protein from equine kidney cortex. *J. Am. Chem. Soc.* **1957**, *79*, 4813-4814.

[5] M. Hambidge, Biomarkers of trace mineral intake and status. *J. Nutr.* **2003**, *133*, 948S-955S.

[6] M. T. Pellecchia, C. Criscuolo, K. Longo, G. Campanella, A. Filla, P. Barone, Clinical presentation and treatment of Wilson's disease: a single-centre experience. *Eur. Neurol.* **2003**, *50*, 48-52.

[7] M. Vašák, N. Romero-Isart, Metallothioneins, in *Encyclopedia of inorganic and bioinorganic chemistry,* John Wiley & Sons, Ltd, **2011**.

[8] J. Hidalgo, M. Aschner, P. Zatta, M. Vašák, Roles of the metallothionein family of proteins in the central nervous system. *Brain Res. Bull.* **2001**, *55*, 133-145.

[9] J. Hidalgo, M. Penkowa, M. Giralt, J. Carrasco, A. Molinero, Metallothionein expression and oxidative stress in the brain. *Methods Enzymol.* **2002**, *348*, 238-249.

[10] M. Vašák, D. W. Hasler, Metallothioneins: new functional and structural insights. *Curr. Opin. Chem. Biol.* **2000**, *4*, 177-183.

[11] G. K. Andrews, Regulation of metallothionein gene expression by oxidative stress and metal ions. *Biochem. Pharmacol.* **2000**, *59*, 95-104.

[12] S. Labbé, D. J. Thiele, Pipes and wiring: the regulation of copper uptake and distribution in yeast. *Trends Microbiol.* **1999**, *7*, 500-505.

[13] P. Liu, C.-J. Goh, C.-S. Loh, E.-C. Pua, Differential expression and characterization of three metallothionein-like genes in Cavendish banana (*Musa acuminata*). *Physiol. Plantarum* **2002**, *114*, 241-250.

[14] A. T. Miles, G. M. Hawksworth, J. H. Beattie, V. Rodilla, Induction, regulation, degradation, and biological significance of mammalian metallothioneins. *Crit. Rev. Biochem. Mol.* **2000**, *35*, 35-70.

[15] M. Chatthai, M. Osusky, L. Osuska, D. Yevtushenko, S. Misra, Functional analysis of a Douglas-fir metallothionein-like gene promoter: transient assays in zygotic and somatic embryos and stable transformation in transgenic tobacco. *Planta* **2004**, *220*, 118-128.

[16] I. Marta Evans, L. N. Gatehouse, J. A. Gatehouse, N. J. Robinson, R. R. D. Croy, A gene from pea (*Pisum sativum* L.) with homology to metallothionein genes. *FEBS Lett.* **1990**, *262*, 29-32.

[17] C. A. Whitelaw, J. A. Le Huquet, D. A. Thurman, A. B. Tomsett, The isolation and characterisation of type II metallothionein-like genes from tomato (*Lycopersicon esculentum* L.). *Plant Mol. Biol.* **1997**, *33*, 503-511.

[18] J. Zhou, P. B. Goldsbrough, Functional homologs of fungal metallothionein genes from Arabidopsis. *Plant Cell* **1994**, *6*, 875-884.

[19] C. S. Cobbett, P. B. Goldsbrough, Phytochelatins and metallothioneins: roles in heavy metal detoxification and homeostasis. *Annu. Rev. Plant Biol.* **2002**, *53*, 159-182.

[20] J. M. Brkljačić, J. T. Samardžić, G. S. Timotijević, V. R. Maksimović, Expression analysis of buckwheat (*Fagopyrum esculentum* Moench) Metallothionein-like gene (*MT3*) under different stress and physiological conditions. *J. Plant Physiol.* **2004**, *161*, 741-746.

[21] S. K. Clendennen, G. D. May, Differential gene expression in ripening banana fruit. *Plant. Physiol.* **1997**, *115*, 43-469.
[22] S. J. Reid, G. S. Ross, Up-regulation of two cDNA clones encoding metallothionein-like proteins in apple fruit during cool storage. *Physiol. Plantarum* **1997**, *100*, 183-189.
[23] I. Kawashima, T. D. Kennedy, M. Chino, B. G. Lane, Wheat E_c metallothionein genes. *Eur. J. Biochem.* **1992**, *209*, 971 -976.
[24] C. N. White, C. J. Rivin, Characterization and expression of a cDNA encoding a seed-specific metallothionein in maize. *Plant Physiol.* **1995**, *108*, 831-832.
[25] E. Freisinger, Metallothioneins in plants. *Met. Ions Life Sci.* **2009**, *5*, 107-153.
[26] L. Hanley-Bowdoin, B. G. Lane, A novel protein programmed by the mRNA conserved in dry wheat embryos. *Eur. J. Biochem.* **1983**, *135*, 9-15.
[27] B. G. Lane, R. Kajioka, T. D. Kennedy, The wheat-germ E_c protein is a zinc-containing metallothionein. *Biochem. Cell Biol.* **1987**, *65*, 1001-1005.
[28] P. Pulido, J. H. R. Kägi, B. L. Vallee, Isolation and some properties of human metallothionein. *Biochemistry* **1966**, *5*, 1768-1777.
[29] E. A. Peroza, R. Schmucki, P. Güntert, E. Freisinger, O. Zerbe, The β_E-domain of wheat E_c-1 metallothionein: a metal-binding domain with a distinctive structure. *J. Mol. Biol.* **2009**, *387*, 207-218.
[30] C. A. Blindauer, M. D. Harrison, J. A. Parkinson, A. K. Robinson, J. S. Cavet, N. J. Robinson, P. J. Sadler, A metallothionein containing a zinc finger within a four-metal cluster protects a bacterium from zinc toxicity. *Proc. Natl. Acad. Sci.* **2001**, *98*, 9593-9598.
[31] C. W. Cody, P. C. Huang, Metallothionein detoxification function is impaired by replacement of both conserved lysines with glutamines in the hinge between the two domains. *Biochemistry* **1993**, *32*, 5127-5131.
[32] C. W. Cody, P. C. Huang, Replacement of all α-domain lysines with glutamates reduces metallothionein detoxification function. *Biochem. Bioph. Res. Co.* **1994**, *202*, 954-959.
[33] P. K. Pan, F. Y. Hou, C. W. Cody, P. C. Huang, Substitution of glutamic acids for the conserved lysines in the α domain affects metal-binding in both the α domain and β domain of mammalian metallothionein. *Biochem. Bioph. Res. Co.* **1994**, *202*, 621-628.
[34] F. Yamasaki, M. Kurasaki, S. Oikawa, T. Emoto, M. Okabe, Y. Kojima, Effects of amino acid replacements on cadmium binding of metallothionein α-fragment. *Cell. Mol. Life Sci.* **1997**, *53*, 459-465.
[35] R. G. Pearson, Hard and soft acids and bases, HSAB, PartII. *J. Chem. Educ.* **1968**, *45*, 643-648.
[36] Ò. Palacios, S. Atrian, M. Capdevila, Zn- and Cu-thioneins: a functional classification for metallothioneins?, *J. Biol. Inorg. Chem.* **2011**, *16*, 991-1009.
[37] H. Irving, R. J. P. Williams, The stability of transition-metal complexes. *J. Chem. Soc.* **1953**, *0*, 3192-3210.
[38] P. A. Cobine, R. T. McKay, K. Zangger, C. T. Dameron, I. M. Armitage, Solution structure of Cu_6 metallothionein from the fungus *Neurospora crassa*. *Eur. J. Biochem.* **2004**, *271*, 4213-4221.
[39] A. Presta, A. R. Green, A. Zelazowski, M. J. Stillman, Copper binding to rabbit liver metallothionein. *Eur. J. Biochem.* **1995**, *227*, 226-240.
[40] M. Vašák, Spectroscopic studies on cobalt(II) metallothionein: evidence for pseudotetrahedral metal coordination. *J. Am. Chem. Soc.* **1980**, *102*, 3953-3955.
[41] M. Vašák, J. H. R. Kägi, H. A. O. Hill, Zinc(II), cadmium(II), and mercury(II) thiolate transitions in metallothionein. *Biochemistry* **1981**, *20*, 2852-2856.
[42] W. Lu, A. J. Zelazowski, M. J. Stillman, Mercury binding to metallothioneins: formation of the Hg_{18}-MT species. *Inorganic Chemistry* **1993**, *32*, 919-926.

[43] R. Dallinger, B. Berger, P. E. Hunziker, J. H. R. Kägi, Metallothionein in snail Cd and Cu metabolism. *Nature* **1997**, *388*, 237-238.

[44] R. Bofill, Ò. Palacios, M. Capdevila, N. Cols, R. González-Duarte, S. Atrian, P. González-Duarte, A new insight into the Ag^+ and Cu^+ binding sites in the metallothionein β domain. *J. Inorg. Biochem.* **1999**, *73*, 57-64.

[45] Ò. Palacios, K. Polec-Pawlak, R. Łobiński, M. Capdevila, P. González-Duarte, Is Ag(I) an adequate probe for Cu(I) in structural copper-metallothionein studies?, *J. Biol. Inorg. Chem.* **2003**, *8*, 831-842.

[46] Research Collaboratory for Structural Bioinformatics (RCSB) RCSB Protein Data Bank, http://www.pdb.org.

[47] M. Eigen, Fast elementary steps in chemical reaction mechanisms. *Pure Appl. Chem.* **1963**, *6*, 97-116.

[48] M. Vašák, Metal removal and substitution in vertebrate and invertebrate metallothioneins. *Methods Enzymol.* **1991**, *205*, 452-458.

[49] M. J. Stillman, Metallothioneins. *Coord. Chem. Rev.* **1995**, *144*, 461-511.

[50] P. Chen, A. Muñoz, D. Nettesheim, C. F. Shaw III, D. H. Petering, Stoichiometry and cluster specificity of copper binding to metallothionein: homogeneous metal clusters. *Biochem. J.* **1996**, *317*, 395-402.

[51] I. J. Pickering, G. N. George, C. T. Dameron, B. Kurz, D. R. Winge, I. G. Dance, X-ray absorption spectroscopy of cuprous-thiolate clusters in proteins and model systems. *J. Am. Chem. Soc.* **1993**, *115*, 9498-9505.

[52] E. Block, M. Gernon, H. Kang, G. Ofori-Okai, J. Zubieta, Coordination chemistry of sterically hindered thiolate ligands. Preparation and structural characterization of the oligomeric homoleptic complexes $[Cu(SC_6H_4\text{-}o\text{-}SiMe_3)]_{12}$ and $[\{Ag(SC_6H_4\text{-}o\text{-}SiMe_3)\}_4]_2$ and a comparison to the structure of the mononuclear species $(Et_4N)_2[Cd(SC_6H_4\text{-}o\text{-}SiMe_3)_4]$. *Inorg. Chem.* **1989**, *28*, 1263-1271.

[53] N. Romero-Isart, M. Vašák, Advances in the structure and chemistry of metallothioneins. *J. Inorg. Biochem.* **2002**, *88*, 388-396.

[54] M. Vašák, A. Galdes, H. A. O. Hill, J. H. R. Kägi, I. Bremner, B. W. Young, Investigation of the structure of metallothioneins by proton nuclear magnetic resonance spectroscopy. *Biochemistry* **1980**, *19*, 416-425.

[55] J. Loebus, E. A. Peroza, N. Blüthgen, T. Fox, W. Meyer-Klaucke, O. Zerbe, E. Freisinger, Protein and metal cluster structure of the wheat metallothionein domain γ-E_c-1: the second part of the puzzle. *J. Biol. Inorg. Chem.* **2011**, *16*, 683-694.

[56] E. A. Peroza, A. Al Kaabi, W. Meyer-Klaucke, G. Wellenreuther, E. Freisinger, The two distinctive metal ion binding domains of the wheat metallothionein E_c-1. *J. Inorg. Biochem.* **2009**, *103*, 342-353.

[57] E. A. Peroza, E. Freisinger, Metal ion binding properties of *Triticum aestivum* E_c-1 metallothionein: evidence supporting two separate metal thiolate clusters. *J. Biol. Inorg. Chem.* **2007**, *12*, 377-391.

[58] J. Domènech, A. Tinti, M. Capdevila, S. Atrian, A. Torreggiani, Structural study of the zinc and cadmium complexes of a type 2 plant (*Quercus suber*) metallothionein: insights by vibrational spectroscopy. *Biopolymers* **2007**, *86*, 240-248.

[59] P. Kille, D. R. Winge, J. L. Harwood, J. Kay, A plant metallothionein produced in *E. coli*. *FEBS Lett.* **1991**, *295*, 171-175.

[60] A. Arseniev, P. Schultze, E. Wörgötter, W. Braun, G. Wagner, M. Vašák, J. H. R. Kägi, K. Wüthrich, Three-dimensional structure of rabbit liver $[Cd_7]$metallothionein-2a in aqueous solution determined by nuclear magnetic resonance. *J. Mol. Biol.* **1988**, *201*, 637-657.

[61] I. Bertini, H.-J. Hartmann, T. Klein, G. Liu, C. Luchinat, U. Weser, High resolution solution structure of the protein part of Cu7 metallothionein. *Eur. J. Biochem.* **2000**, *267*, 1008-1018.

[62] W. Braun, M. Vašák, A. H. Robbins, C. D. Stout, G. Wagner, J. H. R. Kägi, K. Wüthrich, Comparison of NMR solution structure and the x-ray crystal structure of rat metallothionein-2. *Proc. Natl. Acad. Sci.* **1992**, *89*, 10124-10128.

[63] C. Capasso, V. Carginale, O. Crescenzi, D. Di Maro, E. Parisi, R. Spadaccini, P. A. Temussi, Solution structure of MT_nc, a novel metallothionein from the antarctic fish *Notothenia coriiceps*. *Structure* **2003**, *11*, 435-443.

[64] B. A. Messerle, A. Schäffer, M. Vašák, J. H. R. Kägi, K. Wüthrich, Three-dimensional structure of human [$^{113}Cd_7$]metallothionein-2 in solution determined by nuclear magnetic resonance spectroscopy. *J. Mol. Biol.* **1990**, *214*, 765-779.

[65] A. Muñoz, F. H. Försterling, C. F. Shaw, D. H. Petering, Structure of the $^{113}Cd_3\beta$ domains from *Homarus americanus* metallothionein-1: hydrogen bonding and solvent accessibility of sulfur atoms. *J. Biol. Inorg. Chem.* **2002**, *7*, 713-724.

[66] S. S. Narula, M. Brouwer, Three-dimensional solution structure of *Callinectes sapidus* metallothionein-1 determined by homonuclear and heteronuclear magnetic resonance spectroscopy. *Biochemistry* **1995**, *34*, 620-631.

[67] C. W. Peterson, S. S. Narula, I. M. Armitage, 3D solution structure of copper and silver-substituted yeast metallothioneins. *FEBS Lett.* **1996**, *379*, 85-93.

[68] R. Riek, B. Prêcheur, Y. Wang, E. A. Mackay, G. Wider, P. Güntert, A. Liu, J. H. R. Kägi, K. Wüthrich, NMR structure of the sea urchin (*Strongylocentrotus purpuratus*) metallothionein MTA. *J. Mol. Biol.* **1999**, *291*, 417-428.

[69] P. Schultze, E. Wörgötter, W. Braun, G. Wagner, M. Vašák, J. H. R. Kägi, K. Wüthrich, Conformation of [Cd_7]-metallothionein-2 from rat liver in aqueous solution determined by nuclear magnetic resonance spectroscopy. *J. Mol. Biol.* **1988**, *203*, 251-268.

[70] R. B. Turner, D. L. Smith, M. E. Zawrotny, M. F. Summers, M. C. Posewitz, D. R. Winge, Solution structure of a zinc domain conserved in yeast copper-regulated transcription factors. *Nat. Struct. Biol.* **1998**, *5*, 551-555.

[71] H. Wang, Q. Zhang, B. Cai, H. Li, K.-H. Sze, Z.-X. Huang, H.-M. Wu, H. Sun, Solution structure and dynamics of human metallothionein-3 (MT-3). *FEBS Lett.* **2006**, *580*, 795-800.

[72] K. Zangger, I. M. Armitage, Three-dimensional structure and dynamics of a brain specific growth inhibitory factor: metallothionein-3. *Biochemistry* **2001**, *40*, 11433-11441.

[73] K. Zangger, G. Öz, J. D. Otvos, I. M. Armitage, Three-dimensional solution structure of mouse [Cd_7]-metallothionein-1 by homonuclear and heteronuclear NMR spectroscopy. *Protein Sci.* **1999**, *8*, 2630-2638.

[74] A. H. Robbins, D. E. McRee, M. Williamson, S. A. Collett, N. H. Xuong, W. F. Furey, B. C. Wang, C. D. Stout, Refined crystal structure of Cd, Zn metallothionein at 2.0 Å resolution. *J. Mol. Biol.* **1991**, *221*, 1269-1293.

[75] V. Calderone, B. Dolderer, H.-J. Hartmann, H. Echner, C. Luchinat, C. Del Bianco, S. Mangani, U. Weser, The crystal structure of yeast copper thionein: the solution of a long-lasting enigma. *Proc. Natl. Acad. Sci.* **2005**, *102*, 51-56.

[76] Y. Zhan, X. Song, G. W. Zhou, Structural analysis of regulatory protein domains using GST-fusion proteins. *Gene* **2001**, *281*, 1-9.

[77] R. C. Stevens, Design of high-throughput methods of protein production for structural biology. *Structure* **2000**, *8*, R177-R185.

[78] C. K. Liew, R. Gamsjaeger, R. E. Mansfield, J. P. Mackay, NMR spectroscopy as a tool for the rapid assessment of the conformation of GST-fusion proteins. *Protein Sci.* **2008**, *17*, 1630-1635.

[79] J. Loebus, Structural and functional characterization of metallothioneins in plants and fungi. Dissertation, *Universität Zürich,* **2012**.
[80] G. Mir, J. Domènech, G. Huguet, W.-J. Guo, P. B. Goldsbrough, S. Atrian, M. Molinas, A plant type 2 metallothionein (MT) from cork tissue responds to oxidative stress. *J. Exp. Bot.* **2004**, *55*, 2483-2493.
[81] M. Capdevila, J. Domènech, A. Pagani, L. Tío, L. Villarreal, S. Atrian, Zn- and Cd-metallothionein recombinant species from the most diverse phyla may contain sulfide (S^{2-}) ligands. *Angew. Chem., Int. Ed.* **2005**, *44*, 4618-4622.
[82] J. Domènech, R. Orihuela, G. Mir, M. Molinas, S. Atrian, M. Capdevila, The Cd^{II}-binding abilities of recombinant *Quercus suber* metallothionein: bridging the gap between phytochelatins and metallothioneins. *J. Biol. Inorg. Chem.* **2007**, *12*, 867-882.
[83] L. Tío, L. Villarreal, S. Atrian, M. Capdevila, The Zn- and Cd-clusters of recombinant mammalian MT1 and MT4 metallothionein domains include sulfide ligands. *Exp. Biol. Med.* **2006**, *231*, 1522-1527.
[84] R. Orihuela, F. Monteiro, A. Pagani, M. Capdevila, S. Atrian, Evidence of native metal-S^{2-}-metallothionein complexes confirmed by the analysis of Cup1 divalent-metal-ion binding properties. *Chem. Eur. J.* **2010**, *16*, 12363-12372.
[85] R. N. Reese, D. R. Winge, Sulfide stabilization of the cadmium-γ-glutamyl peptide complex of *Schizosaccharomyces pombe*. *J. Biol. Chem.* **1988**, *263*, 12832-12835.
[86] R. N. Reese, R. K. Mehra, E. B. Tarbet, D. R. Winge, Studies on the γ-glutamyl Cu-binding peptide from *Schizosaccharomyces pombe*. *J. Biol. Chem.* **1988**, *263*, 4186-4192.
[87] J. H. R. Kägi, S. R. Himmelhoch, P. D. Whanger, J. L. Bethune, B. L. Vallee, Equine hepatic and renal metallothioneins. *J. Biol. Chem.* **1974**, *249*, 3537-3542.
[88] D. R. Winge, R. Premakumar, K. V. Rajagopalan, Metal-induced formation of metallothionein in rat liver. *Arch. Biochem. Biophys.* **1975**, *170*, 242-252.
[89] I. Bremner, J. H. Beattie, Metallothionein and the trace minerals. *Annu. Rev. Nutr.* **1990**, *10*, 63-83.
[90] S. G. Bell, B. L. Vallee, The metallothionein/thionein system: an oxidoreductive metabolic zinc link. *ChemBioChem* **2009**, *10*, 55-62.
[91] E. Freisinger, Plant MTs-long neglected members of the metallothionein superfamily. *Dalton Trans.* **2008**, *47*, 6663-6675.
[92] W.-J. Guo, M. Meetam, P. B. Goldsbrough, Examining the specific contributions of individual Arabidopsis metallothioneins to copper distribution and metal tolerance. *Plant Physiol.* **2008**, *146*, 1697-1706.
[93] C. Jacob, W. Maret, B. L. Vallee, Control of zinc transfer between thionein, metallothionein, and zinc proteins. *Proc. Natl. Acad. Sci.* **1998**, *95*, 3489-3494.
[94] W. Maret, Redox biochemistry of mammalian metallothioneins. *J. Biol. Inorg. Chem.* **2011**, *16*, 1079-1086.
[95] R. D. Palmiter, The elusive function of metallothioneins. *Proc. Natl. Acad. Sci.* **1998**, *95*, 8428-8430.
[96] J.-H. Kim, Y.-P. Nam, S.-M. Jeon, H.-S. Han, K. Suk, Amyloid neurotoxicity is attenuated by metallothionein: dual mechanisms at work. *J. Neurochem.* **2012**, *121*, 751-762.
[97] Y. Manso, J. Carrasco, G. Comes, P. Adlard, A. I. Bush, J. Hidalgo, Characterization of the role of the antioxidant proteins metallothioneins 1 and 2 in an animal model of Alzheimer's disease. *Cell. Mol. Life Sci.* **2012**, *69*, 3665-3681.
[98] F. Chimienti, Zinc, pancreatic islet cell function and diabetes: new insights into an old story. *Nutr. Res. Rev.* **2013**, 1-11.

[99] D. X. Deng, S. Chakrabarti, M. P. Waalkes, M. G. Cherian, Metallothionein and apoptosis in primary human hepatocellular carcinoma and metastatic adenocarcinoma. *Histopathology* **1998**, *32*, 340-347.
[100] Y. Kondo, J. M. Rusnak, D. G. Hoyt, C. E. Settineri, B. R. Pitt, J. S. Lazo, Enhanced apoptosis in metallothionein null cells. *Mol. Pharmacol.* **1997**, *52*, 195-201.
[101] S. D. Kumar, M. Vijaya, R. P. Samy, S. T. Dheen, M. Ren, F. Watt, Y. J. Kang, B.-H. Bay, S. S. W. Tay, Zinc supplementation prevents cardiomyocyte apoptosis and congenital heart defects in embryos of diabetic mice. *Free Radical Bio. Med.* **2012**, *53*, 1595-1606.
[102] P. Wang, A. Lutton, J. Olesik, H. Vali, X. Li, A novel iron- and copper-binding protein in the Lyme disease spirochaete. *Mol. Microbiol.* **2012**, *86*, 1441-1451.
[103] P. M. Roos, O. Vesterberg, M. Nordberg, Metals in motor neuron diseases. *Exp. Biol. Med.* **2006**, *231*, 1481-1487.
[104] P. J. Thornalley, M. Vašák, Possible role for metallothionein in protection against radiation-induced oxidative stress. Kinetics and mechanism of its reaction with superoxide and hydroxyl radicals. *BBA-Protein Struct. M.* **1985**, *827*, 36-44.
[105] A. W. Foster, N. J. Robinson, Promiscuity and preferences of metallothioneins: the cell rules. *BMC Biology* **2011**, *9*, 1-3.
[106] K. J. Waldron, J. C. Rutherford, D. Ford, N. J. Robinson, Metalloproteins and metal sensing. *Nature* **2009**, *460*, 823-830.
[107] R. B. Martin, Metal ion toxicity, in *Encyclopedia of inorganic and bioinorganic chemistry,* John Wiley & Sons, Ltd, **2011**.
[108] M. P. Richards, Recent developments in trace element metabolism and function: role of metallothionein in copper and zinc metabolism. *J. Nutr.* **1989**, *119*, 1062-1070.
[109] J. C. Amiard, C. Amiard-Triquet, S. Barka, J. Pellerin, P. S. Rainbow, Metallothioneins in aquatic invertebrates: their role in metal detoxification and their use as biomarkers. *Aquat. Toxicol.* **2006**, *76*, 160-202.
[110] D. E. Barañano, C. D. Ferris, S. H. Snyder, Atypical neural messengers. *Trends Neurosci.* **2001**, *24*, 99-106.
[111] T. C. Bartholomew, G. M. Powell, K. S. Dodgson, C. G. Curtis, Oxidation of sodium sulphide by rat liver, lungs and kidney. *Biochem. Pharmacol.* **1980**, *29*, 2431-2437.
[112] S. Cassanelli, J.-M. Moulis, Sulfide is an efficient iron releasing agent for mammalian ferritins. *BBA-Protein Struct. M.* **2001**, *1547*, 174-182.
[113] T. R. Chauncey, J. Westley, Improved purification and sulfhydryl analysis of thiosulfate reductase. *Biochim. Biophys. Acta* **1983**, *744*, 304-311.
[114] R. Hosoki, N. Matsuki, H. Kimura, The possible role of hydrogen sulfide as an endogenous smooth muscle relaxant in synergy with nitric oxide. *Biochem. Biophys. Res. Commun.* **1997**, *237*, 527-531.
[115] W. Maret, Zinc and sulfur: a critical biological partnership. *Biochemistry* **2004**, *43*, 3301-3309.
[116] W. H. Orme-Johnson, Iron-sulfur proteins: structure and function. *Annu. Rev. Biochem.* **1973**, *42*, 159-204.
[117] W. Zhao, J. Zhang, Y. Lu, R. Wang, The vasorelaxant effect of H_2S as a novel endogenous gaseous K_{ATP} channel opener. *EMBO J.* **2001**, *20*, 6008-6016.
[118] H. Beinert, A tribute to sulfur. *Eur. J. Biochem.* **2000**, *267*, 5657-5664.
[119] D. C. Johnson, D. R. Dean, A. D. Smith, M. K. Johnson, Structure, function, and formation of biological iron-sulfur clusters. *Annu. Rev. Biochem.* **2005**, *74*, 247-281.
[120] E. Grill, E.-L. Winnacker, M. H. Zenk, Phytochelatins: the principal heavy-metal complexing peptides of higher plants. *Science* **1985**, *230*, 674-676.

[121] Y. Hayashi, C. W. Nakagawa, A. Murasugi, Unique properties of Cd-binding peptides induced in fission yeast, *Schizosaccharomyces pombe*. *Environ. Health Perspect.* **1986**, *65*, 13-19.
[122] J. C. Steffens, D. F. Hunt, B. G. Williams, Accumulation of non-protein metal-binding polypeptides (γ-glutamyl-cysteinyl)$_n$-glycine in selected cadmium-resistant tomato cells. *J. Biol. Chem.* **1986**, *261*, 13879-13882.
[123] W. E. Rauser, Phytochelatins. *Annu. Rev. Biochem.* **1990**, *59*, 61-86.
[124] N. J. Robinson, A. M. Tommey, C. Kuske, P. J. Jackson, Plant metallothioneins. *Biochem. J.* **1993**, *295*, 1-10.
[125] J. C. Steffens, The heavy metal-binding peptides of plants. *Annu. Rev. Plant Phys.* **1990**, *41*, 553-575.
[126] O. K. Vatamaniuk, S. Mari, Y.-P. Lu, P. A. Rea, Mechanism of heavy metal ion activation of phytochelatin (PC) synthase. *J. Biol. Chem.* **2000**, *275*, 31451-31459.
[127] D. G. Mendoza-Cózatl, R. Moreno-Sánchez, Control of glutathione and phytochelatin synthesis under cadmium stress. Pathway modeling for plants. *J. Theor. Biol.* **2006**, *238*, 919-936.
[128] S.-B. Ha, A. P. Smith, R. Howden, W. M. Dietrich, S. Bugg, M. J. O'Connell, P. B. Goldsbrough, C. S. Cobbett, Phytochelatin synthase genes from Arabidopsis and the yeast *Schizosaccharomyces pombe*. *Plant Cell* **1999**, *11*, 1153-1164.
[129] P. Tennstedt, D. Peisker, C. Böttcher, A. Trampczynska, S. Clemens, Phytochelatin synthesis is essential for the detoxification of excess zinc and contributes significantly to the accumulation of zinc. *Plant Physiol.* **2009**, *149*, 938-948.
[130] R. N. Reese, C. A. White, D. R. Winge, Cadmium-sulfide crystallites in Cd-(γEC)$_n$G peptide complexes from tomato. *Plant Physiol.* **1992**, *98*, 225-229.
[131] T. R. Butt, E. J. Sternberg, J. A. Gorman, P. Clark, D. H. Hamer, M. Rosenberg, S. T. Crooke, Copper metallothionein of yeast, structure of the gene, and regulation of expression. *Proc. Natl. Acad. Sci.* **1984**, *81*, 3332-3336.
[132] V. C. Culotta, W. R. Howard, X. F. Liu, *CRS5* encodes a metallothionein-like protein in *Saccharomyces cerevisiae*. *J. Biol. Chem.* **1994**, *269*, 25295-25302.
[133] J. Domènech, G. Mir, G. Huguet, M. Capdevila, M. Molinas, S. Atrian, Plant metallothionein domains: functional insight into physiological metal binding and protein folding. *Biochimie* **2006**, *88*, 583-593.
[134] F. J. Muñoz, R. V. Ullán, E. Labrador, B. Dopico, Increased expression of two cDNAs encoding metallothionein-like proteins during growth of *Cicer arietinum* epicotyls. *Physiol. Plant.* **1998**, *104*, 273-279.
[135] X. Wan, E. Freisinger, The plant metallothionein 2 from *Cicer arietinum* forms a single metal-thiolate cluster. *Metallomics* **2009**, *1*, 489-500.
[136] X. Wan, E. Freisinger, Incorporation of sulfide ions into the cadmium(II) thiolate cluster of *Cicer arietinum* metallothionein 2. *Inorg. Chem.* **2013**, *52*, 785-792.
[137] L. Zheng, R. H. White, V. L. Cash, R. F. Jack, D. R. Dean, Cysteine desulfurase activity indicates a role for NIFS in metallocluster biosynthesis. *Proc. Natl. Acad. Sci.* **1993**, *90*, 2754-2758.
[138] O. Schicht, E. Freisinger, Spectroscopic characterization of *Cicer arietinum* metallothionein 1. *Inorg. Chim. Acta* **2009**, *362*, 714-724.
[139] E. A. Peroza, E. Freisinger, Tris is a non-innocent buffer during intein-mediated protein cleavage. *Protein Expression Purif.* **2008**, *57*, 217-225.
[140] E. Freisinger, Spectroscopic characterization of a fruit-specific metallothionein: *M. acuminata* MT3. *Inorg. Chim. Acta* **2007**, *360*, 369-380.

[141] M. Knipp, A. V. Karotki, S. Chesnov, G. Natile, P. J. Sadler, V. Brabec, M. Vašák, Reaction of Zn_7-metallothionein with *cis*- and *trans*- [Pt(N-donor)$_2$Cl$_2$] anticancer complexes: *trans*-Pt^{II} complexes retain their N-donor ligands. *J. Med. Chem.* **2007**, *50*, 4075-4086.
[142] D. Hanahan, Studies on transformation of *Escherichia coli* with plasmids. *J. Mol. Biol.* **1983**, *166*, 557-580.
[143] M. E. Woodman, Direct PCR of intact bacteria (colony PCR), in *Curr. Protoc. Microbiol.*, Vol. 9A.3D., John Wiley & Sons, Inc., **2008**, pp. 1-6.
[144] Leland Stanford Junior University, Saccharomyces genome database, http://www.yeastgenome.com/.
[145] C. W. MacDiarmid, L. A. Gaither, D. J. Eide, Zinc transporters that regulate vacuolar zinc storage in *Saccharomyces cerevisiae*. *EMBO J.* **2000**, *19*, 2845-2855.
[146] D. H. Hamer, D. J. Thiele, J. E. Lemontt, Function and autoregulation of yeast copperthionein. *Science* **1985**, *228*, 685-690.
[147] J. M. Cherry, C. Adler, C. Ball, S. A. Chervitz, S. S. Dwight, E. T. Hester, Y. Jia, G. Juvik, T. Roe, M. Schroeder, S. Weng, D. Botstein, SGD: Saccharomyces Genome Database. *Nucleic Acids Res.* **1998**, *26*, 73-79.
[148] C. S. Hoffman, F. Winston, A ten-minute DNA preparation from yeast efficiently releases autonomous plasmids for transformation of *Escherichia coli*. *Gene* **1987**, *57*, 267-272.
[149] C. B. Brachmann, A. Davies, G. J. Cost, E. Caputo, J. Li, P. Hieter, J. D. Boeke, Designer deletion strains derived from *Saccharomyces cerevisiae* S288C: a useful set of strains and plasmids for PCR-mediated gene disruption and other applications. *Yeast* **1998**, *14*, 115-132.
[150] C. Janke, M. M. Magiera, N. Rathfelder, C. Taxis, S. Reber, H. Maekawa, A. Moreno-Borchart, G. Doenges, E. Schwob, E. Schiebel, M. Knop, A versatile toolbox for PCR-based tagging of yeast genes: new fluorescent proteins, more markers and promoter substitution cassettes. *Yeast* **2004**, *21*, 947-962.
[151] M. J. Lafuente, C. Gancedo, Disruption and basic functional analysis of six novel ORFs of chromosome XV from *Saccharomyces cerevisiae*. *Yeast* **1999**, *15*, 935-943.
[152] R. D. Gietz, R. H. Schiestl, High-efficiency yeast transformation using the LiAc/SS carrier DNA/PEG method. *Nat. Protoc.* **2007**, *2*, 31-34.
[153] D. M. Becker, V. Lundblad, Introduction of DNA into yeast cells, in *Curr. Protoc. Mol. Biol.*, Vol. 13.7., John Wiley & Sons, Inc., **1993**, pp. 1-10.
[154] T. Stearns, H. Ma, D. Botstein, Manipulating yeast genome using plasmid vectors. *Methods Enzymol.* **1990**, *185*, 280-297.
[155] GE Healthcare, *GST gene fusion system*, Vol. 18-1157-58, GE Healthcare Bio-Sciences Corporation, Uppsala, Sweden, **2002**.
[156] J. E. Tropea, S. Cherry, D. S. Waugh, Expression and purification of soluble His_6-tagged TEV protease. *Methods Mol. Biol.* **2009**, *498*, 297-307.
[157] K. Türk, A. Puhar, F. Neese, E. Bill, G. Fritz, J. Steuber, NADH oxidation by the Na^+-translocating NADH:quinone oxidoreductase from *Vibrio cholerae*. *J. Biol. Chem.* **2004**, *279*, 21349 -21355.
[158] P. T. Wingfield, Preparation of soluble proteins from *Escherichia coli,* in *Curr. Protoc. Protein Sci.*, Vol. 6.2., John Wiley & Sons, Inc., **2005**, pp. 1-22.
[159] P. T. Wingfield, Protein precipitation using ammonium sulfate, in *Curr. Protoc. Protein Sci.*, Vol. A.3F., John Wiley & Sons, Inc., **1998**, pp. 1-8.
[160] M. Vašák, E. Wörgötter, G. Wagner, J. H. R. Kägi, K. Wüthrich, Metal co-ordination in rat liver metallothionein-2 prepared with or without reconstitution of the metal clusters, and comparison with rabbit liver metallothionein-2. *J. Mol. Biol.* **1987**, *196*, 711-719.

[161] C. O. Dietrich-Buchecker, C. Hemmert, A. K. Khemiss, J. P. Sauvage, Synthesis of dicopper [3]-catenates and [3]-catenands by acetylenic oxidative coupling. Preparation and study of corresponding homodimetallic [3]-catenates [Ag^{+}, Zn^{2+}, Co^{2+}, and Ni^{2+}]. *J. Am. Chem. Soc.* **1990**, *112*, 8002-8008.

[162] C. Simm, B. Lahner, D. E. Salt, A. LeFurgey, P. Ingram, B. Yandell, D. J. Eide, *Saccharomyces cerevisiae* vacuole in zinc storage and intracellular zinc distribution. *Eukaryot. Cell* **2007**, *6*, 1166-1177.

[163] A. O. Pedersen, J. Jacobsen, Reactivity of the thiol group in human and bovine albumin at pH 3-9, as measured by exchange with 2,2'-dithiodipyridine. *Eur. J. Biochem.* **1980**, *106*, 291 -295.

[164] S. Damodaran, Estimation of disulfide bonds using 2-nitro-5-thiosulfobenzoic acid: limitations. *Anal. Biochem.* **1985**, *145*, 200-204.

[165] T. W. Thannhauser, Y. Konishi, H. A. Scheraga, Sensitive quantitative analysis of disulfide bonds in polypeptides and proteins. *Anal. Biochem.* **1984**, *138*, 181-188.

[166] L. M. Siegel, A direct microdetermination for sulfide. *Anal. Biochem.* **1965**, *11*, 126-132.

[167] A. I. Vogel, Sulphides, S^{2-}, in *Vogel's textbook of macro and semimicro qualitative inorganic analysis,* 5th ed., Longman, London and New York, **1979**, pp. 308-310.

[168] G. Meloni, P. Faller, M. Vašák, Redox silencing of copper in metal-linked neurodegenerative disorders. *J. Biol. Chem.* **2007**, *282*, 16068-16078.

[169] H. Willner, M. Vašák, J. H. R. Kägi, Cadmium-thiolate clusters in metallothionein: spectrophotometric and spectropolarimetric features. *Biochemistry* **1987**, *26*, 6287-6292.

[170] H. Schägger, G. von Jagow, Tricine-sodium dodecyl sulfate-polyacrylamide gel electrophoresis for the separation of proteins in the range from 1 to 100 kDa. *Anal. Biochem.* **1987**, *166*, 368-379.

[171] H. Schägger, H. Aquila, G. Von Jagow, Coomassie blue-sodium dodecyl sulfate-polyacrylamide gel electrophoresis for direct visualization of polypeptides during electrophoresis. *Anal. Biochem.* **1988**, *173*, 201-205.

[172] W. Wray, T. Boulikas, V. P. Wray, R. Hancock, Silver staining of proteins in polyacrylamide gels. *Anal. Biochem.* **1981**, *118*, 197-203.

[173] S. Johannsen, S. Paulus, N. Düpre, J. Müller, R. K. O. Sigel, Using *in vitro* transcription to construct scaffolds for one-dimensional arrays of mercuric ions. *J. Inorg. Biochem.* **2008**, *102*, 1141-1151.

[174] H. Akashi, T. Gojobori, Metabolic efficiency and amino acid composition in the proteomes of *Escherichia coli* and *Bacillus subtilis*. *Proc. Natl. Acad. Sci.* **2002**, *99*, 3695-3700.

[175] X. Wan, Characterization of the plant metallothionein 2 from *Cicer arietinum* (chickpea). Dissertation, *Universität Zürich,* **2009**.

[176] J. Cavanagh, W. J. Fairbrother, A. G. Palmer III, M. Rance, N. J. Skelton, *Protein NMR spectroscopy - Principles and practice,* 2nd ed., Elsevier Academic Press, Burlington, MA, USA, **2007**.

[177] F. Lottespeich, J. W. Engels, *Bioanalytik,* 2nd ed., Spektrum Akademischer Verlag, Elsevier GmbH, München, **2006**.

[178] M. P. Williamson, Secondary-structure dependent chemical shifts in proteins. *Biopolymers* **1990**, *29*, 1423-1431.

[179] M. P. Williamson, T. Asakura, Protein chemical shifts, in *Protein NMR techniques*, Vol. 60, Eds. D. G. Reid, Humana Press, Totowa, NJ, **1997**, pp. 53-69.

[180] D. S. Wishart, B. D. Sykes, F. M. Richards, Relationship between nuclear magnetic resonance chemical shift and protein secondary structure. *J. Mol. Biol.* **1991**, *222*, 311-333.

[181] C. M. Dobson, Protein folding and misfolding. *Nature* **2003**, *426*, 884-890.

[182] K. Tamiola, F. A. A. Mulder, Using NMR chemical shifts to calculate the propensity for structural order and disorder in proteins. *Biochem. Soc. T.* **2012**, *40*, 1014-1020.
[183] E. Freisinger, Structural features specific to plant metallothioneins. *J. Biol. Inorg. Chem.* **2011**, *16*, 1035-1045.
[184] K. Hayashi, C. Kojima, Efficient protein production method for NMR using soluble protein tags with cold shock expression vector. *J. Biomol. NMR* **2010**, *48*, 147-155.
[185] D. Eliezer, Characterizing residual structure in disordered protein states using nuclear magnetic resonance. *Methods Mol. Biol.* **2007**, *350*, 49-67.
[186] A. B. Sigalov, A. V. Zhuravleva, V. Y. Orekhov, Binding of intrinsically disordered proteins is not necessarily accompanied by a structural transition to a folded form. *Biochimie* **2007**, *89*, 419-421.
[187] M. R. Jensen, P. R. L. Markwick, S. Meier, C. Griesinger, M. Zweckstetter, S. Grzesiek, P. Bernadó, M. Blackledge, Quantitative determination of the conformational properties of partially folded and intrinsically disordered proteins using NMR dipolar couplings. *Structure* **2009**, *17*, 1169-1185.
[188] W. Bermel, I. Bertini, J. Chill, I. C. Felli, N. Haba, V. Kumar M V, R. Pierattelli, Exclusively heteronuclear ^{13}C-detected amino-acid-selective NMR experiments for the study of intrinsically disordered proteins (IDPs). *ChemBioChem* **2012**, *13*, 2425-2432.
[189] M. Ota, R. Koike, T. Amemiya, T. Tenno, P. R. Romero, H. Hiroaki, A. K. Dunker, S. Fukuchi, An assignment of intrinsically disordered regions of proteins based on NMR structures. *J. Struct. Biol.* **2012**, *181*, 29-36.
[190] L. Salomon, M. R. Jensen, P. Bernardó, M. Blackledge, Measurement and analysis of NMR residual dipolar couplings for the study of intrinsically disordered proteins. *Methods Mol. Biol.* **2012**, *895*, 115-125.
[191] I. G. Dance, A. Choy, M. L. Scudder, Syntheses, properties, and molecular and crystal structures of $(Me_4N)_4[E_4M_{10}(SPh)_{16}]$ (E = S, Se; M = Zn, Cd): molecular supertetrahedral fragments of the cubic metal chalcogenide lattice. *J. Am. Chem. Soc.* **1984**, *106*, 6285-6295.
[192] V. S. Gurin, Electronic structure of CdS cores in Cd thiolate complexes and clusters. *J. Phys. Chem.* **1996**, *100*, 869-872.
[193] V. S. Gurin, *Ab-initio* calculations of small Cd_xS_y and Zn_xS_y (x,y ≤ 6) clusters. *Solid State Comm.* **1998**, *108*, 389-392.
[194] T. Türk, U. Resch, M. A. Fox, A. Vogler, Cadmium benzenethiolate clusters of various size: molecular models for metal chalcogenide semiconductors. *J. Phys. Chem.* **1992**, *96*, 3818-3822.
[195] E. Freisinger, M. Vašák, Cadmium in metallothioneins, in *Met. Ions Life Sci.*, Vol. 11, Eds. A. Sigel, H. Sigel, R. K. O. Sigel, Springer Science + Business Media, Dordrecht, Netherlands, **2013**, pp. 339-371.
[196] S. Pérez-Rafael, A. Kurz, M. Guirola, M. Capdevila, Ò. Palacios, S. Atrian, Is MtnE, the fifth *Drosophila* metallothionein, functionally distinct from the other members of this polymorphic protein family?, *Metallomics* **2012**, *4*, 342-349.
[197] D. J. Plocke, J. H. R. Kägi, Spectral characteristics of cadmium-containing phytochelatin complexes isolated from *Schizosaccharomyces pombe*. *Eur. J. Biochem.* **1992**, *207*, 201-205.
[198] E. Gout, R. Bligny, R. Douce, Regulation of intracellular pH values in higher plant cells. *J. Biol. Chem.* **1992**, *267*, 13903-13909.
[199] T. Huber, E. Freisinger, Sulfide ions as modulators of metal-thiolate cluster size in a plant metallothionein. *Dalton Trans.* **2013**, *42*, 8878-8889.
[200] W. Bae, R. K. Mehra, Cysteine-capped ZnS nanocrystallites: Preparation and characterization. *J. Inorg. Biochem.* **1998**, *70*, 125-135.

[201] A. Torreggiani, J. Domènech, S. Atrian, M. Capdevila, A. Tinti, Raman study of *in vivo* synthesized Zn(II)-metallothionein complexes: structural insight into metal clusters and protein folding. *Biopolymers* **2008**, *89*, 1114-1124.

[202] M. Valls, R. Bofill, N. Romero-Isart, R. González-Duarte, J. Abián, M. Carrascal, P. González-Duarte, M. Capdevila, S. Atrian, *Drosophila* MTN: a metazoan copper-thionein related to fungal forms. *FEBS Lett.* **2000**, *467*, 189-194.

[203] N. Cols, N. Romero-Isart, M. Capdevila, B. Oliva, P. González-Duarte, R. González-Duarte, S. Atrian, Binding of excess cadmium(II) to Cd_7-metallothionein from recombinant mouse Zn_7-metallothionein 1. UV-VIS absorption and circular dichroism studies and theoretical location approach by surface accessibility analysis. *J. Inorg. Biochem.* **1997**, *68*, 1571-1566.

[204] M. Valls, R. Bofill, R. González-Duarte, P. González-Duarte, M. Capdevila, S. Atrian, A new insight into metallothionein (MT) classification and evolution. *J. Biol. Chem.* **2001**, *276*, 32835-32843.

[205] S. S. Narula, R. K. Mehra, D. R. Winge, I. M. Armitage, Establishment of the metal-to-cysteine connectivities in silver-substituted yeast metallothionein. *J. Am. Chem. Soc.* **1991**, *113*, 9354-9358.

[206] G. N. George, D. R. Winge, C. D. Stout, S. P. Cramer, X-ray absorption studies of the copper-beta domain of rat liver metallothionein. *J. Inorg. Biochem.* **1986**, *27*, 213-220.

[207] T. A. Smith, K. Lerch, K. O. Hodgson, Structural study of the Cu sites in metallothionein from *Neurospora crassa*. *Inorg. Chem.* **1986**, *25*, 4677-4680.

[208] J. Bordas, M. H. J. Koch, H.-J. Hartmann, U. Weser, Tetrahedral copper-sulphur coordination in yeast Cu-thionein. An EXAFS study. *FEBS Lett.* **1982**, *140*, 19-21.

[209] U. Weser, H.-J. Hartmann, A. Fretzdorff, G.-J. Strobel, Homologous copper(I)-$(thiolate)_2$-chromophores in yeast copper thionein. *Biochim. Biophys. Acta* **1977**, *493*, 465-477.

[210] D. R. Winge, K. B. Nielson, Formation of the metal-thiolate clusters of rat liver metallothionein. *Environ. Health Perspect.* **1984**, *54*, 129-133.

[211] A. Murasugi, C. Wada, Y. Hayashi, Purification and unique properties in UV and CD spectra of Cd-binding peptide 1 from *Schizosaccharomyces pombe*. *Biochem. Biophys. Res. Commun.* **1981**, *103*, 1021-1028.

[212] A. Murasugi, C. Wada, Y. Hayashi, Cadmium-binding peptide induced in fission yeast, *Schizosaccharomyces pombe*. *J. Biochem.* **1981**, *90*, 1561-1564.

[213] A. Murasugi, C. Wada, Y. Hayashi, Occurrence of acid-labile sulfide in cadmium-binding peptide 1 from fission yeast. *J. Biochem.* **1983**, *93*, 661-664.

[214] A. Murasugi, C. Wada Nakagawa, Y. Hayashi, Formation of cadmium-binding peptide allomorphs in fission yeast. *J. Biochem.* **1984**, *96*, 1375-1379.

[215] M. Bruchez Jr., M. Moronne, P. Gin, S. Weiss, A. P. Alivisatos, Semiconductor nanocrystals as fluorescent biological labels. *Science* **1998**, *281*, 2013-2016.

[216] A. P. Alivisatos, Perspectives on the physical chemistry of semiconductor nanocrystals. *J. Phys. Chem.* **1996**, *100*, 13226-13239.

[217] H. Zeng, R. R. Vanga, D. S. Marynick, Z. A. Schelly, Cluster precursors of uncapped CdS quantum dots via electroporation of synthetic liposomes. Experiments and theory. *J. Phys. Chem. B* **2008**, *112*, 14422-14426.

[218] L. J. Libertini, E. W. Small, The intrinsic tyrosine fluorescence of histone H1. Steady state and fluorescence decay studies reveal heterogeneous emission. *Biophys. J.* **1985**, *47*, 765-772.

[219] J. Beynon, A. Ally, M. Cannon, F. Cannon, M. R. Jacobson, V. L. Cash, D. R. Dean, Comparative organization of nitrogen fixation-specific genes from *Azotobacter vinelandii* and *Klebsiella pneumoniae*: DNA sequence of the *nifUSV* genes. *J. Bacteriol.* **1987**, *169*, 4024-4029.

[220] M. R. Jacobson, K. E. Brigle, L. T. Bennett, R. A. Setterquist, M. S. Wilson, V. L. Cash, J. Beynon, W. E. Newton, D. R. Dean, Physical and genetic map of the major *nif* gene cluster from *Azotobacter vinelandii*. *J. Bacteriol.* **1989**, *171*, 1017-1027.

[221] L. Zheng, D. R. Dean, Catalytic formation of a nitrogenase iron-sulfur cluster. *J. Biol. Chem.* **1994**, *269*, 18723-18726.

[222] L. Zheng, R. H. White, V. L. Cash, D. R. Dean, Mechanism for the desulfurization of L-cysteine catalyzed by the *nifS* gene product. *Biochemistry* **1994**, *33*, 4714-4720.

[223] G. W. I. Luther, S. M. Theberge, D. T. Rickard, Evidence for aqueous clusters as intermediates during zinc sulfide formation. *Geochim. Cosmochim. Ac.* **1999**, *63*, 3159-3169.

[224] M. H. Frey, G. Wagner, M. Vašák, O. W. Sørensen, D. Neuhaus, E. Wörgötter, J. H. R. Kägi, R. R. Ernst, K. Wüthrich, Polypeptide-metal cluster connectivities in metallothionein 2 by novel ^{1}H-^{113}Cd heteronuclear two-dimensional NMR experiments. *J. Am. Chem. Soc.* **1985**, *107*, 6847-6851.

[225] M. Vašák, G. E. Hawkes, J. K. Nicholson, P. J. Sadler, ^{113}Cd NMR studies of reconstituted seven-cadmium metallothionein: evidence for structural flexibility. *Biochemistry* **1985**, *24*, 740-747.

[226] J. H. R. Kägi, *Metallothionein III: Biological roles and medical implications*, Eds. K. Y. Suzuki, N. Imura, M. Kimura, Birkhäuser Verlag, Basel, Switzerland, **1993**.

[227] M. Vašák, *personal communication*.

[228] D. T. Jiang, S. M. Heald, T. K. Sham, M. J. Stillman, Structures of the cadmium, mercury, and zinc thiolate clusters in metallothionein: XAFS study of Zn_7-MT, Cd_7-MT, Hg_7-MT, and Hg_{18}-MT formed from rabbit liver metallothionein 2. *J. Am. Chem. Soc.* **1994**, *116*, 11004-11013.

[229] D. A. Treco, F. Winston, Growth and manipulation of yeast, in *Curr. Protoc. Mol. Biol.*, Vol. 13.2., John Wiley & Sons, Inc., **2008**, pp. 1-12.

[230] S. Fogel, J. W. Welch, Tandem gene amplification mediates copper resistance in yeast. *Proc. Natl. Acad. Sci.* **1982**, *79*, 5342-5346.

[231] J. W. Welch, S. Fogel, G. Cathala, M. Karin, Industrial yeasts display tandem gene iteration at the *CUP1* region. *Mol. Cell. Biol.* **1983**, *3*, 1353-1361.

[232] G. M. Adamo, M. Lotti, M. J. Tamás, S. Brocca, Amplification of the *CUP1* gene is associated with evolution of copper tolerance in *Saccharomyces cerevisiae*. *Microbiology* **2012**, *158*, 2325-2335.

[233] T. Hirasawa, Y. Nakakura, K. Yoshikawa, K. Ashitani, K. Nagahisa, C. Furusawa, Y. Katakura, H. Shimizu, S. Shioya, Comparative analysis of transcriptional responses to saline stress in the laboratory and brewing strains of *Saccharomyces cerevisiae* with DNA microarray. *App. Microbiol. Biotechnol.* **2006**, *70*, 346-357.

[234] H. Zhang, A. F. B. Zeidler, W. Song, C. M. Puccia, E. Malc, P. W. Greenwell, P. A. Mieczkowski, T. D. Petes, J. L. Argueso, Gene copy number variation (CNV) in haploid and diploid strains of the yeast *Saccharomyces cerevisiae*. *Genetics* **2013**, *ahead of print*.

[235] R. Mortensen, Overview of gene targeting by homologous recombination, in *Curr. Protoc. Mol. Biol.*, Vol. 23.1., John Wiley & Sons, Inc., **2006**, pp. 1-12.

[236] V. D. Longo, E. Butler Gralla, J. S. Valentine, Superoxide dismutase activity is essential for stationary phase survival in *Saccharomyces cerevisiae*. *J. Biol. Chem.* **1996**, *271*, 12275-12280.

[237] K. T. Tamai, E. B. Gralla, L. M. Ellerby, J. S. Valentine, D. J. Thiele, Yeast and mammalian metallothioneins functionally substitute for yeast copper-zinc superoxide dismutase. *Proc. Natl. Acad. Sci.* **1993**, *90*, 8013-8017.

[238] C. S. Hoffman, Preparation of yeast DNA, in *Curr. Protoc. Mol. Biol.*, Vol. 13.11., John Wiley & Sons, Inc., **1997**, pp. 1-4.

[239] S. Smolik-Utlaut, T. D. Petes, Recombination of plasmids into the *Saccharomyces cerevisiae* chromosome is reduced by small amounts of sequence heterogeneity. *Mol. Cell. Biol.* **1983**, *3*, 1204-1211.
[240] C. Deng, M. R. Capecchi, Reexamination of gene targeting frequency as a function of the extent of homology between the targeting vector and the target locus. *Mol. Cell. Biol.* **1992**, *12*, 3365-3371.
[241] H. te Riele, E. R. Maandag, A. Berns, Highly efficient gene targeting in embryonic stem cells through homologous recombination with isogenic DNA constructs. *Proc. Natl. Acad. Sci.* **1992**, *89*, 5128-5132.
[242] J. W. Szostak, R. Wu, Insertion of a genetic marker into the ribosomal DNA of yeast. *Plasmid* **1979**, *2*, 536-554.
[243] R. Mortensen, Production of a heterozygous mutant cell line by homologous recombination (single knockout), in *Curr. Protoc. Mol. Biol.*, Vol. 23.5., John Wiley & Sons, Inc., **2008**, pp. 1-11.
[244] G. Richter, *Praktische Biochemie: Grundlagen und Techniken,* 1st ed., Georg Thieme Verlag, Stuttgart, Germany, **2003**.
[245] R. S. Sikorski, P. Hieter, A system of shuttle vectors and yeast host strains designed for efficient manipulation of DNA in *Saccharomyces cerevisiae*. *Genetics* **1989**, *122*, 19-27.
[246] A. Gallego, A. Martín-González, R. Ortega, J. C. Gutiérrez, Flow cytometry assessment of cytotoxicity and reactive oxygen species generation by single and binary mixtures of cadmium, zinc and copper on populations of the ciliated protozoan *Tetrahymena thermophila*. *Chemosphere* **2007**, *68*, 647-661.
[247] D. Lloyd, Flow cytometry of yeasts, in *Curr. Protoc. Cytom.*, Vol. 11.10., John Wiley & Sons, Inc., **1999**, pp. 1-8.
[248] M. Malavolta, L. Costarelli, R. Giacconi, E. Muti, G. Bernardini, S. Tesei, C. Cipriano, E. Mocchegiani, Single and three-color flow cytometry assay for intracellular zinc ion availability in human lymphocytes with Zinpyr-1 and double immunofluorescence: Relationship with metallothioneins. *Cytom. Part A* **2006**, *69A*, 1043-1053.
[249] M. Dabrio, A. R. Rodríguez, G. Bordin, M. J. Bebianno, M. De Ley, I. Sestáková, M. Vašák, M. Nordberg, Recent developments in quantification methods for metallothionein. *J. Inorg. Biochem.* **2002**, *88*, 123-134.
[250] P. Tompa, The interplay between structure and function in intrinsically unstructured proteins. *FEBS Lett.* **2005**, *579*, 3346-3354.
[251] G.-Y. Huang, Y.-S. Wang, Expression and characterization analysis of type 2 metallothionein from grey mangrove species (*Avicennia marina*) in response to metal stress. *Aquat. Toxicol.* **2010**, *99*, 86-92.
[252] O. Schicht, Structural and spectroscopical investigation of metallothionein 1 from *Cicer arietinum*. Dissertation, *Universität Zürich,* **2008**.
[253] A. M. Tommey, J. Shi, W. P. Lindsay, P. E. Urwin, N. J. Robinson, Expression of the pea genePsMTA in *E. coli* - Metal-binding properties of the expressed protein. *FEBS Lett.* **1991**, *292*, 48-52.
[254] R. Bofill, M. Capdevila, N. Cols, S. Atrian, P. González-Duarte, Zinc(II) is required for the *in vivo* and *in vitro* folding of mouse copper metallothionein in two domains. *J. Biol. Inorg. Chem.* **2001**, *6*, 405-417.
[255] J. Domènech, Ò. Palacios, L. Villarreal, P. González-Duarte, M. Capdevila, S. Atrian, MTO: the second member of a *Drosophila* dual copper-thionein system. *FEBS Lett.* **2003**, *533*, 72-78.

[256] L. Tío, L. Villarreal, S. Atrian, M. Capdevila, Functional differentiation in the mammalian metallothionein gene family: metal binding features of mouse MT4 and comparison with its paralog MT1. *J. Biol. Chem.* **2004**, *279*, 24403-24413.

11. Curriculum Vitae

Personal data

Name	Tamara Huber
Date and Place of Birth	23th September 1981 in Luzern (Switzerland)
Nationality	Swiss
Marital status	unmarried

Education

02/2009 – 03/2013	University of Zurich, Zürich Ph.D. studies in bio-inorganic chemistry, finished with a Ph.D. UZH in Inorganic Chemistry.
02/2008 – 03/2009	University of Zurich, Zürich Master studies in biochemistry, finished with a M.Sc. UZH in Biochemistry Chemistry/Biophysics Track.
10/2007 – 08/2008	University of Zurich, Zürich Bachelor studies in biochemistry, finished with a B.Sc. UZH in Biochemistry Chemistry/Biophysics Track.
10/2004 – 08/2007	University of Zurich, Zürich Basic studies in chemistry.
10/2002 – 01/2004	ETH Zurich, Zürich Three semesters of studies in architecture.
08/1994 – 05/2002	Kantonsschule Reussbühl, Luzern High school, finished with maturity type B.
08/1988 – 07/1994	Primary school Reussbühl, Luzern

Publications

"Sulfide ions as modulators of metal-thiolate cluster size in a plant metallothionein"
T. Huber, E. Freisinger, Dalton Transactions 42 (2013) 8878-8889.

"Localization and function of the membrane-bound riboflavin in the Na^+-translocating NADH:Quinone oxidoreductase (Na^+-NQR) from *Vibrio cholerae*"
M. S. Casutt, T. Huber, R. Brunisholz, M. Tao, G. Fritz, J. Steuber, Journal of Biological Chemistry 285 (2010) 27088-270099.

Conference contributions

Oral presentations

13/09/2012	"Investigations on the metal-sulfide-thiolate cluster of metallothioneins" Fall Meeting of the Swiss Chemical Society, Zurich, Switzerland
18-22/06/2012	"Mechanism of sulfide ion incorporation into the metal cluster of metallothioneins" International Symposium on Metal Complexes (ISMEC) 2012, Lisbon, Portugal
8-12/02/2012	"Sulfide incorporation into plant MT2" 4th Graduate School Retreat CMSZH, Zuoz, Switzerland

Poster presentations

13-27/01/2013	5th Graduate School Retreat CMSZH, Charmey, Switzerland
10/10/2011	"Metal cluster and functional analysis of plant metallothioneins" Dorothy Crowfoot Hodgkin Symposium 2011, Zurich, Switzerland
09/10/2011	"Metal cluster and functional analysis of plant metallothioneins" Fall Meeting of the Swiss Chemical Society, Lausanne, Switzerland
07-12/08/2011	"Insights into plant metallothioneins: metal clusters and their functional aspect" International Conference on Biological Inorganic Chemistry (ICBIC) 15, Vancouver, Canada
11/10/2010	"Sulfide ions elevate the metal binding capacity of cicMT2" Dorothy Crowfoot Hodgkin Symposium 2010, Zurich, Switzerland
16/09/2010	"The plant Metallothionein 2 from *Cicer arietinum* increases its metal ion binding capacity by incorporation of sulfide ions" Fall Meeting of the Swiss Chemical Society, Zurich, Switzerland
04-08/09/2010	"Sulfide ions elevate the metal binding capacity of cicMT2" XI International Symposium on Inorganic Biochemistry, Kudowa Zdrój, Poland

Awards

25/01/2013	Poster prize at the 5th Graduate School Retreat CMSZH, Charmey, Switzerland
2012	SCNAT/SCS Chemistry Travel Award